Establishing the zebrafish as a model to study the genetics of nociception

Elisa De Sequeira Couto E Vazão Clemente

University College London

Wolfson Institute for Biomedical Research

London Interdisciplinary Doctoral Programme

Supervisors:

Dr Elena Dreosti, Dr Liam Browne, Professor Maria Fitzgerald

A thesis submitted for the degree of

Doctor of Philosophy

May 2022

DECLARATION

I, Elisa de Sequeira Couto e Vazão Clemente, confirm that the work presented in this thesis is my own. Where information has been derived from other sources, I confirm that this has been indicated in the thesis.

Abstract

Pain is crucial for survival, and the ability to detect potentially harmful stimuli and respond accordingly is evolutionarily conserved. However, pain can also be undesirable in several situations, such as chronic pain. Pain management represents an unmet clinical need, with promising drugs identified in pre-clinical studies in rodents often failing to produce analgesia in clinical trials. This highlights the need for a better understanding of the mechanisms underlying the processing of noxious stimuli. The zebrafish has been increasingly used as an animal model in various fields. In this study, I aimed to establish the zebrafish as a model to study the genetics of nociception.

I first established an infrared laser assay to deliver temporally precise noxious heat stimuli, and studied the behavioural responses of tethered zebrafish larvae upon stimulation. I found that there are two components in these responses, which are temporally separated, have different properties, and can be modulated using chemicals. Then, I generated zebrafish F0 knockouts of *ngfb*, *ntrk1* and *prdm12b*, the zebrafish orthologs of three genes known to play a critical role in human pain, both physiologically and pathologically. I observed anatomical defects in a subset of *ntrk1* and *prdm12b* mutants. *ntrk1* mutants that lacked anatomical defects showed no changes in their response to noxious heat. However, I found that the fast component of the response to the laser was nearly completely abolished in *ngfb* mutants which were otherwise normal.

A genetic approach to the study of zebrafish nociception can be used to gain a mechanistic understanding of the genes, cells and pathways involved in sensing noxious stimuli and generating protective behaviours, which may help the development of better drugs and treatments for pain.

Impact statement

In this work, I establish an assay for the induction and study of zebrafish behavioural responses to acute, temporally precise, noxious heat. I show that this assay can be used to reliably elicit behavioural responses, which can be characterised in detail, and that it is flexible and can be combined with drugs to modulate responses to noxious stimuli. As such, it may be used in the future to test the effectiveness of new candidate analgesics. Moreover, infrared laser stimulation assays can be combined with calcium imaging to study how sensory stimuli, and the resulting protective behaviours, are encoded by different neuronal populations (Haesemeyer et al., 2018; Wee et al., 2019).

I also present new information about zebrafish behavioural responses to noxious stimuli. I show, for the first time, that zebrafish larvae respond to acute noxious heat with both a fast, more stereotyped, response, and a slower response. While a few key areas involved in the processing of noxious stimuli and innocuous heat have been identified in zebrafish (Wee et al., 2019, Haesemeyer et al., 2018), a lot is still unknown about the circuitry underlying sensing noxious stimuli and generating escape behaviours in both zebrafish and mammals. I also show, for the first time, that escape-like responses to acute noxious heat can be modulated by sub-threshold concentrations of an irritant chemical, which raises interesting questions regarding how different modalities of noxious stimuli are encoded by primary afferent neurons, the very first step in the transmission of sensory stimuli. This has not been extensively studied in zebrafish and indeed remains a contentious topic in the mouse literature (Prescott et al., 2014). As such, continuing this work could contribute towards an understanding of the mechanisms underlying nociception in zebrafish, and the similarities and differences compared to mammals.

Lastly, I generate zebrafish F0 knockouts of *ngfb*, *ntrk1* and *prdm12b*, the zebrafish orthologs of three genes known to play a critical role in human pain. The phenotypes shown by *ntrk1* and *prdm12b* mutants suggest a potential role for the ngf/trkA pathway in zebrafish development. This pathway has not been extensively studied in zebrafish, but studies on other neurotrophin receptors have found both similarities and differences in their function in zebrafish, compared to mammals (Gau et al., 2017). I also observed that mutating *ntrk1* does not lead to

clear defects in sensitivity to noxious heat, under my assay conditions, while the fast component of the response is nearly completely abolished in *ngfb* mutants which are otherwise normal. This raises interesting questions regarding the role of the ngf/trkA pathway in the development of the circuitry underlying responses to noxious heat, which could be addressed in future work. In doing so, this would help elucidate the similarities and differences of nociception in zebrafish and mammals. Ultimately, a better understanding of the mechanisms underlying nociception may help the development of better drugs and treatments for pain.

Acknowledgements

This thesis would absolutely not have been possible if it weren't for all of the people below. So a genuine huge thank you to everyone!

I'd like to thank my supervisors, Dr Elena Dreosti, Dr Liam Browne, and Professor Maria Fitzgerald, for guidance and support throughout the project. Elena – for your broad zebrafish and technical lab knowledge, for your decisiveness when identifying critical experiments, and for reminding me to proactively make use of the expertise held by the wider network of "fish floor" people. Liam – for your contagious* enthusiasm for science, and lengthy discussions on experiments, data and pain (*that'll be the only pandemic pun, I promise! - in my defence, Thesaurus failed me, it was either that or "infectious"). And thank you both for your detailed comments on the thesis and all the lessons learnt. Maria – thank you for always asking the best questions and for being one of the best examples of a brilliant, rigorous and knowledgeable, yet compassionate, kind and supportive scientist. Thank you for your empathy, gentle constructive criticism, and encouragement throughout the PhD.

Thank you to all the past and current members of the Dreosti and Browne labs, for discussions and support over the years. Gigantic thanks go to: Ara for always sharing your endless wisdom on all things neuroscience and for all the really fun stuff and very random chats too (side note: I just realised I spent more time sat next to you in the past 4 years than anyone else, so I can only apologise for that!); Tom for a huge amount of help with analysis (especially the free-swimming experiments and a bit of everything during the final push), for thinking about it with me and fixing "small" and big things in my code (including over the weekend!), and for never giving up on making my code more Pythonic; and Hande for showing me the ropes around the lab during those first couple of years. Thanks also to Alizée for unexpected conversations, Isobel for shared experiences, Connie for help with genotyping and nice chats, Flora, Denis and Jonathan for company on those late nights (Jonathan - thanks also for help with the thermistor), and Janka, a talented Master's student I got to supervise, for your hard work and dedication (and for requiring basically no supervision). Ara, Tom, Alizée, Isobel and Connie also deserve a special mention for their patience and

encouragement during the writing stage (I was not fun to be around…!). And thank you to Adam Kampff for help with the tail tracking analysis.

To my upgrade committee, James, Isaac and Sam, for spotting a less than promising project and helping me find an alternative way forward - special thank you to Isaac for very useful discussions on my behaviour data and help with the tap experiments, and James for your kind reassurance, availability, and support, particularly in the final few months.

A huge thank you goes to all the past and current members of the Fish Floor labs (Bianco, Hawkins, Rihel, Tada, Tuschl, Wilson) for an insane amount of feedback and support over the years, and for being some of the kindest, brightest, most passionate and patient people ever - and just an altogether fun bunch to be around! Special thanks to: Ana and Renato for Portuguese companionship (together with Artur!) and Native Scientist; Anya for football; Chintan for helping me think about my data; Declan, the man behind the curtain, for help with the Zebrabox experiments and above all for being almost impossibly empathetic, always checking in and never asking me to shut up (how??); François for kindly answering a record-breaking number of questions on the F0 knockouts; Gaia for useful feedback in the Wilson meetings; Gareth for lots of advice on HL-PCR; Masa for great insight on molecular biology; Paride for help with the blind fish experiments and useful discussions; Stephen for always having helpful suggestions. And also Steve Wilson for invaluable input during the Wilson lab meetings, which I was fortunate enough to take part in throughout the whole PhD.

To all the UCL Fish Facility staff, especially Carole, Heather, Jenna, Karen and Elise, for taking such good care of the fish and for being so patient when dealing with my many many many questions and very last-minute requests. And also the people from Biosciences stores, especially Michael and Tammy, for always having something nice to say.

To the LIDo-DTP programme, community and management team (and the BBSRC), for unbelievably useful, cool and fun training opportunities, socials and experiences I will never forget, an amazing community, a holistic approach to the training of graduate students, and endless support at challenging times - the biggest shout out and sincere thank you goes to Nadine and Geraint for your relentless prioritising of student welfare.

To all the extracurriculars, for being an inexhaustible source of sanity. Special mention to the student societies UCL Taekwondo club and UCL Comedy club for the chance to unwind, connect and try something new (who would have thought I can act? No one, because I definitely can't); various science communication projects (especially Native Scientist, Pain Research Forum, The Brilliant Club and Cartas com Ciência - Mariana and Rafael, thank you for your patience!) for reminding me of why it matters; and comedy for providing me with a healthy way to drown the PhD sorrows (thank you, Steve!).

And now, the people who have suffered the most as a result of my young(er) self's decision to embark on this amazing journey: my friends and family. It cannot have been easy listening to me talk about the same things for the last 1692 days (yes, I actually used an online date calculator for this), and I cannot thank you enough for sticking around. I don't think I'll ever be able to repay you what I owe you in rant-listening, hugs, pep talk and emotional support! UCL thesis length guidelines make it impossible to mention everyone who should be here, but here goes a huge thank you to at least some of you...

My funky, weird, Venn diagram of a friendship group that somehow works, for some of the most fun memories of the past few years. Andreia, Daniela, Eduardo, for letting me in on your jokes; Daniel for being a great lockdown flatmate; Lúcia, for all the lovely surprises, an unexpected connection, your patience, and always saying yes; and my PhD buddies, Clàudia, Greta, João, Marta and Shehrry, for more than some intense few conversations, for always listening, for understanding and for sharing your own experiences with honesty, through tears and laughter. And Kate, of course (more below!).

Annie, for the most peaceful place in London and everything that came from it (how do you always just "get it"…?); Maï-Carmen, for long chats over yummy food; and the people in this incredible group chat that shall remain unnamed, for conversations that allowed me to briefly forget about the thesis.

All the new friendships I made through LIDo, for a sense of companionship and mutual understanding that made everything more enjoyable – a really big shout out to Bethan, Ines, Lisa and Winnie, for always listening and checking in.

And the old ones too: Carolina, Mara, Maria and Rita, for a sense of home in London; Inês, Inês and Maria (again haha), my oldest friends, for always being

there and helping me remember that there's more to me than being a PhD student; and Ismael and Sara, for always randomly checking in and the best catch-ups.

Almost finally – Kate, for being Kate. I'm not sure how I would have got through it without your endless patience and support. Thank you for listening to me talk about it almost every single day for years and somehow managing to care about it throughout (seriously, how?). You really were there through the ups and (many) downs, and you made both better.

Finally, the greatest thank you to the most important people – my family, for your endless love and constant support. A very special and heartfelt thank you to my grandparents, Fernando, João, Lídia, Tina, for your inexhaustible faith in me and for sharing your wisdom of many decades. I am so unbelievably privileged to have you in my life. Your kindness, strength and character are inspiring, and I will always look up to you.

And now, the four people to whom I owe everything: my parents, João and Lídia, and my sisters, Carolina and Maria. Carolina, Maria, thank you for making me laugh when no one else can, the kindly blunt honesty only sisters are allowed to each other, letting me completely take over dinner/family time to whine about minor inconveniences, and your gentle encouragement. You make me the proudest and luckiest big sister! Mãe, Pai, thank you for **ALWAYS** being there. From patiently listening to my 1 am rants, to giving the best advice, putting your foot down when needed, coming to see me when I needed (Mãe!) and even discussing experiments and analysis (also thanks for the help with Python, Pai!), your unconditional support helped me face the PhD challenges with more optimism. I admire you tremendously, and I can only hope to live up to the standard you set. So, thank you.

Em Português (vamos a ver se ainda consigo), porque em Inglês não sabe ao mesmo:

Por fim, um agradecimento gigante às pessoas mais importantes – a minha família, pelo vosso amor interminável e apoio constante. Um obrigada muito especial, do fundo do coração, aos meus avós, Fernando, João, Lídia, Tina, pela vossa fé inesgotável em mim e por partilharem comigo a sabedoria que adquiriram ao longo de tantas décadas. É um privilégio inacreditável ter-vos na

minha vida. A vossa bondade, a vossa força e o vosso carácter são inspiradores, e eu irei sempre admirar-vos.

E, agora, as quatro pessoas a quem devo tudo: os meus pais, João e Lídia, e as minhas irmãs, Carolina e Maria. Carolina, Maria, obrigada por me fazerem rir quando mais ninguém consegue, por aquela “honestidade amavelmente directa”, sem papas na língua, que só irmãs podem ter umas com as outras, por me deixarem monopolizar as horas de jantar em família com queixas sobre pequenos contratempos, e pelo vosso apoio e encorajamento. É uma sorte e um orgulho enormes ser vossa irmã mais velha! Mãe, Pai, obrigada por estarem **SEMPRE** aqui. Da paciência com que ouvem as minhas queixas à uma da manhã, aos conselhos que dão, baterem o pé quando é preciso, virem ver-me quando precisei (Mãe!), e até discutirem experiências e análise (e obrigada pela ajuda com Python, Pai!), o vosso apoio incondicional ajudou-me a enfrentar os desafios do doutoramento com mais optimismo. Admiro-vos imenso e espero conseguir estar à altura do vosso exemplo. Por tudo isto, obrigada.

I'll finish off with the greatest source of inspiration there is – Portuguese proverbs. Here's a select few:

Vozes de burro não chegam ao céu.
A quem muito se abaixa, o rabo lhe aparece.
Água mole em pedra dura, tanto bate até que fura.

Now, on to the actual thesis! Enjoy!

Tudo é ousado para quem a nada se atreve.

Fernando Pessoa

Nothing in life is to be feared; it is only to be understood.

Marie Skłodowska-Curie

CONTENTS

List of figures

List of tables

Abbreviations

ACC	Anterior cingulate cortex
AITC	Allyl isothiocyanate
ASICs	Acid-Sensing Ion Channels
ATL1, ATL3	Atlastin GTPase 1, 3
ATP1a2	ATPase Na+/K+ Transporting Subunit Alpha 2
BDNF	Brain-Derived Growth Factor
BNST	bed nucleus *stria terminalis*
CACNA1A	Calcium Voltage-Gated Channel Subunit Alpha1 A
CEA	Central Amygdala
CGRP	Calcitonin Gene-Related Peptide
CIP, CIPA	Congenital Insensitivity to Pain (with Anhidrosis)
CLTCL1	Clathrin Heavy Chain Like 1
CNS	Central nervous system
CRISPR-Cas9	Clustered regularly interspaced short palindromic repeats – CRISPR-associated protein 9
crRNA	crispr RNA
DLF	dorsal longitudinal fascicle
DMSO	Dimethylsulfoxide
DNMT1	DNA (cytosine-5)-methyltransferase 1
dpf/hpf	Days/hours post-fertilisation (zebrafish)
DRG	Dorsal root ganglia
DRN	Dorsal Raphe Nucleus
DST	Dystonin
E	Embryonic day (mouse)
ELP1	Elongator Acetyltransferase Complex Subunit 1

ENU	Ethylnitrosourea
FAM19A5	Family with sequence similarity 19 (chemokine (C–C motif)-like) member A5
FEPS	Familial Episodic Pain Syndrome
FHM	Familial Hemiplegic Migraine
FISH	Fluorescent in situ hybridisation
FLVCR1	Feline Leukemia Virus subgroup C Receptor 1
GBX1, GBX2	Gastrulation Brain Homeobox 1, 2
gDNA	genomic DNA
GDNF	Glial cell line-Derived Neurotrophic Factor
gRNA	guide RNA
GSX1, GSX2	GS Homeobox 1, 2
HL-PCR	Headloop suppression PCR
HSAN	Hereditary Sensory and Autonomic Neuropathy
IHC	Immunohistochemistry
KIF1A	Kinesin family member 1A
LL response	Long-latency response
LPBN	Lateral Parabrachial Nucleus
LTMR	Low-threshold mechanoreceptor
M-cells	Mauthner cells
MOP, DOP, KOP	mu-, delta-, kappa-opioid receptors
Mrgprs	Mas-related G protein–coupled receptors
NGF	Nerve Growth Factor
Ngn1, Ngn2	Neurogenin-1, -2
nMLF	nucleus of the Medial Longitudinal Fascicle
NSAIDs	Non-Steroidal Anti-Inflammatory Drugs

NT-4/5, NT-3	Neurotrophin-4/5, -3
NTRK1, NTRK2, NTRK3	Neurotrophic Receptor Tyrosine Kinase 1, 2, 3
OPRM1, OPRD1, OPRK1	Opioid Receptor Mu 1, Delta 1, Kapa 1
P2RX2, P2RX3	Purinergic Receptor P2X 2, 3
PAG	Periaqueductal gray area
PAN	Primary afferent neuron
PCR	Polymerase Chain Reaction
PEPD	Paroxysmal Extreme Pain Disorder
PFC	Prefrontal cortex
PRDM12	PR domain zinc finger protein 12
RB neurons	Rohon-Beard neurons
RETREG1	Reticulophagy Regulator 1
RGC	Retinal ganglion cell
RNP	Cas9/gRNA ribonucleoprotein
S1/S2	Primary/Secondary somatosensory cortex
SCN1A, 9A, 10A, 11A	Sodium Voltage-Gated Channel Alpha Subunit 1, 9, 10, 11
SFN	Small-Fibre Painful Neuropathy
SL response	Short-latency response
SNP	Single-Nucleotide Polymorphisms
SP	Substance P
SPTLC1, SPTLC2	Serine Palmitoyltransferase Long Chain Base Subunit 1 and 2
TALENs	Transcription Activator-Like Effector Nucleases
TG	Trigeminal ganglia

tracrRNA	trans-activating crispr RNA
TRKA,B,C	Tropomyosin Receptor Kinase A, B, C
TRP	Transient Receptor Rotential channel family
TRPA1	TRP Cation Channel Subfamily A Member 1
TRPM3, TRPM8	TRP Cation Channel Subfamily M Member 3, 8
TRPV1	TRP Cation Channel Subfamily V Member 1
VPL	Ventral posterolateral (thalamic nucleus)
VPM	Ventral posteromedial nucleus (thalamic nucleus)
vSPN	ventral Spinal Projecting Nuclei
WNK1	with-no-lysine protein kinase 1
WT	Wild-type
ZFHX2	Zinc Finger Homeobox 2
ZFN	Zinc Finger Nucleases

Chapter 1: Introduction

1.1 Pain – why does it matter?

The ability to detect potentially harmful stimuli and respond accordingly is crucial for the survival of organisms. These responses are advantageous from an evolutionary point of view and are shared across different species, from invertebrates, such as *Aplysia californica* (with its widely studied gill withdrawal reflex), *Caenorhabditis elegans* and *Drosophila melanogaster*, to rodents and primates (Castellucci et al., 1970; Wittenburg and Baumeister, 1999; Im and Galko, 2012; Caterina et al., 2000, Chudler et al., 1986). Their protective role is four-fold. Firstly, they prompt immediate behavioural responses that minimise contact with potentially damaging situations (Barik et al., 2018; Khuong et al., 2019). Secondly, they promote identification of the source of danger (Haggard et al., 2013). Thirdly, they lead to the adoption of behaviours that promote tissue repair after injury, such as resting a broken limb (Honore et al., 2000; Huang et al., 2018). Fourthly, lasting associations can be made between specific situations or behaviours and pain, the resulting unpleasant sensation. This allows for internal models of the environment to be updated through higher-order processing and promotes the avoidance of those behaviours in the future (Haggard et al., 2013; Seymour, 2019). The importance of pain for survival is highlighted, for example, by the fact that individuals with congenital inability to experience pain, for instance by loss of function of the voltage-gated sodium channel gene *SCN9A*, often die young, after inadvertently placing themselves in "high-risk" situations, or as a result of unfelt injuries (Cox et al, 2006; Daneshjou et al., 2012).

The International Association for the Study of Pain defines pain as "an unpleasant sensory and emotional experience associated with, or resembling that associated with, actual or potential tissue damage" (IASP, 2020). Despite its critical role for survival, pain can also be undesirable in several situations. One example of when pain is undesirable and becomes maladaptive is chronic pain, that is, pain that lasts or recurs for longer than three to six months. There are several types of chronic pain, such as chronic neuropathic pain (caused by a lesion or disease of the somatosensory nervous system), chronic post-surgical

and post-traumatic pain (which develops after a surgical procedure or a tissue injury and persists at least three months after surgery or tissue trauma), chronic cancer pain (caused by the cancer itself or the cancer treatment), chronic headache, and chronic orofacial, visceral, or musculoskeletal pain (e.g. rheumatoid arthritis) (Treede et al., 2015; Schug et al., 2019). It can be extremely debilitating and negatively affect general and mental health, having been found to be comorbid with sleep disturbances, depression, addiction vulnerability, anxiety, and fatigue, as well as having a negative impact on social and economic wellbeing (Elliott et al., 1999; Elliott et al., 2002; Haack et al., 2019; Chopra and Arora, 2014; Serafini et al., 2020; Boersma et al., 2019; Van Damme et al., 2018). While the exact prevalence of chronic pain varies widely in the literature, it affects a significant proportion of the population, with some studies estimating 20% of Europeans suffer from chronic pain at some point in their lives (Breivik et al., 2006) and others finding chronic pain prevalence in the previous 12 months to be of approximately 40% (Tsang et al., 2008).

Therapeutic advances for chronic pain have been limited (Gilron et al., 2013; Gilron et al., 2022). The majority of drugs typically used fall into the class of opioid analgesics. Opioids are a class of related drugs, such as methadone, codeine and morphine, that act on specific receptors (opioid receptors) in the nervous system. Despite their widespread use, they actually show limited efficacy in the treatment of chronic pain (Serafini et al., 2020). Further, opioid receptors are not exclusively expressed in pain-related pathways. Therefore, the use of opioid analgesics can lead to many problematic side effects, such as constipation, physical dependence and addiction (as a result of activation of reward pathways), as well respiratory depression and, ultimately, death by overdose (due to interactions with parts of the brainstem that control breathing) (Fields and Margolis, 2015; Elman and Borsook, 2016; White and Irvine, 1999). Indeed, opioid misuse is a long-standing issue in the United States, with over 33 thousand deaths per year, as of 2017, and it is sometimes termed the “opioid epidemic” (Soelberg et al., 2017). Furthermore, acute pain, such as postoperative pain or pain resulting from injury or tissue trauma, is also largely undermanaged and often reliant on opioids, in both adults and children (Apfelbaum et al., 2003; Breivik and Stubhaug, 2008; Joshi and Kehlet, 2019; Rosen et al., 2022; Ferland et al., 2019; Hsu et al., 2019). This is also problematic since, for instance,

effective postoperative pain management is important, as it is closely linked with clinical outcome and patient wellbeing (Vadivelu et al., 2010).

In short, pain represents a large unmet clinical need. This largely stems from our incomplete knowledge of the circuits involved in pain processing. As such, the development of better drugs and treatments requires a better understanding of the mechanisms underlying pain and nociception.

1.2 Nociception in mammals

1.2.1 A brief overview of ascending pathways

The International Association for the Study of Pain defines nociception as “the neural process of encoding noxious stimuli”, the consequences of which may be autonomic or behavioural (IASP, 2020). The first step in this process is the activation of nociceptors, a specific type of primary afferent neuron (PAN), by a noxious stimulus. Nociceptors are pseudounipolar neurons, with one axon projecting peripherally, to innervate e.g. skin, muscle and joints, and the other centrally, to the central nervous system (CNS). The cell bodies of nociceptors that transmit noxious information from the body form the dorsal root ganglia (DRG). These neurons project their central axons to the dorsal horn of the spinal cord, where they synapse onto second-order neurons (mainly in the superficial Rexed laminae I and II, but also lamina V - Todd, 2010). The axons of these neurons immediately decussate (cross the midline) and form various pathways which ascend along the spinal cord to synapse onto neurons located in different supraspinal targets. The two main ascending pathways are the spinothalamic tract (Figure 1.1) and the spinoparabrachial tract. Axons of neurons in the spinothalamic tract project to various nuclei in the thalamus, such as the ventral posterolateral (VPL) nucleus and the intralaminar nuclei, while those in the spinoparabrachial tract project to the lateral parabrachial nucleus (LPBN). On the other hand, nociceptors that transmit noxious information from the head and neck have their cell bodies located in trigeminal ganglia (TG) and project their central axons to the brainstem (specifically the spinal trigeminal nucleus), where they synapse onto second-order neurons. As for second-order neurons in the spinal cord, the axons of these neurons also cross immediately and ascend to the

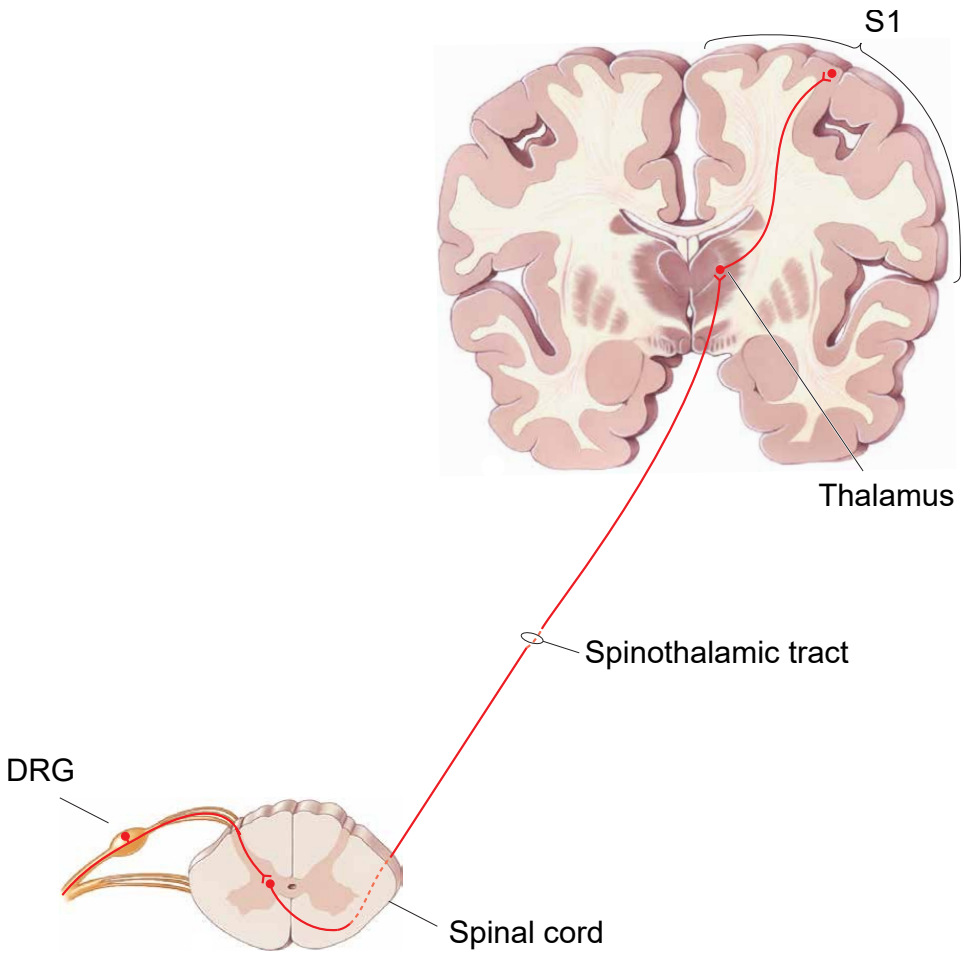

Figure 1.1: **Schematic of the spinothalamic tract, one of the main ascending pathways transmitting noxious information from the body**. Nociceptors with cell bodies in the dorsal root ganglia (DRG) project their central axons to the dorsal horn of the spinal cord, where they synapse onto second-order neurons. The axons of these neurons immediately cross the midline and form the spinothalamic tract, which ascends through the ventral surface of the spinal cord to synapse onto neurons located in various nuclei in the thalamus, such as the ventral posterolateral (VPL) nucleus and the intralaminar nuclei. Thalamic neurons then project to various cortical and sub-cortical areas, which are implicated in sensory-discriminative and/or emotional perception of pain. One of these key areas is the primary somatosensory cortex (S1). Image adapted from Bear et al. (2007).

thalamus, forming the trigeminal lemniscus (also called trigeminothalamic pathway), and synapse onto neurons located in thalamic nuclei, such as the ventral posteromedial nucleus (VPM) and the intralaminar nuclei. Additionally, there are some direct TG projections to the LPBN (McMahon and Koltzenburg, 2005; Dinakar and Stillman, 2016; Peirs and Seal, 2016; Koch et al., 2018; Tan and Kuner, 2021; Rodriguez et al., 2017).

Thalamic neurons then project to various cortical and sub-cortical areas, which are implicated in sensory-discriminative and/or emotional perception of pain. Some of these key areas include the primary and secondary somatosensory cortices (S1 and S2), prefrontal cortex (PFC), anterior cingulate cortex (ACC), insula, periaqueductal gray area (PAG) and the amygdala (McMahon and Koltzenburg, 2005; Dinakar and Stillman, 2016; Peirs and Seal, 2016; Koch et al., 2018; Tan and Kuner, 2021). Neurons in the LPBN project to the PAG, dorsal reticular formation in the medulla and ventromedial hypothalamus (VMH) to drive escape behaviours in rodents, as well as other targets, such as the bed nucleus stria terminalis (BNST) and central amygdala (CEA), the latter being associated with avoidance and generation of an aversive memory in rodents (Barik and Chelser, 2020; Chiang et al., 2020; Barik et al., 2018).

While several of these key players and general steps have been known for decades, a lot remains unknown about the exact mechanisms through which a noxious stimulus is processed to ultimately lead to a painful (or pain-like) experience. These processes are extremely complex and there is significant processing and modulation of the signal taking place at every point, from the very first step in transmission, to descending pathways from the brain, as well as cognitive and affective/emotional pathways (Bushnell et al., 2013).

1.2.2 Nociceptors – somatosensory afferents that sense noxious stimuli

Somatosensation allows animals to monitor both internal and external environments. The first step in the processing of somatosensory stimuli is the activation of somatosensory afferents, which can be interoceptive (autonomic and proprioceptive) or exteroceptive (cutaneous) (Figure 1.2). Interoceptive

afferents carry information about the internal environment of the body. They can largely be divided into visceral sensory afferents and proprioceptors, which provide sensory feedback from internal organs or skeletal muscle, respectively. On the other hand, information about the external environment is transmitted by cutaneous (exteroceptive) afferents. The three main subtypes of cutaneous afferent fibres are Aβ fibres (thickly myelinated, fast-conducting), Aδ (thinly myelinated, fast-conducting), and C fibres (unmyelinated, slow-conducting). Traditionally, Aβ fibres have been associated with sensing light (innocuous) touch (thus being called low-threshold mechanoreceptors – LMTRs), and Aδ and C fibres with noxious stimuli, but this is over-simplistic. For instance, subsets of both Aδ and C fibres have been found to be activated by weak, innocuous mechanical stimuli, displaying thresholds below the noxious range and being classed as LMTRs (Basbaum et al., 2009; Abraira and Ginty, 2013; Koch et al., 2018). This again highlights the complexity of somatosensation. As such, somatosensory neuron subtypes have increasingly been defined by the expression of various markers, often through the use of single-cell RNA sequencing. These classifications, and the functional role of specific subpopulations, are constantly under revision (Usoskin et al., 2015; Li et al., 2016; Zeisel et al., 2018; Kupari et al., 2021; Tavares-Ferreira et al., 2022). For the purposes of this work, I will focus on cutaneous somatosensory neurons that are activated by noxious stimuli – nociceptors.

Information about noxious stimuli is transmitted by nociceptors. These can be Aδ fibres or C fibres, with the former being usually associated with a fast pain, and the latter with a slow pain, as well as itch. Just like other somatosensory neurons, nociceptors can also be divided into subclasses based on gene expression (Usoskin et al., 2015; Li et al., 2016; Zeisel et al., 2018; Zheng et al., 2019; Sharma et al., 2020; Kupari et al., 2021; Tavares-Ferreira et al., 2022). Importantly, the expression of some of these genes determines the tuning of each nociceptor to different stimuli (Koch et al., 2018). A classic example of this is the transient receptor potential (TRP) channel family. For instance, the TRPV1 channel is activated by high temperatures (as well as capsaicin and protons), and its expression in a subset of nociceptors thus confers them sensitivity to noxious heat (as well as capsaicin and protons) (Caterina et al., 1997; Caterina et al., 2000); TRPM8 is sensitive to both innocuous and noxious cold (as well as menthol), being required for cold sensation in mice (Dhaka et al., 2007); and

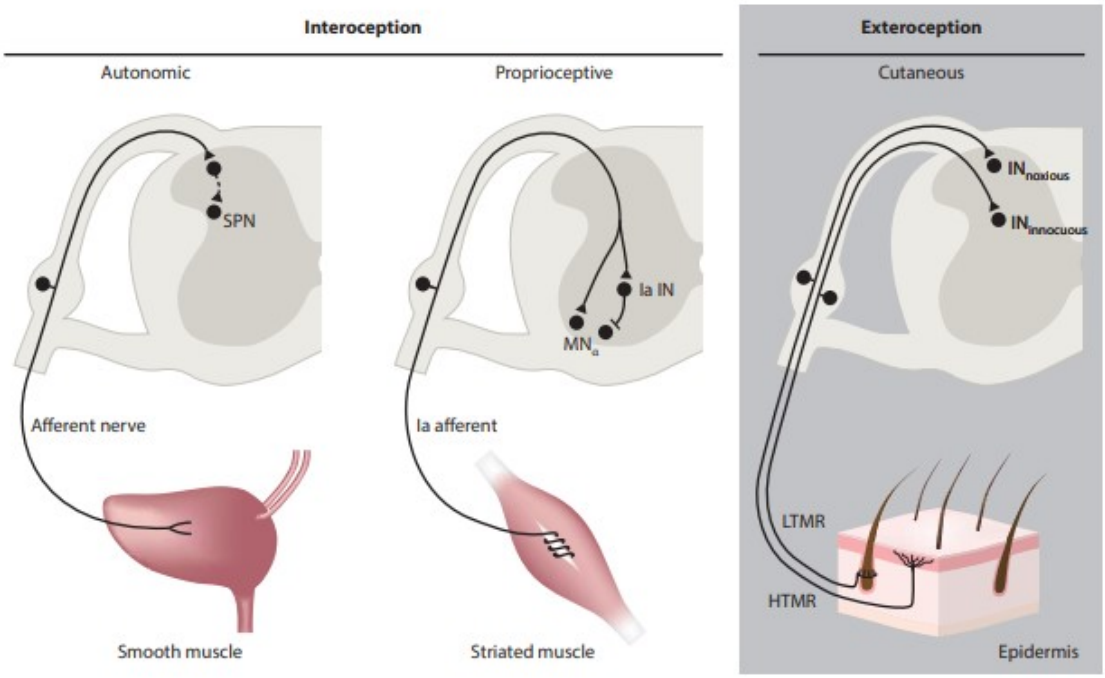

Figure 1.2: **The spinal cord receives and processes information about the internal and external environments**. (Left) Autonomic afferents monitor stretch within smooth muscle to provide information about the activity of internal organs. In the example shown, mechanoreceptors within the bladder wall activate afferent nerves as the bladder fills; in turn, a putative interneuronal pathway (dashed line) within the dorsal horn mediates afferent input onto the sympathetic preganglionic nucleus (SPN), which controls bladder filling. (Center) Proprioceptive afferents monitor tension and stretch within striated muscle to provide information about the position of the body in space. In the example shown, Ia afferents originating in muscle spindles monitor the length and velocity of muscle fibers; in turn, Ia afferents activate agonist alpha motoneurons (MNα s) as well as Ia inhibitory interneurons (INs), which suppress activity of antagonist MNα s. (Right) Cutaneous afferents innervate the hairy and glabrous skin and are activated by mechanical, thermal, noxious, or pruritic stimuli to provide information about the external environment. In the example shown, a low-threshold mechanoreceptor (LTMR) and high-threshold mechanoreceptor (HTMR), which exhibit tuning to the intensity of mechanical stimulation of the skin, activate distinct cohorts of INs within the dorsal horn. Image retrieved from Koch et al. (2018).

TRPA1 is activated by chemicals such as allyl isothiocyanate (AITC, commonly known as mustard oil) as well as having been proposed to be a noxious cold sensor (Bandell et al., 2004). Nociceptors can be polymodal, that is, sensitive to multiple types of noxious stimuli. At the same time, there is a lot of redundancy in the system. For instance, even though TRPV1 is traditionally thought of as the noxious heat sensor, TRPA1 and TRPM3 are also involved in noxious heat sensation, and mice actually retain robust responses to somatosensory heat in the presence of only one of these three channels (Vandewauw et al., 2018). This once again highlights the importance of somatosensation, particularly of noxious stimuli.

As such, many key players in the processing of noxious stimuli have been identified. However, it is still not known exactly how different modalities of noxious stimuli are encoded by PANs to ultimately generate different sensations. PANs are tuned to specific stimulus features, but natural stimuli often activate more than one type of afferent, and it is likely that signals conveyed by different types of afferents interact. In rodents, several theories have been put forward to explain these processes, but this remains a contentious topic, and rodent models have so far been unable to provide us with definite answers (Prescott et al., 2014). This further emphasises the complexity of nociception and pain, from the very first step in the process.

1.2.3 Nociceptor development

Sensory neurons in the DRG derive from multipotent neural crest cells that delaminate from the dorsal neural tube and migrate ventrally. Expression of neurogenin-1 or -2 (Ngn1 and Ngn2, respectively) commits these cells to a neuronal fate. The specification of DRG sensory neurons into various subtypes from their progenitors relies on neurotrophic factors (Figure 1.3). These are factors that regulate the survival, growth and differentiation of specific neuronal populations. DRG sensory neurons differentially express the various neurotrophic factor receptors, primarily TrkA, TrkB, TrkC, Ret, Runx1 and Runx3, which determines their specification into different subtypes. In rodents, neurons showing early Ret expression (at embryonic stage E10.5-11.5 – ‘eRet’ in Figure 1.3) differentiate into myelinated neurons with mechanosensory functions; Ret is

the receptor for members of the GDNF (glial cell line-derived neurotrophic factor) family of neurotrophins. Neurons showing early TrkB expression (but lacking Ret) also differentiate into subtypes of mechanoreceptors, including slowly adapting LTMRs and the lightly myelinated Aδ-LTMR ('TrkB/C' in Figure 1.3); neurotrophin-4/5 (NT-4/5) and brain-derived nerve factor (BDNF) are the preferred ligands at the TrkB receptor. Neurons showing early TrkC expression, combined with Runx3 (a transcription factor which represses the potential for TrkB expression), differentiate into proprioceptive neurons ('TrkB/C' in Figure 1.3); the preferred ligand at the TrkC receptor is neurotrophin-3 (NT-3). Finally, neurons with TrkA expression differentiate into nociceptors. Those with early TrkA expression (E10.5 - 'eTrkA' in Figure 1.3) lack Runx1 expression and develop, from the Ngn2-dependent neurogenesis, into lightly myelinated Aδ fibres. Those with late TrkA expression (E12.5) express Runx1 at E12.5 and develop, largely from the Ngn1-dependent neurogenesis, into unmyelinated C fibres ('lTrkA' and 'lRet' in Figure 1.3). Myelinated Aδ fibres then go on to express neuropeptides such as calcitonin gene-related peptide (CGRP) or substance P (SP), which makes them peptidergic nociceptors. Neuropeptides are thought to have a modulatory role on nociception. For instance, CGRP has been suggested to have a "pronociceptive" role (that is, facilitating nociceptive processing) upon its release from the central terminals of PANs (Trang et al., 2005). Indeed, CGRP antagonists can increase the latency of withdrawal responses to both thermal and mechanical stimuli in rats (Yu et al., 1994). Unmyelinated C fibres further differentiate into other subtypes, defined by expression of either TrkA (identifying heat-sensitive and mechanically sensitive peptidergic nociceptors); or Ret, isolectin B4 (IB4), and one of many Mas-related G protein–coupled receptors (Mrgprs) (nonpeptidergic nociceptors). Nerve growth factor (NGF) is the preferred ligand for TrkA (McMahon and Koltzenburg, 2005; Fitzgerald, 2005; Marmigere and Ernfors, 2007; Lallemend and Ernfors, 2012; Koch et al., 2018). A final key player in the development of nociceptors in the mouse DRG is Prdm12, a transcription factor specifically expressed in myelinated Aδ- and unmyelinated C-fiber nociceptors from as early as E9.5 into adulthood. It is necessary for the initiation of the nociceptive neuron lineage through the initiation and maintenance of TrkA expression (Usoskin et al., 2015; Desiderio et al., 2019; Bartesaghi et al., 2019; Landy et al., 2021).

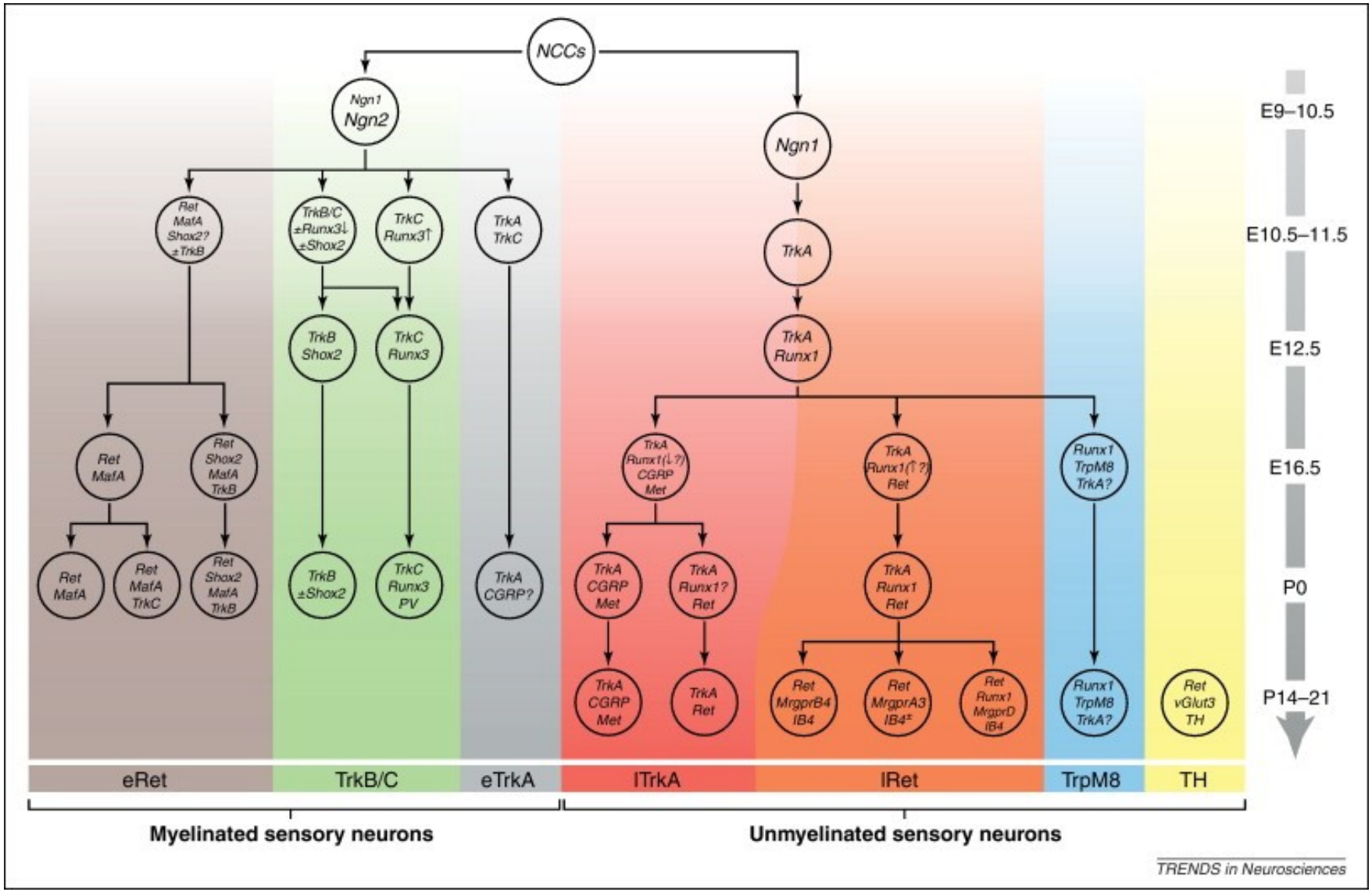
NCCs
Ngn1
Ngn2
Ngn1
Ret
MafA
Shox2?
±TrkB
TrkB/C
±Runx3↓
±Shox2
TrkC
Runx3↑
TrkA
TrkC
TrkA
TrkA
Runx1
TrkB
Shox2
TrkC
Runx3
Ret
MafA
Ret
Shox2
MafA
TrkB
TrkA
Runx1(↓?)
CGRP
Met
TrkA
Runx1(↑?)
Ret
Runx1
TrpM8
TrkA?
Ret
MafA
Ret
MafA
TrkC
Ret
Shox2
MafA
TrkB
TrkB
±Shox2
TrkC
Runx3
PV
TrkA
CGRP?
TrkA
CGRP
Met
TrkA
Runx1?
Ret
TrkA
Runx1
Ret
TrkA
CGRP
Met
TrkA
Ret
Ret
MrgprB4
IB4
Ret
MrgprA3
IB4±
Ret
Runx1
MrgprD
IB4
Runx1
TrpM8
TrkA?
Ret
vGlut3
TH
E9–10.5
E10.5–11.5
E12.5
E16.5
P0
P14–21
eRet
TrkB/C
eTrkA
lTrkA
lRet
TrpM8
TH
Myelinated sensory neurons
Unmyelinated sensory neurons
TRENDS in Neurosciences

Figure 1.3: **Dorsal root ganglion (DRG) neuron diversification during development**. Schematic representation of the different main lineages (outlined by color shading) during the course of sensory neuron differentiation in mouse. All sensory neurons arise from neural crest cells (NCCs). The far-right column refers to development stages in mouse, where E and P represent embryonic and postnatal stages, respectively. Hence, within the myelinated populations, light-brown, green and gray identify the early Ret (eRet), tropomyosin-receptor kinase (Trk)B/TrkC and early TrkA (eTrkA) lineages, respectively. The unmyelinated populations are divided into four main categories: the late TrkA (lTrkA), the late Ret (lRet), the TrpM8 and the TH lineages, identified by the red, orange, blue and yellow color codes, respectively. The ancestors of vesicular glutamate transporter type 3 (VGLUT3+)/tyrosine hydroxylase (TH+) neurons are unknown; therefore, this type of neuron is not connected to any early immature neuronal population. Factors with question marks remain to be clarified and plus and minus signs refer to expression in some but not all neurons in the indicated subtype of neurons. Furthermore, the arrow within cells of the eTrkA lineage remains to be clarified for definite assignment. Image retrieved from Lallemend and Ernfors (2012).

Neurotrophins can also bind to the p75 neurotrophin receptor ($p75^{NTR}$), a single membrane spanning protein in the tumor necrosis factor (TNF) receptor family. Unlike the Trk receptors, which autophosphorylate after ligand binding, the $p75^{NTR}$ does not have intrinsic catalytic activity. Instead, it partners with the three neurotrophin receptors, TrkA, TrkB, TrkC, as well as non-neurotrophin receptors (Meeker and Williams, 2015). Interactions between Trk receptors and $p75^{NTR}$ can lead to changes in the binding affinity for neurotrophins. For instance, high-affinity NGF binding requires co-expression of and binding to both TrkA and $p75^{NTR}$ (Hempstead et al., 1991). $p75^{NTR}$ also plays a role in sensory neuron differentiation. For example, $p75^{NTR}$ has been found to be required for the development of nonpeptidergic nociceptors by fine-tuning Ret-mediated trophic support (Chen et al., 2017).

It is important to note that recent studies have shed light on considerable differences between the transcriptome of mouse and human DRG (Rostock et al., 2018; Tavares-Ferreira et al., 2022). In particular, Tavares-Ferreira et al. (2022) found a blended expression of markers of peptidergic and nonpeptidergic nociceptors in human DRG, contrary to what is commonly seen in rodents.

There are also some differences between TG and DRG neurons, both with regards to their gene expression and developmental origin. Indeed, transcriptional and translational profiling have identified several genes that are differentially expressed in rodent DRG and TG (Price and Flores, 2007; Manteniotis et al., 2013; Kogelman et al., 2017; Megat et al., 2019). Moreover, unlike DRG neurons, TG neurons have a dual developmental origin, being formed by cranial neural crest cells and trigeminal ectodermal placodes (Lallemend and Ernfors, 2012). The specification of all TG neurons depends on Ngn-1 function, with Ngn-1 null mutants showing a complete loss of TG (Ma et al., 1998). However, as detailed in the previous sections, TG and DRG neurons have equivalent functional roles, and there are many similarities between these two populations. For instance, Lopes et al. (2017) found that more than 99% of mRNA showed consistent expression between TG and DRG neurons (suggesting that the greater differences reported by others, such as Megat et al. (2019), might be attributable to non-neuronal populations), and single-cell RNA sequencing of TG neurons identified several clusters of sensory neurons, some of which were well conserved in DRG (Nguyen et al., 2017; Sharma et al., 2020). Additionally,

despite the differences in developmental origin, several of the key players involved in the differentiation and specification of different populations of DRG neurons are also important in TG development. For instance, Runx1−/− mice show a decrease in total number of neurons in the TG, TrkB is expressed in mechanoreceptors, and Runx3 is required for the specification of TrkC-expressing mechanoreceptive TG neurons (Theriault et al., 2004; Dykes et al., 2010; Marmigere et al., 2006; Senzaki et al., 2010). Importantly, as for mouse DRG, Prdm12 is also expressed in TG neurons from as early as E9.5, selectively in TrkA+ (but not TrkB/C+) neurons, which differentiate into nociceptors, and a loss of Prdm12 leads to a complete loss of TrkA+ neurons (Desiderio et al., 2019; Bartesaghi et al., 2019). Finally, TG neurons also express neuropeptides (e.g. CGRP and SP) as well as some of the key molecules activated by noxious stimuli such as TRP channels (e.g. TRPV1, TRPA1, TRPM8) (Messlinger et al., 2020; Dux et al., 2020).

In short, there are a number of key molecules involved in the differentiation and specification of nociceptors in DRG and TG neurons. In the next section, I will detail how mutations in these (and other) genes can lead to severe defects in the ability to sense noxious stimuli.

1.3 Human genetic pain disorders

1.3.1 Human phenotypes

Human Mendelian genetic disorders of pain sensing are extreme phenotypes characterised by either painlessness or paroxysmal (excess) pain. They are usually caused by one or two mutations in a single gene, typically single-nucleotide changes, and are inherited and fully penetrant. Even though they are quite rare, studying these disorders is extremely valuable for pain research, as it can help us gain insight into the role of these genes and their pathways. This can ultimately aid the development of new drugs (Cox et al., 2019).

Mendelian disorders of painlessness can be classified as developmental (with sensory neuropathy – nociceptors are either not generated or undergo apoptosis during development) or functional (without sensory neuropathy –

nociceptors are present but have functional defects). Developmental Mendelian disorders of painlessness are typically referred to as hereditary sensory and autonomic neuropathies (HSANs) and can be caused by mutations in several genes (Table 1.1; Figure 1.4). They are a clinically and genetically heterogeneous group of disorders, broadly classified into eight types: HSAN Types1-6, HSAN Type 8 and FLVCR1-associated pain loss (which presents features of HSAN but is not classed as one of the different types of HSAN – Chiabrando et al., 2016; Chiabrando et al., 2021). Their main pathological feature is the progressive degeneration of (predominantly) sensory and autonomic neurons, which underlies the inability to experience pain but also a range of other symptoms, including variable autonomic and motor disturbances (Rotthier et al., 2012; Cox et al., 2019). On the other hand, functional Mendelian disorders of painlessness are those where patients report pain insensitivity in the absence of neuropathy, showing normal nerve fibre density: Nav 1.7 Congenital Insensitivity to Pain (CIP), Nav 1.9 CIP, or Marsili Syndrome (Table 1.1; Cox et al., 2019).

Table 1.1: **Human Mendelian genetic disorders of pain sensing and genes affected**. Human gene symbol and UniProtKB ID of the corresponding protein are shown.

Gene Symbol	UniProtKB ID	Disorder(s)	References
ATL1	Q8WXF7	HSN1D	Guelly et al., 2011 Cox et al., 2019
ATL3	Q6DD88	HSN1F	Kornak et al., 2014 Fischer et al., 2014 Cox et al., 2019
ATP1a2	P50993	FHM type II	De Fusco et al. 2003 Cregg et al., 2010
CACNA1A	O00555	FHM type I	Ophoff et al. 1996 Cregg et al., 2010
CLTCL1	P53675	HSAN9	Nahorski et al., 2015a Nahorski et al., 2015b
DNMT1	P26358	HSN1E	Klein et al., 2011 Cox et al., 2019
DST	Q03001	HSAN6	Ferrier et al., 2015 Cox et al., 2019
ELP1 / IKAP	O95163	HSAN3 (also called Riley-Day syndrome)	Anderson et al., 2001 Cox et al., 2019
FLVCR1	Q9Y5Y0	FLVCR1-Associated Pain Loss	Chiabrando et al., 2016 Cox et al., 2019
KIF1A	Q12756	HSAN2C	Nemani et al., 2020 Cox et al., 2019
MPV17	P39210	Navajo neurohepatopathy	Karadimas et al., 2006 Nahorski et al., 2015b
NGFB	P01138	HSAN5	Einarsdottir et al., 2004 Cox et al., 2019
NTRK1	P04629	HSAN4 (also called CIPA)	Mardy et al., 1999 Cox et al., 2019
PRDM12	Q9H4Q4	HSAN8 MiTES	Chen et al., 2015 Cox et al., 2019
***RETREG1* (previously FAM134B)**	Q9H6L5	HSAN2B	Kurth et al., 2009 Cox et al., 2019
SCN10A	Q9Y5Y9	FEPS2 SFN	Faber et al., 2012b Cox et al., 2019
SCN11A	Q9UI33	FEPS3 SFN Nav1.9 CIP	Zhang et al., 2013 Huang et al., 2014 Leipold et al., 2013 Leipold et al., 2015 Cox et al., 2019
SCN1A	P35498	FHM type III	Dichgans et al. 2005 Cregg et al., 2010
SCN9A	Q15858	HSAN2D Nav1.7 CIP PEM PEPD SFN	Cox et al., 2006 Yuan et al., 2013 Faber et al., 2012a Yang et al., 2004 Fertleman et al., 2006 Cox et al., 2019
SPTLC1	O15269	HSAN1A	Bejaoui et al., 2001 Dawkins et al., 2001 Cox et al., 2019
SPTLC2	O15270	HSAN1C	Rotthier et al., 2010 Cox et al., 2019
TRPA1	O75762	FEPS1	Kremeyer et al., 2010 Cox et al., 2019
WNK1	Q9H4A3	HSAN2A	Shekarabi et al., 2008 Cox et al., 2019
ZFHX2	Q9C0A1	Marsili Syndrome	Habib et al., 2018 Cox et al., 2019

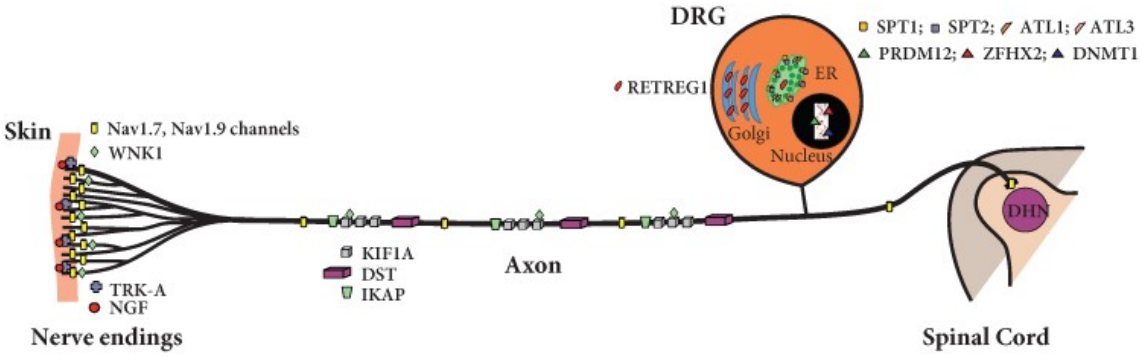

Figure 1.4: **Schematic of a primary sensory neuron showing subcellular location of proteins encoded by pain insensitivity genes**. Transcriptional regulators PRDM12, ZFHX2, and DNMT1 localize to the nucleus within the DRG soma. RETREG1 is found within the endoplasmic reticulum (ER) and is also a structural protein of the cis-Golgi body. SPT1 and SPT2 are involved in sphingolipid biosynthesis and localize to the ER. ATL1 and ATL3 regulate ER architecture. Voltage-gated sodium channels are expressed at both the peripheral and central terminals and along axons of primary afferents. WNK1 is a regulator of ion channels and also interacts with KIF1A, a kinesin family motor protein involved in axonal transport of synaptic vesicles. DST is involved in intracellular transport and maintains cytoskeletal integrity. IKAP mutations are associated with neuronal migration defects and impaired neurotrophic retrograde transport. NGF and its receptor, TRKA, are important for neuronal development and survival. DHN = dorsal horn neuron. Image retrieved from Cox et al. (2019).

The second main group of human genetic pain disorders are those where there is paroxysmal pain: Primary Erythromelalgia (PE, which can be sub-classed into familial (inherited) and sporadic forms); Paroxysmal Extreme Pain Disorder (PEPD); Familial Episodic Pain Syndrome Types 1–3 (FEPS1-3); Familial Hemiplegic Migraine Types 1-3 (FHM1-3); and Small-Fibre Painful Neuropathy (SFN). Most of these disorders are channelopathies, that is, they are caused by mutations in genes that encode ion channels, such as sodium channels (*SCN1A*, *SCN9A*, *SCN10A* and *SCN11A*), calcium channels (*CACNA1A*), or TRP channels (*TRPA1*) (Table 1.1; Cregg et al., 2010; Cox et al., 2019; Bennett and Woods, 2014; Tang et al., 2015; Raouf et al., 2010). These are typically gain-of-function mutations that lead to neuronal hyperexcitability.

It is interesting to note that different mutations in the same gene can have drastically different consequences. For instance, loss-of-function mutations in *SCN9A* can lead to painlessness with or without sensory neuropathy (HSAN2D or Nav1.7 CIP, respectively), while gain-of-function mutations in the same gene can lead to various disorders of extreme pain, namely PE, PEPD or SFN (Yuan et al., 2013; Cox et al., 2006; Yang et al., 2004; Dib-Hajj et al., 2005; Fertleman et al., 2006; Faber et al., 2012a).

1.3.2 Mouse studies of human genetic pain disorders

Understanding the genetic basis of human Mendelian pain disorders can give insight into the pathophysiology of pain and the role that key proteins play in the process. With that aim, many of these disorders have been modelled and studied in rodent models. For instance, knock-in mice carrying a *Scn11a* mutation (which causes Nav 1.9 CIP in humans) had reduced sensitivity to pain (Leipold et al., 2013), and knock-in mice carrying a *Cacna1a* mutation associated with FHM-1 had several gain-of-function effects, including a reduced threshold and increased velocity of cortical spreading depression (a wave of transient intense cortical spike activity which is thought to underlie the migraine aura in humans) (van den Maagdenberg et al., 2004; Pietrobon and Brennan, 2019). On the other hand, the phenotype of mouse knockout studies has also informed the discovery of genes implicated in human genetic pain disorders (Mogil, 2009). For example, conditional knockout of *Scn9a* in sensory neurons resulted in mice with

decreased sensitivity to noxious thermal and mechanical stimuli (Nassar et al., 2004) and mutations in this gene in humans were later found to lead to Nav1.7 CIP (Cox et al., 2006). Similarly, homozygous *Ntrk1*-knockout mice have congenital loss of responses to noxious stimuli and a complete loss of nociceptors in the DRG, as well as sympathetic ganglia neurons and cholinergic neurons of the basal forebrain (Smeyne et al., 1994; Snider, 1994), and mutations in *NTRK1* in humans have been shown to lead to congenital insensitivity to pain with anhidrosis (CIPA), also known as HSAN4 (Indo et al., 1996; Mardy et al., 1999; Indo 2001). Finally, a good example of mechanistic insight deriving from animal models of these disorders can be seen in *PRDM12*. In humans, several mutations in *PRDM12* have been shown to lead to HSAN8, with affected individuals being unable to feel acute or inflammatory pain and showing severe loss of nociceptive fibres (Chen et al., 2015). Subsequently, several key mouse studies helped unveil the role of *PRDM12* in sensory neuron development. Desiderio et al. (2019) found that *Prdm12* is required for the development of nociceptors by regulating the initiation and maintenance of TrkA expression, with constitutive knockouts of *Prdm12* showing selective loss of nociceptor precursors. Indeed, Bartesaghi et al. (2019) found that all remaining neurons in the DRG of *Prdm12*-null mice were myelinated LTMRs (TRKC+, TRKB+, RET+). Finally, Landy et al. (2021) showed that embryonic conditional knockout of *Prdm12* in sensory neurons leads to decreased responses to various noxious stimuli, including mechanical, noxious cold and capsaicin, while responses to innocuous stimuli were intact, which replicates several aspects of the human phenotype (Chen et al., 2015).

The mechanistic understanding gained from animal and human studies has sometimes translated into effective analgesics. For instance, a mutation in *NGF* has been found to lead to HSAN5, with patients showing insensitivity to pain accompanied by a severe reduction of unmyelinated fibres and a moderate loss of thinly myelinated fibres (Einarsdottir et al., 2004). This is likely caused by a loss of trophic support as a result of reduced availability of mature NGF (mutant NGF is mainly found as proNGF in both neuronal and non-neuronal cells) (Larsson et al., 2009). Homozygous *Ngf*-knockout mice fail to respond to noxious stimuli and show loss of sensory and sympathetic neurons (Crowley et al., 1994). Moreover, heterozygous mice harbouring the same point mutation identified in humans (661C>T) have recently been found to show impaired sensitivity to noxious stimuli (heat, cold and capsaicin) and reduced skin innervation, with loss

of unmyelinated axons (Testa et al., 2019). These and other studies have suggested NGF as a potential target drug. Indeed, drugs targeting NGF have emerged as promising clinical targets for various forms of chronic pain over the past few years (Watson et al., 2008; Denk et al., 2017; Dakin et al., 2019).

Nevertheless, many promising drugs identified in pre-clinical studies in rodents fail to produce an analgesic effect in clinical trials. For instance, voltage-gated sodium channels are considered promising analgesic drug targets, due to their role in neuronal excitability and signalling, as well as having been implicated in human genetic pain disorders and chronic pain conditions. However, success in clinical trials has been limited so far, with antagonists targeting specific sodium channels, such as Nav1.7 and Nav1.8, often showing no to weak analgesic activity, despite showing anti-nociceptive properties in rodents (Momin and Wood, 2008; Emery et al., 2016; Jarvis et al., 2007; Yekkirala et al., 2017). This may stem from our incomplete knowledge of the mechanisms underlying the processing of noxious stimuli and pain. For example, Minett et al. (2015) showed that sensitivity to pain can be restored by naloxone, an opioid antagonist, in both Nav1.7-null mice and a human lacking Nav1.7. This suggests an increased opioid drive may partly underlie the painlessness phenotype and has led some to propose that the loss of pain sensation in mutants is not simply due to a functional loss of Nav1.7 channels, which could help explain the lack of efficiency of several Nav1.7 antagonists developed (Emery et al., 2016; Yekkirala et al., 2017). In short, there is a clear need for a better mechanistic understanding of the processing of noxious stimuli and pain. In the following sections, I will review the advantages of the zebrafish as an animal model, as well as the similarities and differences of its nociceptive system, compared to mammals.

1.4 The zebrafish as an animal model

The teleost zebrafish (*Danio rerio* – previously, *Brachydanio rerio*) is a small fish native to Southeast Asia, typically found in small streams and stagnant or slow-moving pools. Over the past few decades, the zebrafish has established itself as a model organism in a broad range of fields, such as aquatic toxicology, regeneration, development, drug discovery, and several disorders, including cancer and hematopoietic, cardiovascular, kidney, eye, ear, neurological and

neuropsychiatric disorders (Streisinger et al., 1981; Kalueff et al., 2016; d'Amora and Giordani, 2018; Patton et al., 2021; Fazio et al., 2020; Fontana et al., 2018; Gemberling et al., 2013; Marques et al., 2019; Blanco-Sanchez et al., 2017; Ganz, 2017; Dooley and Zon, 2000; Glass and Dahm, 2004; Kalueff et al., 2014b).

There are several advantages of the zebrafish as an animal model. It is small (and as such cost- and space-efficient) and it has a fast development: several structures are distinguishable from 24 hours post-fertilisation (hpf), such as the notochord, the heart, and the eyes; and embryonic development is complete at 3 days post-fertilisation (dpf). They generate a large number of offspring (hundreds of eggs per female), which develop externally and are optically clear, and as such allow for visual analyses of developmental processes (Gonzalez-Nunez and Rodriguez, 2009). Further, the zebrafish is a vertebrate, with sufficient physiological complexity and high physiological homology to humans, and thus permits the study of vertebrate biology, physiology and disease, contrary to the fruit fly (*Drosophila melanogaster*) and nematode (*Caenorhabditis elegans*) (Kalueff et al., 2014a). Moreover, the zebrafish has a fully sequenced, diploid genome, with high (80-85%) homology to humans, which allows for genetic studies to be carried out (Howe et al, 2013). Early large-scale mutagenic screens with ethylnitrosourea (ENU) allowed for the identification of hundreds of genes critical for a variety of developmental processes (Haffter et al., 1996; Driver et al., 1996). The zebrafish is particularly amenable to genetic manipulation, allowing for both forward and reverse genetic screens, and there are currently a wide range of genetic tools available, including the Gal4-UAS system, heat-inducible promoters (hsp70), Cre-mediated recombination, morpholinos, zinc finger nucleases (ZFNs), transcription activator-like effector nucleases (TALENs) and the CRISPR-Cas9 system (Hwang et al., 2013; Gemberling et al., 2013). The zebrafish is also particularly well-suited for drug discovery, allowing for high-throughput screening of drugs and their effects on a variety of physiological and pathological phenotypes (Rihel and Schier, 2011; Emran et al., 2008; Rihel et al., 2010; Stewart et al., 2014).

Zebrafish show a variety of behaviours, from prey hunting and shoaling, to learning and social preference towards conspecifics, and thus has been increasingly used as a model in sensory, developmental, and cognitive, as well

as translational, Neuroscience (Bianco et al., 2011; Spence et al., 2008; Tunbak et al., 2020; Oliveira, 2013; Stewart et al., 2014). They have smaller, simpler brains than rodents, and are easily genetically manipulated, which allows for the identification of circuits underlying various behaviours and developmental processes through imaging and manipulation of neuronal activity in a vertebrate (Antinucci and Hindges, 2016; Lau et al., 2019; Haesemeyer et al., 2018, Wee et al., 2019; Kalueff et al., 2014). For these reasons, the zebrafish has been increasingly seen as a potential model for nociception (Gonzalez-Nunez and Rodriguez, 2009; Malafoglia et al., 2013a; Taylor et al., 2017; Ohnesorge et al., 2021). This will be discussed in the next section.

1.5 Nociception in zebrafish

1.5.1 Nociceptors

As detailed above, the ability to detect and respond to potentially harmful stimuli is crucial for survival and conserved across many animal species. There are several similarities between somatosensory neurons in zebrafish and mammals (Malafoglia et al., 2013a). Focusing on cutaneous (exteroceptive) afferents, which transmit information about the external environment, these are also pseudounipolar neurons with cell bodies in either TG or DRG. TG neurons innervate and transmit sensory information from the head, with their peripheral axons arborising on the surface of the head and central axons projecting into the hindbrain (Kimmel et al., 1990; Metcalfe et al., 1990; Sagasti et al., 2005). DRG neurons innervate and transmit sensory information from the body, with their central axons projecting to the dorsal horn of the spinal cord (McGraw et al. 2008; Knafo et al., 2017; Figure 1.5).

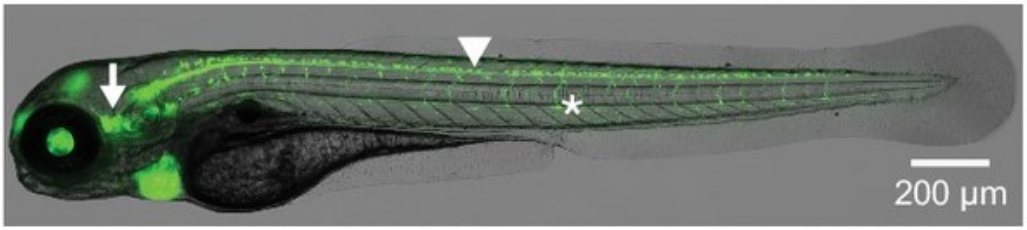

Figure 1.5: **Sensory neuron populations in larval zebrafish**. In vivo fluorescence image of 4 dpf Tg(*isl2b:gal4,cmlc2:eGFP*; *UAS:GFP-aequorin-opt*) double transgenic zebrafish larva shows expression of GFP-aequorin in sensory neurons: trigeminal ganglia (arrow), Rohon-Beard neurons (arrowhead) and dorsal root ganglia (*). Image retrieved from Knafo et al. (2017).

In zebrafish, there are two additional sources of somatosensory input: the lateral line and a temporary population of sensory neurons (present only during the early stages of development) called Rohon-Beard (RB) neurons. The lateral line detects water motion and pressure, allowing fish to sense movements of other animals, which is important for prey detection, for instance. It is made up of neuromasts, which are clusters of cells, including the sensory cells, supporting cells and mantle cells (Ghysen and Dambly-Chaudiere, 2007). The sensory cells are ciliated mechanosensory hair cells, similar to those in the inner ear, which convert mechanical stimuli into electrochemical signals (Montalbano et al., 2021). While the lateral line is not often seen as relevant to nociception, several acid-sensing ion channels (ASICs) have been detected in all three neuromast cell types, as well as the nerves supplying neuromasts (Paukert et al., 2006; Abbate et al., 2016). ASICs are proton-gated cation channels, which can be activated by a drop in extracellular pH as well as some non-proton ligands such as guanidine-4-methylquinazoline (GMQ) (Waldmann et al., 1997; Yu et al., 2010). In mammals, they have been proposed to have several roles, including mechanosensation, chemosensation and nociception (Price et al., 2000; Price et al., 2001; Ziemann et al., 2009; Wemmie et al., 2013). In zebrafish, several ASICs have also been found to be activated by extracellular protons (acidic solutions) (Paukert et al., 2006), and adult zebrafish show behavioural responses to acetic acid, such as increased ventilation rate and decreased swimming (Reilly et al., 2008; Correia et al., 2011). As such, zebrafish ASICs have been proposed by some as possibly playing a role in sensing some noxious chemicals, particularly acids (Taylor et al., 2017; Costa et al., 2019). Indeed, recent work by Adedara et al. (2022) found that amiloride, a non-selective ASICs blocker, abolished pain-like responses (writhing-like response and impaired locomotion) induced upon intraperitoneal injection of acetic acid in a zebrafish model of visceral pain. Therefore, the zebrafish lateral line may play a role in chemosensation.

RB neurons are a temporary cell population formed during early embryogenesis and present during embryonic and larval stages. They have similar functions to DRG neurons: their peripheral axons arborize extensively over the surface of the trunk from 16 hpf, and they extend ascending and descending central axons which form the dorsal longitudinal fascicle (DLF) of the spinal cord, transmitting sensory information from the body (Yeo et al., 2004; Malafoglia et al., 2013a). They undergo programmed cell death during

development. While early studies suggested populations of RB neurons to disappear completely by 5 dpf, they have since been reported to be present after 7 dpf, and up to 2 weeks (Williams et al., 2000; Kucenas et al., 2006; Slatter et al., 2005; Palanca et al., 2013). Therefore, RB and DRG neurons co-exist in larval stages, with the former being located in the very dorsal regions of the spinal cord, and the latter ventrally, just outside the spinal cord (Slatter et al., 2005; Figure 1.5).

While the different types of cutaneous afferent fibres have not been characterised in zebrafish, electrophysiological and anatomical studies have characterised them in other teleost fish, such as the rainbow trout (*Oncorhynchus mykiss*) (Malafoglia et al., 2013a; Sneddon, 2017; Sneddon, 2019). Similarly to mammals, Aβ, Aδ and C-fibres were identified in the TG of the rainbow trout (*Oncorhynchus mykiss*; the fibre type was determined based on the diameter of nerve fibres found in higher vertebrates), and their cell body size correlated with fibre diameter (Sneddon, 2002). Electrophysiological recordings of individual neurons identified populations tuned to different combinations of mechanical, thermal and chemical stimuli (Sneddon, 2003).

1.5.2 Nociceptor gene expression

As described previously, some of the genes expressed by somatosensory neurons determine their tuning to different sensory stimuli. Zebrafish larvae have been found to express orthologs of several genes crucial for nociception in mammals. For instance, all three TRP channels required for noxious heat sensation in mammals (Vandewauw et al, 2018) are expressed in zebrafish larvae, although only trpv1 and trpa1b (one of the two isoforms of TRPA1 – trpa1a and trpa1b) are expressed in cutaneous sensory neurons (TG and/or RB neurons), with trpm3 being found in the brain (Gau et al., 2013; Prober et al., 2008; Kastenhuber et al., 2013). Further, P2X receptors have also been found in zebrafish. P2X receptors are purinergic ionotropic receptors activated by ATP. P2X3, encoded by *P2RX3*, is a marker of non-peptidergic nociceptors in mammals (Usoskin et al., 2015). In rodents, P2X2/3 receptors at the trigeminal primary afferent terminals are thought to play a role in central sensitization in trigeminal brainstem nociceptive neurons, and have been implicated in

inflammatory pain and neuropathic pain (Hu et al., 2002; Ballini et al., 2011; Oliveira et al., 2009; Jarvis et al., 2002). The two zebrafish orthologs of P2RX3, p2rx3.1 and p2rx3.2, are expressed in TG and RB neurons from larval stages (Appelbaum et al., 2007). Finally, neuropeptides such as CGRP have been found in the TG of larval zebrafish (Pan et al., 2012). Importantly, there is some degree of conservation between zebrafish and mammals at the functional level too. Particularly, trpv1 seems to be crucial for noxious heat sensation in zebrafish larvae: trpv1-expressing neurons in zebrafish are activated by heat, and knock down of *trpv1* blocks noxious heat-induced locomotion in zebrafish larvae (Gau et al., 2013). Moreover, trpa1b underlies behavioural responses to chemical irritant AITC: trpa1b channels are activated by AITC *in vitro* and *trpa1b*-null mutants lose the behavioural responses to AITC (Prober et al., 2008).

Nevertheless, there are also some differences between species. Firstly, while the zebrafish trpv1 is activated by heat and acidic pH, it has not been found to be activated by capsaicin, which can be explained by the fact that two residues required for capsaicin-mediated activation of TRPV1, Ser-512 and Thr-550, are different at the analogous zebrafish positions (Thr-480 and Ile-518, respectively) (Gau et al., 2013; Jordt and Julius, 2002; Gavva et al., 2004). Further, TRPM3 plays a role in noxious heat sensation in rodents, but trpm3 expression in zebrafish has not been detected in sensory neurons (only in the brain), which would argue against it playing a role in somatosensation (Vandewauw et al, 2018; Kastenhuber et al., 2013). Similarly, TRPA1 plays a role in noxious heat sensation in mammals, but it is unclear if its zebrafish orthologs, trpa1a and trpa1b, have the same function, since fish where trpa1a and/or trpa1b are mutated show no defects in noxious heat sensation (Vandewauw et al, 2018; Prober et al., 2008). Nevertheless, studies in rodents have suggested there is some redundancy in the system. For example, while ablation of Trpv1-expressing neurons in mice results in almost complete absence of acute noxious heat sensing (Pogorzala et al., 2013), this is not seen to the same extent in *Trpv1*-knockout mice (Caterina et al., 2000). Additionally, double knockout mice lacking two of the three key channels involved in sensing noxious heat in mammals (Trpv1, Trpa1, Trpm3) show reduced but not abolished responses to heat (Vandewauw et al, 2018). As such, it is still possible for zebrafish trpa1 channels to play some role in heat sensation, which perhaps is not apparent in the presence of functional trpv1 channels in Prober et al. (2008). Overall,

acknowledging the differences between zebrafish and mammals is important as it helps to inform experimental design and the interpretation of results.

1.5.3 Nociceptor development

Similarly to mammals, zebrafish TG neurons have a dual origin (from neural crest cells and the epidermal placode), while DRG neurons originate from the neural crest (Malafoglia et al., 2013a). ngn1 is key for the development of both TG and DRG neurons: in the absence of ngn1, DRG neural precursor cells adopt a glial fate and early-born TG neurons do not form (Andermann et al., 2002; Caron et al., 2008; McGraw et al., 2008). RB neurons originate from the neural plate (Cornell and Eisen, 2000). During development, repulsive interactions between developing RB and TG sensory neurons limit each other's territories (Sagasti et al., 2005).

The development and differentiation of the different populations of somatosensory neurons has not been as extensively studied in zebrafish as it has in mammals. Nevertheless, the expression pattern of key genes such as neurotrophins suggests some degree of conservation, as well as some differences, between species. In zebrafish, there are two orthologs of the human *NGF* gene, *ngfa* and *ngfb* (this is seen across many zebrafish genes as a result of a teleost-specific whole genome duplication event; Meyer and Schartl, 1999; Howe et al., 2013). In the early stages of development, *ngfb* is expressed in the TG and in the brain; it is also widely expressed across the brain and spinal cord of adult zebrafish (Nittoli et al., 2018; Cacialli et al., 2019; Hui et al., 2017; Sun et al., 2018). *ntrk1*, which encodes trkA (the receptor that ngf binds to), has been found to be expressed in RB neurons and TG in zebrafish larvae, although expression in DRG neurons has not been detected (Gau et al., 2017; Pan et al., 2012; Hahn et al., 2020; Martin et al., 1995; Palanca et al., 2013). There are two orthologs to TRKB and TRKC: *ntrk2a* and *ntrk2b* encode trkB1 and trkB2, and *ntrk3a* and *ntrk3b* encode trkC1 and trkC2, respectively (Martin et al., 1995). Of these, *ntrk2a* and *ntrk3a* have consistently been found to be expressed in TG and RB neurons (Martin et al., 1995; Gau et al., 2017; Nittoli et al., 2018); *ntrk3b* has been detected in the TG by some (Pan et al., 2012) but not others (Martin et al., 1995; Martin et al., 1998).

Some studies have also looked at the expression of neurotrophins in specific subpopulations of sensory neurons, which again highlighted both similarities and differences compared to mice. As detailed previously, in mice, expression of TrkA in developing somatosensory neurons specifies nociceptors; genes such as Trpv1 and Trpa1 are found exclusively in those neurons (Fitzgerald 2005; Marmigère and Ernfors, 2007; Lallemend and Ernfors, 2012; Usoskin et al., 2015). In zebrafish larvae, a subset of trpv1+ TG neurons (and a small subset of trpa1b+ neurons) also expresses trkA, replicating what is seen in peptidergic and non-peptidergic unmyelinated DRG neurons in adult mice (Gau et al., 2017; Usoskin et al., 2015). However, contrary to what is seen in rodents, a subset of trkC1+ TG neurons have also been found to express trpa1b and trpv1 in zebrafish larvae (Pan et al., 2012; Gau et al., 2017). One study by Gau et al. (2017) explored the role of neurotrophins in the development of sensory neurons, finding both similarities and differences compared to mammals. In zebrafish, runx3 is expressed in TG, RB and DRG neurons. Loss of runx3 leads to increased expression of trkB and decreased expression of trkC. This suggests that, like in mammals, it acts to consolidate a solitary trkC phenotype by repressing the potential for trkB expression and maintaining the expression of trkC. However, runx3 also controlled the expression of trpa1b, a role analogous to that of the mammalian Runx1, but not trkA, cgrp, or trpv1 (which would be expected of a transcription factor acting like Runx1). On the other hand, zebrafish runx1 was only found to be expressed in RB neurons (and only transiently, up to 24 hpf), and it seemed to play a role in facilitating runx3 expression in RB neurons, with loss of runx1 leading to loss of runx3 in those neurons.

In short, while there are some differences between zebrafish and mammals in the development and differentiation of somatosensory neurons (and specifically nociceptors), several key factors are still conserved across species. Furthermore, the dominance of nociceptive markers in larval zebrafish (with nearly 90% of TG neurons expressing trpv1 and/or trpa1b at 3 dpf – Gau et al., 2017) suggests that early nociceptive development is critical for survival of the free-swimming larvae.

1.5.4 Behaviour

Understanding behaviour is an essential question in neuroscience (Pereira et al., 2020). Zebrafish larvae naturally swim in bouts that are segmented in time, separated by longer periods of rest, which has allowed for the swimming patterns used in different behavioural contexts to be identified and categorised (Budick and O'Malley, 2000; Wolman and Granato, 2011; Kalueff et al., 2013; Marques et al., 2018). For instance, "J-turns" are defined by two or more unilateral "J-bends", which have high tail bend amplitude (>90°) and a caudal bend location close to the end of the tail, thus forming the trunk and tail into a 'J' shape. They are exclusively used during prey-tracking, and serve to orient larvae toward their prey (McElligott and O'Malley, 2005; Bianco et al., 2011; Mearns et al., 2020). "C-starts", also called "C-bends", are fast startle responses typically elicited upon touching the head, in which the fish body first curves to form a C-shape, and then the fish propels itself away at an angle (120°–180°) from its previous position using a fast swim (Kimmel et al., 1974; Burgess and Granato, 2007b). Finally, "O-bends" are slower escape responses that can be elicited by dark flashes, for instance, in which the larval zebrafish body curves to change the orientation (180°) of swimming (Burgess and Granato, 2007a).

Zebrafish larvae show behavioural responses to noxious stimuli such as temperature and chemicals (Lima et al., 2012; Gau et al., 2013; Prober et al., 2008; Barrios et al., 2020). These behaviours are critical for survival. For instance, temperatures in the natural habitat of zebrafish can fluctuate widely, since they typically live in shallow pools, and zebrafish can be exposed to chemicals as well (for example, AITC is a biodegradation product used by plants from the Brassicaceae family as defence) (Engeszer et al., 2007; Haesemeyer 2020; Overby et al., 2015). Free-swimming zebrafish larvae show increased locomotor activity upon exposure to noxious heat (beyond 37°C) or AITC, as well as also robustly avoiding the hot (36°C) side of a dual heat/cool plate in a place preference assay (Gau et al., 2013; Prober et al., 2008; Esancy et al., 2018; Ko et al., 2019; Kroll et al., 2021). Moreover, head-fixed larvae execute large-angle tail bends upon optovin-based trpa1 stimulation (Wee et al., 2019). In short, zebrafish use a wide repertoire of behaviours to escape noxious (and innocuous) stimuli.

1.5.5 Analgesic drugs

One of the main goals of research on pain and nociception is the development of analgesic drugs that address pain. The two main classes of analgesics currently used are non-steroidal anti-inflammatory drugs (NSAIDs) and opioids, although anaesthetics can also be used for the purpose of analgesia. Effectiveness of these drugs in zebrafish would highlight the similarities between zebrafish and mammals, thus providing further support to the use of zebrafish for basic nociception research, as well as for drug discovery (Ohnesorge et al., 2021). Indeed, several drugs across all classes have been successfully used in zebrafish for analgesic purposes.

Anaesthetics act by blocking sodium channels, which reduces the excitability of neurons, including nociceptors. They can be used as analgesics at low doses. In zebrafish, lidocaine has been shown to prevent the behavioural changes induced by a noxious stimulus (acetic acid) at 5 dpf, as well as preventing the associated reduction in activity and distance swum after fin clipping in adults (Schroeder and Sneddon, 2017; Lopez-Luna et al., 2017; Deakin et al., 2019).

NSAIDs block prostaglandin synthesis by inhibiting cyclooxygenase enzyme 1 or 2 (COX-1 or COX-2). Several NSAIDs have been found to be effective analgesics in zebrafish, in both adults and larvae. For instance, acetylsalicylic acid and flunixin prevented the post-nociceptive behavioural patterns seen after fin clipping of adult fish (Schroeder and Sneddon, 2017; Deakin et al., 2019), and acetylsalicylic acid prevented the behavioural changes induced by acetic acid in larvae, although ibuprofen failed to ameliorate the sensitised temperature aversion observed in zebrafish larvae after AITC administration (Lopez-Luna et al., 2017; Curtright et al., 2015).

In humans, opioids act on the endogenous opioid system, through central mu-, delta- and kappa-opioid receptors (MOP, DOP and KOP), encoded by *OPRM1*, *OPRD1* and *OPRK1*, respectively. Zebrafish have orthologs for all three of these genes (*oprm1*, *orpd1a* and *oprd1b*, and *oprk1*, respectively), with the resulting amino acid sequences sharing about 70% homology to the human sequences (Demin et al., 2018). Opioid drugs have been found to have similar effects in zebrafish as in mammals. For instance, morphine has been shown to

prevent the behavioural changes induced by acetic acid in larvae, and various noxious chemicals in adults (including histamine, cinnamaldehyde, mustard oil, acetic acid and complete Freund's adjuvant). Moreover, naloxone, a non-selective opioid antagonist, prolongs the behavioural responses to these chemicals in a dose-dependent manner (Taylor et al., 2017; Lopez-Luna et al., 2017; Deakin et al., 2019; Costa et al., 2019). Furthermore, the side effects of opioids (e.g. respiratory depression and addiction) can also be replicated in zebrafish. For instance, fentanyl depresses the rate of respiratory mandible movements in freely-swimming zebrafish larvae, an effect which is reversed by naloxone, and zebrafish adults show signs of addiction to hydrocodone (continued self-administration despite adverse consequences) and withdrawal effects (stress and anxiety) after removal of the drug (Zaig et al., 2021; Bosse and Peterson, 2017).

In short, several commonly used analgesics have been successfully used in zebrafish for analgesic purposes, which supports the use of zebrafish for basic nociception research, as well as for drug discovery.

1.6 Aims

The zebrafish is an attractive animal model with a nociceptive system that shares several similarities with that of mammals, from a developmental, genetic, molecular, and cellular point of view. Further, zebrafish larvae show behavioural responses to both noxious and innocuous stimuli, which can be modulated by chemicals such as irritants or analgesics. The simplicity of the zebrafish, compared to rodents, means it can help us reach a mechanistic understanding of the circuits underlying sensing noxious stimuli and the generation of protective behaviours. The zebrafish has a fully sequenced, diploid genome, with high homology to humans, and is particularly amenable to genetic manipulation, allowing for both forward and reverse genetic screens. Currently, there are a wide range of genetic tools available, including the Gal4-UAS system and the CRISPR-Cas9 system (Hwang et al., 2013; Gemberling et al., 2013; Howe et al, 2013). However, to date, very few studies have explored the functional role of different nociception-related genes in zebrafish.

The overall aim of my project was to establish the zebrafish as a model to study the genetics of nociception. Specifically, I aimed to answer the following questions:

1. Do zebrafish show fast behavioural responses to noxious heat?
2. Can these responses be manipulated by mutating specific genes?

To answer these questions, I set out to do the following:

1. Establish an assay for the study of fast escape-like responses to noxious heat;
2. Validate the infrared laser stimulation setup as an assay for noxious thermal stimulation of zebrafish larvae; and
3. Generate and characterise zebrafish F0 knockout of genes involved in human genetic pain disorders.

Chapter 2: Methods

2.1 Animals

Adult zebrafish were reared by University College London's Fish Facility on a 14 hr:10 hr light:dark cycle. Embryos were raised in 10-cm Petri dishes filled with system water in a 28°C incubator on a 14 hr:10 hr light:dark cycle. Wild-type (WT; refers to *AB* × *Tup LF* fish) zebrafish larvae up to 7 days post-fertilisation (dpf) were used for all experiments, except for the blind fish experiments and the fluorescent in situ hybridisation/immunohistochemistry (FISH/IHC) experiments. To generate larvae used for blind fish experiments, double-transgenic *Tg(atoh7:gapRFP)*^{cu2Tg} (Kay et al., 2001) and *Tg(elavl3:ITETA-PTET:Cr.Cop4-YFP)*^{fmi2Tg} (Fajardo et al., 2013) adults carrying *mitfa*$^{w2/w2}$ (Lester et al., 1999) and *atoh7*$^{+/th241}$ (Kay et al., 2001) mutations were used. Larvae with *Tg(elavl3:ITETA-PTET:Cr.Cop4-YFP)*^{fmi2Tg} expression were excluded. Blind *atoh7*$^{th241/th241}$ fish were selected based on *Tg(atoh7:gapRFP)*^{cu2Tg} expression being visible only in the eye but with no retinal ganglion cell (RGC) projections in the brain, while sighted controls were selected based on *Tg(atoh7:gapRFP)*^{cu2Tg} expression being visible in both the eye and RGC projections in the brain. To generate larvae used for FISH/IHC experiments, *Tg(elavl3:jGCaMP7f)*^{u343} adults were used. Larvae were selected based on trigeminal ganglia expression *Tg(elavl3:jGCaMP7f)*^{u343} at 4 dpf. All experiments were conducted in accordance with the United Kingdom Animals (Scientific Procedures) Act, 1986. After all experiments, animals were culled by tricaine methanesulfonate (Sigma; from here on: tricaine) overdose.

2.2 Sequence homology analysis

The amino acid sequences of various proteins were compared in human (*Homo sapiens*; GRCh38.p13), mouse (*Mus musculus*; GRCm39) and zebrafish (*Danio rerio*; GRCz11). They were obtained by using Ensembl (version 99; Cunningham et al., 2019) to find the human gene and its mouse and zebrafish orthologs, and identifying their UniProtKB (The UniProt Consortium, 2021) IDs. Where multiple UniProtKB IDs were found for the same Ensembl ID, the

UniProtKB ID with a "Reviewed" annotation status was selected. If this was not possible, the one with the highest annotation score was chosen; if multiple IDs had the same score, a rating of 'Experimental evidence at transcript level' was preferred over that of 'Protein inferred from homology'. If many UniProtKB IDs still fulfilled these conditions, the one with the longest amino acid sequence was selected.

Identity matrices and phylogenetic trees were then obtained through the EMBL-EBI online ClustalOmega Multiple Sequence Alignment tool (Sievers et al., 2011; Madeira et al., 2019). Amino acid sequences were then aligned using BLAST (Altschul et al., 1990).

2.3 Infrared laser stimulation assay

2.3.1 Infrared laser stimulus characterisation

A 980 nm infrared laser was used in these experiments (Figure 2.1). To measure the relationship between laser power and current used for stimulation (infrared laser: Thorlabs, L980P200), an optical power meter (Thorlabs, PM100USB) connected to a photodiode power head with silicon detector (Thorlabs, S121C) was used. A silicon, biased detector (Thorlabs, DET36A, discontinued) connected to a data acquisition board (National Instruments, NI USB-6001; NI-DAQ) was then used to determine the laser rise and decay times, with analogue input data from the NI-DAQ being collected using the Bonsai software (Lopes et al., 2015). To estimate the laser beam size, a beam profiler (Thorlabs, BP209-VIS) was positioned at the same distance from the laser as the zebrafish larvae.

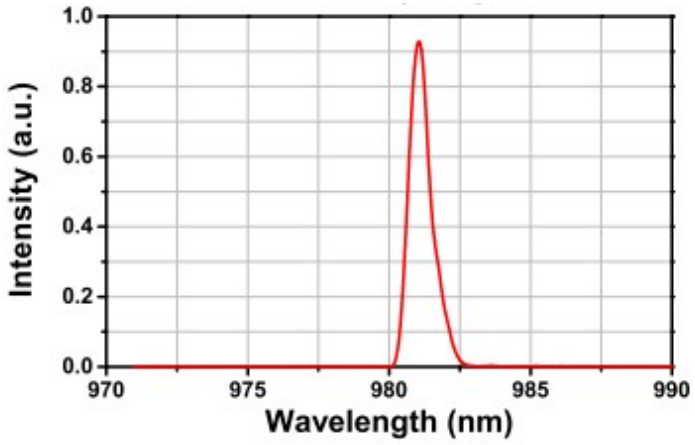

Figure 2.1: **Sample spectrum of the infrared laser used in the infrared laser stimulation assay**. Source: Thorlabs website.

To estimate the temperature induced in larval zebrafish by the laser stimulus, a thermistor with similar dimension and absorption characteristics as larval zebrafish was used (TDK; Haesemeyer et al., 2015). The thermistor was first calibrated by submersing it in water at increasing temperatures, and recording the voltage output at each temperature using the NI-DAQ. These recordings were converted into resistance values and used to generate a calibration curve relating temperature to resistance. The thermistor was then embedded in the same 2% low-melting point agarose that is used for behaviour experiments using larval zebrafish and positioned in the same place as a fish would. For each stimulus used, voltage output from the thermistor was recorded and converted into resistance values, and temperature changes in the thermistor were subsequently calculated from the calibration curve using the Steinhart-Hart equation (Steinhart and Hart, 1968).

2.3.2 Infrared laser stimulation of head-fixed zebrafish larvae

Larval zebrafish at 6-7 dpf were anaesthetised with tricaine and embedded in 2% low- melting point agarose (Sigma) in a 6 cm petri dish filled with 12mL of fresh system water. To allow the tail to move freely, the agarose caudal to the swim bladder was cut at 135° to the anterior-posterior axis and removed. After a recovery and habituation period of at least 30 minutes, animals were inspected for motor responsiveness to somatosensory stimulation by gently touching the tail with a pipette tip. Responsive larvae were positioned below an infrared camera (Blackfly S BFS-U13-13Y3C) and illuminated from below with a visible light LED array. To avoid image pixel saturation during laser activation, which could interfere with the analysis, a filter (Edmund Optics, Schott KG-1, 45-648) was added to the camera lens. Videos were recorded at 400Hz.

Heat stimulation was delivered using a 980 nm laser (Thorlabs, L980P200), focused to a beam size that allowed the targeting mainly of the head of larvae. Real-time thermal stimuli were generated using a high-power laser driver (Thorlabs, LDC240C) controlled by a NI-DAQ. Before the beginning of the assay, a 1-minute baseline recording was made. Each stimulation protocol consisted of six 500-millisecond stimulations of different intensities (selected in a random order from a list of pre-set intensities, 0.729 V, 0.853 V, 0.977 V, 1.1 V, 1.224 V,

and 1.323 V, such that each intensity was selected once and only once); and a 2-minute interval between them. Each fish was exposed to 3 consecutive rounds of stimulation. The experimental pipeline was written in Bonsai (Lopes et al., 2015).

2.3.3 Infrared laser stimulation behavioural assay – analysis pipeline

Initial analysis of the obtained raw data was performed using a Python script written by Dr Adam Kampff (Python v3.8). Briefly, the tail base was first defined manually and this was taken as the centre point of a 180° downwards search arc of fixed radius, used to find the maximum (smoothed) pixel value. This pixel was then taken as the centre point of the next arc and this was repeated 12 times, segmenting the tail into a total of 12 segments of equal length (Figure 2.2.A). The x and y coordinates of each centre point were extracted and different tail kinematics were then calculated for each video frame: cumulative tail angle (sum of all Δθ, where Δθ is the difference between consecutive angles, θ1 and θ2, and each angle is the angle between adjacent segments; tail curvature (mean of the absolute value of all Δθ); tail motion (sum of $\sqrt{\Delta x^2 + \Delta y^2}$), where Δx and Δy are the difference in the x and y coordinates of each centre point across neighbouring frames n and n+1) (Figure 2.2.B).

I then used these three kinematics (cumulative tail angle, curvature and motion) as a starting point to analyse the tail-flick behaviour in response to stimulation with different infrared laser intensities. The beginning of a response or bout was defined as the frame when tail motion became greater than our “beginning of response” threshold (baseline motion plus 10 times the standard deviation, SD). Only responses starting within a 1 second window of stimulus presentation (the frame when the laser was switched on, t=0) were recorded. The end of the response or bout was defined as the point in time when tail motion returned to values lower than our “end of response” threshold (baseline motion plus 2 times the SD). For a response to be recorded, tail motion must remain below the “end of response” threshold for 95% of the frames in the 100 ms window after the “end of response” frame (the frame when tail motion first

returned to values below the “end of response” threshold). This ensured individual bouts were captured.

The following response parameters were then analysed: peak cumulative tail angle, curvature and motion (maximum cumulative tail angle, curvature and motion, respectively); response latency (time of the beginning of the first bout); response probability; and peak response vigour (response vigour was calculated as the mean absolute difference in consecutive values of cumulative tail angle over a full bout).

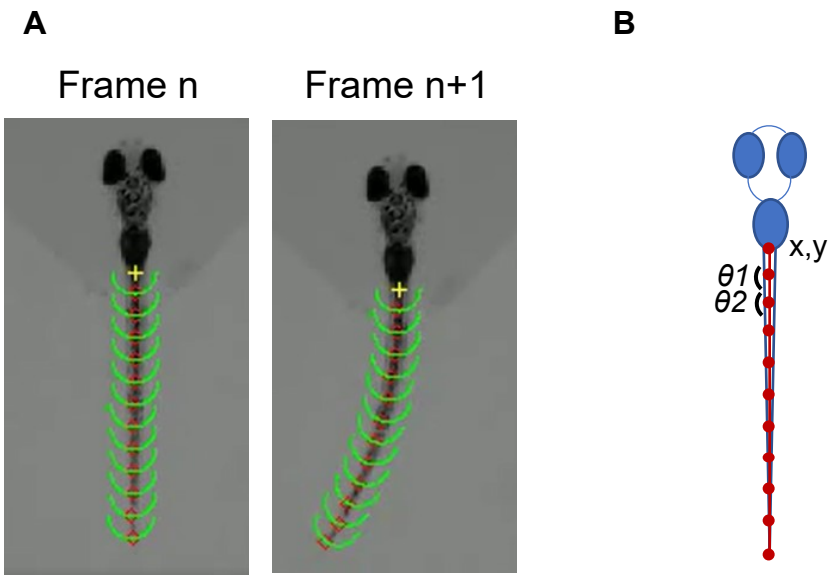

Figure 2.2: **Analysis of video recordings of zebrafish larvae during the infrared laser stimulation behavioural assay**. A: For each frame n in the video, the tail base is first defined manually (yellow cross), and this is taken as the centre point of a 180° downwards search arc of fixed radius (green arc), used to find the maximum (smoothed) pixel value (red diamond). This pixel is then taken as the centre point of the next arc and this is repeated 12 times, segmenting the tail into a total of 12 segments of equal length. The process is repeated for the subsequent frame n+1, until the end of the video. B: Different tail kinematics are calculated for each video frame: cumulative tail angle (sum of all Δθ, where Δθ is the difference between consecutive angles and each angle is the angle between adjacent segments, θ1 and θ2; tail curvature (mean of the absolute value of all Δθ); tail motion (sum of $\sqrt{\Delta x^2 + \Delta y^2}$), where Δx and Δy are the difference in the x and y coordinates of each centre point across neighbouring frames n and n+1).

2.4 Drug experiments

2.4.1 Free-swimming behaviour of zebrafish larvae upon exposure to lidocaine or AITC (Zebrabox)

Single larvae at 3 or 5 dpf were transferred, using a Pasteur pipette, into the individual wells of the mesh filter plate of a MultiScreen-MESH Filter Plate (Merck, MANM10010), which had been placed on the up-turned plastic lid of the plate and filled with fresh system water. To record each animal's behaviour, each plate was placed into a Zebrabox (ViewPoint Life Sciences) running quantization mode with the following settings: detection sensitivity, 15; burst, 50; and freezing, 4. Baseline swimming behaviour was recorded for approximately 1 hour (50-70 min), at which point the mesh filter plate was transferred into the receiver 96-well plate, pre-filled with 400µL of different concentrations of Allyl isothiocyanate (AITC, commonly known as mustard oil; Sigma-Aldrich) in 0.5% Dimethylsulfoxide (DMSO; Sigma), or lidocaine hydrochloride (from here on simply lidocaine; Hameln). The plate was returned to the Zebrabox and behaviour was recorded for at least a further 90 min. Larval behaviour was video-tracked at 25 Hz. Raw behavioural data was acquired and analysed with support from Dr Declan Lyons and Dr François Kroll, using custom analysis software from Professor Jason Rihel's lab at University College London, as described in Ghosh and Rihel (2020). Briefly, behavioural data was recorded by subtracting subsequent pairs of frames from each other and determining the number of pixels that changed intensity (within each well of the 96-well plate) between each pair of frames (Δ pixels). These Δ pixels values were summed into 1 s bins and smoothed with a running average within a 15 min sliding window. This was used as a proxy for movement.

2.4.2 Infrared laser stimulation of head-fixed zebrafish larvae exposed to lidocaine or AITC

Each individual larval zebrafish first went through the standard infrared laser behavioural assay (as described in 2.3.2). Then, the drug of choice was pipetted into each petri dish and fish were incubated in it for 45 minutes, after which they

went through the standard infrared laser behavioural assay again (remaining incubated in the drug). The drugs used were lidocaine (at either 5 mg/L or 10 mg/L; control: water) and AITC (at either 0.015 µM or 0.06 µM in 0.1% DMSO; control: 0.1% DMSO).

2.5 Generation of F0 knockouts using CRISPR-Cas9

The protocol for the generation of F0 knockout larvae was based on that developed by Kroll et al. (2021), as detailed below.

2.5.1 crRNA selection

The crRNA (Alt-R CRISPR-Cas9 crRNA; Integrated DNA Technologies, IDT) was the only component of the Cas9/gRNA ribonucleoprotein (RNP) which was specific to the target locus. Three crRNAs were selected per target gene (Table 2.1), targeting two (*prdm12b*) or three (*ntrk1*) distinct exons (*ngfa* and *ngfb* are single-exon genes so all three guides targeted the same exon). They were selected from IDT's database of predesigned crRNAs based on: on- target and off-target scores; rank according to the web tool CHOPCHOP (v3; Labun et al., 2019; Labun et al., 2016; Montague et al., 2014); and, for genes where the same exon was targeted multiple times, position within the exon (to prevent guides from interfering with each other).

Table 2.1: **crRNAs selected for the generation of zebrafish F0 knockouts with CRISPR-Cas9**. At least three targets per gene were selected.

Gene	Target	Exon	Strand	crRNA sequence	PAM sequence
ngfb	a	1	Antisense	GACTAGCATGGACCACCGCA	TGG
	b	1	Antisense	TGGCTGTGACATCTTGACCG	TGG
	c	1	Sense	CATTCAAGAACCTGGTGGCG	TGG
ngfa	a	1	Sense	TGACGAACTAATTCCCACCG	TGG
	b	1	Antisense	CCGAGTACTCACCACGATGC	AGG
	c	1	Antisense	GTTGATTCGGATGAACCTCC	AGG
ntrk1	a	17	Antisense	AGACGGGTGGGTTTTTGACG	AGG
	b	1	Antisense	CCACAACCGGGGCCACCCTA	TGG
	c	13	Sense	TTGAAGTGGGAACTGGGTGA	AGG
	d	5	Antisense	CCAGTAAATGTCACACGAGC	AGG
prdm12b	a	1	Sense	GCTGGGGGAACACCTGTTCG	AGG
	b	1	Antisense	CCCCCAGCACGTTCCTCCAG	CGG
	c	3	Sense	TTTCATCGATGCCAGTCAAG	AGG

2.5.2 RNP preparation

Unless stated otherwise, all steps were performed on ice and all reagents were stored at -80°C before use. The tracrRNA (Alt-R CRISPR-Cas9 tracrRNA; IDT) and each crRNA were received as pellets, which were resuspended in Duplex buffer (IDT) to a concentration of 200 µM. To form the gRNA, 1 µL crRNA 200 µM, 1 µL tracrRNA 200 µM, and 1.51 µL Duplex buffer were mixed (final concentration: 57 µM) and incubated at 95°C for 5 minutes. For each RNP, equal volumes of gRNA and Cas9 (Alt-R S.p. Cas9 Nuclease V3, 61 µM; IDT) solutions were mixed (typically 1 µL gRNA; 1 µL Cas9) and incubated at 37°C for 5 minutes, generating a 28.5 µM RNP solution. The three RNP solutions (one per target) were pooled in equal amounts (here termed “pooled RNP”), with the exception of *ngf* double-knockouts, where six RNP solutions were pooled (one per target for each of the two *ngf* genes, *ngfa* and *ngfb*). The resulting solution was aliquoted in 1.2-1.5 µL aliquots, which were stored at -80°C.

2.5.3 Scrambled RNPs

For all experiments, three scrambled crRNAs (Alt-R CRISPR-Cas9 Negative Control crRNA #1, #2, #3; IDT) were prepared into RNPs as detailed above.

2.5.4 Injections

On the morning of injections, one aliquot of scrambled pooled RNP and one aliquot of pooled RNP for a gene of interest were thawed on ice. Phenol red (1:10) was added to each solution. Using a glass needle, approximately 1 nL of the pooled RNP was injected into the yolk at the single-cell stage, except for the *ngf* double-knockouts, where approximately 2 nL of the six-RNP mix were injected so the amount of RNP per gene would remain equal to when a single gene is targeted. Two to four batches of embryos were injected each day.

2.6 Phenotype of mutants

2.6.1 Viability

The percentage of viable embryos was quantified daily from 1 dpf to 4 dpf (viability was not assessed at 0 dpf, as unviable eggs were likely either unfertilised eggs or eggs damaged by the needle). For some experiments, viability was also assessed at 6 dpf and 7 dpf. “Viable embryos” refers to embryos that were alive and showed no obvious anatomical or behavioural defects on each day. Common anatomical defects included, but were not limited to, heart oedema (assessed from 3 dpf), tail curvature (assessed from 4 dpf), visibly smaller size (assessed from 3 dpf), absence of an inflated swim bladder after 5 dpf, or other obvious anatomical deformations (assessed from 3 dpf). Common behavioural defects included spiral swimming (along the “z axis”; assessed from 4 dpf), and unbalanced swimming (sideways or along the “z axis”; assessed from 6 dpf). Dead and ill embryos were removed daily, with the exception of embryos displaying a deflated swim bladder or behavioural defects, as pilot data suggested this to be a specific phenotype resulting from the mutation. The viability of injected embryos was compared to that of scrambled-injected (from here on, scrambled) and uninjected controls and, for most experiments, was assessed blinded to the condition (injected or scrambled).

2.6.2 Imaging

Representative brightfield images of uninjected, scrambled and injected fish were taken at 7 dpf using a light microscope (Leica). Generally, fish were lightly anaesthetised with tricaine, mounted in 1%-2% agarose on a glass slide or the plastic lid of a petri dish, and imaged dorsally and ventrally. Some images were taken on awake and unmounted fish.

2.6.3 Free-swimming behaviour of mutants

Individual larvae at 6-7 dpf were transferred, using a Pasteur pipette, into a square arena (10 x 10 cm) filled with fresh system water, and allowed to swim

freely for 20 minutes. Videos were recorded at 100-120 Hz with a camera (PointGrey, Grasshopper 2), with illumination from below from an infrared light source (Advanced Illumination, US, 880 nm) uniformly covering the whole arena. For looming experiments on *ngfb* F0 knockout fish, a series of eight looming stimuli were presented to the larvae after a 20 min baseline (free swimming in the absence of a looming stimulus). To achieve this, larvae were tracked in real time and a dark spot of increasing diameter (the looming stimulus), centred around the centroid of the fish, was projected from below every 2 min. The looming stimulation experimental pipeline was written in Bonsai (Lopes et al., 2015) by Dr Thomas Ryan, and the looming stimulation protocol, which is time-locked with the video recording, was saved for further analysis (see below).

2.6.4 Free-swimming behaviour of mutants – analysis pipeline

Analysis of raw data from the free-swimming behaviour experiments was carried out using a Python script written by Dr Thomas Ryan (unless stated otherwise), based on a tracking method previously established in our laboratory (Tunbak et al., 2020). Briefly, fish were first tracked by computing the image background, identifying the contour of the largest particle (i.e. the fish) and calculating the fish centroid, eye centroid, and body centroid for each frame. The x and y coordinates of each of these three points were then used for further analysis.

Firstly, individual bouts were extracted using a Python script written by Dr Adam Kampff. Briefly, bouts are computed from a “motion signal”, which is the sum of the frame by frame spatial and angular velocities (calculated from the x and y coordinates of the body centroid). The threshold for “a bout” was set as 10% of the median of the 100 largest motion signal values, which was determined by empirical observation to identify bouts accurately. Once all bouts have been extracted, the start frame of each individual bout (“bout start frame”) is computed. Secondly, the distance travelled across two frames (“distance per frame”) was calculated by computing the straight line distance between every frame, given the x and y coordinates of tracking data.

These two initial metrics, “bout start frame” and “distance per frame”, were used for further bout and swimming analysis, by computing total distance, peak bout velocity and average bout velocity. “Total distance” is the sum of all “distance per frame” values (for the full duration of the experiment). “Bout velocity” is the distance travelled across each frame, with “peak bout velocity” referring to the maximum bout velocity over a bout (that is, the 400 ms after “bout start frame”), and “average bout velocity” being the mean “bout velocity” over a bout.

For looming experiments, the beginning of each looming stimulus (“loom start”) was identified from the looming stimulation protocol. Looming escape response rate was measured as the probability of a “looming escape response” occurring within a 1 s window of “loom start”. The latency of those responses was also measured. To distinguish fast looming escape responses from slower spontaneous bouts that simply happened to fall within 1 s of the presentation of a looming stimulus, a filter was applied such that only responses with a high peak velocity were considered, since fast escape bouts are rarely performed spontaneously. This threshold was set as the mean “peak bout velocity” plus two times the standard deviation (SD), over the 20 min baseline period (during which no looming stimuli were presented). Escape bouts can be reliably distinguished from this threshold (see also: Chapter 5).

2.6.5 Vibration experiments and analysis

The behavioural arena consisted of a 35 mm Petri dish filled with 3.5 mL of fresh system water, which was placed on a horizontal platform. Images were acquired under 850 nm illumination using a high-speed camera (Mikrotron MC1362, 700 fps, 500 µs shutter-time) equipped with a machine vision lens (Fujinon HF35SA-1) and a 850 nm bandpass filter to block visible light. A solenoid ‘tapper’ was placed such that the piston, when extended, would contact the optomechanical frame of the rig. The solenoid was controlled using an Arduino Uno.

Larvae acclimated to the Petri dish for at least 30 minutes, after which the dish was moved to the horizontal platform and they were allowed to acclimate for around 1 minute before starting the experiment. Mechano-acoustic ‘tap’ stimuli

were then delivered with an inter-stimulus interval of 15 seconds for at least 10 minutes. During experiments, eye and tail kinematics were tracked online as described in Henriques et al. (2019). Accurate tracking relied on the body centroid being within a predefined central region (‘in middle’, 11 mm from the edge of the arena). Whenever the fish left this region, a concentric grating was projected (AAXA P2 Jr), via a cold mirror, from below, that drifted towards the centre of the arena to attract the fish to the central region. Only responses occurring when the fish was ‘in middle’ were considered.

Camera control, online tracking and stimulus presentation were implemented using custom software written in LabView and MATLAB. Raw data analysis was performed using custom MATLAB scripts written by Dr Isaac Bianco at University College London. Briefly, images were first background-subtracted using a continuously updated background model and this was then thresholded to find the ‘body’ and ‘eye’ centroids. The tail was tracked by performing consecutive annular line-scans, starting from the body centroid and progressing toward the tip of the tail so as to define 9 equidistant x-y coordinates along the tail. Inter-segment angles were computed between the 8 resulting segments. Tail curvature was computed as the sum of these inter-segment angles. Swim bouts were identified using a velocity threshold (500◦/s) applied to smoothed cumulative tail angles. Escape responses to tap stimuli were identified if instantaneous speed of the body centroid exceeded 75 mm/s. To calculate response latencies, an LED is placed adjacent to the petri dish (within the camera field of view) and is triggered at the same time as the solenoid tapper. The response latency is calculated in relation to the LED being switched on (t=0). Because the LED is switched on almost instantaneously but there is a slight delay between the tapper being triggered and the tap being delivered to the bottom of the petri dish, escape latencies calculated in relation to the LED being switched on are overestimated.

2.7 Genomic DNA extraction

Larvae were culled by tricaine overdose and their genomic DNA (gDNA) was extracted from either the tail or the whole body by HotSHOT (Meeker et al., 2007), as follows. If extracting DNA from the whole body, individual larvae were transferred to a 96-well PCR plate. If extracting DNA from the tail, individual

larvae were placed laterally on the lid of a petri dish, and a microscalpel (FEATHER®; type: P-730) was used to cut along the dorso-ventral axis by applying steady downward pressure to make the incision. The cut was done posterior to the swim bladder, at approximately 1/3 of the full length of the body. The tail was then transferred to a 96-well PCR plate using a P1000 micropipette. Excess liquid was removed from each well before adding 15 µL (for tail extractions) or 25 µL (for whole-body extractions) of base solution (25 mM KOH, 0.2 mM EDTA in water). Plates were sealed and incubated at 95°C for 30 minutes, then cooled down before the addition of corresponding volumes of neutralisation solution (40 mM Tris-HCL in water). gDNA was stored at 4°C.

2.8 Genotyping with Headloop PCR

An adaptation of the Rand et al. (2005) headloop suppression PCR protocol (HL-PCR) was used to determine if a target locus had been efficiently mutated in F0 embryos, as described in Kroll et al. (2021). For each sample, two separate reactions were set up: one using standard forward and reverse PCR primers and another one using either a forward or a reverse HL primer (combined with a standard reverse or forward primer, respectively) (Table 2.2). Standard PCR primers (“base primers”) were designed using the NCBI Primer Designing Tool, Primer-BLAST (Ye et al., 2012), such that the resulting amplicon included the sequence targeted by the crRNA. HL primers were designed using a Python-based tool (available at: https://github.com/GTPowell21/Headloop (Powell, 2020)).

For the PCR, each well contained: 4 µL 5× Phusion HF buffer (New England Biolabs, NEB), 0.4 µL dNTPs (10 mM), 1 µL forward primer (10 µM), 1 µL reverse primer (10 µM), 0.2 µL Phusion® High-Fidelity DNA Polymerase (NEB), 1 µL to 2 µL gDNA and water up to 20 µL. PCR amplification was performed using an Eppendorf MasterCycler Pro S PCR machine. The PCR program was: 98°C – 30 seconds; then 25 to 35 cycles of: 98°C – 10 seconds, 66°C – 30 seconds, 72°C – 18 to 33 seconds, depending on amplicon length (NEB recommended extension time for gDNA is 30 seconds per kb); then 72°C – 5 minutes. Amplification was assessed by electrophoresis by loading 7.5 µL of PCR product with 1.5 µL of 6x loading dye on a 1% agarose gel.

Table 2.2: **Primer sequences used in HL-PCR**. For each standard PCR, two standard primers were used (“base forward” and “base reverse”). For each HL-PCR, a forward or a reverse HL primer was combined with a standard (base) reverse or forward primer, respectively. FwB = “base forward” primer. RvB= “base reverse” primer.

Gene	Target	Base Forward	Base Reverse	Headloop Forward	Headloop Reverse
ngfb	a	ACGATGGCAACAAAAACTGC	ATGAAGTCAGCGCACGTACA	CACCGCATGGGCTCAACGTGACGATGGCAACAAAAACTGC	Rv-B
	b	ACGATGGCAACAAAAACTGC	ATGAAGTCAGCGCACGTACA	Fw-B	CGGTCAAGATGTCACAGCCAATGAAGTCAGCGCACGTACA
	c	AGGCAATGAGGTCACCGTTT	AGCCTGCGGTTTTCAAGCAT	Fw-B	TGGTGGCGTGGAGACTCATAAGCCTGCGGTTTTCAAGCAT
ngfa	a	-	-	-	-
	b	-	-	-	-
	c	-	-	-	-
ntrk1	a	GCACCTGCCCAAAAGAAGTG	ATGGTGAGTACATTTTTGGGTGT	TTTTGACGAGGGCCACGAGGGCACCTGCCCAAAAGAAGTG	Rv-B
	b	CCCTGCTACACGGCTCAATA	CAGCTCGCAGAACTTACCCAA	CCACCCTATGGTCAGCCATGCCCTGCTACACGGCTCAATA	Rv-B
	c	TGAGAGTGCTGACACTTATTGC	AGCAACCAGCATCTTGTCAGT	Fw-B	GGGTGAAGGAGCTTTTGGCAAGCAACCAGCATCTTGTCAGT
	d	GCCTCTAATGCACTGACGCA	AAATCCACCTCCAAACACACAG	Fw-B	GCTCGTGTGACATTTACTGGAAATCCACCTCCAAACACACAG
prdm12b	a	GCATATAAAGCCCACCGGGA	GGGCGAACCATCTCCTCATC	TCGAACAGGTGTTCCCCCAGGCATATAAAGCCCACCGGGA	Rv-B
	b	GCATATAAAGCCCACCGGGA	GGGCGAACCATCTCCTCATC	CTCCAGCGGCCGTACAGGAAGCATATAAAGCCCACCGGGA	Rv-B
	c	GCATGCATGGGCATGATTTT	CTTCCGATCTGCACGACCTC	CTCTTGACTGGCATCGATGAGCATGCATGGGCATGATTTT	Rv-B

2.9 *In situ* hybridisation (ISH)

2.9.1 Probe generation

RNA antisense probes for *trpv1*, *trpa1b*, *trpm3*, *p2rx2*, and *cgrp* were made. For *trpv1*, *trpm3*, *p2rx2*, and *cgrp*, total RNA extracted from WT adult zebrafish was used to generate cDNA by reverse transcription using SuperScript™ II Reverse Transcriptase (Invitrogen). The cDNA was then amplified by PCR with Taq polymerase (Invitrogen), using forward and reverse primers shown in Table 2.3, and cloned into an ampicillin-resistant pCRII-TOPO vector (Invitrogen). For *trpa1b*, the cDNA in a pBluescriptSK(+) plasmid was provided by Professor Ajay Dhaka (University of Washington). The different vectors were linearised with NEB restriction enzyme XbaI (*trpa1b*), or Promega restriction enzymes EcoRV (*trpv1*, *p2x2*), NotI (*trpm3*), BamHI (CGRP), and transcribed with either T7 (*trpa1b*, *cgrp*) (Promega) or SP6 (*trpm3*, *trpv1*, *p2rx2*) (Promega) to generate digoxigenin (DIG)-labelled riboprobes according to manufacturer's instructions. The *trpm3* probe was generated by Ms Hande Tunbak. The probes were purified using Qiagen RNeasy Mini Kit, eluted in 30 µL of nuclease-free water and tested on 1% RNase-free agarose gel in Tris-acetate-EDTA (TAE) buffer (40 mM Tris, 20 mM acetic acid, 1 mM EDTA).

Table 2.3: **Primer sequences used to amplify cDNA for the generation of RNA probes.**

Gene (Protein)	Gene name	ENSEMBL Gene ID	ENSEMBL Transcript ID	Primers	cDNA length (bp)
trpv1 **(trpv1)**	*transient receptor potential cation channel, subfamily V, member 1*	ENSDARG00000059883	ENSDART00000083731.5	Fw: TGACGTGGTGGAACCCTCTA	1141
				Rv: TTGATTCGCGTAATCCTTCC	
trpm3 **(trpm3)**	*transient receptor potential cation channel, subfamily M, member 3*	ENSDARG00000039181	ENSDART00000147188.3	Fw: GCAAGTCTTCGGCAAAGGTC	1046
				Rv: GGGGCAGGTTACCCTTTTTC	
p2rx2 **(p2rx2)**	*purinergic receptor P2X, ligand-gated ion channel, 2*	ENSDARG00000002300	ENSDART00000190310.1	Fw: ATCCTGGTGTCCCATTGAGG	541
				Rv: TCCAACTGAAGTCATGGCCG	
calca **(cgrp)**	*calcitonin/calcitonin-related polypeptide, alpha*	ENSDARG00000056590	ENSDART00000079112.6	Fw: CTAATGTGGGCTCCCAGGC	511
				Rv: TCAAGGCACAAGACACATCCA	

2.9.2 Whole mount ISH

Whole mount colorimetric ISH was performed as described previously (Thisse and Thisse, 2008), with a few modifications. Briefly, 7 dpf WT larvae (for NBT-BCIP *in situs*) or 7 dpf *Tg(elavl3:jGCaMP7f)*^{u343} larvae (Fast Red *in situs*) were fixed in 4% PFA (w/v; Sigma) in PBS and 4% sucrose (Sigma) overnight at 4°C, and dehydrated through a graded series (25%, 50%, 75% and 100%) of methanol/PBSTw (PBS with 0.1% TWEEN®20, Sigma), after which they were stored at -20°C for at least one overnight. After rehydration through a graded series of methanol/PBSTw (75%, 50% and 25%), larvae were washed in PBSTw, permeabilised with Proteinase K (100 µM/mL) for 20 minutes, bleached in the dark for 30 minutes with hydrogen peroxide, post-fixed in 4% PFA (w/v) in PBS for 30 minutes, and incubated in standard hybridisation buffer containing 50% formamide for at least 3 hours at 65°C. Samples were then incubated in each probe at 65°C, either overnight (for *p2rx2*, *trpm3* and *cgrp*) or for 2.5 days (for *trpa1b* and *trpv1*). The next day, samples were washed at 65°C through a graded series of hybridisation solution (50%, 25%, 0%, 0%) and saline sodium citrate (SSC) (2x, 2x, 2x, 0.2%) for 10 minutes each, followed by two 10-minute PBSTw washes, and then they were blocked with 10% Normal Goat Serum in PBSTw for at least one hour at room temperature. Samples were then incubated overnight at 4°C with anti-DIG-AP Fab fragment (alkaline phosphatase conjugated antibody; 1:3000 in block solution) (Roche). The following day, they were washed thoroughly (at least four 15-minute washes in PBSTw).

DIG-labelled probes were then detected either by standard Nitro Blue Tetrazolium (NBT) and 5-Bromo-4-chloro-3-indolyl phosphate (BCIP) (Roche) protocol for colorimetric ISH, or using Fast Red (Sigma) for fluorescent ISH (FISH). For NBT-BCIP staining, samples were first equilibrated in freshly prepared “AP buffer” (staining buffer without NBT-BCIP: 0.1M Tris buffer (pH 9.5), 50 mM MgCl2, 0.1 M NaCl, 0.01 % TWEEN®20) by washing three times for 15 minutes, after which they were incubated in the staining solution (1 µL NBT and 3 µL BCIP per 1 mL of AP buffer) and allowed to develop in the dark at room temperature, being monitored under a light microscope regularly (at around 30- to 60-minute intervals) for the development of a blue precipitate. For Fast Red staining, the Fast Red solution was prepared by first separately dissolving one Fast Red TR salt tablet and one NAMP tablet in 1 mL of ddH2O each, after which

the resulting solutions were filtered and mixed together. Since Fast Red is a chromogenic substrate to alkaline phosphatase (Hauptmann et al., 2016), Fast Red staining also gives a colorimetric precipitate in addition to fluorescent signal, which allows following of the reaction while the signal develops. Thus, samples were incubated in the Fast Red staining solution and allowed to develop in the dark at room temperature, being monitored under a light microscope regularly (at around 30- to 60-minute intervals) for the development of a red precipitate. The specific staining time for both NBT-BCIP and Fast Red staining varied depending on the probe. If no clear staining was observed at the end of the day, staining was paused by replacing staining solutions with either AP buffer (NBT-BCIP) or PBS (Fast Red) and samples were left overnight at 4°C, with staining being resumed the following day by incubating samples in fresh staining solutions. Reactions were stopped with either PBSTw (NBT-BCIP) or PBS (Fast Red) washes.

For NBT-BCIP, samples were then post-fixed in 4% PFA/PBS for 20 minutes, dehydrated in methanol, and kept overnight at -20°C, after which they were rehydrated, transferred into 80% glycerol (Sigma) in PBSTw through a graded series, and imaged using a light microscope (Leica). For Fast Red, samples were examined under a light microscope for staining. IHC was then combined with the FISH before imaging (as described below).

2.9.3 FISH/IHC

IHC against HuC/D, a neuronal marker in larval zebrafish (Kim et al., 1996), was combined with the Fast Red FISH (described in 2.9.2). After stopping the Fast Red reaction with PBS washes, samples were incubated with a mouse anti-HuC/D monoclonal antibody (16A11) (1:500 in PBSTw; Molecular Probes Cat# A-21271) overnight at 4°C, washed (at least six 30-minute washes) and incubated with an anti-mouse Alexa 488 (1:500 in PBSTw; Thermofisher) and 4′,6-diamidino-2-phenylindole (DAPI) (1:500 in PBSTw; Tocris Bioscience, Cat# 5748) overnight at 4°C in the dark. After washing (at least six 30-minute washes in the dark), samples were transferred to 80% glycerol in PBSTw through a graded series, and mounted for confocal imaging.

2.9.4 Confocal microscope image acquisition

Confocal imaging was carried out using a Zeiss LSM-880 with Airyscan (Zeiss). Whole mount FISH/IHC samples were mounted in mounting medium (1:1 2% low melting point agarose:80% glycerol), using glass rings fitted on a slide by silicone grease and VWR Thickness No.1 coverslips (approximately 130-170 μm). Imaging was performed by scanning with 1024x1024 pixel resolution, 8-bit, and z-step size of approximately 0.42 μm.

Chapter 3: Establishing an assay for the study of fast escape-like responses to noxious stimuli

3.1 Introduction

The ability to escape from and avoid potentially harmful situations is critical for survival and is present across the animal kingdom, from invertebrates, such as *Aplysia californica* (with its widely studied gill withdrawal reflex), *Caenorhabditis elegans* and *Drosophila melanogaster*, to rodents and primates (Castellucci et al., 1970; Wittenburg and Baumeister, 1999; Im and Galko, 2012; Caterina et al., 2000, Chudler et al., 1986). Zebrafish larvae also show a variety of behavioural responses to noxious stimuli and stimuli that signal threats. These stimuli include temperature, chemicals (e.g. allyl isothiocyanate (AITC), commonly known as mustard oil), touch, vibration and visual (e.g. looming) stimuli (Gau et al., 2013; Prober et al., 2008; Lam et al., 2005; Barrios et al., 2020). With regards to temperature, such behaviours are necessary because temperatures in the natural habitat of zebrafish can fluctuate widely, since zebrafish are typically found in the wild in shallow pools and streams which can be heated by sunlight (Engeszer et al., 2007; Haesemeyer 2020). As for vibration, the ability to sense water motion is critical for survival, as it allows for the detection of predators (Odstrcil et al., 2022; Stewart and McHenry, 2010). Regarding chemicals, AITC is a biodegradation product used by plants from the Brassicaceae family as defence (Overby et al., 2015). AITC has been found to activate *TRPA1* channel orthologs (formerly known as *ANKTM1*) in Drosophila and mammals, as well as zebrafish, leading to sensory neuron activation, pain-like sensations and ultimately aversive responses (Bandell et al., 2004; Jordt et al., 2004; Bautista et al., 2006; Prober et al., 2008; Al-Anzi et al., 2006; Kang et al., 2010). Finally, looming stimuli can be perceived as threatening by the fish as they may represent an approaching predator (Dunn et al., 2016).

When exposed to these various stimuli, zebrafish respond with changes in their behaviour. For instance, zebrafish larvae increase their swimming activity in

response to AITC being added to the water (Prober et al., 2008). They can also execute very fast, stereotyped escape responses, such as fast C-starts, in response to both acoustic and tactile stimuli, as well as the slightly slower O-bends, in response to visual stimuli (Wolman and Granato, 2011; Kalueff et al., 2013; Marques et al., 2018; Lam et al., 2005; Mu et al., 2012; Budick and O'Malley, 2000). Finally, a variety of behaviours can be elicited by both noxious and innocuous heat: a generalised increase in water temperature beyond 37°C (considered noxious in zebrafish) leads to increased swimming activity in zebrafish larvae; in a place preference assay, they robustly avoid the hot (36°C) side of a dual heat/cool plate; and when exposed to acute innocuous heat in the form of an infrared laser, free-swimming larvae show escape responses and head-fixed larvae show tail-flick "escape-like" responses (Prober et al., 2008; Gau et al., 2013; Haesemeyer et al., 2018; Haesemeyer et al., 2015). In short, zebrafish use a wide repertoire of behaviours to escape noxious (and innocuous) stimuli. Together with the similarities of their nociceptive system to that of mammals (discussed in Chapter 1), this suggests zebrafish may be used to study nociception.

As detailed in Chapter 1, there are several advantages to using zebrafish larvae as an animal model. In particular, their simplicity compared to mammals means zebrafish can help us reach a mechanistic understanding of the circuits sensing noxious stimuli and generating the resulting behavioural responses, with clear hypotheses that can then be tested in other animal models. For instance, Haesemeyer et al. (2018) used larval zebrafish to produce a brain-wide circuit model of tail-flick behaviours evoked by innocuous heat, and Wee at al. (2019) identified novel neuronal populations and circuits driving nocifensive behaviours in response to trpa1 channel activation. Moreover, zebrafish allow for higher throughput experiments, which is advantageous for drug discovery (Curtright et al., 2015). Finally, they are particularly amenable to genetic techniques, and have been used to perform large-scale phenotypic screens of gene variants linked to human disorders such as psychiatric disorders, as well as establishing models of various diseases, from cancer to eye and inner ear diseases (Thyme et al., 2019; Tang et al., 2020; Feitsma and Cuppen, 2008; Blanco-Sanchez et al., 2017; Link and Collery, 2015).

The overall aim of my project was to establish the zebrafish as a model to study the genetics of nociception. As such, my first goal was to set up an assay in our laboratory that would allow me to study fast escape-like responses to noxious heat in zebrafish larvae. Characterising these responses (in wild-type fish and mutants) would then allow me to infer a role for these genes in zebrafish. To be able to do that, the assay used needed to allow for the tracking of these fast behaviours after exposure to the stimulus and for a fine control of the stimulus, which needed to be short and temporally precise, and to reach temperatures in the noxious range. Hence, I based my behavioural assay on that described by Haesemeyer et al. (2018) where an infrared laser is used to deliver short, temporally-precise stimuli to 6-7 dpf head-fixed larvae. The laser, pointing to the head, generates heat, which promotes a tail-flick “escape-like” response. This is recorded by a high-speed camera and analysed offline. I adjusted the original assay, which used innocuous heat (24°C to 29°C), so that the laser intensities used stimulated fish with temperatures in the noxious range. In the zebrafish literature, the threshold for noxious heat is normally agreed to be between 34°C and 37°C, with exposure to temperatures of 48°C for only a few seconds having been shown to induce tissue and nerve damage (Gau et al., 2013; Prober et al., 2008; Haesemeyer et al., 2015; Haesemeyer et al., 2018; Malafoglia et al., 2013b).

In this chapter, I set up the infrared laser stimulation assay. I characterised the properties of the stimulus and found it to be temporally precise and to generate heat at temperatures which I estimate to be in the noxious range for zebrafish larvae. When stimulated with the laser, zebrafish show tail-flick responses, which I can track for further analysis.

3.2 Results

3.2.1 Setting up an infrared laser assay to study the behaviour of zebrafish larvae in response to noxious stimuli

To deliver temporally-precise heat stimuli of different intensities, I established an infrared laser stimulation assay in our laboratory (Figure 3.1) based on that used by Haesemeyer et al. (2018). In this assay, 6-7 dpf larvae are tethered (head-fixed) in agarose, with the tail free to move, and stimulated with a 980 nm laser infrared laser (Figures 3.1.A and B). The energy of the infrared laser beam is absorbed by the black pigment in the skin of the fish, which generates heat, causing a tail-flick escape-like response. The laser beam is focused to allow the targeting mainly of the head. Real-time thermal stimuli are generated using a high-power laser driver, which provides current to the laser diode. The laser driver is controlled by a National Instruments Data Acquisition Device (NI-DAQ), a device to perform input/output electrical measurements (Figures 3.1.C and D), which receives digital input from a computer where the stimulation protocol is programmed. This allowed me to precisely control the duration and intensity of the laser stimulus. The experimental pipeline was written in Bonsai (Lopes et al., 2015) by Dr Adam Kampff. Behavioural data was recorded using a camera and analysed offline using Python.

Before performing the behaviour experiments, I first sought to characterise the properties of the laser and stimulus. My aims were to ensure: firstly that my stimulus was temporally precise, secondly that the infrared laser generated heat in the noxious range, thirdly that this was sufficient to elicit tail-flick behavioural responses, and finally that these responses could be tracked successfully for further analysis. To determine this, I started by performing a series of measurements of the stimulus (data summarised in Table 3.1).

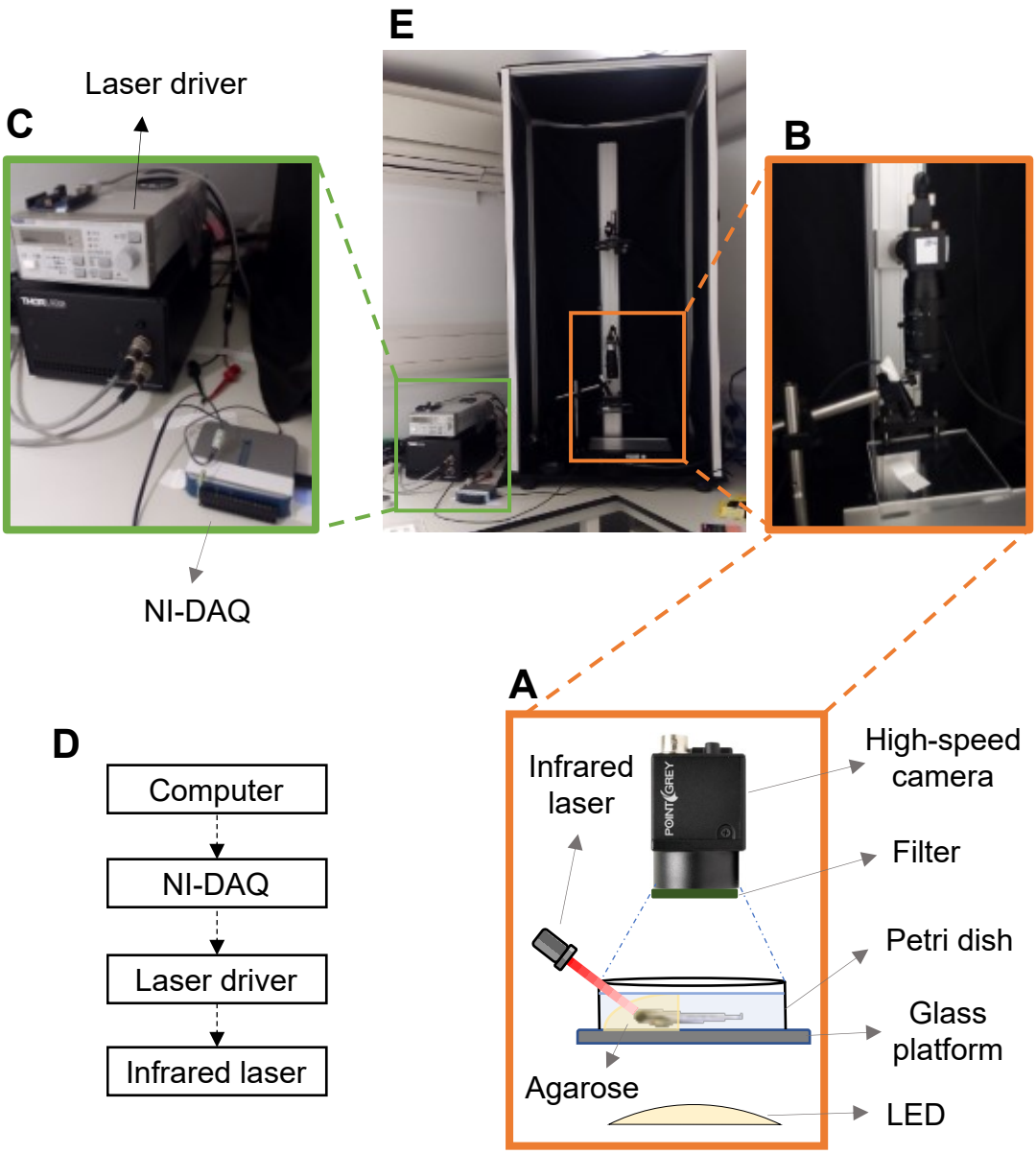

Figure 3.1: **The infrared laser stimulation assay**. A: Zebrafish larvae are tethered in agarose, with the tail free to move. The petri dish is placed on a glass platform, which is illuminated from below with a visible light LED. They are stimulated with an infrared laser (980 nm) and their behaviour is recorded from above using a high-speed camera (to which a filter was added after pilot experiments), which is connected to a computer (not shown). B: Picture of the setup components represented schematically in A. C and D: The infrared laser is controlled by a laser driver, according to voltage outputs from the NI-DAQ. The NI-DAQ is connected to a computer and controlled through a Bonsai script (Lopes et al., 2015). E: Picture of the full setup.

Table 3.1: **Infrared laser stimulus properties.** For each voltage (in V), the corresponding laser driver current (intensity, in mA; rounded to the nearest 5), average power (determined using an optical power meter, in mW; n=3 measurements; SEM is shown) and temperature (estimated using a thermistor, in °C; n=1 measurement) are shown.

Voltage (V)	Intensity (mA)	Average Power (mW)	Peak temperature (°C)
0.729	300	184.07±4.9E-4	41
0.853	350	215.22±3.2E-4	46
0.977	400	242.37±3.0E-4	48
1.100	450	264.99±1.3E-3	51
1.224	500	-	54
1.323	540	296.21±5.0E-4	61

First, I used a silicon biased detector to determine the temporal profile of the laser. My goal was to measure laser kinetics (rise and decay times), in order to confirm they were fast and similar between intensities. I did this for three different intensities: 80 mA, 120 mA and 160 mA. These intensities were lower than those later used in the behavioural assay due to a technical limitation of the silicon biased detector. To record the signal from the detector, I used NI-DAQ USB-6001, which is a multifunction DAQ device that offers analogue I/O and digital I/O. Figure 3.2 shows the signal recorded from the detector through the NI-DAQ plotted over time. I found the rise and decay times of the laser to be less than 50 µs (the sample rate of the NI-DAQ). This was the same for all three intensities tested. Therefore, the laser rise and decay are negligible compared to the 500 ms-long stimulus I apply to the fish.

I also used an optical power metre (Thorlabs, PM100USB) connected to a photodiode power head with silicon detector (Thorlabs, S121C) to measure the relationship between laser power and current for the different current intensities used (Figure 3.3 and Table 3.1).

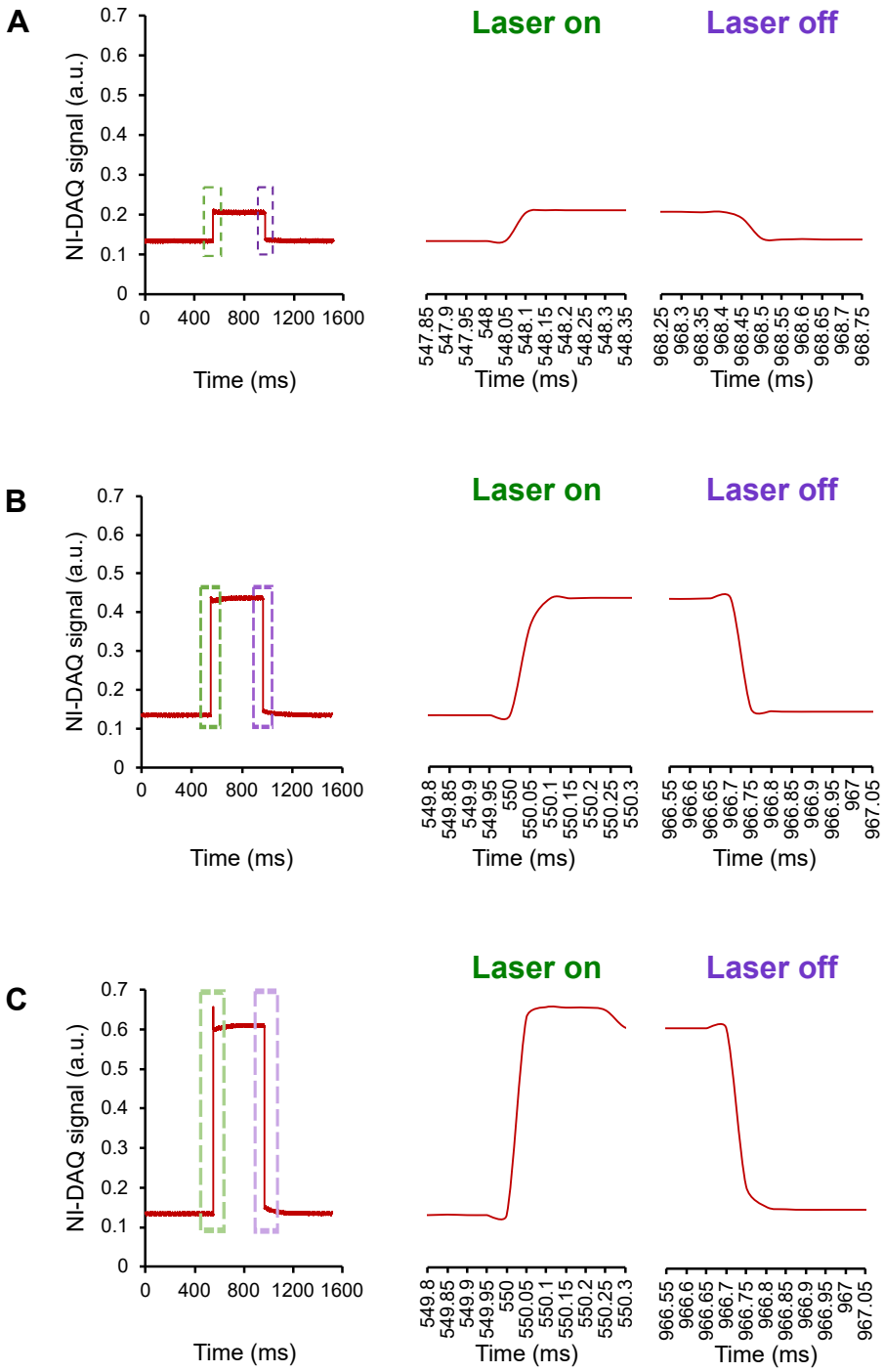

Figure 3.2: **Infrared laser profile over time**. Analogue signal recorded from a silicon detector using a NI-DAQ, for three different laser intensities: 80 mA (A), 120 mA (B) and 160 mA (C). In each figure, the left panel shows the NI-DAQ analogue signal recorded over the full 500-ms infrared laser stimulus. The middle and right panels in each figure show the same NI-DAQ analogue signal zoomed in around the time when the laser was switched on ("Laser on") and off ("Laser off"), respectively (green and purple dashed rectangles in the left panel). As can be seen, the rise and decay times of the laser were less than 50 µs for all intensities tested.

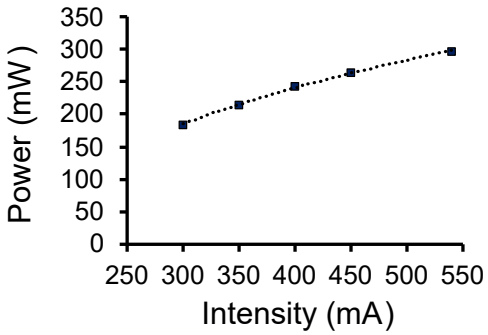

Figure 3.3: **Relationship between laser intensity (mA) and power (mW).** For each intensity set on the laser controller, the output power from the laser was determined using an optical power meter. This was done three times for each intensity. Each point on the graph represents the mean output power for each intensity. Error bars, representing the standard error of the mean (SEM), and a line of best fit (dashed line) are also shown.

Then, I used a calibrated thermistor (see Chapter 2 – Methods) with approximately the same size as the head of a larval zebrafish (Figure 3.4.D) to estimate the temperatures that the fish would be exposed to when stimulated with different laser intensities (as done in Hasemeyer et al., 2018). To do these experiments, the thermistor was embedded in the same 2% low-melting point agarose that would be used for behaviour experiments using larval zebrafish and positioned in the same place as a fish would (Figure 3.4.A). The stimulation protocol used was identical to what I would be using in each round of the behaviour experiments: 1 minute of baseline; six 500-millisecond stimulations of different intensities (selected in a random order from a list of pre-set intensities, 0.729 V, 0.853 V, 0.977 V, 1.1 V, 1.224 V, and 1.323 V, such that each intensity was selected once and only once); and 2 minutes between each stimulus. This was to mimic the conditions of the experiment as much as possible. For each stimulus used, voltage output from the thermistor was recorded and converted into resistance values, and temperature changes in the thermistor were subsequently calculated from the calibration curve using the Steinhart-Hart equation (Steinhart and Hart, 1968). The temperature traces obtained are shown in Figure 3.4.B. For each laser intensity, temperature rises non-linearly after a delay from when the laser is switched on, peaks, and then declines after the laser is switched off. The delay times (time to reach peak temperature) vary between ~500 ms and ~740 ms but are not related to laser intensity (300 mA: 640 ms; 350 mA: 600 ms; 400 mA: 690 ms; 450 mA: 550 ms; 500 mA: 740 ms; 540 mA: 500 ms). Importantly, as predicted, higher laser intensities lead to higher peak temperatures recorded. These ranged from ~41°C to ~61°C (Figure 3.4.C and Table 3.1). As such, all of my estimated peak temperatures are above the noxious threshold of around 34°C-37°C (Hasemeyer et al., 2018). In short, using this setup allows me to deliver a series of noxious heat stimuli of different intensities.

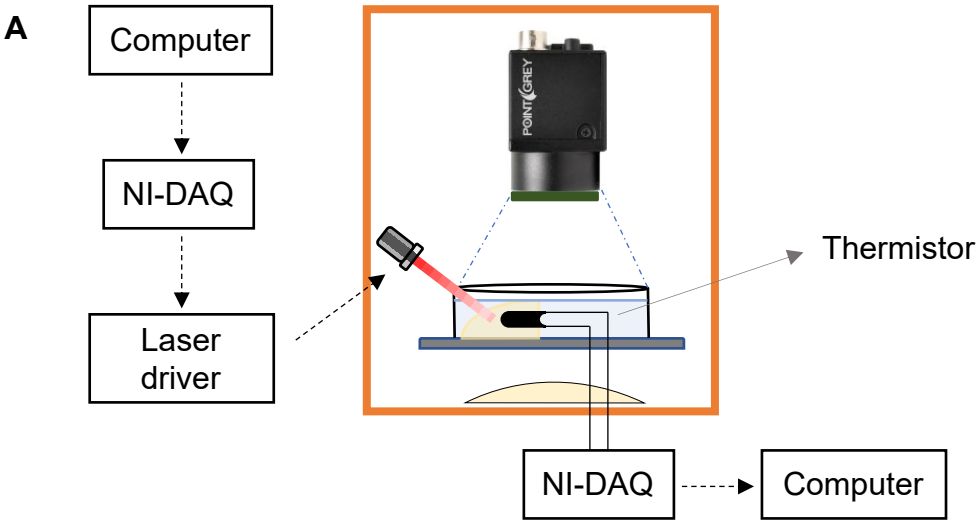
A
Computer
NI-DAQ
Laser driver
Thermistor
NI-DAQ
Computer

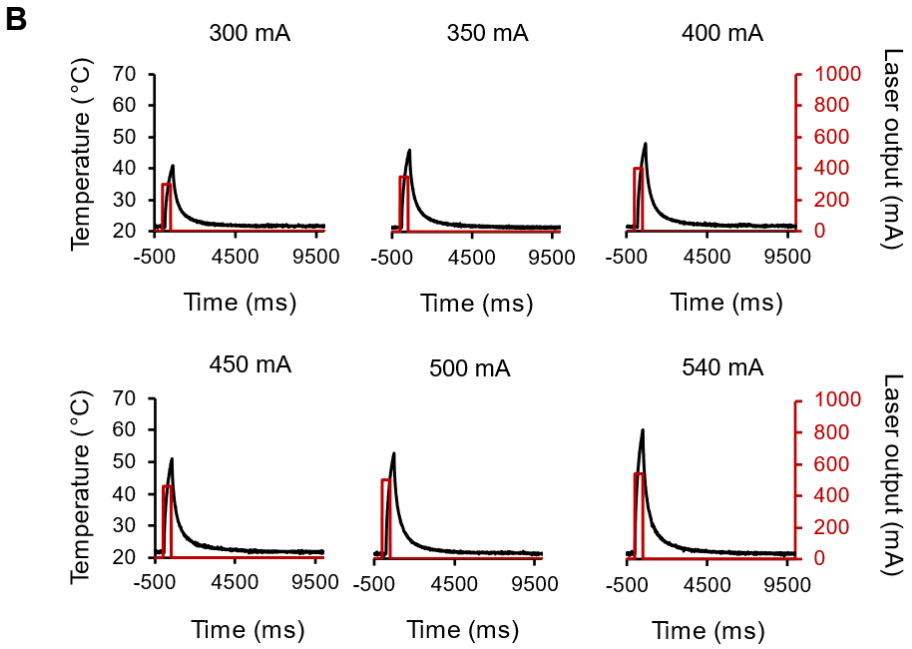
B
300 mA
350 mA
400 mA
450 mA
500 mA
540 mA
Temperature (°C)
Laser output (mA)
Time (ms)

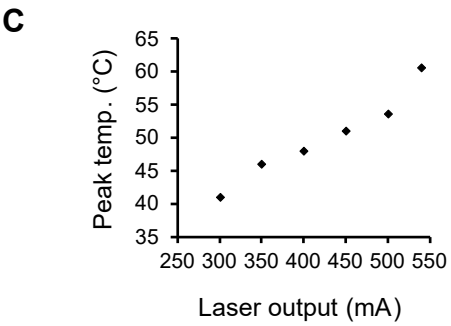
C
Peak temp. (°C)
Laser output (mA)

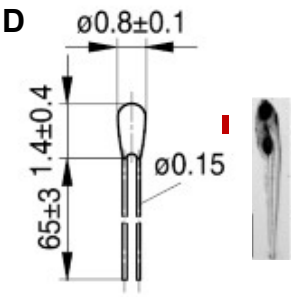
D
ø0.8±0.1
1.4±0.4
65±3
ø0.15

Figure 3.4: **Using a thermistor to estimate the stimulus temperature**. A: The thermistor is embedded in the same 2% low-melting point agarose that is used for behaviour experiments using larval zebrafish and positioned in the same place as a fish would. The standard infrared laser stimulation protocol is carried out. Real-time thermal stimuli are generated using a high-power laser driver, which provides current to the laser diode. The laser driver is controlled by a NI-DAQ, which receives digital input from a computer where the stimulation protocol is programmed. For each stimulus used, voltage output from the thermistor is then recorded through an NI-DAQ, and later converted into resistance values. Temperature changes in the thermistor are subsequently calculated from a calibration curve using the Steinhart-Hart equation (Steinhart and Hart, 1968). B: Temperature recordings (black) from the thermistor for different laser intensities (red). Results are shown for every laser intensity. C: The peak temperature for each laser intensity, as estimated with the thermistor, increases with intensity. D: Diagram showing the dimensions (in mm) of a typical thermistor (left), compared to a zebrafish larva (right). The red rectangle represents the laser beam (approximately to scale).

Some pilot experiments were then carried out to test the setup and its ability to drive behaviour in zebrafish larvae. The stimulation protocol consisted of three rounds of six 500-millisecond stimulations of different intensities (selected in a random order from a list of pre-set intensities, 0.729 V, 0.853 V, 0.977 V, 1.1 V, 1.224 V, and 1.323 V, such that each intensity was selected once and only once) at 2-min intervals. I found that the infrared laser could elicit tail-flick behaviours in zebrafish larvae (Figure 3.5.A). These pilot experiments also revealed the need for a series of technical optimisation steps so that the tail of the fish could be tracked. Firstly, I found that pixel saturation while the laser was switched on covered most of the fish (Figure 3.5.A, t=0). This is problematic because it makes it challenging to accurately track its full tail, and fish often respond while the laser is still on (Figure 3.5.A, t=490, for example). To address this, a filter was added to the camera lens to block the infrared light, avoiding pixel saturation. Multiple filters, with different properties and absorbance spectra, were tested (Figure 3.5.B). My aim was to identify a filter that blocked the majority of the infrared light, while allowing a small amount to pass through, to allow for visual confirmation that the laser was switched on at the correct times. It would also need to allow most of the visible light to pass through, so that there was enough contrast between the fish and the background, so the tail of the fish could be tracked. Based on those criteria, filter 3 was selected (Edmund Optics SCHOTT KG-1). Secondly, the movements I elicit with the laser are too fast for the recording frame rate initially used (100 Hz): the tail of the fish often appears blurred, which would also interfere with the tracking, and “jumps” from one location to the other between consecutive frames (Figure 3.5.A e.g. t=850 ms and t=860 ms). To overcome this, my initial camera was replaced with a high-speed camera (400 Hz), and illumination with the visible light LED was maximised so that exposure time could be decreased to reduce tail blurring. Finally, the whole tail often hit the agarose when it was cut at the initial 90° angle. As such, the agarose was subsequently cut at an angle of 135° so the tail could move more freely. As shown in Figure 3.6, these measures largely resolved the previously identified issues: the tail is no longer blurred, and its movement can be clearly followed frame-by-frame. Therefore, I then proceeded to carry out the behavioural experiments.

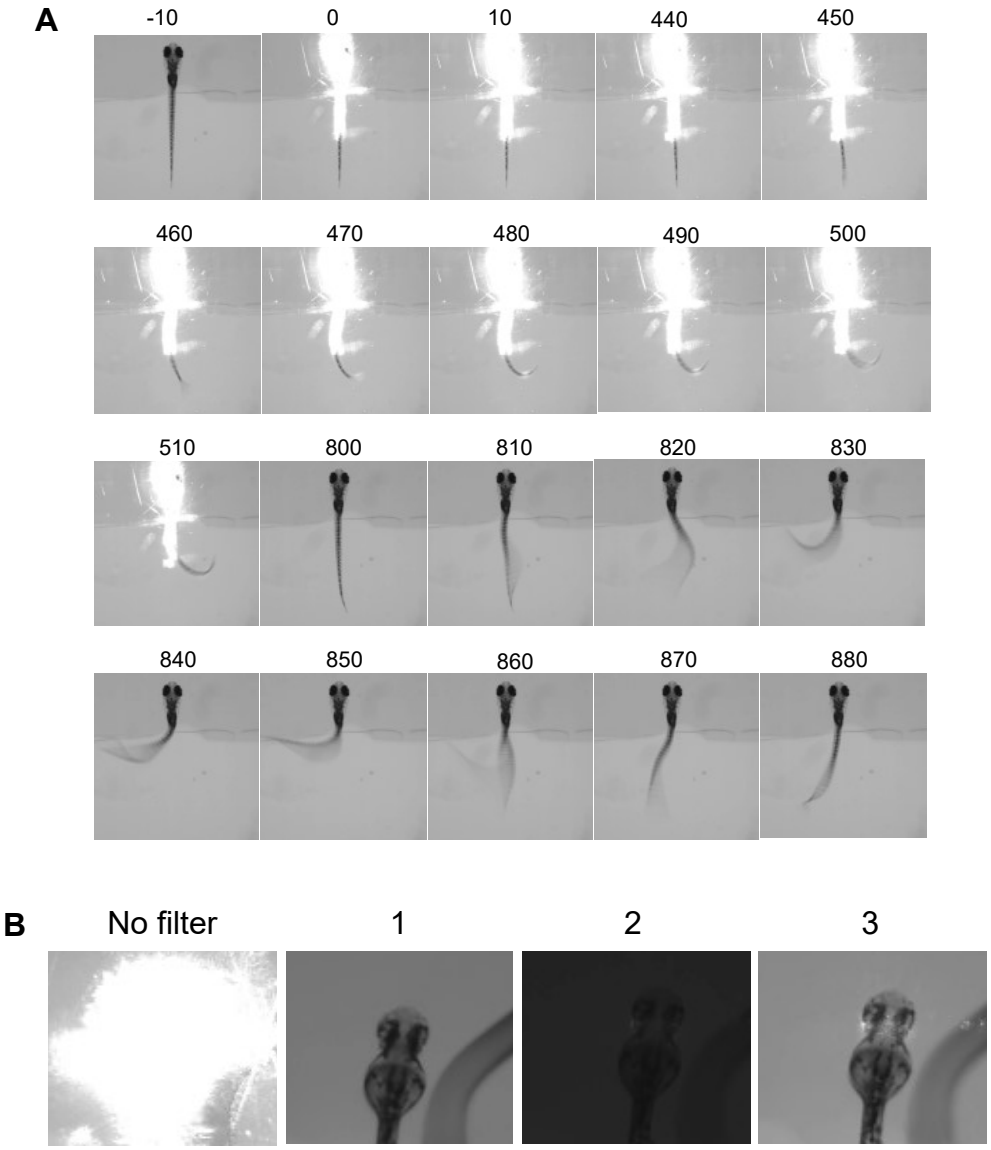

Figure 3.5: **Pilot experiments on the infrared laser setup revealed a need for optimisation of the system**. A: Representative images taken from a video recording of one of the pilot experiments (taken at a recording rate of 100 Hz). The number on each image refer to time in ms, with t=0 indicating the time when the laser is switched on. Under these assay conditions, pixel saturation from the infrared laser covers most of the tail (e.g., see t=500 ms), the tail sometimes hits the agarose (e.g., t=850) and it often cannot be tracked, "jumping" between locations across frames. B: To avoid pixel saturation in the video recordings, a filter was added to the camera lens. Three different filters, with different properties and absorbance spectra, were tested (1, 2 and 3, corresponding to Edmund Optics SCHOTT filters BG-38, VG-9, KG-1, respectively).

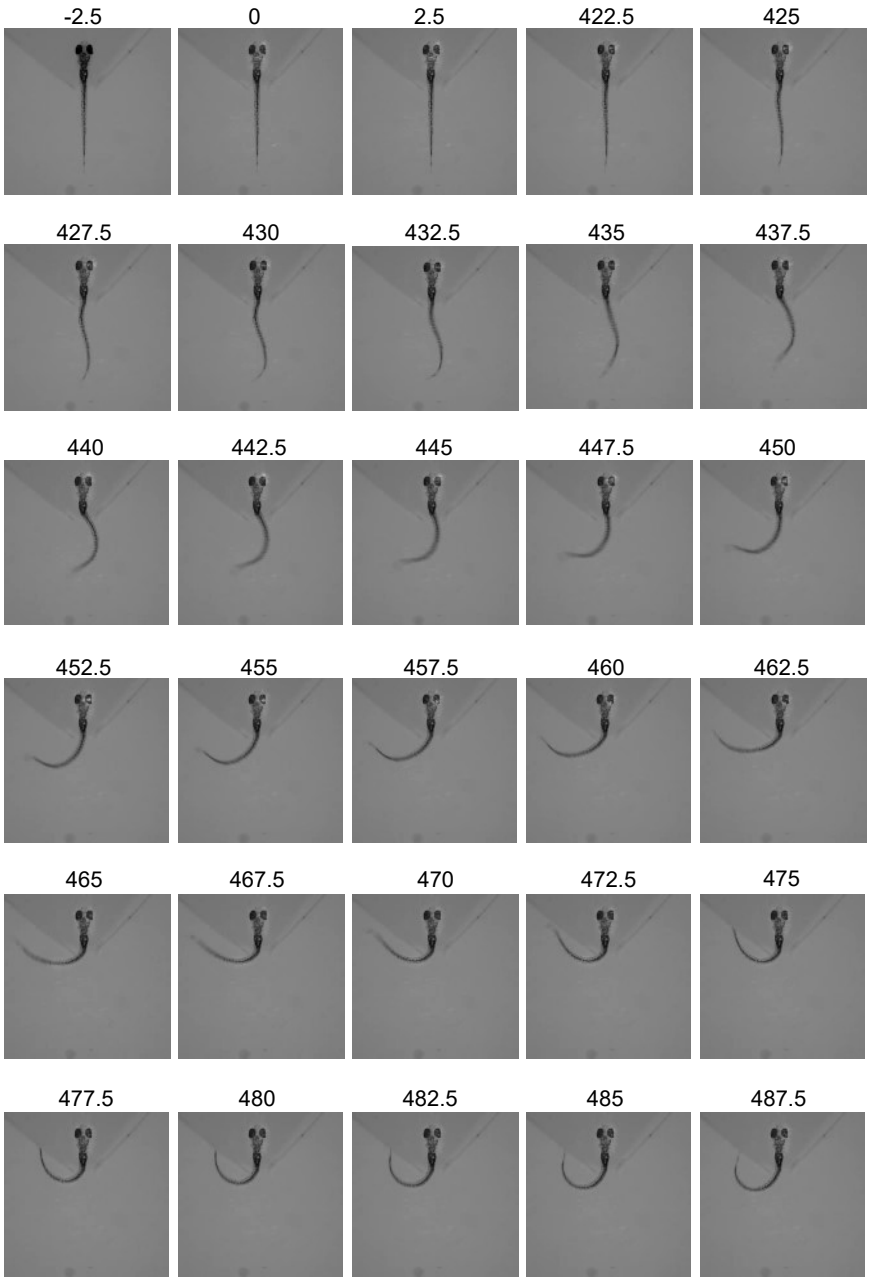

Figure 3.6: **Representative images from a video recording of one of the pilot experiments after optimisation of the system.** Images were taken at a recording rate of 400 Hz. The number on each image refer to time in ms, with t=0 indicating the time when the laser is switched on. Under these improved assay conditions, the tail of the fish can be followed across frames and is no longer covered by the infrared laser.

3.2.2 Head-fixed zebrafish larvae show escape-like responses to noxious heat delivered with an infrared laser

Larval zebrafish at 6-7 dpf were anaesthetised and embedded in agarose (to allow the tail to move freely, the agarose caudal to the swim bladder was cut at 135° to the anterior-posterior axis and removed). After a recovery and habituation period of at least 30 mins, animals were inspected for motor responsiveness to somatosensory stimulation by gently touching the tail with a pipette tip. Responsive larvae were exposed to three rounds of six 500-millisecond stimulations of different intensities (selected in a random order from a list of pre-set intensities, 0.729 V, 0.853 V, 0.977 V, 1.1 V, 1.224 V, and 1.323 V, such that each intensity was selected once and only once) at 2-min intervals. Recordings were analysed offline and the tail was tracked (see Chapter 2 – Methods). Different parameters were then calculated for each frame: cumulative tail angle (sum of all tail angles); tail curvature (mean of the absolute value of all tail angles); tail motion (which compared the x and y coordinates of the edges of tail segments across neighbouring frames). Tail angle (here, cumulative tail angle and tail curvature) is routinely used in the zebrafish literature to characterise tail-flick and swimming behaviours (e.g. Marques et al., 2018; Wee at al., 2019). Tail motion was used as a measure of movement.

Representative plots of the raw traces of each of these parameters around the time of stimulation are shown in Figures 3.7 and 3.8. Tail-flick behaviours can be elicited across all six laser intensities, as shown by the changes in the tail cumulative angle, curvature and motion values from baseline (Figure 3.7). Bouts of different amplitudes are detected. Cumulative angle traces reveal fish can respond with unilateral or bilateral tail movements (Figure 3.7, left: blue and green arrows, respectively), with negative cumulative angle values corresponding to a tail flick to the right, and positive values to a tail flick to the left. As predicted, different bouts are reflected differently in each parameter. For example, unilateral bouts can show similar motion values to bilateral bouts, and bouts with similar peak motion values can have different curvatures and cumulative angles (e.g. Figure 3.7 at 500 mA, blue and green arrows). Tail-flick behaviours can be elicited reliably across all three rounds of stimulation (Figure 3.8). In short, head-fixed zebrafish larvae show escape-like responses to noxious heat delivered with an infrared laser.

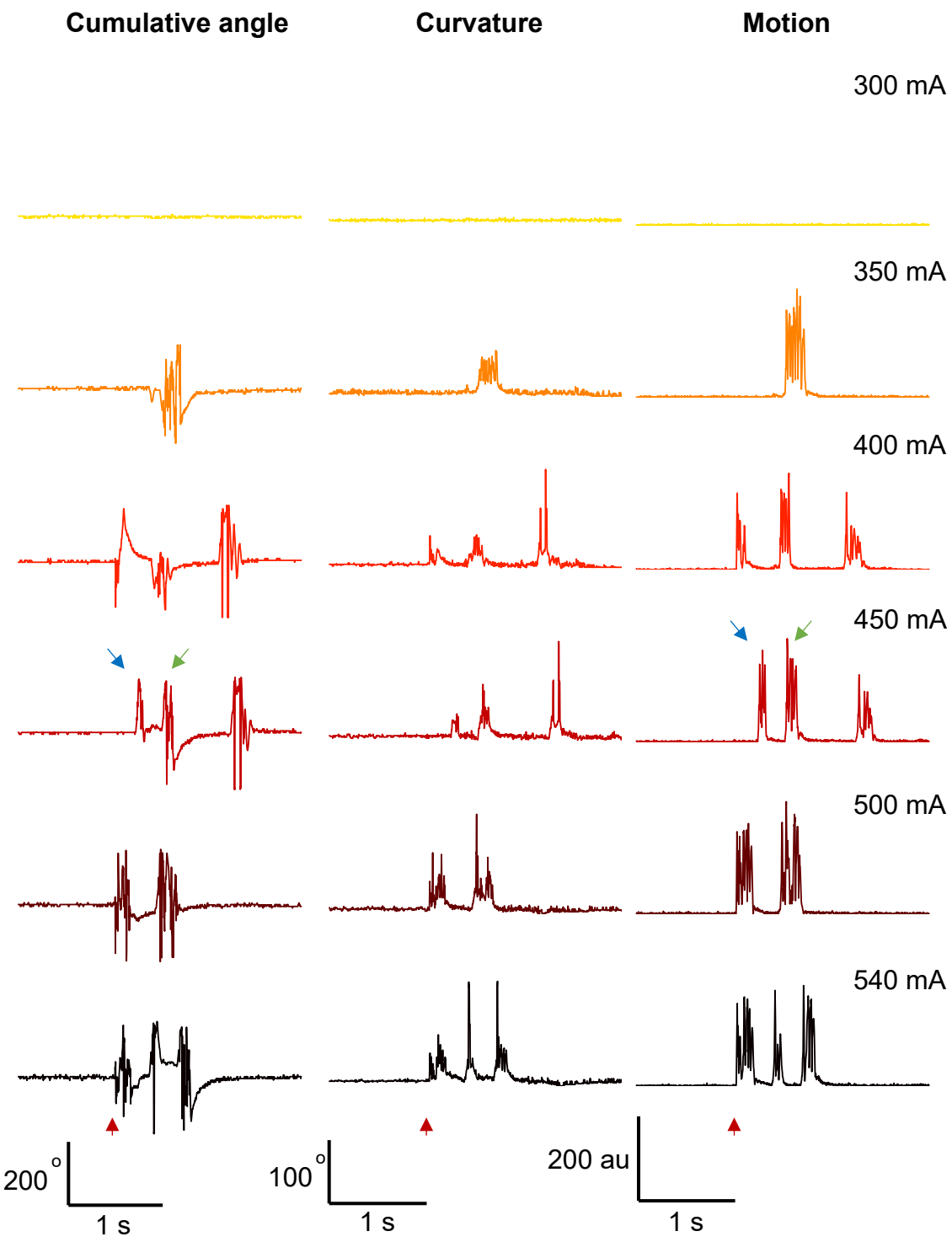

Figure 3.7: **Representative cumulative angle (left), curvature (middle) and motion traces of a single fish over the first round of stimulation**. The red arrow indicates when the laser was switched on (t=0). Traces are shown from 500 ms before the laser was switched on to 2 s after the laser was switched on. The blue and green arrows indicate unilateral and bilateral bouts. Cumulative angle y axis ranges from -200° to 200°; curvature y axis ranges from 0° to 100°; motion y axis ranges from 0 a.u.. to 300 a.u. X axis shows time in ms.

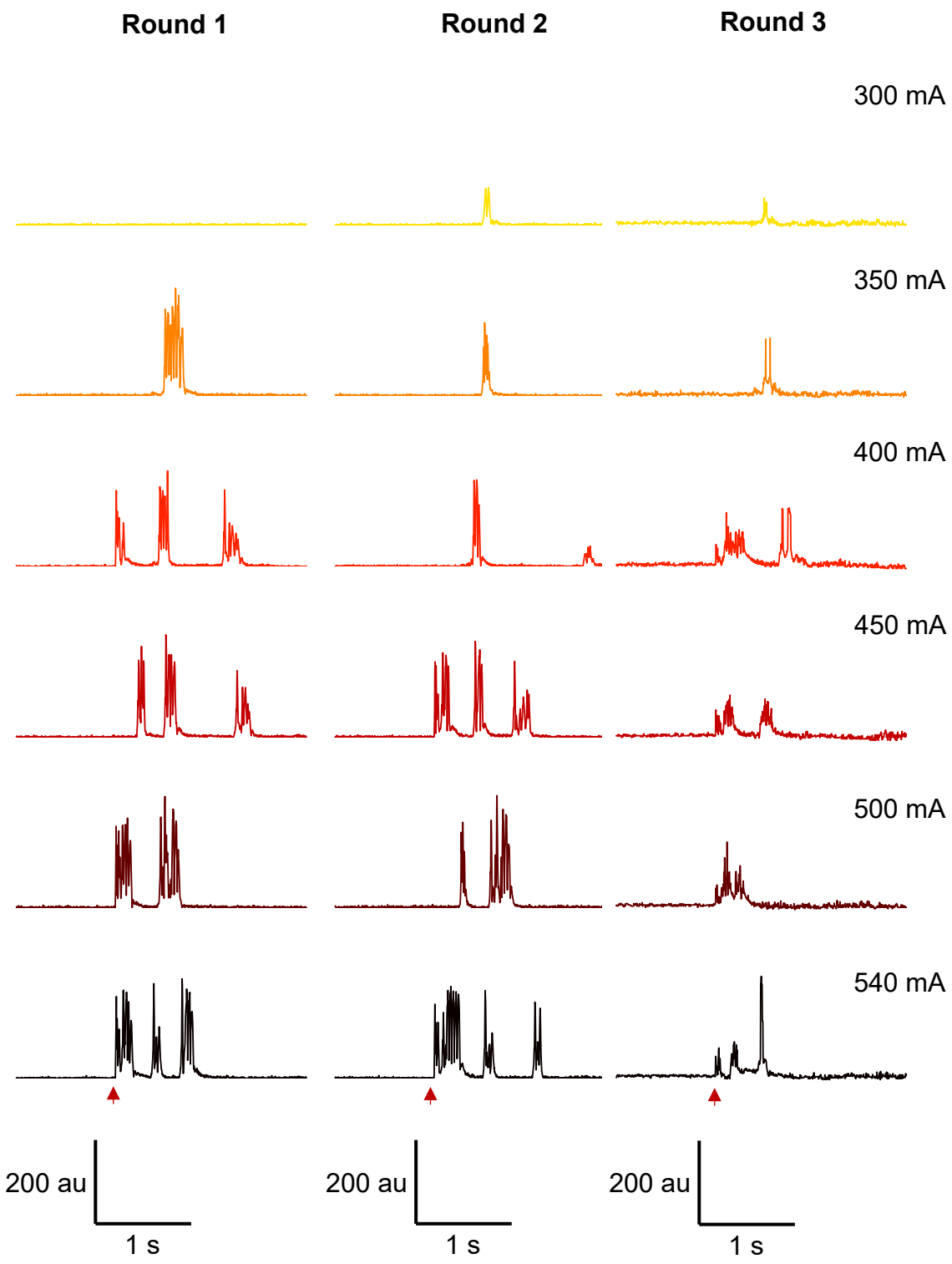

Figure 3.8: **Representative motion traces of a single fish over the three rounds of stimulation**. Motion y axes range from 0 a.u. to 300 a.u.. X axis shows time in ms. The red arrow indicates when the laser was switched on (t=0).

Exposure of whole zebrafish larvae to temperatures of 48°C for only a few seconds has been shown to induce clear anatomical defects, as well as tissue and nerve damage; conversely, exposure to 45°C for the same period of time had no effects on anatomy, neuroanatomy or behaviour (Malafoglia et al., 2013b). According to my thermistor estimates, the peak temperature reached upon stimulation with the laser was equal to or greater than 48°C at the four highest intensities used (Table 3.1). Therefore, I visually inspected larvae after each experiment. I did not observe any obvious anatomical defects and I also found larvae to retain the ability to respond to the light touch of a pipette tip. Therefore, I deemed these laser intensities safe to use for subsequent experiments.

3.2.3 Quality control

A subset of the tracking videos was manually inspected for quality control purposes. Tracking videos show the computed tracked tail segmentation overlaid on top of the original video recording. I observed that, while our script usually successfully tracked the tail of the fish, including during movement, it occasionally failed to do so. Representative examples of what “failed tracking” often looked like on the tracking video are shown in Figure 3.9.A. I found this to be mainly caused by: instances where the swim bladder of the fish was not fully embedded in the agarose, meaning it could move slightly during fast movements, which disrupted the tracking; bright reflections from the infrared laser (Figure 3.9.A at 540 mA); or dirt (e.g. dust) in the water in close proximity to the tail of the fish. Upon matching these videos to the resulting tail motion traces, I observed they corresponded to abnormally high peak motion values (e.g. Figure 3.9.C at 540 mA), often reaching 1000 a.u., which were much higher than the usual motion values, normally peaking at a maximum of 300 a.u.. After plotting the distribution of peak motion values, I initially planned to exclude bouts where peak motion was greater than 400 a.u, since most peak motion values were below this cut-off. Nevertheless, upon manual examination of bouts that would be excluded according to this criterion, I found several where peak motion was greater than 400 a.u. but tracking had not failed. Consequently, I decided to implement an alternative method to solve tracking failures. I next considered applying a filter to the data, such that abnormally high values were smoothed out. However, this did

not appear to be a good solution, as it would significantly alter the properties data (e.g. response latency). Therefore, we sought to find an alternative method.

We observed that, as shown in Figure 3.9.A at 540 mA, “failed tracking” normally meant the tail was momentarily “lost” and the head of the fish was “found” instead. As such, a region of interest (ROI) was defined between the blue and orange diagonal lines shown in Figure 3.9.B, and this was set as an exclusion region, such that any tail coordinates falling within this ROI would be flagged as “failed tracking”. That ROI encompasses the agarose, so it would not be possible for real tail movements to fall there. The values of the x and y coordinates flagged as “failed tracking” were then replaced with the result of a linear interpolation carried out across them. The script for this was written by Dr Thomas Ryan. This successfully removed the abnormally high motion values caused by failed tracking and so I was able to include these bouts in the analysis. Strikingly, this method performed better than a hard motion threshold and provided us with more accurate data, as it successfully identified and corrected both large and small tracking failures (Figure 3.9.A at 540 mA and 350 mA, respectively), leaving “real” high motion values unaffected. For instance, as seen in Figure 3.9.A, at 350 mA, part of the tail was momentarily lost and entered the ROI, resulting in a slightly higher motion value for this particular bout. Because this was still well within a typical “real” motion, it would be missed by a hard threshold, but it was corrected by our interpolation method (Figure 3.9.C at 350 mA, green arrow). The abnormal peak at 540 mA was also corrected (Figures 3.9.A and C). On the other hand, manually inspecting the video recording after stimulation at 500 mA revealed that, despite the exceptionally high motion value (Figure 3.9.C at 500 mA - blue arrow), the tracking never actually failed. Accordingly, the high motion peak was unaffected by interpolation.

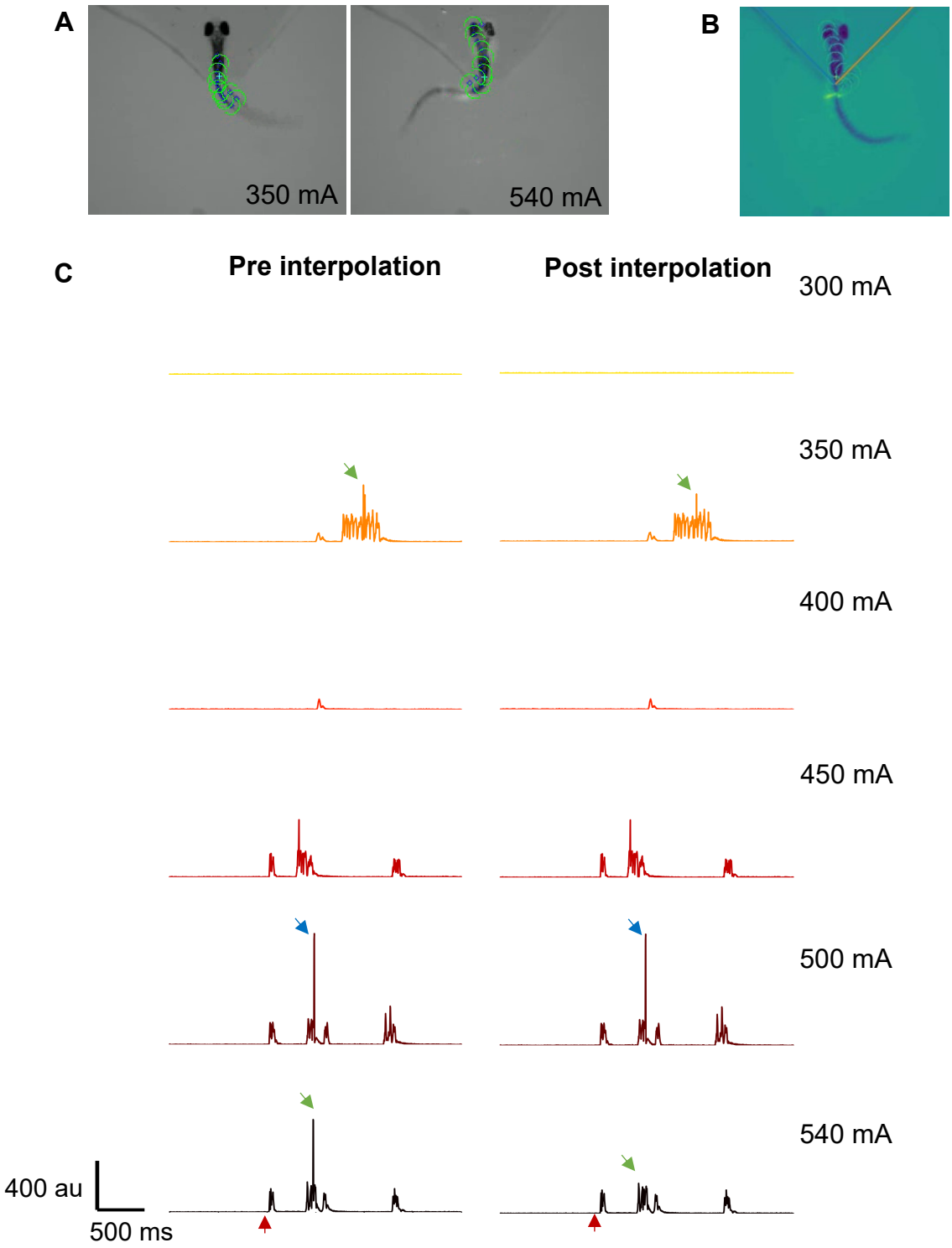

Figure 3.9: **Implementation of a linear interpolation method fixes instances where the tracking of the tail fails**. A: Examples of failed tracking. A blurred tail (left) or a spot of light (right) can affect tracking momentarily, with the tail of the fish being partly (left) or fully (right) "lost". B: An exclusion ROI was defined as the pixel coordinates between the blue and orange lines. C: Motion trace of a representative example of failed tracking before (left) and after (right) the linear interpolation method is applied to data points where tracking fails. This method successfully corrects the motion artifacts generated by failed tracking (green arrow), while "real" motion data points are not changed (blue arrow). Motion y axes range from 0 a.u. to 1000 a.u.. The red arrow indicates when the laser was switched on (t=0).

3.3 Discussion

The overall aim of my project was to establish the zebrafish as a model to study the genetics of nociception. In this chapter, I established an assay for the study of fast escape-like responses to noxious heat in zebrafish larvae (based on Haesemeyer et al., 2018). Here, an infrared laser is used to deliver short, temporally-precise noxious heat stimuli to 6-7 dpf head-fixed larvae. The laser generates heat, which induces a tail-flick “escape-like” response.

My first aim when setting up this assay was for the stimulus used to be short and temporally-precise, so that I could study fast escape-like behaviours. I measured laser kinetics and found them to be very fast and similar between intensities.

Secondly, I sought to deliver a noxious heat stimulus, since my goal was to study behavioural responses to noxious stimuli. To do that, I adapted the original assay developed by Haesemeyer et al. (2018) so that fish were stimulated with temperatures in the noxious range (greater than 34°C-37°C; Gau et al., 2013; Prober et al., 2008; Haesemeyer et al., 2015; Haesemeyer et al., 2018). Using a calibrated thermistor, I estimated the temperatures generated by my infrared laser. I found that higher laser intensities led to higher peak temperatures, and that peak temperatures across all intensities ranged from ~41°C to ~61°C. Contrary to what was described in the literature, with Malafoglia et al. (2013b) finding exposure to temperatures greater than 48°C-50°C to lead to severe damage or even death, I did not observe any obvious tissue damage after the full experiment, and larvae retained the ability to respond to light touch. This is to be expected, since my stimulus was more restricted than that used in Malafoglia et al. (2013b), both spatially (directed at a small area of the skin, rather than a full body immersion) and temporally (500 ms, less than 10% of the duration used in Malafoglia et al. (2013b)).

My third and final goal was to be able to elicit and record behavioural responses for further analysis. Pilot experiments showed fish to perform tail-flick responses upon exposure to the infrared laser but revealed a need for a series of optimisation steps. Using a high-speed camera with a specific filter added to it, I was able to record high quality, high-speed videos that could be analysed offline by segmenting and tracking the tail to then extract three initial tail kinematics

(cumulative angle, curvature and motion). I found that my infrared laser stimulus was able to reliably elicit fast tail-flick escape-like behaviours over a range of stimulus intensities, across the full duration of the experiment.

In short, I used an infrared laser to stimulate head-fixed zebrafish larvae with temperatures which I estimate to be in the noxious range, eliciting tail-flick behaviours (over a range of stimulus intensities) which can be successfully tracked for further analysis. In the following chapter, I will detail a series of experiments performed with this assay in order to validate it in a range of conditions. I will also look more closely at the behavioural responses generated by the infrared laser.

Chapter 4: Validating the infrared laser stimulation setup as an assay for noxious thermal stimulation of zebrafish larvae

4.1 Introduction

The role of the nervous system is ultimately to generate behaviour (Gomez-Marin and Ghazanfar, 2019; Datta et al., 2019). Indeed, behaviour is how nociception is functionally expressed. Animals can exhibit a variety of behaviours in response to noxious stimuli, from simple motor withdrawal reflexes to complex nocifensive behaviours. For instance, mice have been shown to respond to noxious stimuli with both fast withdrawal reflexes and full-body movements, and even stereotyped facial expressions (Schorscher-Petcu et al., 2021; Dolensek et al., 2020). Zebrafish larvae show increased locomotor activity upon exposure to noxious heat or chemicals such as allyl isothiocyanate (AITC), commonly known as mustard oil (Gau et al., 2013; Prober et al., 2008; Esancy et al., 2018; Ko et al., 2019). They are also capable of executing fast escape-like responses to acute noxious stimuli, with large-angle tail bends having been observed upon optovin-based trpa1 stimulation of head-fixed larvae (Wee et al., 2019). When studying nociception in non-human animals (and non-verbal humans), we rely on behavioural outputs as a proxy for the felt experience.

Ultimately, the overall aim of my project was to establish the zebrafish as a model to study the genetics of nociception. In this chapter, I sought to validate the infrared laser stimulation setup described in Chapter 3 as an assay for noxious thermal stimulation of head-fixed zebrafish larvae. I had three main aims.

The first aim was to characterise the behaviours elicited upon infrared laser stimulation. This characterisation of the tail-flick responses to noxious heat in wild-type fish will later allow me to infer a role for different genes in zebrafish, by comparing the responses of wild-type fish to the responses of mutants.

The second aim was to verify that the infrared laser is generating these behaviours exclusively (or at least primarily) through noxious heat rather than other types of sensory stimuli (e.g. auditory or visual). This was important because many of the behaviours displayed by zebrafish in response to noxious stimuli can be elicited by other types of stimuli as well. For instance, adult zebrafish show increased locomotor activity following acute restraint stress (Ghisleni et al., 2012); free-swimming zebrafish larvae can execute very fast, stereotyped escape responses, such as fast C-starts (latencies of less than 10 ms), in response to both acoustic and tactile stimuli, as well as O-bends (slightly slower but with latencies of still only a few hundred milliseconds), in response to visual stimuli (Wolman and Granato, 2011; Kalueff et al., 2013; Marques et al., 2018); and head-fixed larvae can perform tail-flick responses upon exposure to acoustic stimuli (Barrios et al., 2020).

The third and final aim was to test if my setup can be used to identify modulation of behavioural responses to noxious stimuli (in my case, heat). This would later ease the interpretation of any phenotypes I might observe in my mutants. To test that, I sought to modulate the response to the infrared laser using two chemicals: a local anaesthetic, lidocaine, and an irritant, AITC. Lidocaine, a sodium channel blocker, has an analgesic effect at low doses, having been shown to decrease sensitivity to noxious heat in mice (Binshtok et al., 2009). AITC has long been known to induce thermal hyperalgesia (increased sensitivity to heat) in both rodents and humans (Merrill et al., 2008; Albin et al., 2008).

I found that tail-flick escape-like responses can be elicited reliably across the full duration of the experiment using a range of laser intensities. These responses have two components: a fast one with a short-latency, and a slower one with a long-latency. I also demonstrated that these responses are elicited by (noxious) thermal stimulation, with minimal to no input from auditory or visual sensory stimuli, and can be modulated with a chemical irritant, AITC.

4.2 Results

4.2.1 There are two components in the tail-flick response to noxious heat

With the aim of better understanding the tail-flick behaviours elicited by different intensities of the infrared laser across the whole population, I looked at the average cumulative angle, curvature and motion traces across all trials of all fish (Figure 4.1.A). Focusing on average cumulative angles (Figure 4.1.A, left), it can be seen that while no bias is observed during baseline and from 2 s after the stimulus (cumulative angle values are close to zero), during the response there seems to be a bias towards a negative cumulative angle, which here corresponds to a tail flick to the right. Regarding the average curvature and motion across all fish (Figure 4.1.A middle and left, respectively), we can see that higher laser intensities lead to responses which are larger in amplitude and happen sooner, as predicted. Strikingly, all three traces reveal that there are two components in the response to the laser: a fast, short-latency (SL) response (purple arrows in Figure 4.1.A), and a slower, long-latency (LL) response. Plotting the cumulative distribution of response latencies across all trials shows these responses are clearly separated by latency, with the SL response taking place consistently at around 25 ms and the LL response after 100 ms (Figure 4.1.B). The two components were then further analysed separately, with a response being classed as SL if its latency was lower than 100 ms and LL if it was longer than 100 ms, as indicated by the purple dotted line in Figure 4.1.B.

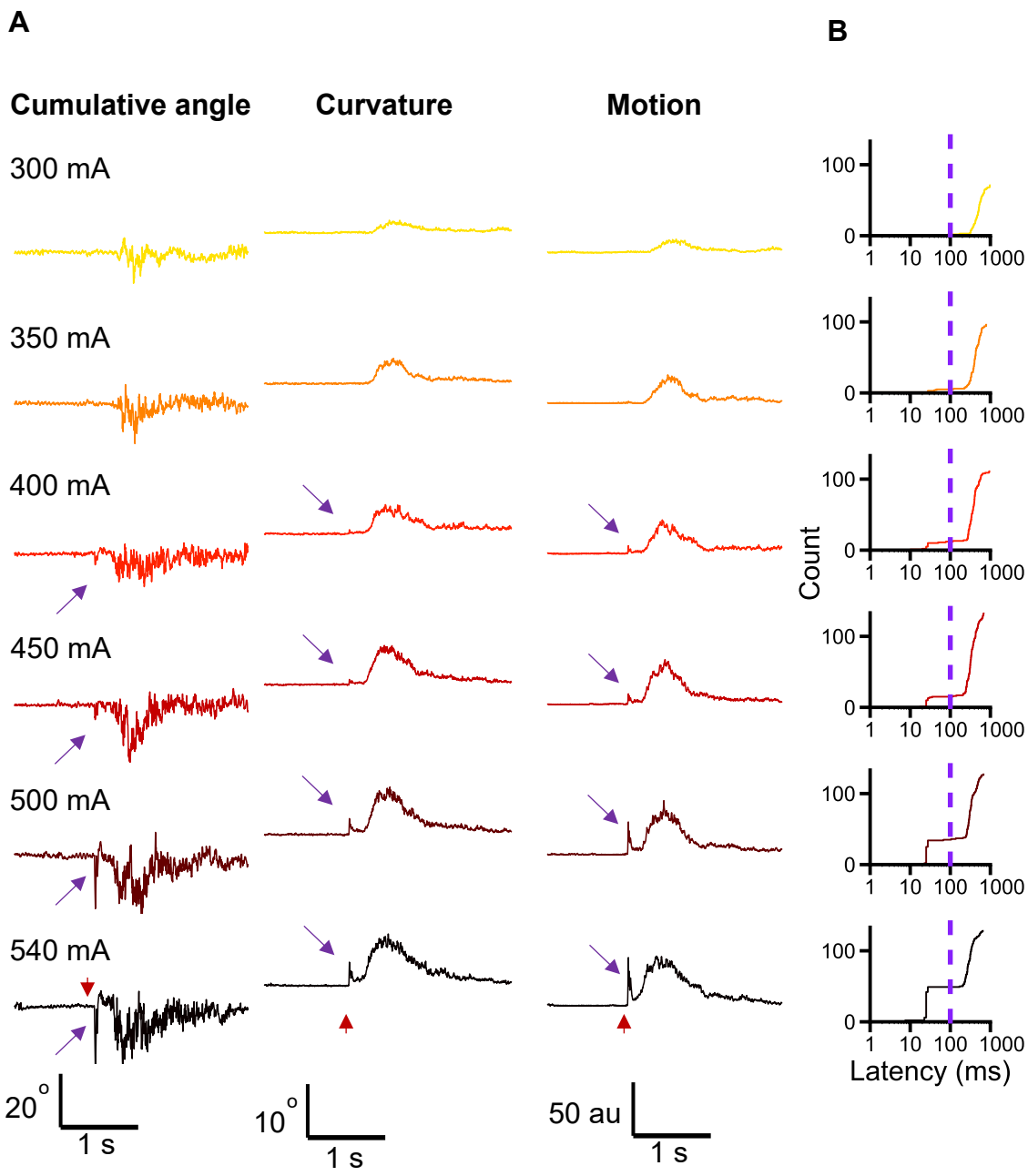

Figure 4.1: **There are two temporally distinct components in the tail-flick response to the infrared laser**. A: Average cumulative angle (left), curvature (centre) and motion (right) traces across all fish (n=59 fish). At the highest laser intensities, a short-latency (SL) response becomes apparent (purple arrows), followed by a long-latency (LL) response. Cumulative angle y axis ranges from -20° to 20°; curvature y axis ranges from 0° to 20°; motion y axis ranges from 0 a.u. to 100 a.u.. X axis shows time in ms. B: Cumulative distribution of response latencies across all three trials (n=177 trials). The x axis is shown on a logarithmic scale. There is a clear temporal separation between the SL (happening at approximately 25 ms) and LL responses (happening after 100 ms). For all subsequent analysis, a threshold was drawn at 100 ms (as indicated by the purple dotted line) to class a response to the laser as either SL or LL. The red arrow indicates when the laser was switched on (t=0).

As predicted, increasing the intensity of our stimulus leads to a higher LL and SL response probability (Figures 4.2.A and B, respectively). Interestingly, the LL response probability peaks at 450 mA (0.69±0.04) and decreases at higher laser intensities (0.60±0.04 at 500 mA and 0.56±0.05 at 540 mA). This could be explained by the fact that, at higher laser intensities, there is a higher chance that a fish will execute a SL response (Figure 4.2.B), and so fish might not be able to perform a second, “LL”, bout within the 1 s response window. Indeed, at higher laser intensities there is a higher probability of fish executing only SL responses (Figure 4.2.C). I also looked at total response probability, that is, the probability of a fish responding to the stimulus, regardless of whether the response was a LL or SL response (Figure 4.2.D). I found this to also increase with laser intensity and peak at 450 mA, however it does not decrease noticeably beyond that and instead reaches a *plateau* (total response probability is 0.75±0.04 at 450 mA, 0.72±0.04 at 500 mA, and 0.72±0.04 at 540 mA). This suggests a saturation of the response to the laser, which provides further evidence to the hypothesis that my stimulus is operating within the noxious range. Regarding response latency, LL response latencies decrease with increasing laser intensities and also reach a *plateau* from 450 mA (Figure 4.2.E: 525.3±25.6 ms at 300 mA; 455.8±17.2 ms at 350 mA; 416.0±19.3 ms at 400 mA; 383.5±14.7 ms at 450 mA; 378.6±16.7 ms at 500 mA; 379.1±18.0 ms at 540 mA). This again indicates we are saturating the response to the laser and that our stimulus is noxious. On the other hand, the latency of the SL response does not vary with laser intensity and is instead consistently around 25 ms, with the exception of SL responses at 300 mA (Figures 4.1.B and 4.2.F; 48.8±27.4 ms at 300 mA; 28.0±7.0 ms at 350 mA; 28.0±3.6 ms at 400 mA; 25.9±1.1 ms at 450 mA; 26.5±2.3 ms at 500 mA; 24.2±0.7 at 540 mA). This is likely because at lower intensities there are fewer SL responses (SL response probabilities: 0.011±7.853E-3 at 300 mA; 0.028±0.012 at 350 mA; 0.068±0.025 at 400 mA; 0.085±0.023 at 450 mA; 0.198±0.039 at 500 mA; 0.277±0.044 at 540 mA) and there is a mix between “real” SL responses and responses that simply happen to fall in the SL window, as suggested by the large SEM at lower intensities, especially 300 mA (Figure 4.2.F).

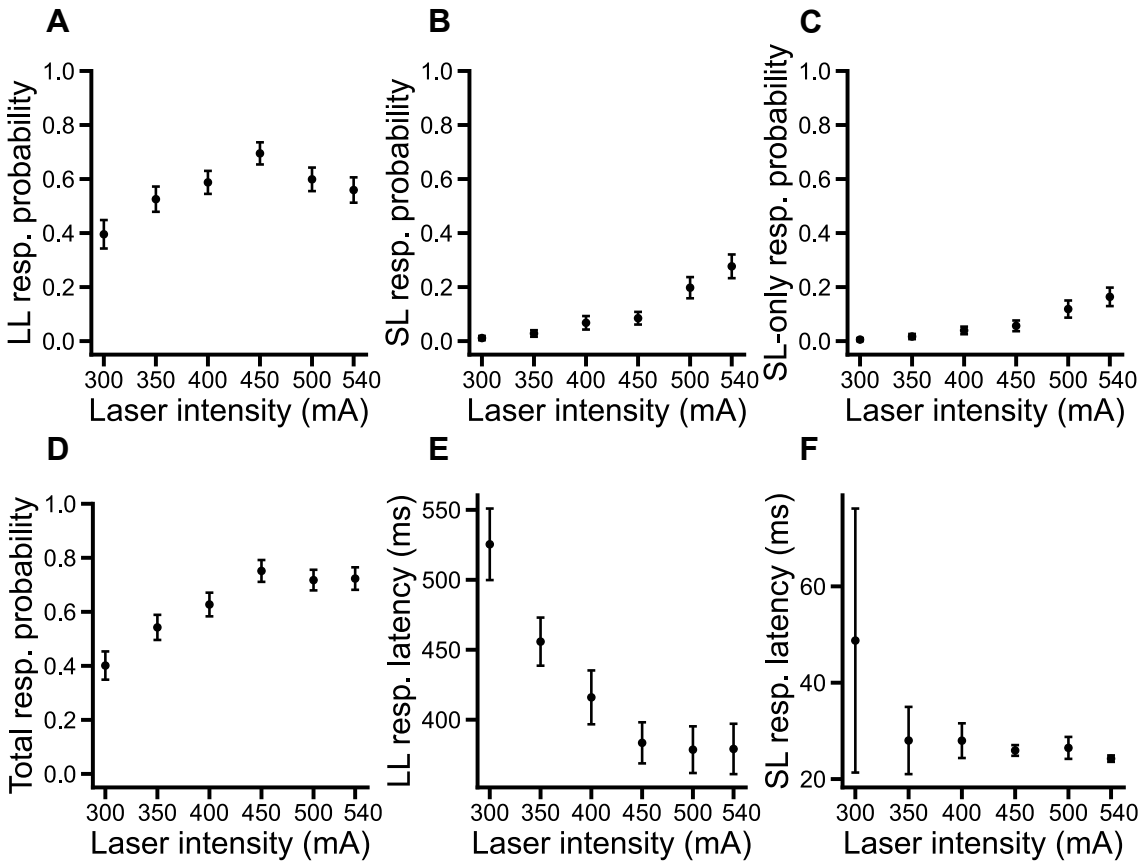

Figure 4.2: **Effect of laser intensity on response ("resp.") probability and response latency**. LL response probability increases with increasing laser intensity between 300 mA and 450 mA, peaks at 450 mA and then decreases (A). This decrease is mediated by the higher SL response probability seen at higher laser intensities (B), as shown by the higher rate of "SL-only" trials at those intensities (C). Total response probability reaches a plateau at 450 mA (D), which suggests a saturation of the response. The average LL response latency decreased with increasing laser intensities and also reaches a plateau from 450 mA (E). Conversely, the SL response latency did not change with laser intensity (F). N=59 fish. Error bars represent SEM.

I then looked at various metrics to characterise the LL (Figure 4.3) and SL (Figure 4.4) responses. Higher laser intensities elicit LL responses which are faster, as shown by the rightward shift in the cumulative distribution (CD) curves of peak motion and peak vigour as laser intensity increases (Figures 4.3.C and D) (vigour is calculated as the mean absolute difference in consecutive values of cumulative tail angle over a full bout). At higher intensities, LL responses to the laser appear to become more stereotyped (less variable), as indicated by the greater slope of the CD curves for peak motion and peak curvature (Figures 4.3.C and B). Peak cumulative angle, on the other hand, does not appear to be a very informative metric, seeing as it saturates at 180° across most trials at all laser intensities (Figure 4.3.A). I then focused on the SL response (Figure 4.4). To do that, I looked exclusively at the three highest intensities, since they elicit SL responses more reliably (Figure 4.2.F). Strikingly, the CD curves of all metrics analysed (peak cumulative angle, curvature, motion and vigour) do not appear to change across intensities, with the possible exception of peak motion and peak vigour at 450 mA (Figure 4.4). This suggests a generally stereotyped, possibly reflex-like, response. Finally, I sought to compare these metrics between the SL and LL responses. Figure 4.5 shows the CD curves of peak cumulative angle, curvature, motion and vigour for LL and SL responses at 540 mA (the intensity that elicits SL responses most reliably). The differences in the shapes of the CD curves of peak cumulative angle and peak curvature could suggest different bout types might be used in the LL and SL responses.

In short, infrared laser stimulation of tethered zebrafish larvae can elicit tail flick responses over a range of intensities. These responses have two components which appear temporally and kinematically distinct.

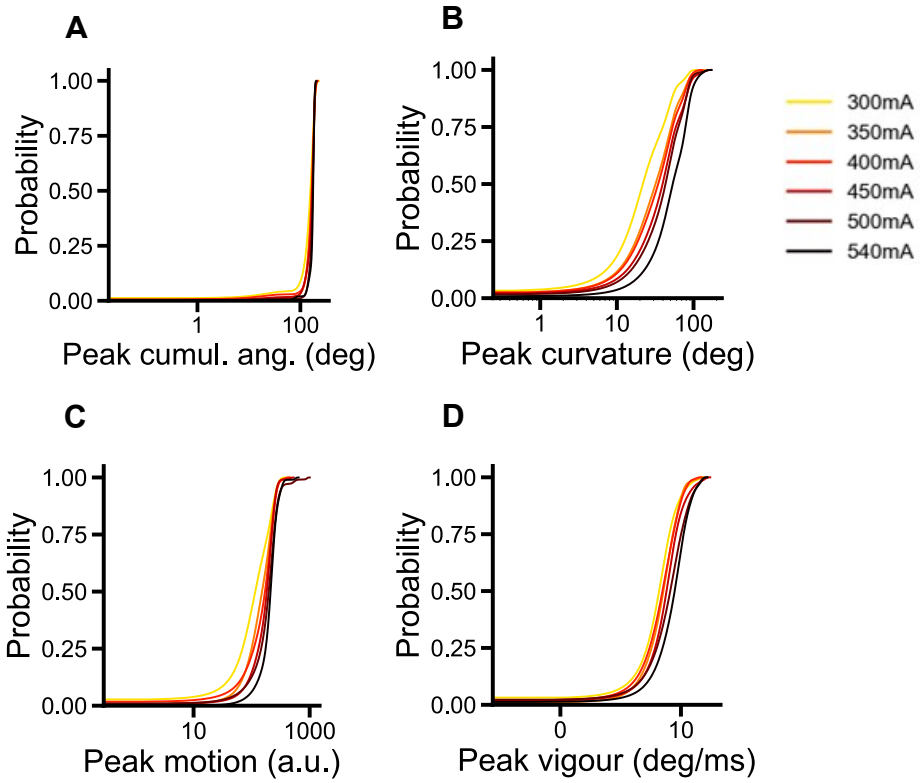

Figure 4.3: **The kinematics of LL responses change with increasing laser intensities**. Cumulative distribution plots of peak cumulative angle (A), curvature (B), motion (C), and vigour (D) are shown. The rightward shift in the cumulative distribution curves of peak motion (C) and peak vigour (D) at higher intensities indicates faster responses. Peak curvature also increases with laser intensity (B). Conversely, peak cumulative angle saturates at 180° across most trials at all laser intensities (A). The x axis is shown on a logarithmic scale.

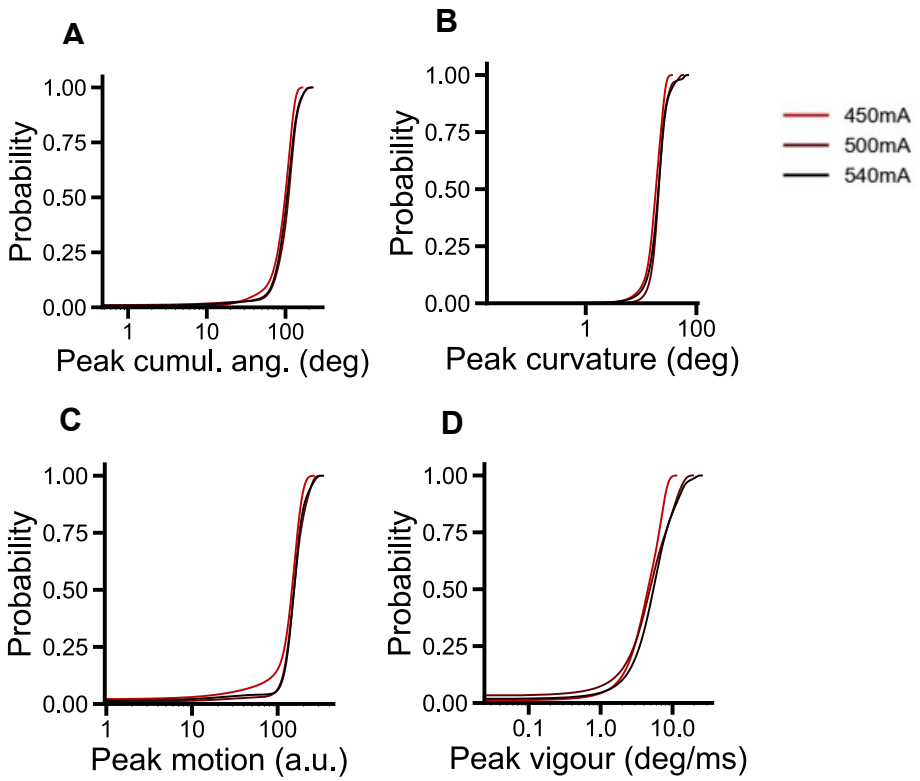

Figure 4.4: **The kinematics of SL responses do not change with increasing laser intensities**. Cumulative distribution plots of peak cumulative angle (A), curvature (B), motion (C), and vigour (D) are shown. Here, only responses to stimulation with the three highest intensities were analysed (450 mA, 500 mA, 540 mA), as they elicit SL responses more reliably. No clear difference is seen in any of the metrics analysed. The x axis is shown on a logarithmic scale.

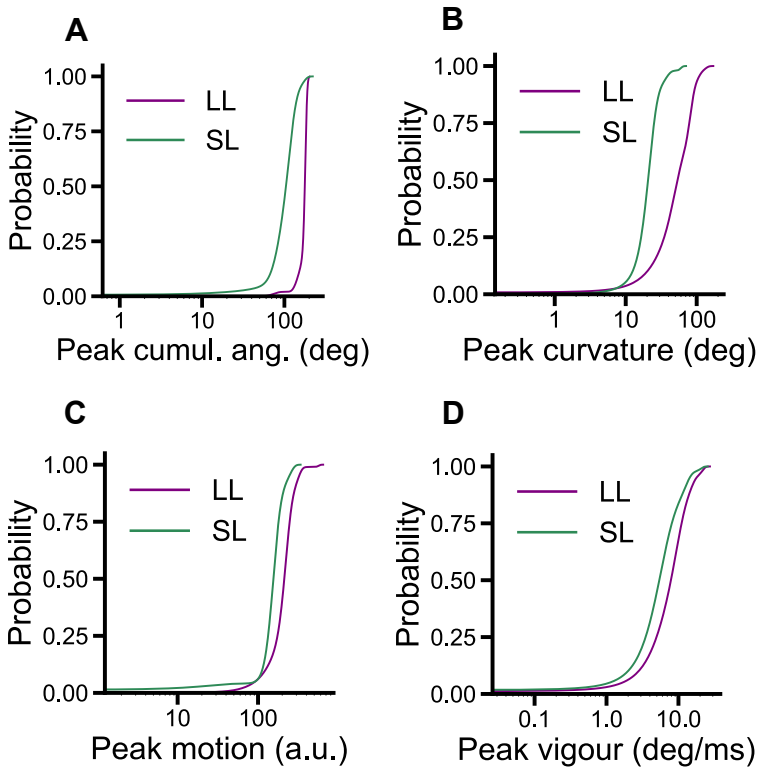

Figure 4.5: **The kinematics of LL and SL responses are different**. Cumulative distribution plots of peak cumulative angle (A), curvature (B), motion (C), and vigour (D), for LL and LL responses are shown. Here, only responses to stimulation with the highest intensity, 540 mA, were analysed, as it elicits SL responses more reliably. The differences in the shapes of the cumulative distribution curves of peak cumulative angle and peak curvature suggest different bout types might be used in the LL and SL responses. The x axis is shown on a logarithmic scale.

4.2.2 Individual factors underlying response to the infrared laser

It was intriguing to observe that the SL response happened reliably at around 25 ms (e.g. at 540 mA, 24.2±0.7 ms) and displayed little variability across the various bout kinematics analysed, which might suggest a stereotyped, reflex-like response, but that the probability of the response was low (less than 30% for all intensities). I hypothesised that there were two populations of fish, one that responded with a high response rate (100%), and another with a low response rate (0%) (Figure 4.6.A, right, “Model”). To test this hypothesis, I looked at the SL response probability of each fish at the highest laser intensity (the intensity which elicited a SL response most reliably) across the three trials (Figure 4.6.A, right, “Expt”). Contrary to what was hypothesised, there appeared to be a mixed population within the responding fish, with some responding in one of the three trials, some in two, and only a small percentage in all three trials. A mixed population was also observed with regards to the LL response probability across the three trials (Figure 4.6.A, left). I then looked at whether there was an effect of fish age or mounting time (how long fish were mounted in agarose prior to the beginning of the experiment) on overall LL or SL response probability across all intensities and the whole experiment. There was no significant difference between the LL or SL response probabilities of fish that undertook the experiment aged 6 dpf compared to those that were 7 dpf (Figure 4.6.B). I also could not detect any clear effect of mounting time on LL or SL response probabilities (Figure 4.6.C).

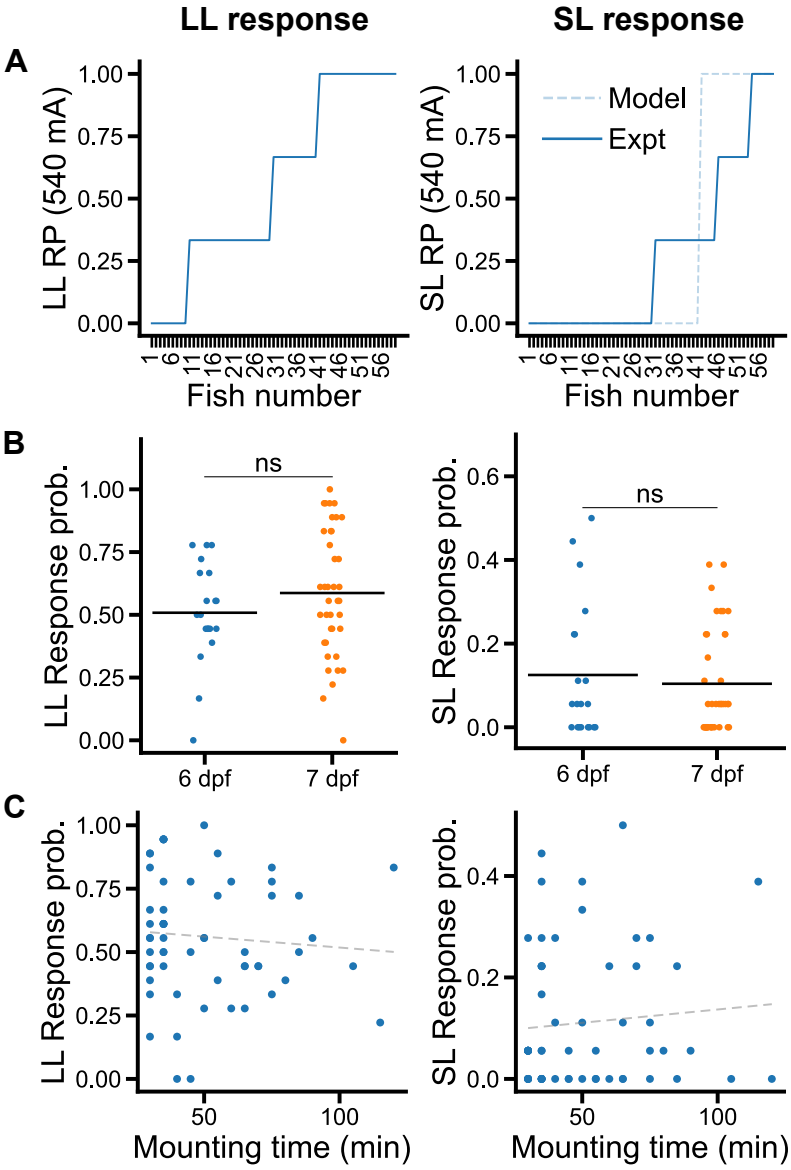

Figure 4.6: **Individual factors underlying response to the infrared laser**. A: There was a mixed population within the responding fish, with some responding in one of the three trials, others in two, and others in all three trials (at 540 mA; RP: response probability). This was true for both the LL (left) and SL (right) responses. The fish number on the x axis does not correspond to a specific fish (that is, Fish 1 on the LL response plot is not necessarily the same as Fish 1 on the SL response plot). The dashed line on the SL response plot illustrates a Model where two populations of fish exist, one that responds with a high response rate (100%), and another with a low response rate (0%). This Model did not match the data ('Expt'). B: Fish age does not affect the LL (left) or SL (right) response probability (n=59; LL response: F=-1.202, p=0.234 with an Independent Samples t-Test; SL response: F=402, p=0.848 with a Mann-Whitney U test). C: Mounting time does not have a clear effect on LL (left) or SL (right) response probability (n=59). Dashed lines represent a line of best fit across the data.

4.2.3 Repeated stimulation does not impact on response probability

Habituation and sensitisation to various sensory stimuli, including noxious stimuli, have been extensively reported across species upon repeated stimulation (Thompson, 2001; Purves et al, 2004; Jepma et al., 2014; Rennefeld et al, 2010). In larval zebrafish, for example, habituation in the acoustic startle reflex has been observed (Pantoja et al., 2016; López-Schier, 2019). Therefore, it was also important to determine whether repeated exposure to the heat stimulus could lead to changes in behaviour over time, for example due to sensitisation or habituation, which would lead to increased or decreased response probability, respectively. First, I looked at whether the intensity of the previous stimulus affected the LL or SL response probability to the current stimulus (Figure 4.7). The matrices in Figure 4.7 (left panel) show the LL (Figure 4.7.A) or SL (Figure 4.7.B) response probability to each pair of previous-current stimuli. For each 'previous stimulus intensity', there is a trend for increased response probabilities as 'current stimulus intensity' increases. This is true for both the LL and SL responses (Figures 4.7.A and B, respectively, middle panel). This can be seen more clearly after flattening the data along the X axis of the matrix, that is, averaging across 'columns' for each 'current stimulus intensity', as shown in the middle panel in the same figure. On the other hand, for each 'current stimulus intensity' no trend is observed in the matrix as the intensity of the 'previous stimulus' increases. Again, this is true for both the LL and SL responses. This can be seen clearly after flattening the data along the Y axis of the matrix, that is, averaging across 'rows' for each 'previous stimulus intensity' (Figures 4.7.A and B, respectively, right panel).

Finally, I also looked at the responses across the duration of the experiment (Figure 4.8). For each individual laser intensity, no clear difference was observed in the cumulative distributions of response latencies across the three rounds of stimulation. Overall, this suggests that, under my current assay conditions, the response to each stimulation is independent of the preceding stimulus and is consistent across the experiment, with no clear sensitisation or habituation to the infrared laser stimulus.

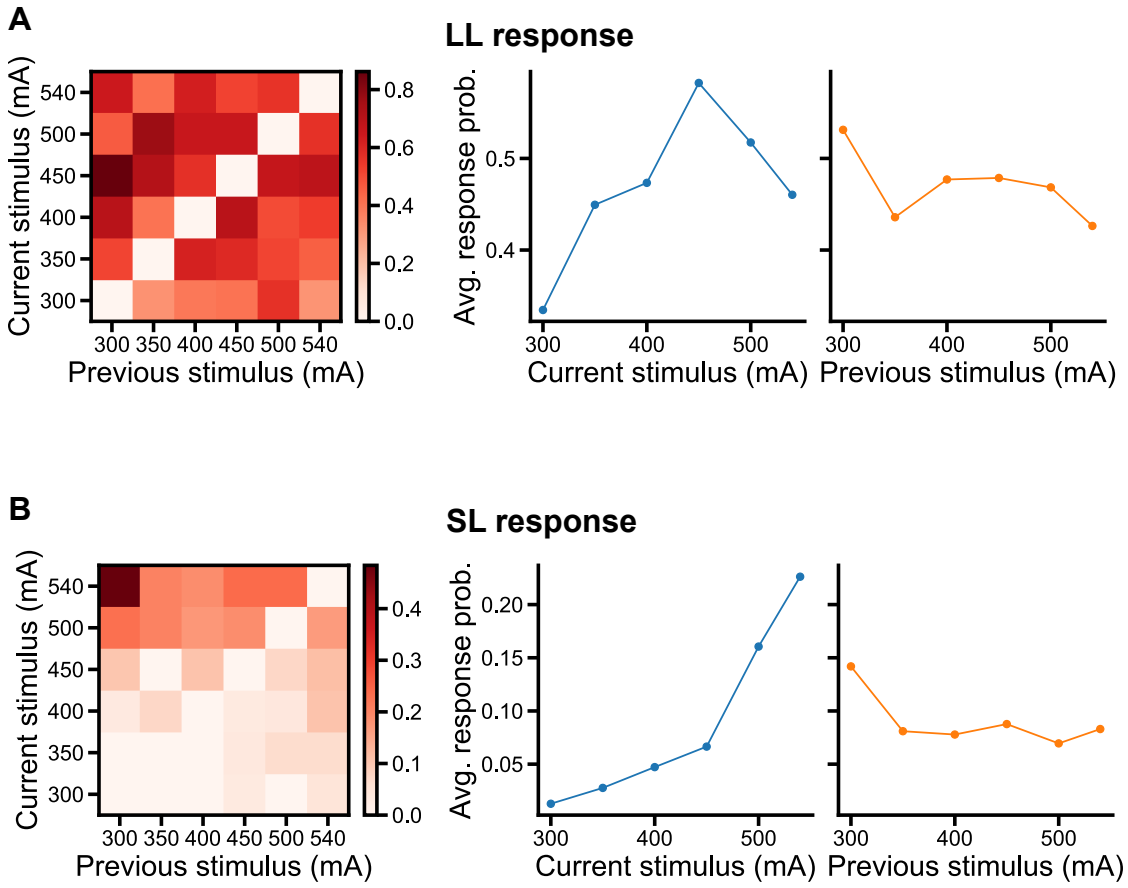

Figure 4.7: **The intensity of the previous stimulus does not affect the LL or SL response probability to the current stimulus**. The matrices (left) show the LL (A) and SL (B) response probability for each combination of previous/current stimulus (since each round was analysed separately, the intensities of the previous and current stimulus can never be the same). Averaging all response probabilities to each current stimulus (middle) shows, as observed previously, the LL response probability (A) increases with laser intensity up to a point where a plateau is reached (450 mA) and decreases after that, while the SL response probability (B) increases with intensity. On the other hand, averaging all response probabilities for each previous stimulus shows no effect of intensity on either LL (A) or SL (B) response probabilities, indicating the intensity of the previous stimulus doesn't affect the response probability to the current stimulus. N=59 fish.

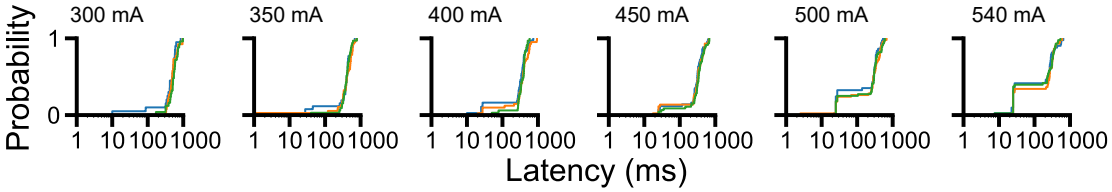

Figure 4.8: **The LL and SL response probabilities do not change over the three rounds of stimulation**. Cumulative distributions of response latencies across the three rounds of stimulation show no clear differences (blue: round 1; orange: round 2; green: round 3). The x axis is shown on a logarithmic scale.

4.2.4 Infrared laser elicits escape-like responses through thermal, not visual or auditory, stimulation

My goal was to determine whether the infrared laser was eliciting a response through heat and/or other sensory stimuli, for instance auditory or visual. An auditory stimulus could perhaps come from the laser being switched on, and a visual stimulus from the light of the laser itself. In the first experiment, fish were first positioned immediately adjacent to the position normally targeted by the laser (‘off-target’; Figure 4.9.A), and underwent the regular stimulation protocol. Each fish was then moved to the regular ‘on-target’ position for an additional round of stimulation. As shown in the representative motion traces of an individual fish (Figure 4.9.B), the response to the infrared laser is completely absent, at all intensities, when the fish is placed off-target, but it is present when the same fish is moved to the normal on-target position. In all the fish analysed, I recorded no tail-flick movements across all intensities of one round of stimulation when they were placed off-target, but observed normal responses, with both a SL and LL component, when they were moved back on-target for one round of stimulation (Figure 4.9.C). This strongly suggests that auditory stimuli did not contribute towards the behaviour elicited by the infrared laser.

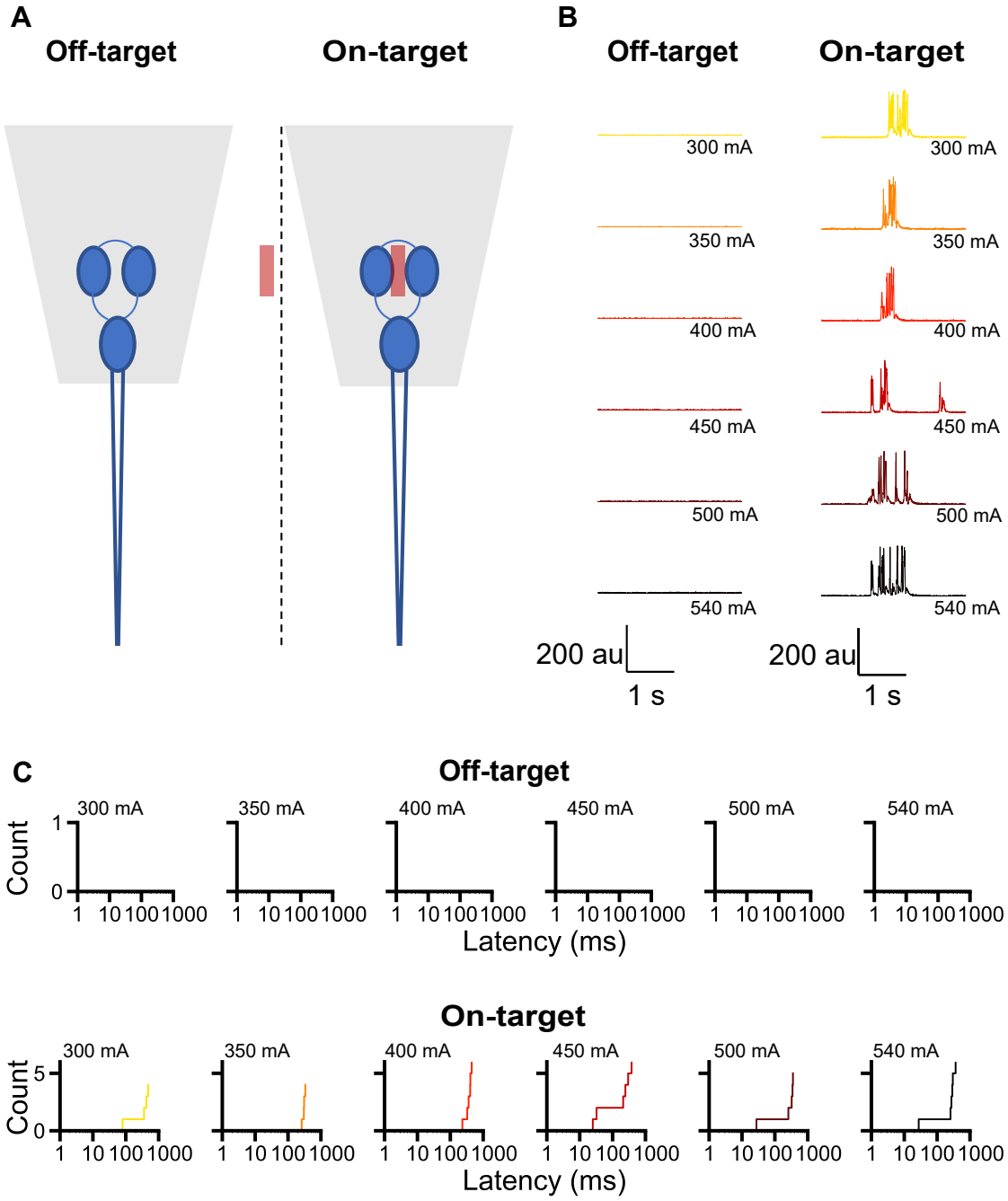

Figure 4.9: **Auditory input does not contribute to the response to the infrared laser**. A: Schematic showing the off- and on-target positions of the fish. The red rectangle represents the position targeted by the infrared laser beam and the agarose is shown in grey. B: Representative motion traces of a single fish across a single round of stimulation. No responses were observed in the "off-target" position. Once the fish is moved to the regular "on-target" position, responses can be observed again. X axis shows time in ms and ranges from -500 ms (before laser is switched on) to 2000 ms. C: Cumulative distributions of response latencies over one round of stimulation across the whole population of fish (n=8 fish). No responses were recorded when the fish were in the "off-target" position for one round of stimulation, but LL and SL responses could be recorded once they were placed in the normal "on-target" position for another round of stimulation. The x axis is shown on a logarithmic scale.

A visual response to our infrared laser was theoretically unlikely since none of the eight zebrafish opsins present in cones have been reported to show absorbance at wavelengths beyond 700 nm (Chinen et al., 2003; Nelson et al., 2019). Nevertheless, zebrafish larvae have been shown to exhibit negative phototaxis to near-infrared light at 860 nm, suggesting they can perceive light beyond 700 nm (Hartmann et al., 2018). Additionally, recent studies in rats have shown conserved visual capacity under red light, despite the fact that they are dichromats that possess ultraviolet and green cones, but not red cones (Nikbakht and Diamond, 2021). Moreover, my setup uses very strong light and, for the same wavelength, light intensity has been shown to positively correlate with light detection in mice (Naarendorp et al., 2010). Therefore, in my second experiment, I aimed to rule out with certainty a role of vision in eliciting these responses in the conditions of my assay. To do that, I used the retinally-blind *lakritz* fish, which are blind as a result of complete absence of retinal ganglion cells (RGCs; Kay et al., 2001). While *lakritz* mutants are normally darker than WT fish because they fail to adapt to bright, ambient light (hence the name “lakritz”, German for “liquorice”), the *lakritz* fish I had access to carried an additional mutation which leads to strongly reduced skin pigmentation, below WT levels (Lester et al., 1999). Therefore, to control for a potential effect of that decreased pigmentation on sensitivity to the laser, I performed these experiments on three groups of fish (Figure 4.10.A): retinally-blind fish (from here on referred to as ‘blind’), which were selected based on a lack of expression of RFP in the optic tectum (see Chapter 2 – Methods); sighted controls from the same batch (from here on referred to as ‘controls’), which were selected based on expression of RFP in the projections to the optic tectum and in the optic tectum; and pigmented WT fish from the same day (‘WT’).

Since accurate tracking of the tail of the fish relies on the contrast between the tail and background, which was largely decreased in the fish lacking pigmentation, I carefully examined a subset of the tracking videos from these experiments to reassess tracking performance in these fish. Indeed, I observed that tracking of the tip of the tail often failed, even when fish were stationary (Figure 4.10.B), something I had never previously observed in my experiments on WT fish. Since these tracking failures were normally restricted to the tip of the tail, they could not be detected and corrected by the quality control we had implemented previously (see Chapter 3). I sought to test whether excluding the

last third of the tail from the analysis (for these experiments only) would still allow me to detect tail movements in WT pigmented fish. Excluding the last four segments of the tail during analysis leads to motion traces where bouts have smaller motion values, as seen in the individual representative traces shown in Figure 4.10.C. This is to be expected, since motion values result from the sum of the changes in the position of the segment edges across the whole tail, so taking into account a smaller number of points would naturally lead to smaller motion values. Nevertheless, the cumulative distribution of response latencies obtained when analysing the whole tail versus the top two thirds, for the same six WT fish, suggests tail-flick responses are still being largely captured after excluding the last third of the tail from the analysis (Figure 4.10.D). Since the aim of these experiments was not to characterise the escape-like responses in detail, but simply to assess whether blind fish were capable of executing these behaviours in response to the laser, I proceeded to analyse these experiments taking into account only the top two thirds of the tail.

As shown in Figure 4.11, blind fish show LL response probabilities comparable to those of sighted controls, which suggests the LL response is not driven by visual cues. Focusing on the LL response at the highest intensity, 540 mA, Kruskal-Wallis test for ranks revealed a main effect of the experimental group (“WT” – n=6; “Control” – n=8; “Blind” – n=8) on LL response probability ($F=7.230$; $p=0.027$). Importantly, this was driven by the significantly higher LL response probability of the “WT” group, compared to the other two: post-hoc analysis using Dunn's multiple comparison test revealed no significant differences between the LL response probability in the “Control” and “Blind” groups ($p=0.588$). This difference in the LL response probability of pigmented and non-pigmented fish indicates that, as expected, the pigment on the skin of WT fish is important for the infrared laser to produce enough heat to reliably elicit a response, under my assay conditions. Regarding the SL response, my data is inconclusive, as the response probabilities were negligible, even at the highest laser intensity (WT=0.06; sighted controls=0; blind=0.04 at 540 mA). At 540 mA, only one WT fish and one Blind fish responded with a SL response (out of six or eight fish, for WT fish or blind fish, respectively), and only in 1/3 trials. The low SL response probability of pigmented WT fish was likely due to the small sample size (n=6). The occurrence of a SL response in blind fish appeared promising, despite the low response probability, as it would suggest blind fish retain the ability to respond

to the infrared laser with a SL response, indicating this response is not driven by visual cues. Since it only occurred in one trial, I then looked more closely at the original video file of that trial, to confirm the response was real. Unfortunately, I observed that it was not. In that particular trial, the fish executed a spontaneous bout, which started immediately before the laser was switched on, initially with the movement of just the end of the tail, and continued through the stimulation, increasing in amplitude and eventually involving the whole tail. Normally, this response would have been automatically excluded from the analysis, because its beginning preceded the stimulus start. However, since in these experiments only the top two thirds of the tail were considered for the analysis, and these only started moving after the laser was switched on (halfway through the actual bout), it was mistakenly counted as a SL response. As such, I was unable to detect SL responses in the blind fish. This is not unexpected given the low sample size (n=8) and since these fish are not pigmented, which significantly decreased the LL response probability. Further experiments are needed.

In short, the infrared laser elicits LL escape-like responses largely through thermal, not visual or auditory, stimulation. As for SL responses, I have ruled out a role of acoustic stimulation however, at present, I cannot conclusively rule out a visual contribution to the response.

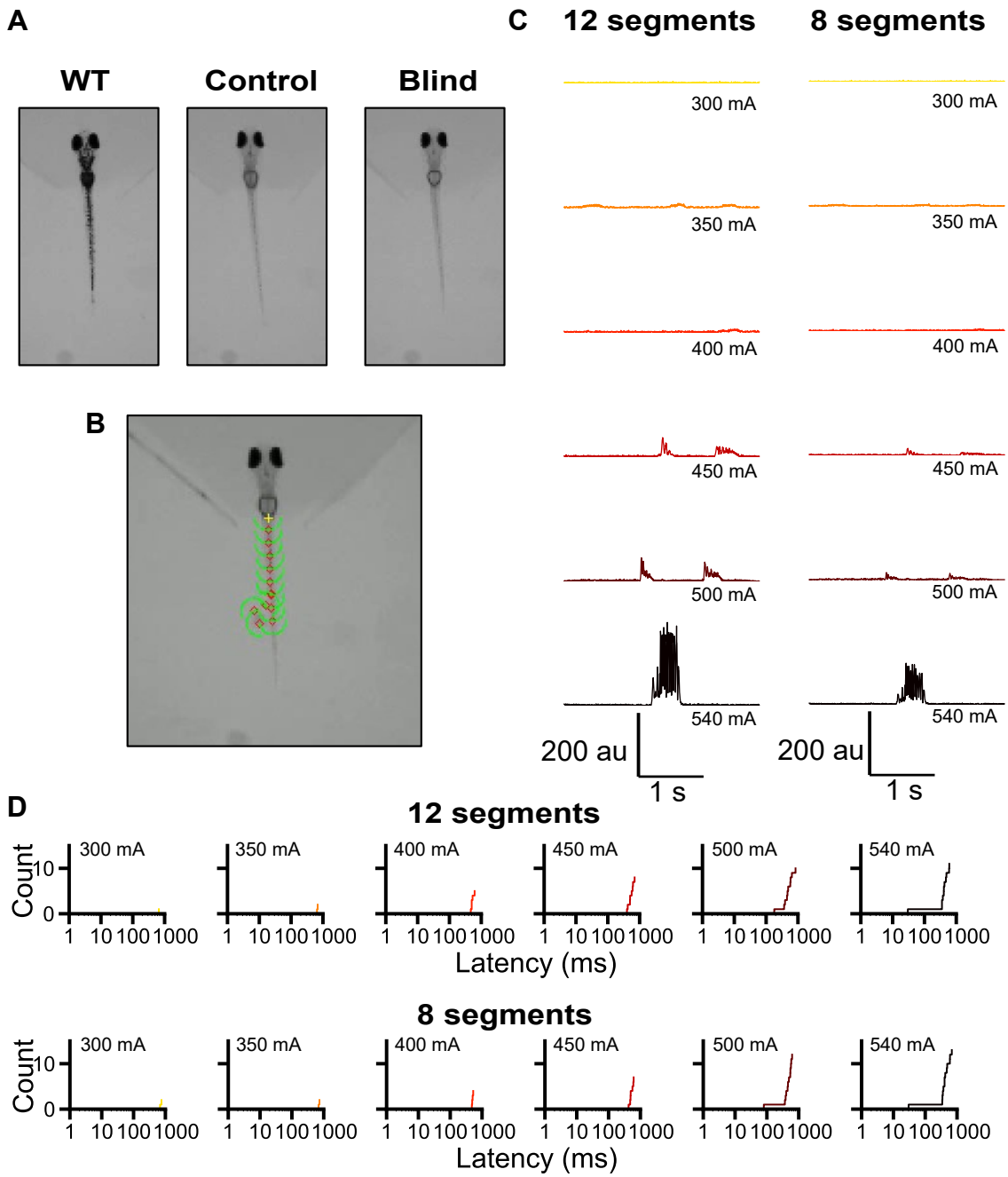

Figure 4.10: **Analysis of control experiments using blind fish**. A: To rule out a role of vision in eliciting the responses to the infrared laser, control experiments using retinally-blind lakritz mutants were carried out. Since the fish used in these experiments carried an additional mutation which strongly reduces skin pigmentation, three groups of fish were used in these experiments: retinally-blind fish ('blind', n=8); sighted controls ('controls', n=8); and pigmented WT fish ('WT', n=6). B: In fish lacking skin pigmentation, the contrast between the tail and the background is decreased, which often leads to failed tracking, even when the fish is stationary. C: Representative motion traces of a pigmented WT fish where either the full tail ('12 segments') or the top two thirds of the tail are analysed ('8 segments'). Motion y axes range from 0 a.u. to 300 a.u.. X axis shows time in ms and ranges from -500 ms (before laser is switched on) to 2000 ms. D: Cumulative distribution of response latencies obtained when analysing the whole tail versus the top two thirds suggests tail-flick responses are still captured (n=18 trials). The x axis is shown on a logarithmic scale.

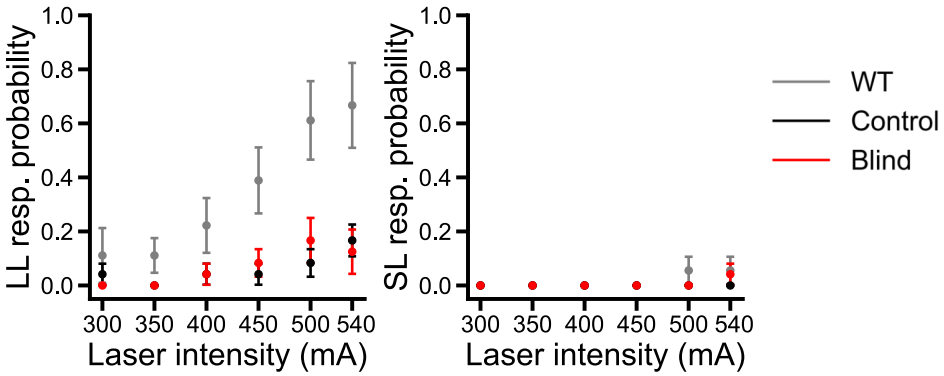

Figure 4.11: **The LL response is not visually driven, but a visual contribution to the SL response cannot be ruled out**. LL (left) and SL (right) response probabilities for WT (n=6), control (n=8) and blind (n=8) fish. The LL response is not visually driven, but skin pigmentation affects the response to the infrared laser: Kruskal-Wallis test for ranks revealed a main effect of experimental group on LL response probability (F=7.230; p=0.027), driven by the significantly higher LL response probability of the “WT” group, compared to the other two. Post-hoc analysis with Dunn's multiple comparison test revealed no significant differences between the LL response probability in the “Control” and “Blind” groups (p=0.588), which suggests the LL response is not visually driven. The data on the SL response is inconclusive, as the SL response probability was too low across all groups.

4.2.5 Sensitivity to the infrared laser can be changed using an irritant chemical

To test if my setup can be used to identify modulation of behavioural responses to noxious heat, I used two different chemicals: a local anaesthetic, lidocaine, and an irritant chemical, allyl isothiocyanate (AITC). They are known to have opposite modulatory effects on the sensitivity to noxious stimuli in humans, rodents, and zebrafish. Lidocaine has been shown to decrease sensitivity to noxious heat in mice and to prevent the behavioural changes induced by a noxious stimulus (acetic acid) in 5 dpf zebrafish fish (Binshtok et al., 2009; Lopez-Luna et al., 2017). AITC has long been known to induce thermal and mechanical hyperalgesia (increased sensitivity to heat or mechanical stimuli, respectively) in both rodents and humans, and it has been shown to lead to increased locomotor activity in zebrafish larvae (Koltzenburg et al., 1992; Merrill et al., 2008; Albin et al., 2008; Kroll et al., 2021; Prober et al., 2008). For both substances, the doses tested were selected after first performing a literature search to identify a preliminary range of concentrations, and then performing some pilot experiments, as detailed below.

For lidocaine, administration of 2 or 5 mg/L lidocaine 45 mins before a stressor (e.g. fin clipping) has been shown to reduce post-nociceptive behavioural patterns in adult fish, and administration of 5 mg/L lidocaine 40 mins before a noxious stimulus (acetic acid) prevented the behavioural changes induced by that noxious stimulus in 5 dpf fish (Schroeder and Sneddon, 2017; Lopez-Luna et al., 2017). Therefore, I selected 5 mg/L as my preliminary dose. Since lidocaine acts predominately by blocking voltage-gated sodium channels, having been shown to also block motor fibres (Gokin et al., 2001; Hermanns et al., 2001), it was important to first confirm that it did not have any general effects on locomotor activity at the concentration used. This was so that, should I observe a decreased response to the laser, this could be attributed with confidence to decreased sensitivity to noxious heat, rather than a generalised decrease in motility. To perform these experiments, I used a commercially available setup called Zebrabox (see Chapter 2 – Methods), which allows for high-throughput behavioural analysis of up to 96 free-swimming zebrafish larvae at any one time (one fish per well of a standard 96-well plate) (Lee et al., 2017, Lee et al., 2022), and studied the free-swimming activity of larvae after treatment with 5 mg/L

lidocaine. I also tested two other doses: 0.1 mg/L and 500 mg/L. 0.1 mg/L was a much lower dose which should show mild effects on behaviour, if any. Conversely, 500 mg/L was a much higher dose which should lead to a strong decrease of swimming behaviour due to anaesthesia or death. Indeed, lidocaine has been shown to abolish ventricular action potentials recorded from spontaneously beating hearts isolated from 48 hpf zebrafish embryos (Alday et al., 2014), and to induce light sedation or anaesthetic overdose in adult zebrafish at concentrations of 300 mg/L or 350 mg/L-1 g/L, respectively (Collymore et al., 2014; Collymore et al., 2016; von Krogh et al., 2021). The ability to induce death by overdose in larvae has not been as widely reported and remains a controversial issue in the literature (Collymore et al., 2016), but some studies have been able to demonstrate this (Mocho et al., 2022). Thus, treatment with 500 mg/L worked as a positive control to confirm the batch of lidocaine used was working. I performed these experiments on fish aged 5 dpf, since they are of similar age to those used in the infrared laser experiments (6-7 dpf) and show high basal levels of activity, which should allow me to detect an effect of lidocaine on free-swimming behaviour.

Figure 4.12 shows fish activity over the course of the experiment for each dose of lidocaine tested (water was used as negative control). This preliminary analysis of the raw data was performed with support from Dr Declan Lyons and Dr François Kroll, using custom analysis software from Professor Jason Rihel's lab at University College London, as described in Ghosh and Rihel (2020). To determine whether lidocaine affected locomotor activity, I compared total activity after exposure to the drug across groups (that is, after the time point indicated by the black arrow, t=0). "Total activity" was defined as the total area under the curve after fish were moved into the solution containing lidocaine (or water for the control). Kruskal-Wallis test for ranks revealed a main effect of lidocaine dose on total activity post drug ($F=18.582$; $p=3.335E-4$). As expected, post-hoc analysis using Dunn's multiple comparison test revealed that the highest concentration of lidocaine caused a significant and sharp decrease in locomotion (likely due to anaesthesia/death), which confirms that the lidocaine batch used was working. In contrast, the two lower doses showed no changes in locomotor activity compared to the water control. As such, 5 mg/L lidocaine may be used to test if lidocaine can modulate responses to infrared laser stimulation.

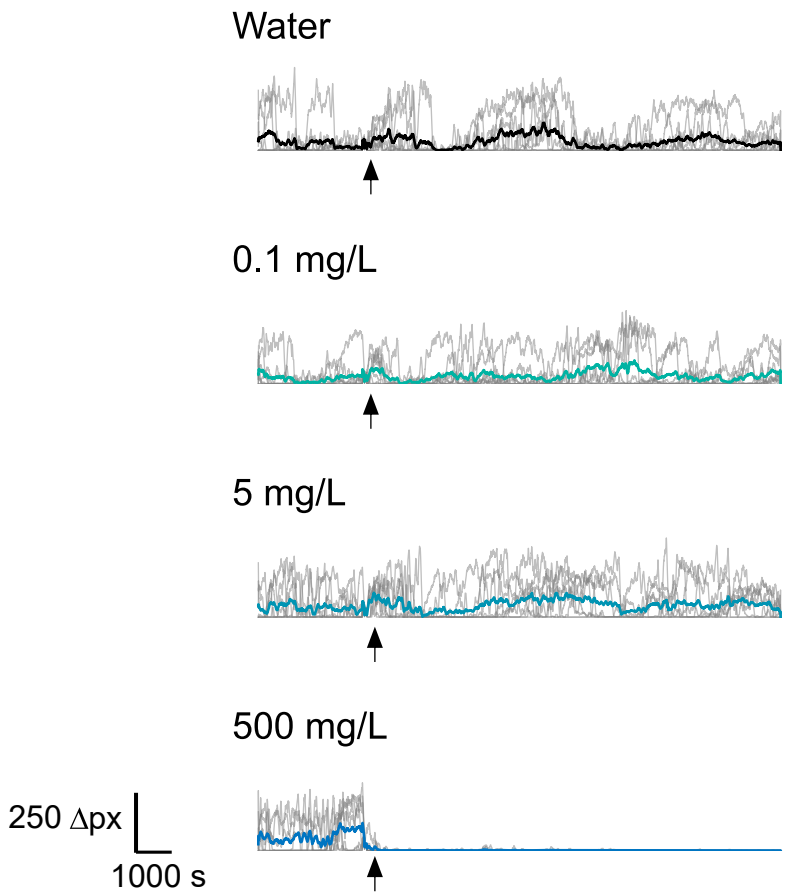

Figure 4.12: **Effect of lidocaine on the locomotor activity of 5 dpf zebrafish larvae in the free-swimming Zebrabox assay**. Grey traces represent the locomotor activity of individual fish over time; black or coloured traces represent the averages of all fish (n=8 fish per dose). The black arrow indicates t=0, when fish were treated with different doses of lidocaine (or water, for the controls). X axes show time in seconds; Y axes show Δ pixels (Δpx; total/second). Behavioural data was recorded by subtracting subsequent pairs of frames from each other and determining the number of pixels that changed intensity between each pair of frames (Δ pixels). These Δ pixels values were summed into 1 s bins and smoothed with a running average within a 15 min sliding window. Total activity post drug (total area under the curve after the black arrow) was compared across groups. Kruskal-Wallis test for ranks revealed a main effect of lidocaine dose on total activity post drug (F=18.582; p=3.335E-4). Post-hoc analysis using Dunn's multiple comparison test revealed the highest concentration of lidocaine caused a significant and sharp decrease in locomotion (p=0.002), while the two lower doses showed no changes in locomotor activity compared to the water control (p=0.9787 for 0.1 mg/L and p=0.3509 for 5 mg/L).

In this experiment (Figure 4.13.A), each fish first underwent three rounds of stimulation ('First half'), after which water (n=14 fish) or lidocaine were added to the dish (to a final concentration of 5 mg/L; n=14 fish; fish from five different clutches over five days of experiments were used). Following a 45 min incubation period, fish were put through another three rounds of stimulation ('Second half'). Surprisingly, no difference in LL response probability was detected during the second half of the experiment between fish treated with 5 mg/L lidocaine and water controls. Additionally, fish in the lidocaine-treated group had uncharacteristically low SL response probabilities (close to zero across all laser intensities, even at the highest intensities: 0.02 at 540 mA) during the first half of the experiment. As such, it would not be possible for me to test my hypothesis that 5 mg/L lidocaine would decrease the SL response to the laser. I was also unable to detect a clear effect of 5 mg/L lidocaine on the LL response probability.

Consequently, I next decided to test a higher dose of lidocaine, 10 mg/L (n=10 fish). In addition, I focused only on the responses to the four highest laser intensities (400 mA, 450 mA, 500 mA and 540 mA), because they elicit more reliably a response in untreated WT fish, meaning I should be able to more clearly detect an effect of lidocaine at these intensities. The experimental design was otherwise identical to that used to test 5 mg/L lidocaine. It is worth noting that, due to time constraints of the project, I did not carry out the preliminary testing of 10 mg/L lidocaine on the Zebrabox setup to look for potential effects of this dose on free-swimming locomotor behaviour. Instead, I decided to only perform these experiments if an effect on the sensitivity to the infrared laser were detected. Surprisingly, I was unable to detect any clear effect of 10 mg/L lidocaine on the response to the infrared laser: there was no clear change in the LL or SL response probability across all intensities (Figure 4.13.B). Additionally, there was a lot of variability across fish, particularly in the lidocaine-treated group, as shown by the large error bars (SEM). In my assay, lidocaine was administered by pipetting it into the water. I sought to do this consistently across fish, but there could have been small differences in exactly where and how it was pipetted, which might underlie part of this variability. In short, I tested two doses of lidocaine and was unable to detect an effect of either on the response to the infrared laser stimulus. This was unexpected since previous studies (Schroeder and Sneddon, 2017; Lopez-Luna et al., 2017) reported an effect of lidocaine in reducing behavioural responses to noxious stimuli. Compared to those studies, I administered

lidocaine using a similar method (diffusion in the water), with the same incubation time (45 min), and at the same (5 mg/L) or even higher (10 mg/L) concentration than those reported. The same strain of fish were used, and at similar ages (6-7 dpf in my study, compared to 5 dpf in Lopez-Luna et al., 2017). Strikingly, Schroeder and Sneddon (2017) used adult fish and still reported an effect at 5 mg/L. Future experiments testing higher concentrations are needed. For this, it would be interesting to first create a dose-response curve of the effect of different concentrations of lidocaine on the free-swimming behaviour of zebrafish larvae on the Zebrabox setup, and then selecting the highest doses that did not affect their behaviour to be tested on the infrared laser setup.

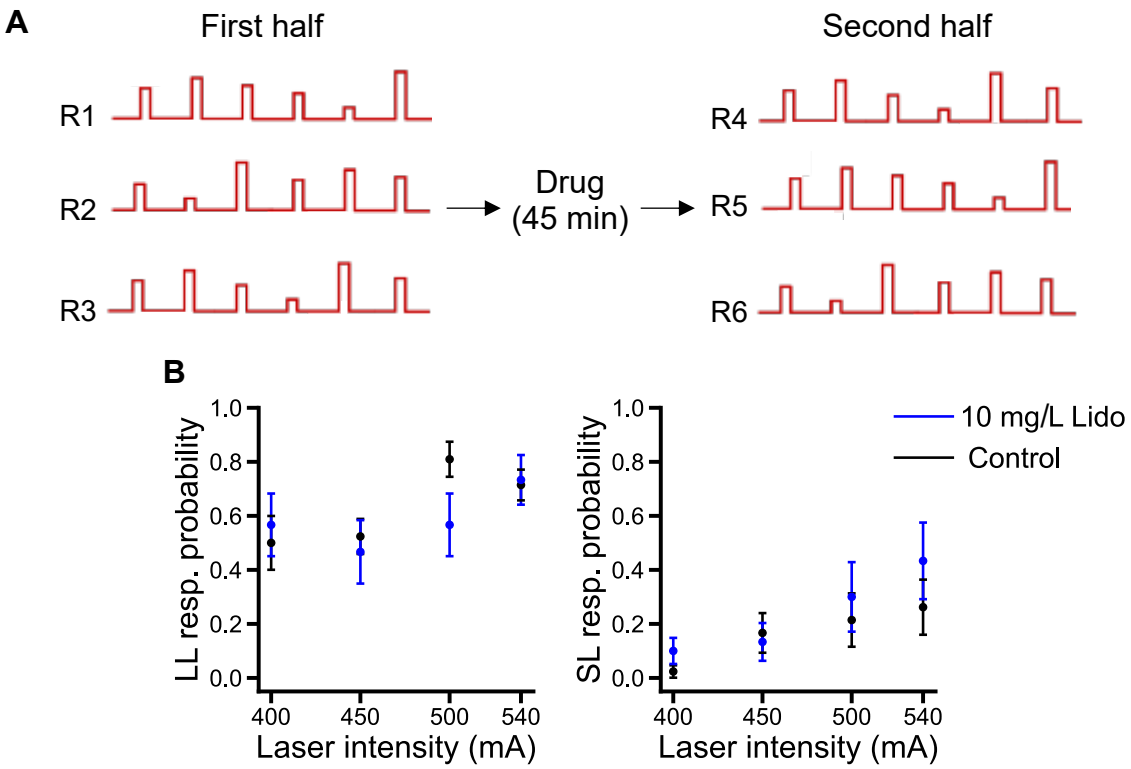

Figure 4.13: **Combining infrared laser stimulation experiments with lidocaine treatment**. A: Each experiment consists of a first half, during which fish go through the three rounds of laser stimulation, followed by a 45 min incubation in lidocaine (or water for controls), followed by a second half, during which fish go through another three rounds of laser stimulation. The LL and SL response probabilities in the second half of the experiment are then compared between fish treated with lidocaine and water controls. B: Incubation with 10 mg/L lidocaine has no clear effect on LL or SL response probability (n=10 for 10 mg/L lidocaine; n=14 for controls). Here, only the four highest intensities are shown, as they more elicit a response more reliably and, as such, any effect of lidocaine on decreasing the response probability should be more noticeable. Error bars represent SEM.

For AITC, the concentrations reported in the literature to affect the locomotor activity of larval zebrafish vary widely, from as low as 0.66 µM to 100 µM (Kroll et al., 2021; Prober et al., 2008). Importantly, since I wanted to explore the modulatory effect of AITC on the behavioural response to the laser, my aim was to select a subthreshold dose of AITC, that is, a dose that did not have an effect on behaviour on its own, but which might still potentiate the response to heat. With that in mind, I first tested seven different doses of AITC on 3 dpf fish using the same Zebrabox setup described above. I used 3 dpf fish as they have very low basal levels of locomotor activity, due to their swim bladders not being fully inflated at that developmental stage (Winata et al., 2009; Robertson et al., 2007). This would allow me to more clearly detect changes induced by AITC in their swimming behaviour. I selected both doses known to have an effect on behaviour (1 µM, 4 µM and 10 µM), which I used as positive control, and doses below that range (0.5 µM, 0.125 µM, 0.0625 µM, 0.03125 µM). To account for variability within clutches, I measured the activity of two batches of fish, collected on different days (for each dose of AITC, n=3 for batch 1 and n=4 for batch 2). Responses to each dose of AITC are shown in Figure 4.14. As predicted, 10 µM reliably increased the locomotor activity of fish (3/3 fish in batch 1 and 3/4 fish in batch 2), whereas the lowest doses (0.125 µM and below) did not induce any behavioural changes in any of the fish tested. Based on these results, I then proceeded to test the two lowest doses (0.03125 µM and 0.0625 µM) on 5 dpf fish, with the aim of confirming whether these doses still had no effect on the behaviour of larvae which are closer in age to those used in the infrared laser setup. As predicted, these fish have much higher basal levels of activity, which are maintained throughout the experiment (Figure 4.15). One-way ANOVA was unable to detect a main effect of AITC dose on total activity, defined as the total area under the curve after fish were moved into the solution containing AITC (or 0.5% DMSO; $F=1.884271$; $p=0.177$; n=8 fish per group), suggesting 0.03125 µM and 0.0625 µM do not lead to clear increases in the locomotor activity of 5 dpf larvae. To ensure that a sub-threshold concentration of AITC was used in the infrared laser experiments, I was conservative in my final selection of the doses to test on the infrared laser setup. As such, I selected 0.06 µM AITC and an even lower dose, 0.015 µM AITC.

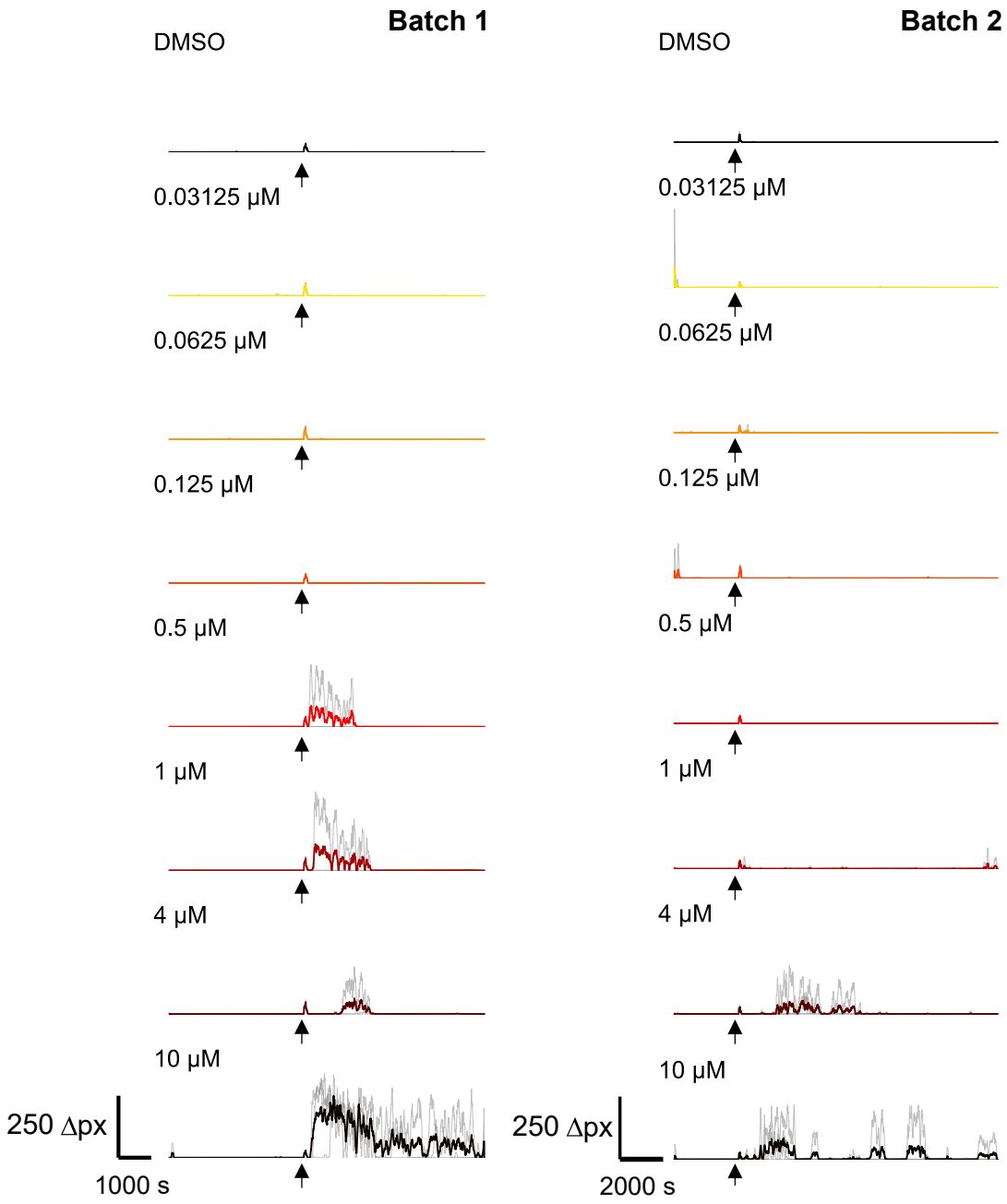

Figure 4.14: **Effect of different doses of AITC on locomotor activity of 3 dpf zebrafish larvae in the free-swimming Zebrabox assay**. Light grey traces represent the locomotor activity of individual fish over time; black or coloured traces represent the averages of all fish for two batches of embryos from two different days (n=3 per dose per batch). The black arrow indicates t=0, when fish were treated with different doses of AITC (or DMSO, for the controls). X axes show time in seconds; Y axes show Δ pixels (Δpx; total/second). Behavioural data was recorded by subtracting subsequent pairs of frames from each other and determining the number of pixels that changed intensity between each pair of frames (Δ pixels). These Δ pixels values were summed into 1 s bins and smoothed with a running average within a 15 min sliding window. Total activity post drug (total area under the curve after the black arrow) was compared across groups. 10 µM AITC reliably increased the locomotor activity of fish (3/3 fish in batch 1 and 3/4 fish in batch 2), whereas the lowest doses (0.125 µM and below) did not induce any behavioural changes in any of the fish tested.

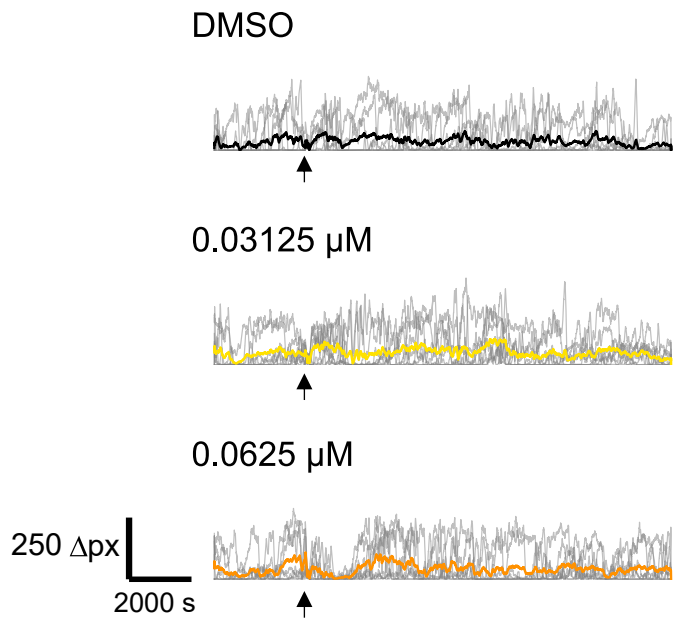

Figure 4.15: **Low doses of AITC do not affect the locomotor activity of 5 dpf zebrafish larvae in the free-swimming Zebrabox assay**. Light grey traces represent the locomotor activity of individual fish over time; black or coloured traces represent the averages of all fish (n=8 fish per dose). The black arrow indicates t=0, when fish were treated with different doses of AITC (or DMSO, for the controls). X axes show time in seconds; Y axes show Δ pixels (Δpx; total/second). Behavioural data was recorded by subtracting subsequent pairs of frames from each other and determining the number of pixels that changed intensity between each pair of frames (Δ pixels). These Δ pixels values were summed into 1 s bins and smoothed with a running average within a 15 min sliding window. Total activity post drug (total area under the curve after the black arrow) was compared across groups. One-way ANOVA was unable to detect a main effect of AITC dose on total activity ($F=1.884$; $p=0.177$; n=8 fish per group), suggesting 0.03125 µM and 0.0625 µM do not lead to increases in the locomotor activity of 5 dpf larvae.

Strikingly, treating zebrafish larvae with 0.015 µM AITC (n=9 fish), a very low concentration of AITC, led to a modest increase in the LL response probability at some laser intensities compared to controls (n=9 fish) (Figure 4.16.A, left), which was significant at 450 mA (with a Mann-Whitney U test: F=16.5, p=0.02), but not at 500 mA (with a Mann-Whitney U test: F=23, p=0.119). No clear effect was observed on the SL response probability (Figure 4.16.A, right). Therefore, I then tested a slightly higher (still subthreshold) dose, 0.06 µM AITC (n=10 fish). As predicted, treating zebrafish larvae with 0.06 µM AITC led to a stronger increase in the LL response probability (Figure 4.16.B, left). This increase was now significant across more laser intensities, from 400 mA to 500 mA (with a Mann-Whitney U test: F=20.5, p=0.038 at 400 mA, F=13.5, p=7.807E-3 at 450 mA; F=9.5, p=2.668E-3 at 500 mA). Interestingly, while there was now a trend towards an increase in the LL response probability at 540 mA, this was still not significant (with a Mann-Whitney U test: F=28, p=0.156). Regarding the SL response (Figure 4.16.B, right), while there appeared to be a slight trend towards a higher SL response probability at 540 mA, this was not significant (with a Mann-Whitney U test: F=26.5, p=0.115). As detailed previously, I was conservative in my selection of AITC doses to test, so it is likely that higher (still subthreshold) doses would significantly increase the SL response probability.

Looking more closely at the LL response probabilities of control fish (Figures 4.16.A and B), I observed these appeared lower than usual. For instance, my previous experiments had shown LL response probabilities of 0.69±0.04 at 450 mA, 0.60±0.04 at 500 mA, and 0.56±0.05 at 540 mA, which were much higher than those now shown by the control fish in these experiments (0.11±0.05, 0.26±0.09 and 0.48±0.11, respectively). To determine if this was due to these fish belonging to a particularly unresponsive batch of fish, I looked at the LL response probabilities of control fish during the first half of the experiment (rounds 1-3, before any drug was added), and compared them to those of fish that would later be treated with AITC, also during the first half of the experiment (before any drug treatment) (Figure 4.16.C). I did not observe any clear differences between groups. Therefore, it is likely that the low response probabilities of control fish in the second half of the experiment (Figures 4.16.A and B) are due to the length of the experiment, and not an unresponsive batch of fish.

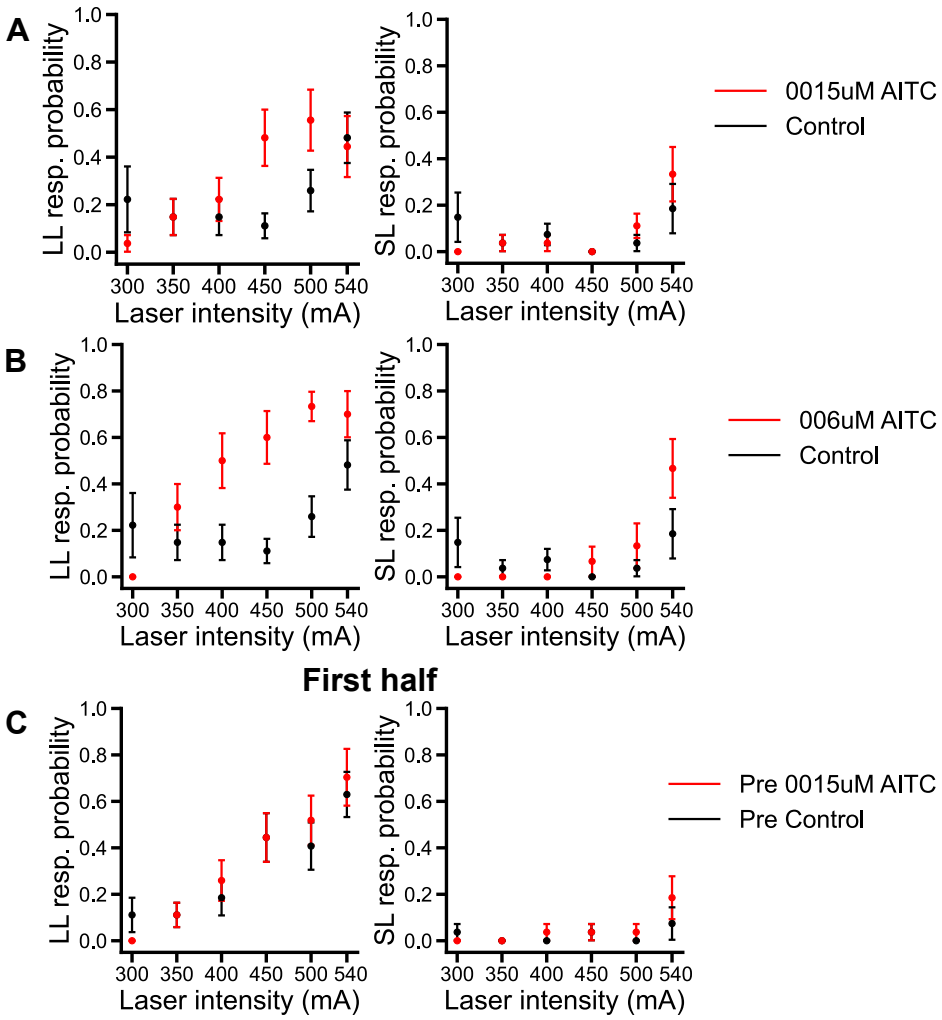

Figure 4.16: **AITC sensitises the response to the infrared laser in a dose-dependent manner.** Each experiment consists of a first half, during which fish go through the three rounds of laser stimulation, followed by a 45 min incubation in AITC (or DMSO for controls), followed by a second half, during which fish go through another three rounds of laser stimulation. In A and B, the LL and SL response probabilities in the second half of the experiment were compared between fish treated with AITC and DMSO controls. In C, the LL response probabilities in the first half of the experiment (rounds 1-3) were compared between fish that would later be treated with AITC and those that would be DMSO controls; this was to assess variability across batches. n=9 fish for DMSO controls, n=9 fish for 0.015 µM AITC; n=10 for 0.06 µM AITC. Error bars represent SEM. A: Incubation with 0.015 µM AITC led to a modest increase in the LL response probability at some laser intensities, which was significant at 450 mA (with a Mann-Whitney U test: F=16.5, p=0.02), but not at 500 mA (with a Mann-Whitney U test: F=23, p=0.119). No clear effect was seen on the SL response probability. B: Incubation with 0.06 µM AITC led to an increase in the LL response probability, which was significant from 400 mA to 500 mA (with a Mann-Whitney U test: F=20.5, p=0.038 at 400 mA, F=13.5, p=7.807E-3 at 450 mA; F=9.5, p=2.668E-3 at 500 mA). There was a trend towards an increase in the LL and SL response probabilities at 540 mA, however these were not significant (with a Mann-Whitney U test: F=28, p=0.156 for the LL response; F=26.5, p=0.115 for the SL response). C: In the first half of the experiment, no clear differences between any of these groups were observed.

In short, I was able to modulate the response to the infrared laser using AITC. Very low, sub-threshold concentrations of AITC significantly increased the LL response to the infrared laser, in a dose-dependent manner. I could not observe a significant effect of these doses on the SL response probability, but a trend was observed with the highest AITC dose tested. As such, it would be interesting to test the effect of higher doses of AITC on the SL response probability in future experiments. This suggests that my setup can be used to detect modulation of behavioural responses to noxious heat.

4.3 Discussion

In this chapter, I have characterised the tail-flick escape-like behaviours elicited in tethered zebrafish larvae by infrared laser stimulation. I found zebrafish larvae respond reliably to a range of infrared laser intensities over the full course of the experiment. I have shown for the first time that these responses have two components: a fast, short latency (SL) response, which happens less frequently but at constant latencies, when elicited; and a slower, long latency (LL) response, which happens more frequently, at variable latencies. Importantly, my data strongly suggests the infrared laser induces a response through thermal stimulation, with minimal to no input from other sensory stimuli (auditory or visual), and that this can be modulated with an irritant chemical, AITC. This, together with the temperature estimates from the thermistor experiments shown in the previous chapter, indicates this behavioural setup can be used to study and characterise fast escape-like responses to noxious stimuli in zebrafish larvae.

4.3.1 Infrared laser-induced escape-like responses in zebrafish larvae

As predicted, increasing the intensity of the infrared laser increased the response probability and elicited responses that were faster and larger (Figure 4.1). Zebrafish larvae have been shown to execute 13 distinct swim bout types, which are used in different contexts (Marques et al., 2018). Since my experiments were carried out in a head-fixed preparation, it is not possible to directly compare the kinematics of the bouts elicited with the infrared laser to those observed in freely swimming fish. Nevertheless, the large values of cumulative tail angles I describe (between 145.25± 7.03° at the lowest intensity and 171.39± 2.74° at the highest intensity, for the LL response) are consistent with those seen in swim bouts typically associated with escape behaviours, such as long- and short-latency C-starts (LLC and SLC). Indeed, Wee et al. (2019) reported similar values (100.11 ± 1.93°) in head-fixed fish in response to an aversive stimulus (optovin-based trpa1 stimulation). Interestingly, while cumulative angle values average out to zero (across the whole population of fish) during baseline and from 2 s after the stimulus (indicating a straight tail), there seems to be a bias towards a

negative cumulative angle during both the SL and LL response to the laser. This would indicate an overall bias towards a tail flick to the right (Figure 4.1.A). Individual zebrafish larvae have been shown to display an internal bias towards the left or the right in their initial response to heat (Li, 2012). This internal bias has also been observed in other behaviours, such as dark-induced circling and acoustic startle reflexes evoked in the dark (Horstick et al., 2020). However, if there were an equal probability of each individual fish having an internal bias towards the left or the right, there would be equal chances of each of them turning left or right in that first response to the laser, and so cumulative angle values would in principle be averaged out to zero over the whole population of fish, which is not what we observed. Instead, there appears to be a group bias. This could be explained by two main reasons. The first one would be experimental bias, for example, due to a bias in how the fish were mounted or positioned in relation to the laser. The second one would be that zebrafish have a collective bias (laterality) in their initial response to heat. Indeed, behavioural laterality in response to other sensory stimuli, particularly visual, has been widely studied in zebrafish larvae and it has been shown to partly correlate with neuroanatomical asymmetries in the brain (Miklosi et al., 1997; Watkins et al., 2004; Sovrano and Andrew, 2006; Barth et al., 2005).

4.3.2 Modulating the infrared laser-induced escape-like responses with lidocaine and AITC

I could not detect an effect of lidocaine on the response to the infrared laser, using concentrations previously reported to show an analgesic effect in both zebrafish larvae and adults (Schroeder and Sneddon, 2017; Binshtok et al., 2009; Lopez-Luna et al., 2017). I also tested a higher concentration (10 mg/L) and still observed no effect. As detailed previously, I was conservative in my dose selection, because lidocaine is a sodium channel blocker, which has been shown to block motor (as well as sensory) fibres (Gokin et al., 2001; Hermanns et al., 2001), which would be a confounding factor in my experiments. Higher doses of lidocaine should be tested in the future.

Conversely, I was able to modulate the response to my infrared laser stimulus using AITC, with larvae treated with AITC showing increased LL

response probabilities over a range of laser intensities. This was striking, because I was very conservative in my dose selection and used only sub-threshold concentrations (0.015 μM and 0.06 μM AITC) that were much lower than those reported to have a noxious effect (0.66 μM and higher - Kroll et al., 2021; Prober et al., 2008). This observed AITC-induced sensitisation to heat in zebrafish larvae is in line with previous work by Curtright et al. (2015), who found that free-swimming larvae showed sensitised temperature aversion upon incubation with 0.5 μM AITC. Compared to controls, they displayed increased avoidance of temperatures greater than or equal to 31.5°C and preferred normally neutral cooler (26.5°C) and aversive cooler (22.5–24.5°C) temperatures compared to 28.5°C. In the future, it would be interesting to test whether higher concentrations of AITC can also lead to changes in the SL response probability.

In short, I demonstrated my setup can be used to identify modulation of behavioural responses to noxious heat.

4.3.3 Understanding the two-component response to infrared laser stimulation

Cumulative distributions of response latencies to the laser revealed two components in the response: a fast, short latency (SL) response, only occurring in some of the trials; and a slower, long latency (LL) response, occurring in a higher number of trials. There was a clear temporal separation between the two components of the response, with the SL happening at around 25 ms, and the LL occurring in the hundreds of milliseconds range. To understand these responses and the mechanisms behind them, I first looked to determine whether they were at least partly driven by other sensory stimuli.

LL responses

An auditory contribution is ruled out. I first wanted to rule out conclusively a possible auditory contribution to the LL response that might originate from the laser being switched on. To do that, I placed the fish immediately adjacent to the position normally targeted by the laser during the assay. I found that this

completely abolished the LL response (Figure 4.9), which rules out an auditory contribution.

A retinal visual contribution is ruled out. A visual response to our infrared laser was theoretically unlikely since none of the eight zebrafish opsins present in cones have been reported to show absorbance at wavelengths beyond 700 nm (Chinen et al., 2003; Nelson et al., 2019), and the emission spectrum of our laser was restricted to 980 nm (as per the information on the supplier's website; see Chapter 2 – Methods). Nevertheless, it was important to completely rule out a visual contribution for the LL response under my specific assay conditions. This is because my assay uses strong light and, for the same wavelength, light intensity has been shown to positively correlate with light detection in rodents (Naarendorp et al., 2010). Moreover, zebrafish larvae show negative phototaxis to near-infrared light at 860 nm, suggesting they can perceive light beyond 700 nm (Hartmann et al., 2018), and they have been shown to perform visually-evoked responses to other wavelengths of light with latencies comparable to the LL response (Antinucci et al., 2020; Burton et al., 2017). Therefore, I performed the infrared laser stimulation assay on retinally-blind *lakritz* fish, which lack retinal ganglion cells (RGCs) (Kay et al., 2001). Since these blind fish showed LL response probabilities and latencies identical to those of sighted controls from the same batch, I have demonstrated that these responses are not visually-mediated. It is worth mentioning that both control and blind fish showed lower LL response probabilities than those of WT fish. This can likely be explained by their reduced skin pigmentation, which results from the *mitfa*$^{w2/w2}$ mutation that they also carried (Lester et al., 1999). Indeed, Haesemeyer et al. (2015) previously reported that the heat stimulus induced by an infrared laser normally acts by directly heating the fish pigmentation, rather than the water around it. The reduced LL response probability in non-pigmented fish, compared to WT controls, provides further evidence to the hypothesis that the LL response is elicited by heating the skin of the fish. Importantly, however, the fact that I still observed reliable responses in fish lacking pigmentation, particularly at the highest laser intensities, opens promising avenues for future work, by allowing for the infrared laser stimulation assay to be combined with whole-brain calcium imaging experiments (which require the use of non-pigmented fish). These experiments will be crucial to identify the key brain areas involved in the processing of noxious stimuli, similarly to what Haesemeyer et al. (2018) did for innocuous heat.

A non-retinal visual contribution is unlikely. It has to be noted that LL responses could also be driven by other visual, RGC-independent processes. For instance, deep brain photoreceptors have been shown to respond to light and drive behaviour, largely through the photopigment melanopsin (opn4; which is also the canonical marker of intrinsically photosensitive RGCs (ipRGCs); Berson et al., 2002). In fact, the pineal "light on" response is preserved in the retinally-blind *lakritz* mutants, with opn4xa+ projection neurons in the pineal of dark-adapted embryos showing induced *c-fos* expression after exposure to a 30 min pulse of white light. Moreover, photosensitive neurons in the preoptic area (likely those expressing *opn4a*) can drive light-seeking behaviour triggered by loss of illumination ("dark photokinesis") in larvae lacking eyes and pineal (Sapède et al., 2020; Fernandes et al., 2012). However, there are no records of visually evoked fast escape responses that do not involve the retina. For example, fast escape responses to looming stimuli have been shown to be completely abolished in the *lakritz* mutants, and the startle response observed when lights are abruptly switched off is abolished in *chokh* (*chk*) mutants, which completely lack eyes from early in development, as well as fish whose eyes have been surgically removed (Temizer et al., 2015; Emran et al., 2008; Easter and Nicola, 1996). Moreover, none of the zebrafish melanopsins have been reported to show absorbance at wavelengths beyond 700 nm (Davies et al., 2011; Matos-Cruz et al., 2011).

Integration of temperature information. Finally, previous reports have suggested that free-swimming larval zebrafish integrate temperature information over timescales of 400 ms, which would be compatible with our observed LL response times (Haesemeyer et al., 2015).

Taken together, this strongly suggests that the LL response was primarily, if not fully, driven by the heat stimulus.

SL responses

An auditory contribution is ruled out. With regards to the SL response, zebrafish have been shown to execute fast escape responses to acoustic, mechanical and visual stimuli, with latencies of less than 12 ms (Medan and Preuss, 2014). Moving the fish offset from the position targeted by the laser

completely abolished the SL response to the laser (Figure 4.9), which rules out an auditory component.

Possible retinal visual contribution. However, data from the blind fish experiments did not allow us to completely rule out a role of vision in generating the SL response, since the SL response probability was too low across all experimental groups. This was not unexpected, given the lack of pigmentation of these fish and the low probability of this response even in pigmented larvae. While I have largely ruled out a visual component in the LL response, it would be theoretically conceivable for a visual, RGC-dependent pathway driving the SL response to co-exist with the somatosensory pathway driving the LL response. Indeed, RGC-dependent fast C-start escapes to visual (looming) stimuli have been observed, with latencies as low as 9 ms (Temizer et al., 2015). Nevertheless, previous reports have also shown that free-swimming larval zebrafish can respond to heat stimuli within 50 ms, which would be compatible with my observed SL response times and suggest this response may be driven by heat (Haesemeyer et al., 2015). In the future, it would be interesting to carry out these experiments on large cohorts of pigmented blind fish, in order to conclusively rule out a visual contribution to this response.

4.3.4 A proposed nociceptive circuit in zebrafish larvae

The described two-component response to noxious heat suggests a complex, multi-pathway circuit underlying these behaviours. While it is beyond the scope of this thesis to identify and study this circuitry, a few potential regions of interest are identified below, and a simple circuit is proposed. Briefly, I propose that the noxious heat stimulus activates somatosensory neurons with cell bodies in the trigeminal ganglia, which project to different neurons in the hindbrain, which then either directly elicit the fast SL response, or elicit the slower LL response via the midbrain and forebrain (Figure 4.17). Some key neurons, nuclei and brain areas are highlighted schematically in Figure 4.18 and detailed below.

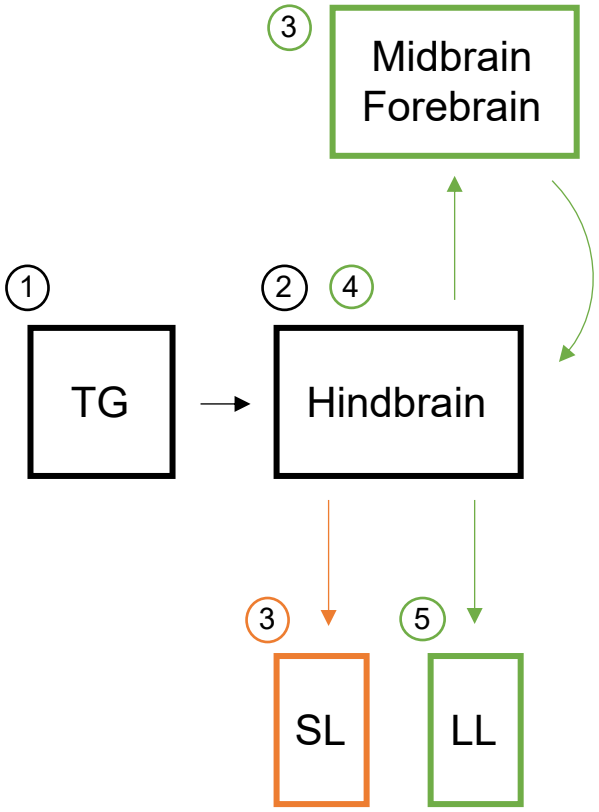

Figure 4.17: **Proposed step-by-step processing of noxious stimuli in zebrafish larvae to generate behaviour**. A noxious heat stimulus activates somatosensory neurons with cell bodies in the trigeminal ganglia (TG; 1), which project to different neurons in the hindbrain (2) which then either directly elicit the fast SL response (3 in orange) or elicit the slower LL response via the midbrain and forebrain (3-5 in green).

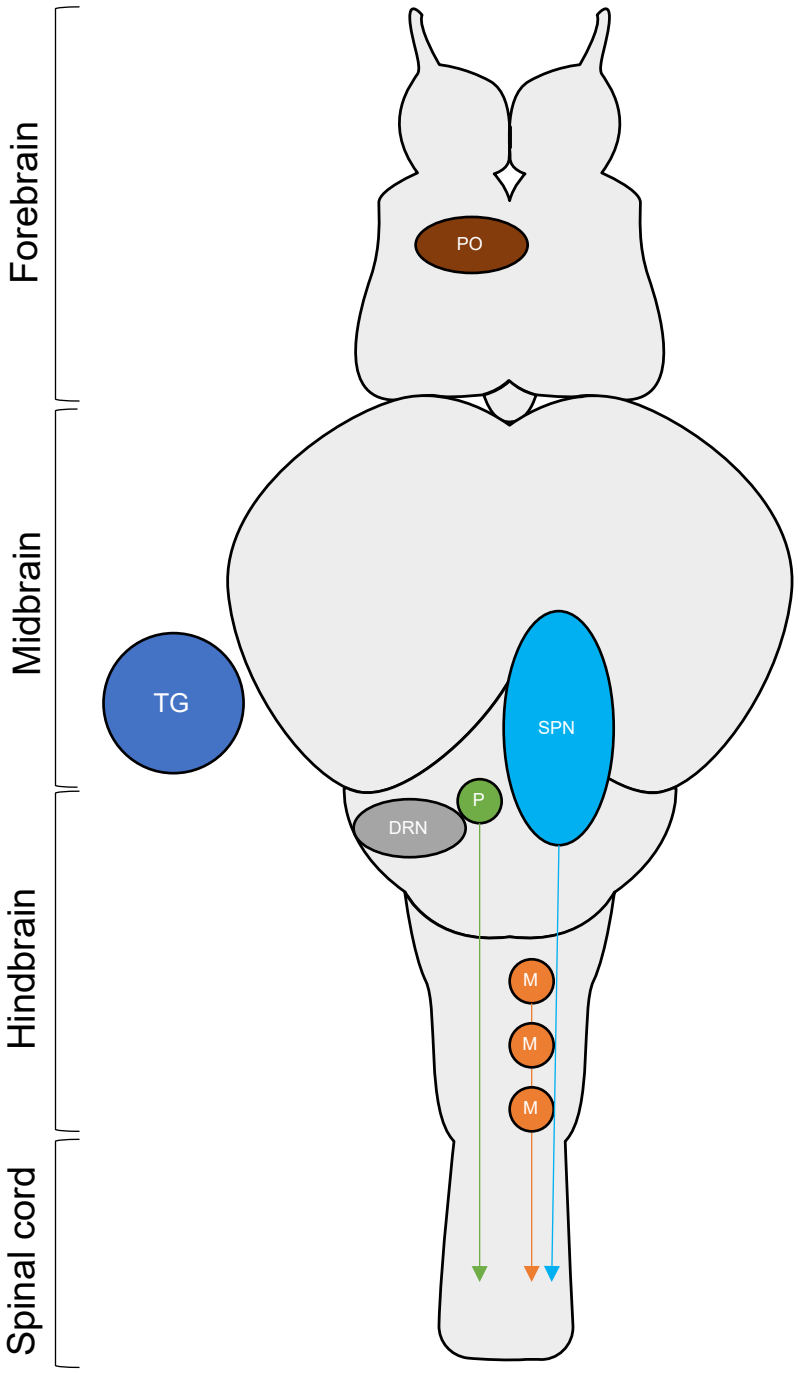

Figure 4.18: **Schematic showing a selection of neurons, nuclei and brain areas that are key for the processing of noxious stimuli**. Arrows indicate known spinal projections. SPN = ventral spinal projection neurons (including nMLF, in the midbrain), M = M-system (top to bottom: M-cell, MiD2cm, MiD3cm), P = prepontine neurons, TG = trigeminal ganglia, DRN = dorsal raphe nucleus. For bilateral structures (e.g., TG, M-system), only one is shown. Locations are approximate and sizes are not to scale. The original drawing of the brain was adapted from Gil Costa at SciDraw.

The M-system as a potential key player driving SL responses

The first component in the response to the infrared laser, which we termed SL response, was observed with increasing frequency at higher laser intensities (Figure 4.2.B), showed latencies of around 25 ms (Figure 4.2.F) and appeared stereotyped (Figure 4.4). The most promising candidate pathway to be mediating the SL response is that involving descending projections from Mauthner cells (M-cells), a bilateral pair of giant reticulospinal neurons that can trigger ballistic C-start escape responses with a single action potential, and their two homologs, MiD2cm and MiD3cm (from here on referred to collectively as the M-system). They have been extensively studied in various teleost fish (particularly goldfish and zebrafish) and shown to be at the centre of the fast escape behaviours executed by zebrafish in response to acoustic, mechanical and visual stimuli (Chang et al., 1987; Korn and Faber, 2005; Medan and Preuss, 2014). M-cell axons exit the medulla through the spinal cord to make direct contact with primary motoneurons and indirect contact with other motoneurons through a set of interneurons (Medan and Preuss, 2014). Reciprocal inhibition between the two M-cells, mediated by the excitatory cranial relay neurons (Ta1 and Ta2), is required for good escape performance (Shimazaki et al., 2019). Calcium imaging has revealed the M-cell responds during the large escapes produced by mechanical stimulation of the tail, and all three cells respond together upon stimulation on the head (O'Malley et al., 1996). Accordingly, laser ablating M-cells abolishes fast C-start responses to tail- (but not head-) directed tactile stimuli, while ablating all three cells abolishes fast C-start responses to both head- and tail-directed stimuli (Liu and Fetcho, 1999). With regards to the acoustic startle response, hair cells in the otic vesicle stimulate eighth (VIII) nerve fibres that directly activate the M-cell (at mixed chemical and electrical synapses), which in turn activates motor neurons, leading to the initiation of the stereotyped C-start response (Yao et al., 2014; Marsden and Granato, 2015). Finally, an escape response to threatening visual stimuli mediated by the M-system has also been described, where information is conveyed from the retina to the optic tectum (the zebrafish homolog to the mammalian superior colliculus), which sends afferents that contact both M-cells to then generate fast C-start escapes (Medan and Preuss, 2014; Preuss et al., 2006; Yao et al., 2016; Dunn et al., 2016; Marquez-Legorreta et al., 2020).

Importantly for us, the M-cell has long been known to receive input from trigeminal ganglia (TG) sensory neurons, which are pseudounipolar neurons, with peripheral axons arborising on the surface of the head and central axons projecting to the hindbrain (Kimmel et al., 1990; Metcalfe et al., 1990; Takahashi et al., 2002). Interestingly, while earlier studies suggested TG fibres enter the hindbrain at stereotypically defined points at the level of rhombomere 2 (Yeo et al., 2004; Metcalfe et al., 1990), more recent studies have found subtypes of TG sensory neurons, namely those expressing *trpa1b*, to project to rhombomeres 5 and 6, where the two M-cell homologs are located, as well as directly to the spinal cord (Pan et al., 2012). While trpa1b is not thought to play a significant role in heat sensation in zebrafish larvae (Prober et al., 2008), contrary to what is seen in rodents (Vandewauw et al., 2018), the existence of these projections nevertheless suggests that TG sensory neurons carrying information about aversive stimuli project to hindbrain regions that would be relevant for the generation of fast escape behaviours. Importantly, Haesemeyer et al. (2018) also identified a prominent cluster of heat-sensing cells in rhombomeres 5/6. Finally, indirect evidence from laser ablation experiments suggests that stimulation of TG neurons may be involved in generating fast responses. In these experiments, ablating one TG in zebrafish larvae resulted in the abnormal expansion of the trigeminal sensory arbour of the remaining TG across the midline of the head, and this led to behavioural defects in the laterality of the response to mechanical stimulation to the head (Sagasti et al. 2005). This demonstrates TG neurons can mediate stereotyped escape behaviours to somatosensory stimulation.

Our observed response latencies (25 ms) were longer than those typically elicited by the M-system (4-10 ms; Marquart et al., 2019, Temizer et al., 2015). However, this could easily be explained by the differences between the types of sensory stimuli used: while the acoustic and visual stimuli are almost instantaneous, our heat stimulus is not, and a delay is to be expected between the laser being switched on and the temperature of the skin of the fish reaching the threshold that would activate nociceptors (see also Chapter 3). Indeed, our response latencies are in line with previous experiments, where photoactivation of somatosensory neurons using channelrhodopsin-2 (ChR2) triggered escape behaviours with latencies of around 30 ms (Douglass et al., 2008).

Our SL response probability was relatively low across the whole population of WT fish, even at the highest laser intensities (0.277±0.044 at 540 mA – Figure 4.2.B). Further, I found variability in the SL response probability within each SL responding fish, with some responding in one of the three trials, some in two, and only a small percentage in all three trials (Figure 4.6.A). Conversely, Lacoste et al. (2015) found that a tap stimulus could elicit fast escape-like responses in tethered zebrafish larvae with almost 100% probability (99.7%), with over 90% of those showing short latencies (12 ms or less) and the others slightly longer latencies (13-25 ms). There are many factors that could explain my results. Firstly, there could have been slight inconsistencies when mounting the fish (e.g. depth along the agarose) or positioning them under the infrared laser, but this is unlikely to explain the variability seen within each fish. Instead, this suggests that the SL response may be modulated by other factors or circuits. This is not unexpected. Indeed, variability in the probability of a noxious stimulus eliciting a reflex withdrawal response has been seen in mice (Browne et al., 2017; Schorscher-Petcu et al., 2021). Moreover, internal states can affect behaviour in zebrafish. For instance, Johnson et al. (2020) found that the bout types and interbout intervals selected by free-swimming fish can be affected by internal hunger states, as well as behavioural history. Interestingly, in zebrafish, neuromodulatory input from serotonergic neurons in the **dorsal raphe nucleus** (DRN) has been found to mediate inter-individual variability in short-term habituation to the M-cell-mediated acoustic startle response (Pantoja et al., 2016). Pantoja et al. (2016) found that both M-cells and DRN neurons, which project into the vicinity of M-cells, are activated by the acoustic stimulus. DRN neuron responses were evoked more frequently when the sound stimulus also induced an acoustic startle response, suggesting a possible causal link between DRN neuron activation and behaviour. DRN neuron responses varied widely across individuals, with individuals with low habituation to the acoustic stimulus showing sound-evoked activity in a larger number of DRN neurons than individuals with high habituation. Overall, this suggests that DRN neuron activation by the acoustic stimulus suppresses acoustic startle response habituation, and inter-individual variability in this activity mediates inter-individual variability in habituation to the stimulus. It would be interesting to explore whether this or other circuits are also modulating the SL response to the infrared laser.

In short, the M-system appears to be a promising candidate pathway driving the SL response, which may also be modulated by other circuits. Future experiments could help clarify this. These include: imaging *c-fos* expression in M-cells after the infrared laser assay (*c-fos* is an immediate early gene whose expression is associated with increased neural activity – Herrera and Robertson, 1996); performing the infrared laser stimulation experiments on zebrafish transgenic lines expressing genetically encoded calcium indicators in the M-system, such that the activity of the M-system in response to the laser can be monitored in real time (Tian et al., 2012; O'Malley et al., 1996); and performing laser ablations of the M-system prior to exposure to our assay, to determine a causal link between M-system activity and SL responses (Liu and Fetcho, 1999).

Other promising nuclei possibly driving SL responses

The circuitry mediating escape behaviours is complex and is known to involve various interconnected reticulospinal neurons in the hindbrain other than the M-system. Their role in controlling behaviour has been extensively studied (Mendelson 1986; Orger et al., 2008; Lau et al., 2019). Indeed, in the M-system laser ablation studies by Liu and Fetcho (1999) mentioned above, “escape” responses with sharply increased response latencies (tens of ms) were still observed, with bend angle and angular velocities that otherwise resembled those of normal C-starts. Accordingly, it has since been found that the majority of descending brainstem neuronal subtypes respond to escape-eliciting mechanical stimuli (Gahtan et al., 2001). Additionally, dark-flash stimuli have been shown to evoke large angle C-start (O-bend) responses which are M-cell-independent (Burgess and Granato, 2007a). Finally, Bhattacharyya et al. (2017) found that slow looming stimuli were less likely to recruit the M-system than fast looms, and instead recruited other **ventral spinal projecting nuclei**, such as RoV3, MiR1, MiM1, MiV1, MiR2, and MiV2, which resulted in escapes that were more delayed and more variable in their kinematics. All of these nuclei could potentially be driving or contributing towards the SL response.

Promising brain/spinal areas driving LL responses

The second component in the response to the infrared laser, which we termed LL response, was observed with increasing probability at higher laser intensities, up to a point where a *plateau* was reached (Figure 4.2.A), showed decreasing latencies for increasing laser intensities (again up to a point where a *plateau* was reached – Figure 4.2.E), and appeared less stereotyped than the SL response, showing shifts in the CD curves of different kinematics with increasing laser intensity (Figure 4.3). There are a number of possible brain regions that could be involved in its generation. The **ventral spinal projecting nuclei** mentioned above may be playing a role in this response. A particularly promising candidate would be the **nucleus of the medial longitudinal fascicle (nMLF)**, a nucleus of projecting neurons located in the midbrain that synapse onto motor neurons in the spinal cord (Severi et al., 2014). Cells in the nMLF show increased calcium activity in response to taps to the head, which correlate with fast "escape-like" behaviours in head-fixed larvae (Gathan et al., 2002; Sankrithi and O'Malley, 2010). The activity of these neurons has also been shown to correlate with locomotor kinematics and to modulate the duration and oscillation frequency of tail movements, with laser ablation of these cells leading to a decrease in maximum swimming speed in response to visual stimuli, which was not seen upon ablation of M-cells (Severi et al., 2014). Most importantly, their activity correlates strongly with heat-induced swimming behaviours (Haesemeyer et al., 2018). Other promising ventral spinal projecting nuclei include RoM2, RoM3, RoL3, MiV1 and MiV2 (based on data by Wee et al., 2019 – see below).

It is unclear whether **trigeminal nucleus motor neurons** themselves could be mediating our behavioural responses. On the one hand, Haesemeyer et al. (2018) found "motor-related" cells in the trigeminal in a cluster distinct from the "(innocuous) heat-sensitive" cluster, perhaps corresponding precisely to trigeminal motor neurons. On the other hand, TG motor neurons project stereotypically from rhombomeres 2 and 3 to innervate a small number of target muscles in the mandibula (Pan et al., 2012; Higashijima et al., 2000; Tanaka et al., 2007; Moens and Prince, 2002). So far, no other direct targets of these neurons have been identified.

There are a number of higher-order brain areas that could be involved in the generation of the LL responses. Indeed, Haesemeyer et al. (2018) found the

forebrain to display widespread (innocuous) heat-related activity, particularly in the **sub-pallium, habenula and preoptic areas**. The latter is of particular interest to us, since optogenetic activation of hypothalamic dopaminergic neurons promoted locomotor behaviour in timescales comparable to our LL responses (hundreds of ms), likely through neurons in the preoptic area, which send long-range projections to spinal projection neurons in the midbrain (nMLF) and hindbrain (RoL1 and RoM1). Interestingly, a subset of neurons in this area responded to acoustic/vibrational stimuli, and optogenetic stimulation of the whole dopaminergic population was found to reduce acoustic startle reflex threshold (Barrios et al., 2020). Moreover, oxytocin neurons in the preoptic area have been found to be strongly activated by several noxious stimuli, namely mustard oil (AITC), electric shock and noxious (37°C) heat (Wee et al., 2019). Optogenetic activation of these neurons was sufficient to generate defensive behaviours (large-angle tail bends) via the recruitment of brainstem reticulospinal neurons, including RoM2, RoM3, RoL3, MiV1 and MiV2. Interestingly, the M-cell was one of the downstream targets detected. However, bilateral M-cell ablation had no effect on most behavioural parameters in response to optogenetic stimulation of oxytocin neurons or optovin-based trpa1 stimulation. It only led to an increase in response latency to optogenetic stimulation but not optovin-based trpa1 stimulation (Wee et al., 2019). This suggests that, in a naturalistic scenario, the M-cell might not play a significant role in the generation of these responses. This would strengthen our hypothesis that it might be more important for faster responses that do not require involvement of higher order brain areas.

Modulation of SL and LL responses

Finally, it would be interesting to consider whether the integration of other sensory modalities can modulate the SL and/or LL responses to noxious heat. As described previously, serotonergic neurons in the **dorsal raphe nucleus** could be a promising pathway to be modulating the SL response (Pantoja et al., 2016). Further, the **nMLF and other reticulospinal cells** have been proposed by some as attractive candidates for playing a role in sensorimotor integration (Severi et al., 2014). For instance, escape responses to acoustic stimuli may be modulated by, and result from the integration of, multiple sensory cues: **prepontine neurons** in rhombomere 1 have been shown to drive “delayed”, long latency (16-50 ms)

C-start escapes to acoustic stimuli, the trajectories of which are guided by visual information, in parallel with the M-system-driven short latency C-starts, which happen within 12 ms of the stimulus and are more stereotyped (Marquart et al., 2019). **Higher order brain areas** could also be involved. For example, light-responsive dopaminergic neurons in the caudal hypothalamus have been shown to be required for the visual enhancement of M-cell-mediated auditory escape responses (Mu et al., 2012), and a reduction in the number of dopaminergic cells in the diencephalon correlated with a weaker and shorter-lasting response to touch to the head (Lam et al., 2005). Interestingly, **posterior tubercular dopaminergic neurons** have been shown to innervate the TG, with catecholaminergic fibres in the skin showing arborization patterns that seem to overlap with those of sensory free nerve endings. Moreover, specific subgroups of these neurons have been shown to respond to sensory stimuli, with some far-projecting neurons responding to mechanosensory stimuli and others to visual stimuli (Haehnel-Taguchi et al., 2018; Reinig et al., 2017).

In short, in this chapter, I have characterised the tail-flick escape-like behaviours elicited in tethered zebrafish larvae by infrared laser stimulation. I have shown for the first time that these responses have two components that are temporally separated. This raises interesting questions about the circuitry underlying them, which could be addressed in future work. Importantly, my data strongly suggests that the infrared laser induces a response through thermal stimulation and that this can be modulated with an irritant chemical, AITC. As such, this behavioural setup can be used to study and characterise fast escape-like responses to noxious stimuli in zebrafish larvae, as well as allowing for the detection of changes in the properties of these responses. Therefore, with the overall aim of establishing the zebrafish as a model to study the genetics of nociception, I next sought to generate zebrafish knockouts of various genes and to characterise their responses to the infrared laser. This is discussed in the following chapter.

Chapter 5: Generation and characterisation of zebrafish F0 knockout of genes involved in human genetic pain disorders

5.1 Introduction

5.1.1 Human genetic pain disorders

Human Mendelian disorders of pain sensing are extreme phenotypes characterised by either painlessness or paroxysmal (excess) pain, with or without sensory neuropathy. They are usually caused by one or two mutations in a single gene and are fully penetrant. Even though they are quite rare, studying these disorders is extremely valuable for pain research, as it can help us gain insight into the role of these genes and their pathways. This can ultimately aid the development of new drugs (Cox et al., 2019). For instance, mutations in *NGF* have been found to lead to congenital insensitivity to pain, and drugs targeting NGF have emerged as promising clinical targets for various forms of chronic pain over the past few years (Einarsdottir et al., 2004; Watson et al., 2008; Denk et al., 2017; Dakin et al., 2019). Many of these disorders have been studied in rodent models, which has helped elucidate the role of some of these genes in nociception (Crowley et al.,1994; Smeyne et al., 1994; Desiderio et al., 2019; Landy et al., 2021; see more below). Nevertheless, a lot is still unknown about these processes, which is highlighted by the fact that many promising drugs fail to produce an analgesic effect in clinical trials. For instance, mutations in *SCN9A*, encoding the α-subunit of the voltage-gated sodium channel, Nav1.7, have been shown to lead to congenital insensitivity to pain, but specific Nav1.7 antagonists have weak analgesic activity (Cox et al., 2006; Emery et al., 2016). As detailed in previous chapters, the zebrafish is an attractive animal model. Its simplicity, compared to mammals, means zebrafish can help us reach a mechanistic understanding of the circuits underlying sensing noxious stimuli.

The overall aim of my PhD is to establish the zebrafish as a model to study the genetics of nociception. In this chapter, I describe the generation and characterisation of F0 knockout of zebrafish orthologs of genes known to be involved in human genetic pain disorders. First, I selected promising candidate genes that have been shown to play a role in those disorders. Then, I generated zebrafish F0 knockouts of the zebrafish orthologs of those genes. Finally, I characterised the phenotype of the resulting mutants.

The first step was to select the target genes. Upon researching a combination of review articles and primary research articles, a comprehensive but not exhaustive list of potential candidate genes was compiled. This was summarised in Table 1.1 (see Chapter 1 – Introduction). In order to narrow down this list on a few promising candidates, three criteria were employed sequentially, as outlined in the flowchart in Figure 5.1. Firstly, only genes associated exclusively with a loss of pain in humans were considered. Secondly, I selected genes based on their expression pattern and function. Finally, to confirm the suitability of the remaining genes as targets, sequence homology analysis was performed. Each step is outlined in more detail below.

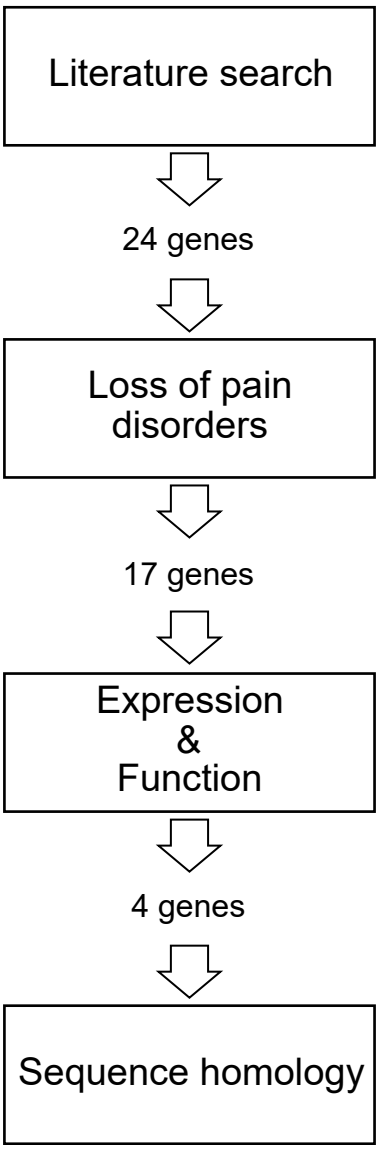

Figure 5.1: **Selecting target genes for mutant generation**. A literature search was performed to compile a list of potential candidate genes (see Table 1.1 in Chapter 1 – Introduction). Then, two criteria were applied sequentially to narrow down the search: only genes involved exclusively in loss of pain disorders were selected; genes with very widespread expression and function (particularly those known a known role in locomotion) were excluded. Finally, sequence homology analysis was performed to confirm the suitability of the final candidates.

5.1.2 Selecting genes associated with loss of pain

As detailed above, the majority of human pain disorders fall into one of two categories: extreme (paroxysmal) pain or painlessness (loss of pain). I chose to focus on the latter category because those disorders have been extensively studied in rodent models, which provides a useful framework for what phenotypes to expect (Crowley et al.,1994; Smeyne et al., 1994; Desiderio et al., 2019; Landy et al., 2021). Additionally, reductions in sensitivity to noxious stimuli such as heat (Gau et al., 2013) and chemicals (Prober et al., 2008) have already been achieved in zebrafish by knocking down different genes. This again provides a useful reference for my experiments.

According to this criterion, genes implicated in human pain disorders of extreme pain were excluded from this study: *ATP1a2*, *CACNA1A*, *SCN1A*, *SCN9A*, *SCN10A*, *SCN11A*, and *TRPA1*. As shown in Table 1.1, these genes have been associated with Familial Hemiplegic Migraine (FHM) type I (*CACNA1A*), FHM type II (*ATP1a2*), FHM type III (*SCN1A*), Familial Episodic Pain Syndrome-1 (FEPS-1: *TRPA1*), FEPS-2 (*SCN10A*), FEPS-3 (*SCN11A*), small fibre neuropathy (SFN: *SCN9A*, *SCN10A* and *SCN11A*), primary erythromelalgia (PEM: *SCN9A*), and paroxysmal extreme pain disorder (PEPD: *SCN9A*) (Cregg et al., 2010; Cox et al. 2019).

5.1.3 Selecting genes based on expression and functional role

Then, I selected genes based on their expression pattern and function (in humans and, if known, rodent and zebrafish). I decided to focus on genes known to be expressed primarily in sensory neurons, and, importantly, to exclude those that lead to motor defects when mutated. This is because knocking out genes with widespread expression throughout the body could result in unexpected side effects, and mutating those with a known effect on behaviour would constitute a confounding factor (since we use behavioural changes as the main readout for changes in sensitivity to noxious stimuli). Based on these two criteria, the following genes were excluded: *ATL1, ATL3, CLTCL1, DNMT1, DST, ELP1, FLVCR1, KIF1A, RETREG1, SPTLC1, SPTLC2* and *WNK1*. This is outlined below.

ATL1 and ATL3 (atlastin GTPase 1 and atlastin GTPase 3, respectively) are members of the dynamin superfamily of large GTPases. In mammals, *ATL1* is expressed primarily in the brain, particularly in the hippocampus and pyramidal neurons (Zhu et al., 2003). Mutations in this gene have been shown to cause autosomal dominant hereditary spastic paraplegia in humans (Zhao et al., 2001). In zebrafish, it has been shown to control motility and spinal motor axon architecture, with knockdown of *atl1* inducing a loss of motility of zebrafish larvae, associated with increased branching of spinal motor axons (Fassier et al., 2010). In humans, mutations in *ATL3* have been linked to destruction of distal bones of the lower extremities (Kornak et al., 2014), with some patients also showing a decrease in motor nerve conduction velocities, indicative of axonal damage (Fischer et al., 2014).

CLTCL1 (Clathrin Heavy Chain Like 1) encodes CHC22 (Clathrin Heavy Chain 22), which is upregulated in the developing human brain (Nahorski et al., 2015b) and expressed post-natally in high levels in skeletal muscle, heart and testes (Drissi et al., 2020). It is responsible for trafficking the glucose transporter 4 (GLUT4) in skeletal muscle and fat (Vassilopoulos et al., 2009) and has increased expression during myogenesis and muscle regeneration (Towler et al., 2004). In humans, mutations in this gene can lead to severe non-progressive learning disability and a delay in central nervous system myelination, with no motor defects (Nahorski et al., 2015a).

DNMT1 (DNA (cytosine-5)-methyltransferase 1) is the main DNA methyltransferase in mammalian cells (Svedružić 2011). In humans, mutations in *DNMT1* also cause autosomal dominant cerebellar ataxia, deafness and narcolepsy (Winkelmann et al., 2012). In zebrafish, *dnmt1* is required for the development and maintenance of the lens (Tittle et al., 2010).

DST (dystonin) is an adhesion junction protein involved in intracellular transport and the maintenance of cytoskeletal integrity (Cox et al., 2019). In humans, mutations in *DST* lead to a loss of autonomic neurons (Manganelli et al., 2017) and a range of dysautonomic symptoms, as well as muscle hypotonia and severe psychomotor retardation (Edvardson et al., 2012).

ELP1 (Elongator Acetyltransferase Complex Subunit 1, also known as IKBKAP) is a scaffolding protein. In humans, mutations in *ELP1* leading to

decreased levels of ELP1 protein have been linked to sympathetic neuron death and sympathetic nervous system dysfunction (Li et al., 2020). In zebrafish, morpholino-induced depletion of *elp1* leads to aganglionosis and a reduced number of enteric neurons (Cheng et al., 2015).

FLVCR1 (Feline Leukemia Virus subgroup C Receptor 1) encodes a broadly expressed heme exporter. Mutations in this gene have been linked to vision impairment and posterior column ataxia in humans (Rajadhyaksha et al., 2010). In mice and zebrafish, the two heme exporters encoded by *flvcr1*, *flvcr1a* and *flvcr1b*, have been shown to control erythropoiesis (Mercurio et al., 2015).

KIF1A (Kinesin family member 1A) is a neuron-specific motor protein responsible for the transport of membranous organelles and synaptic vesicles. In humans, some mutations in *KIF1A* have been associated with a range of disorders, including hereditary spastic paraparesis (Citterio et al., 2015) and cerebellar atrophy (Lee et al., 2014). In zebrafish, a rare *kif1a* mutation detected in patients with epilepsy was shown to result in epileptic seizure-like activity (Guo et al., 2020).

RETREG1 (Reticulophagy Regulator 1, also known as FAM134B), encodes a Golgi protein responsible for apoptosis regulation (Khaminets et al., 2015). While its function in zebrafish is unknown (Subedi et al., 2021), it has been shown to be necessary for the survival of autonomic neurons in humans, with loss-of-function mutations in this gene leading to autonomic dysfunction (Kurth et al., 2009).

SPTLC1 and *SPTLC2* (Serine Palmitoyltransferase Long Chain Base Subunit 1 and 2, respectively) encode the long chain base subunit 1 and 2 of serine palmitoyltransferase, respectively. Serine palmitoyltransferase is the key enzyme in sphingolipid biosynthesis (Murphy et al., 2013). In humans, mutations in *SPTLC1* lead to progressive degeneration of motor neurons, with symptoms including distal muscle wasting and weakness (Dawkins et al., 2001; Bejaoui et al., 2001), and mutations in *SPTLC2* can lead to gait difficulties (Rotthier et al., 2010), motor weakness, muscle atrophy and slow motor conduction velocities (Murphy et al., 2013; Suriyanarayanan et al., 2019).

WNK1 (with-no-lysine protein kinase 1) is a ubiquitous serine-threonine kinase. It has been shown to be essential for angiogenesis and heart

development in mice (Xie et al., 2009) and angiogenesis in zebrafish (Lai et al., 2014).

After applying the above criteria, four genes remained: *NGF*, *NTRK1*, *PRDM12* and *ZFHX2*. From these, *NGF*, *NTRK1*, and *PRDM12* seemed particularly promising, due to the role of the NGF/TRKA pathway in the specification of nociceptors (see Chapter 1 – Introduction). NGF (Nerve Growth Factor) is a member of the family of neurotrophins, structurally related proteins required for the development and function of the vertebrate nervous system, particularly sensory neuron specification (Fitzgerald, 2005). Closely-related members of this family include BDNF (Brain-Derived Neurotrophic Factor), NT-3 (Neurotrophin-3) and NT-4/5 (Neurotrophin-4/5). Each neurotrophin preferentially binds to and activates one of the three tyrosine kinase receptors: NGF to TRKA (encoded by *NTRK1*; Kaplan et al., 1991); BDNF and NT-4/5 to TRKB (encoded by *NTRK2*; Klein et al., 1991, Klein et al., 1992); and NT-3 to TRKC (encoded by NTRK3; Lamballe et al., 1991). In humans, mutations in *NGF*, *NTRK1* and *PRDM12* (a transcription factor that regulates the expression of TRKA) have been shown to lead to developmental pain insensitivity disorders, namely Hereditary Sensory and Autonomic Neuropathy Types V, IV and VIII, respectively (Einarsdottir et al., 2004; Mardy et al., 1999; Chen et al., 2015; Cox et al., 2019). In mice, mutations in all three of these genes have also been found to lead to decreased sensitivity to noxious stimuli and loss of sensory neurons (Crowley et al.,1994; Smeyne et al., 1994; Desiderio et al., 2019; Landy et al., 2021). To confirm their suitability as targets for our study, sequence homology analysis was performed to determine the similarities between these genes in human, mouse and zebrafish.

5.1.4 Sequence homology analysis confirms *NGF*, *NTRK1* and *PRDM12* as good candidate genes

The amino acid sequences of the human (*Homo sapiens*) proteins encoded by *NGF*, *NTRK1* (TRKA), and *PRDM12* were compared to the mouse (*Mus musculus*) and zebrafish (*Danio rerio*) sequences. There are two zebrafish

orthologs of the human *NGF* gene, *ngfa* and *ngfb*. This is commonly seen across many zebrafish genes as a result of a teleost-specific whole-genome duplication event (Meyer and Schartl, 1999; Howe et al., 2013). Each of the amino acid sequences of interest was also compared to several known phylogenetically related proteins (Lanave et al., 2007; Hohenauer and Moore, 2012). This was to confirm that the sequences of the zebrafish orthologs of interest were more similar to those of the corresponding human protein than those of closely related proteins, which would further support their evolutionary proximity and conservation. To do that, the amino acid sequences were obtained using Ensembl (version 99; Cunningham et al., 2019) and UniProtKB (The UniProt Consortium, 2021) (Table 5.1). Identity matrices (Figure 5.2.A) and phylogenetic trees (Figure 5.2.B) were then obtained through the EMBL-EBI online ClustalOmega Multiple Sequence Alignment tool (Sievers et al., 2011; Madeira et al., 2019). As predicted, for every gene analysed, the human and mouse orthologs are evolutionarily closer to each other than to the zebrafish ortholog(s), as indicated by the phylogenetic trees (Figure 5.2.B). They also have higher identity scores (Figure 5.2.A), which measure the number of identical residues ("matches") in relation to the length of the alignment. For instance, when compared to human NGF, mouse Ngf scores 85.06%, while the two zebrafish orthologs, ngfa and ngfb, score 49.77% and 50.79%, respectively. This was also true for NTRK1 (mouse TrkA score: 86.81%; zebrafish trkA score: 53.51%) and PRDM12 (mouse Prdm12 score: 98.63%; zebrafish prdm12b score: 84.59%). Importantly, the score of our zebrafish orthologs of interest, when compared to the corresponding human protein, was generally higher than when compared to other closely related proteins. For example, zebrafish ngfa scored 49.77% against human NGF, but only 35.60% against human BDNF and 38.83% against human NTF-3. This was also true for ngfb (score against human NGF: 50.79%; score against human BDNF: 35.26%; score against human NT-3: 41.36%), and prdm12b (PRDM12: 84.59%; PRDM14: 32.58%; PRDM6: 33.43%), but not for trkA (TRKA (NTRK1): 53.51%; TRKB (NTRK2): 50.19%; TRKC (NTRK3): 53.56%). Most importantly, I also checked whether the specific amino acids that are mutated in the corresponding human pain disorders are conserved in zebrafish. This is because it is likely that those amino acids are key for the function of each protein, seeing as a single amino acid change can have such a dramatic phenotypic effect. To do this comparison, the amino acid sequences

were aligned using BLAST (Altschul et al., 1990). I found that all those amino acids were conserved across the three species for all genes (Figure 5.2.C). This conservation again indicates that those amino acids are key for protein function and also provides support to the use of zebrafish as an animal model for nociception.

Taken together, the expression pattern, known function and amino acid sequence conservation between human *NGF*, *NTRK1* and *PRDM12* and the zebrafish orthologs made these three genes attractive targets to mutate.

Table 5.1: **Ensembl and UniProtKB IDs of proteins compared by sequence homology analysis.**

	Human		Mouse		Zebrafish	
Gene	**ENSEMBL**	**UniProtKB**	**ENSEMBL**	**UniProtKB**	**ENSEMBL**	**UniProtKB**
BDNF	ENSG00000176697	P23560	ENSMUSG00000048482	P21237	ENSDARG00000018817	Q6NZ01*
NGF	ENSG00000134259	P01138	ENSMUSG00000027859	P01139	-	-
ngfa	-	-	-	-	ENSDARG00000058961	O73797
ngfb	-	-	-	-	ENSDARG00000014050	Q6YBR5
NTF3	ENSG00000185652	P20783	ENSMUSG00000049107	P20181	ENSDARG00000059043	F1QR36
NTRK1	ENSG00000198400	P04629	ENSMUSG00000028072	Q3UFB7	ENSDARG00000004586	F6P1M3*
NTRK2	ENSG00000148053	Q16620	ENSMUSG00000055254	P15209	-	-
ntrk2a	-	-	-	-	ENSDARG00000059897	B8JLJ1*
ntrk2b	-	-	-	-	ENSDARG00000098511	A0A0R4ITX7*
NTRK3	ENSG00000140538	Q16288	ENSMUSG00000059146	Q6VNS1	-	-
ntrk3a	-	-	-	-	ENSDARG00000077228	A0A0R4ITE7*
ntrk3b	-	-	-	-	ENSDARG00000086214	A0A0H2UKW5*
PRDM12	ENSG00000130711	Q9H4Q4	ENSMUSG00000079466	A2AJ77	-	-
prdm12b	-	-	-	-	ENSDARG00000007430	Q5U3V3 *
PRDM14	ENSG00000147596	Q9GZV8	ENSMUSG00000042414	E9Q3T6	ENSDARG00000045371	F1QWQ9*
PRDM6	ENSG00000061455	Q9NQX0	ENSMUSG00000069378	Q3UZD5	-	-

An asterisk indicates an unreviewed annotation score on UniProtKB. A dash indicates the particular ortholog cannot be found on Ensembl for that species. B8JLJ1 is not an Ensembl-predicted ortholog. The zebrafish ngfa is also known as NT-7.

A

ID | Name — Percent Identity Matrix

			1	2	3	4	5	6	7	8	9	10
NGF	1	P01138|NGF_HUMAN	100.00	85.06	49.77	50.79	35.50	39.91	40.38	35.68	42.42	42.67
	2	P01139|NGF_MOUSE	85.06	100.00	46.05	50.26	34.20	38.03	38.50	34.80	39.83	40.52
	3	O73797|NTF7_DANRE	49.77	46.05	100.00	57.73	32.52	35.60	35.60	38.05	38.83	39.61
	4	Q6YBR5|NGF_DANRE	50.79	50.26	57.73	100.00	35.87	35.26	35.26	40.31	41.36	41.67
BDNF	5	Q6NZ01|Q6NZ01_DANRE	35.50	34.20	32.52	35.87	100.00	75.30	74.70	36.75	37.60	37.60
	6	P23560|BDNF_HUMAN	39.91	38.03	35.60	35.26	75.30	100.00	97.57	38.32	40.17	40.17
	7	P21237|BDNF_MOUSE	40.38	38.50	35.60	35.26	74.70	97.57	100.00	37.96	39.83	39.83
NTF-3	8	F1QR36|F1QR36_DANRE	35.68	34.80	38.05	40.31	36.75	38.32	37.96	100.00	53.53	53.31
	9	P20783|NTF3_HUMAN	42.42	39.83	38.83	41.36	37.60	40.17	39.83	53.53	100.00	96.11
	10	P20181|NTF3_MOUSE	42.67	40.52	39.61	41.67	37.60	40.17	39.83	53.31	96.11	100.00

			1	2	3	4	5	6	7	8	9	10	11
NTRK3	1	Q16288|NTRK3_HUMAN	100.00	97.21	74.76	72.17	56.95	57.27	55.87	54.18	53.56	51.93	50.39
	2	Q6VNS1|NTRK3_MOUSE	97.21	100.00	74.42	72.41	56.70	57.14	55.74	53.93	53.18	51.68	50.13
	3	A0A0R4ITE7|A0A0R4ITE7_DANRE	74.76	74.42	100.00	78.67	55.23	55.43	54.46	53.95	52.24	49.81	48.64
	4	A0A0H2UKW5|A0A0H2UKW5_DANRE	72.17	72.41	78.67	100.00	55.84	55.71	54.85	53.40	51.42	50.00	48.83
NTRK2	5	Q16620|NTRK2_HUMAN	56.95	56.70	55.23	55.84	100.00	94.03	64.74	63.26	50.19	50.32	49.17
	6	P15209|NTRK2_MOUSE	57.27	57.14	55.43	55.71	94.03	100.00	65.08	63.08	50.38	50.52	49.36
	7	B8JLJ1|B8JLJ1_DANRE	55.87	55.74	54.46	54.85	64.74	65.08	100.00	69.01	51.97	51.13	50.47
	8	A0A0R4ITX7|A0A0R4ITX7_DANRE	54.18	53.93	53.95	53.40	63.26	63.08	69.01	100.00	49.68	48.55	46.98
NTRK1	9	F6P1M3|F6P1M3_DANRE	53.56	53.18	52.24	51.42	50.19	50.38	51.97	49.68	100.00	53.51	52.61
	10	P04629|NTRK1_HUMAN	51.93	51.68	49.81	50.00	50.32	50.52	51.13	48.55	53.51	100.00	86.81
	11	Q3UFB7|NTRK1_MOUSE	50.39	50.13	48.64	48.83	49.17	49.36	50.47	46.98	52.61	86.81	100.00

			1	2	3	4	5	6	7	8
PRDM14	1	F1QWQ9|F1QWQ9_DANRE	100.00	54.28	52.09	28.54	27.80	30.46	31.90	31.79
	2	Q9GZV8|PRD14_HUMAN	54.28	100.00	69.77	30.04	30.39	32.58	34.20	34.20
	3	E9Q3T6|PRD14_MOUSE	52.09	69.77	100.00	30.19	30.33	33.44	33.88	33.88
PRDM6	4	Q9NQX0|PRDM6_HUMAN	28.54	30.04	30.19	100.00	95.78	33.43	34.56	34.56
	5	Q3UZD5|PRDM6_MOUSE	27.80	30.39	30.33	95.78	100.00	33.73	34.56	34.56
PRDM12	6	Q5U3V3|Q5U3V3_DANRE	30.46	32.58	33.44	33.43	33.73	100.00	84.59	85.35
	7	Q9H4Q4|PRD12_HUMAN	31.90	34.20	33.88	34.56	34.56	84.59	100.00	98.63
	8	A2AJ77|PRD12_MOUSE	31.79	34.20	33.88	34.56	34.56	85.35	98.63	100.00

B

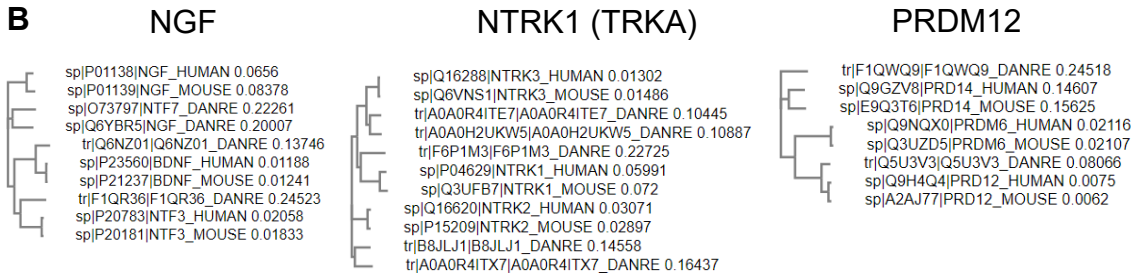

C

Figure 5.2: **Sequence homology analysis confirms *NGF*, *NTRK1* and *PRDM12* as good candidate genes**. The amino acid sequences of the human (Homo sapiens) proteins encoded by *NGF*, *NTRK1* (TRKA), and *PRDM12* were compared to the mouse (Mus musculus) and zebrafish (Danio rerio) sequences. Each sequence was also compared to phylogenetically related proteins (BDNF, NTF-3, TRKB (encoded by NTRK2), TRKC (encoded by NTRK3), PRDM6, PRDM8). A: Percent Identity Matrices created by Clustal2.1. ID and name refer to the UniProtKB ID and name, respectively. B: Phylogenetic trees created by Clustal2.1. C: Alignment of the amino acid sequence of NGF (A), TRKA (B), and PRDM12 (C) in human (h), mouse (m) and zebrafish (zf). The amino acids mutated in different human pain disorders, shown in red, are conserved in the mouse and zebrafish orthologs. Dashed lines represent omitted amino acids.

5.1.5 Generation of transient F0 knockouts

Since its first implementation, CRISPR-Cas9 has been extensively used to generate zebrafish mutant lines, often with the aim of gaining a mechanistic understanding into the role of genes known to be associated with various human disorders (Hwang et al., 2013; Thyme et al., 2019). However, traditional CRISPR-Cas9 strategies require two generations of adult animals to generate homozygous mutants, which can take up to six months to achieve. This places time and ethical constraints on screens of several genes (Sorlien et al., 2018). Recently, Kroll et al. (2021) developed a method for reliably generating biallelic knockouts directly in the injected embryos, termed the F0 generation. Using a set of three synthetic gRNAs per gene, this protocol allows for the generation of biallelic F0 knockouts with fully penetrant phenotypes in >90% of injected animals, and can be adapted to generate biallelic mutations simultaneously in up to three genes per animal.

In this chapter, I use CRISPR-Cas9 to generate F0 knockouts of *NGF*, *NTRK1* and *PRDM12* zebrafish orthologs (*ngfb*, *ntrk1*, *prdm12b*). These three genes are known to play a critical role in human pain, both physiologically and pathologically. My aim was to study their role in the sensitivity of zebrafish larvae to noxious heat. Single knockouts of *ntrk1* or *prdm12b* lead to a subset of zebrafish larvae showing severe developmental defects which affect locomotion, but sensitivity to noxious heat is not abolished in these mutants. Single knockouts of *ngfb* lead to mutants with no obvious anatomical, developmental or locomotor defects. These fish show normal LL responses to stimulation with the infrared laser but nearly completely absent SL responses. These results open several promising avenues of future work and help establish the zebrafish as a model to study the genetics of nociception.

5.2 Results

5.2.1 Using CRISPR-Cas9 to generate F0 knockouts of zebrafish orthologs of *NGF*, *NTRK1* and *PRDM12*

The experimental pipeline is shown in Figure 5.3. To generate F0 knockouts of *ngfa*, *ngfb*, *ntrk1* and *prdm12b*, crRNA was designed to target three different loci in each gene (see Table 2.1 for the crRNA sequences – Chapter 2, Methods). As mentioned previously, there are two zebrafish orthologs of the human *NGF* gene (*ngfa* and *ngfb*); crRNA was designed separately for each ortholog. Embryos were then injected at single-cell stage and checked daily for viability between 1 and 4 days post-fertilisation (dpf). At 6-7 dpf, the phenotype of injected embryos was assessed, both anatomically and behaviourally (in free-swimming and/or infrared laser experiments). Finally, they were genotyped individually to confirm mutations were successful (only embryos with at least one successful mutant locus were included in the analysis).

crRNA was designed as described in Chapter 2 (Methods). Three crRNAs were selected per target gene (Table 2.1). They were selected from IDT's database of predesigned crRNAs based on on-target and off-target scores, and rank according to the web tool CHOPCHOP (v3; Labun et al., 2019; Labun et al., 2016; Montague et al., 2014). Where possible, each target locus was on a distinct exon (while proceeding down the list from the best predicted crRNAs), as this might negate any potential compensatory mechanisms (such as skipping of the mutated exon), thus further decreasing the likelihood of production of a functional protein in the F0 knockouts (Anderson et al., 2017; Lalonde et al., 2017; Kroll et al., 2021). Moreover, previous studies where F0 knockouts are generated by simultaneously targeting multiple loci of the same gene have shown that this method sometimes leads to large deletions between two targeted sites (Wu et al., 2018; Kroll et al, 2021). As such, I typically targeted exon 1, with the second and third targets falling towards the middle and/or end of the gene. Finally, for *ntrk1*, exons 13 and 17 were selected since, in humans, exons 13 to 17 encode the tyrosine kinase domain of TRKA, which is phosphorylated in response to NGF and is critical for the intracellular signalling of the NGF/TRKA pathway (Mardy et al., 1999).

For each gene, the exons targeted by each crRNA are shown in Figure 5.4.A. Two distinct exons were targeted when mutating *prdm12b*, and three distinct exons when mutating *ntrk1*. *ngfa* and *ngfb* are single-exon genes so all three guides targeted the same exon. For all genes (apart from *ngfa*), three crRNA per gene were initially designed and their ability to induce mutations was tested, before carrying out any further experiments, using headloop PCR (HL-PCR) (Figure 5.4.B; Rand et al., 2005; Kroll et al., 2021). In WT or scrambled-injected controls (S1, S2 and S3 in Figure 5.4.C), normal amplicon amplification, obtained using a pair of standard PCR primers (std in Figure 5.4.C) is suppressed when one of the primers is replaced with a primer containing a headloop tag, complementary to the target locus (HL in Figure 5.4.C). If the target locus is mutated, the tag is no longer complementary to it, and so normal amplicon amplification can occur (HL in sample N1 in Figure 5.4.C). If the mutation is not successful, amplicon amplification will be suppressed, like in WT fish, when one of the primers is replaced with a primer containing a headloop tag (HL in sample N2 in Figure 5.4.C). This preliminary testing was used to optimise the HL-PCR conditions for each headloop primer pair, which were later used when genotyping mutants. It also allowed me to select which crRNA were effective at generating mutations.

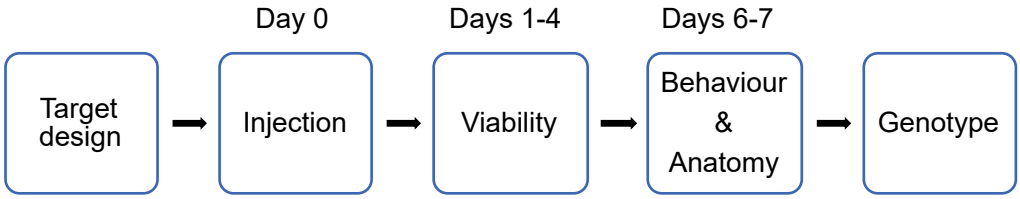

Figure 5.3: **Pipeline of F0 knockout experiments**. First, three crRNA per gene are designed. Embryos are injected at single-cell stage and their viability is monitored from 1 to 4 dpf. At 6 or 7 dpf, behavioural experiments are carried out and embryos are examined for gross anatomical defects. Then, gDNA is extracted and used for genotyping.

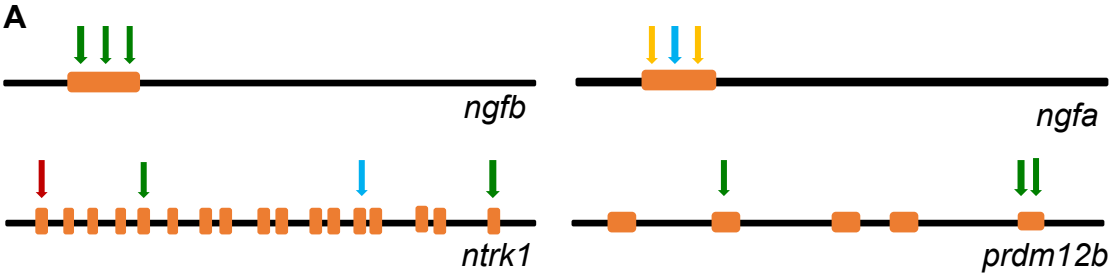

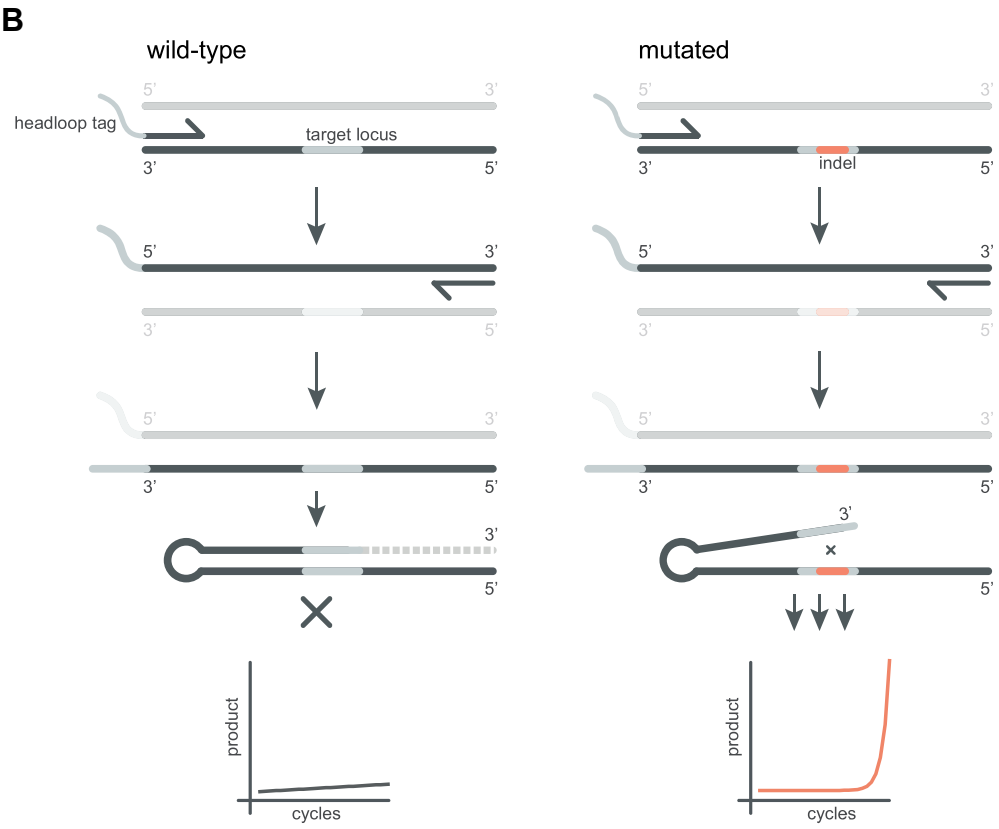

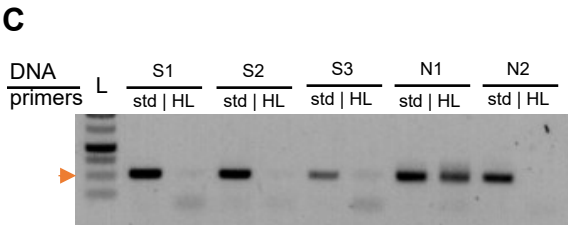

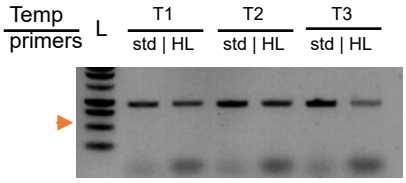

E

--AACCTCTAGCTGTCGTGGCATTGACAGCAAGCACTGGAACTCTTACTGCACCAACACACACACCTATGTGCGGG
CGCTAACGTCCTACAA**AAACCAGATCGCCTGGAGGT**TCATCCGAATCAACGCCGCATGCGTCTGTGTGCTCAGCCG
TAACTCCTGGAGGCATGGACTGAAGTATTGACTGCTATCTCAGCAATCCAATGCAGCCTCCTGTTGAAAGTCCC--

Figure 5.4: **Designing and testing crRNA for the generation of F0 knockouts**. A: Schematic illustrating the exons targeted by each crRNA. Orange rectangles represent exons. Each arrow represents one crRNA (green: crRNA successfully generates mutations; blue: efficiency of crRNA could not be confirmed; red: crRNA not successful at generating mutations). For all genes, the reverse strand is shown. Not to scale. B: Principle of HL-PCR. A headloop tag complementary to the target locus is added to one PCR primer. During PCR, the first elongation incorporates the primer and its overhang; the second elongation synthesises the headloop tag. (left) If the template is wild-type, the complementary tag base-pairs with the target locus and directs elongation (hatched sequence). The amplicon forms a hairpin secondary structure, which prevents its subsequent use as template. (right) If the targeted locus is mutated, the tag is no longer complementary to the locus. The amplicon remains accessible as a template, leading to exponential PCR amplification. Image retrieved from Kroll et al. (2022). C: Target locus D of *ntrk1* amplified with the standard (std) PCR primers or when one is replaced by a headloop primer (HL). For each DNA sample, S represents DNA extracted from a single scrambled-injected fish and N from a fish injected with 3 guides targeting the *ntrk1* gene. Orange arrowheads mark the 500 bp ladder (L) band. D: Target locus of *ngfa* amplified with std PCR primers or when one is replaced by a HL primer. Three primer annealing temperatures were tested: T1= 58°C; T2= 62°C; T3= 66°C. Image courtesy of Ms Connie Whiting. E: 5’ to 3’ nucleotide sequence of part of the *ngfa* exon. Highlighted nucleotides represent variants registered on ensemble.org, as of April 2022. The nucleotides underlined and in bold indicate the sequence that one of the failed headloop tags is complementary to. Dashed lines represent omitted nucleotides.

For *ngfb* and *prdm12b*, all three crRNA initially designed were successful at inducing mutations and were therefore used for the following experiments. For *ntrk1*, two of the three crRNA were successful at reliably inducing mutations (the third one only generated one mutant out of 45 injected fish); therefore, a fourth crRNA was designed with the aim of identifying a third working crRNA. Due to time constraints, I was unable to test the fourth crRNA in preliminary experiments and simply used it alongside the two whose efficiency had been confirmed for subsequent experiments. Indeed, Kroll et al., (2021) showed that using only two crRNA per gene can be sufficient to achieve a high rate of F0 biallelic knockouts (> 75%).

For *ngfa*, I was also unable to carry out the preliminary testing, due to time constraints, and simply used the three crRNA initially designed in subsequent experiments. I found that one of the three crRNAs injected was not successful at generating mutations (zero mutants generated out of 14 injected fish). Unfortunately, I could not successfully use the HL-PCR method to genotype the other two targets on *ngfa*. This is because the headloop tag in both our forward and reverse headloop primers was unable to suppress DNA amplification in WT fish, even after extensive optimisation of various PCR parameters, largely carried out by Ms Connie Whiting (Figure 5.4.D). One possible explanation for this could be the presence of single nucleotide polymorphisms (SNPs) in the sequence the headloop tag would normally be complementary to. HL-PCR has been shown to be highly sensitive, detecting even 1-bp deletions in stable mutant lines (Kroll et al., 2021). This means that SNPs in WT fish could affect the ability of the headloop tag to suppress DNA amplification, preventing its use as a genotyping method for those specific target sites. Indeed, for the third crRNA targeting *ngfa*, subsequent analysis did reveal a record on Ensembl of a synonymous mutation located within the sequence the tag should be complementary to (Figure 5.4.E).

5.2.2 F0 knockout of *ntrk1* or *prdm12b* leads to reduced embryo viability and severe anatomical defects

To assess whether mutating these genes affected embryo survival, embryo viability after injections was monitored from 1 to 4 dpf across three groups: “uninjected” (WT embryos from the same batch that did not receive any

injections), “scrambled” (embryos injected with ‘scrambled’ crRNA, as detailed in Chapter 2 - Methods), and “*ntrk1*-inj” or “*prdm12b*-inj” (embryos injected with crRNA targeting *ntrk1* or *prdm12b*, respectively). The percentage of viable fish at 4 dpf was lower in the *ntrk1*-inj and *prdm12b*-inj groups, compared to scrambled controls (Figures 5.5 A and C). The striking drop in viability from 3 to 4 dpf was due to some developmental defects only becoming apparent at that age – namely, the “curved spine” phenotype, which made up the majority of unviable embryos at 4 dpf in the *ntrk1*-inj and *prdm12b*-inj groups. This refers to fish whose spine was curved, either along the dorso-ventral axis or along the left-right axis, as well as those with abnormal (“spiral-like”) swimming. This phenotype was still observed at 7 dpf. As well as that, several fish showed defects in the inflation of their swim bladder at 7 dpf. Brightfield images of a subset of larvae from each group (“scrambled”, “*ntrk1*-inj” and “*prdm12b*-inj”) were taken. Then, each larva was euthanised and its gDNA was extracted for genotyping. As predicted, many of the fish with anatomical defects were mutants. A representative image of three “curved spine” *ntrk1* F0 knockout fish is shown in Figure 5.5.B (under “*ntrk1* F0 knockout”), with the top and bottom images showing a spine bent along the left-right, and the middle image showing a spine bent along the dorso-ventral axis. Additionally, *ntrk1* and *prdm12b* F0 knockout fish often showed defects in the inflation of their swim bladder at 7 dpf, as indicated by the arrows in Figures 5.5.B and D. In *ntrk1* mutants this was usually a deflated swim bladder, but some *prdm12b* mutants actually showed an overinflated swim bladder, as shown in the bottom panel of Figure 5.5.D (under “*prdm12b* F0 knockout”). In short, F0 knockout of *ntrk1* or *prdm12b* leads to reduced embryo viability and severe anatomical defects in some fish.

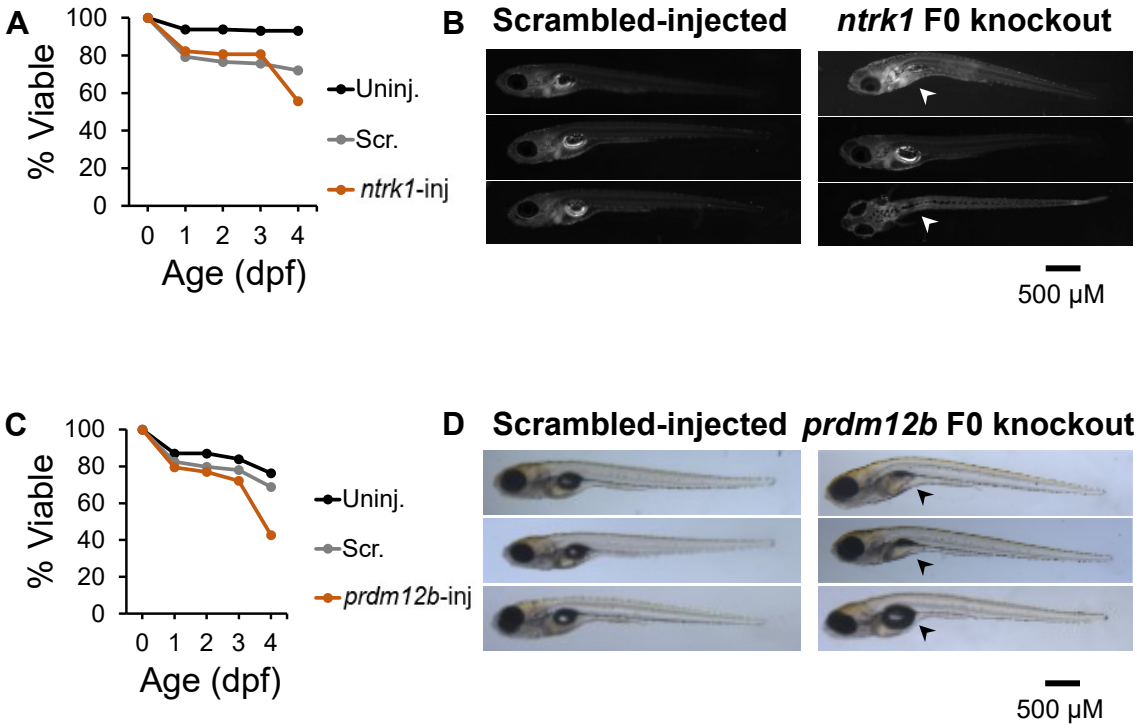

Figure 5.5: **F0 knockouts of *ntrk1* and *prdm12b* lead to reduced embryo viability and severe anatomical defects**. A and C show the percentage of injected embryos that were viable on each day (Day 0: injection day). The percentage of viable fish at 4 dpf was lower in the '*ntrk1*-inj' and '*prdm12b*-inj' groups, compared to scrambled controls. The striking drop in viability from 3 to 4 dpf was due to some developmental defects becoming apparent at that age. B and D show representative brightfield images of scrambled controls (B, D), *ntrk1* mutants (B) or *prdm12b* mutants (D) at 7 dpf. Several *ntrk1* mutants and *prdm12b* mutants show a bent spine and swim bladder inflation defects (arrowhead). 'Uninj.': uninjected controls; 'Scr.': controls injected with scrambled crRNA; '*ntrk1*-inj': embryos injected with crRNA targeting *ntrk1*; '*prdm12b*-inj': embryos injected with crRNA targeting *prdm12b*; 'Scrambled-injected': controls injected with scrambled crRNA; '*ntrk1* F0 knockout': confirmed *ntrk1* F0 knockout; '*prdm12b* F0 knockout': confirmed *prdm12b* F0 knockout.

5.2.3 F0 knockout of *ntrk1* or *prdm12b* leads to swimming defects in a subset of larvae, but sensitivity to noxious stimuli is not abolished

To assess the effect of the observed anatomical defects on swimming behaviour, *ntrk1* and *prdm12b* F0 knockout fish were allowed to freely explore an open arena for 20 minutes and their behaviour was analysed. Only genotyped fish with at least one confirmed successful mutation were included in the analysis. Regarding *ntrk1* mutants, a mixed population was found. Some *ntrk1* F0 knockouts lacked obvious anatomical abnormalities and resembled scrambled-injected fish in their swimming behaviour. They maintained their balance throughout the experiment (Figure 5.6.A, “Normal *ntrk1* F0 knockout”, top panel) and explored the whole arena (Figure 5.6.A, “Normal *ntrk1* F0 knockout”, bottom panel). I refer to these fish as “Normal *ntrk1* F0 knockout”. Conversely, other *ntrk1* F0 knockout fish showed the “curved spine” phenotype and abnormal swimming behaviour (“Curved spine” *ntrk1* F0 knockout). They could not maintain an upright position and often swam sideways (Figure 5.6.A, “Curved spine *ntrk1* F0 knockout”, top panel), which translated into decreased exploration of the arena (Figure 5.6.A, “Curved spine *ntrk1* F0 knockout”, bottom panel). A mixed population of mutants was also observed for *prdm12b* F0 knockout fish (Figure 5.6.B), with similar characteristics: *prdm12b* mutants lacking obvious anatomical abnormalities showed normal swimming (“Normal *prdm12b* F0 knockout”), while those with the “curved spine” phenotype (which was often coupled with swim bladder inflation defects) had abnormal swimming (“Curved spine” *prdm12b* F0 knockout”).

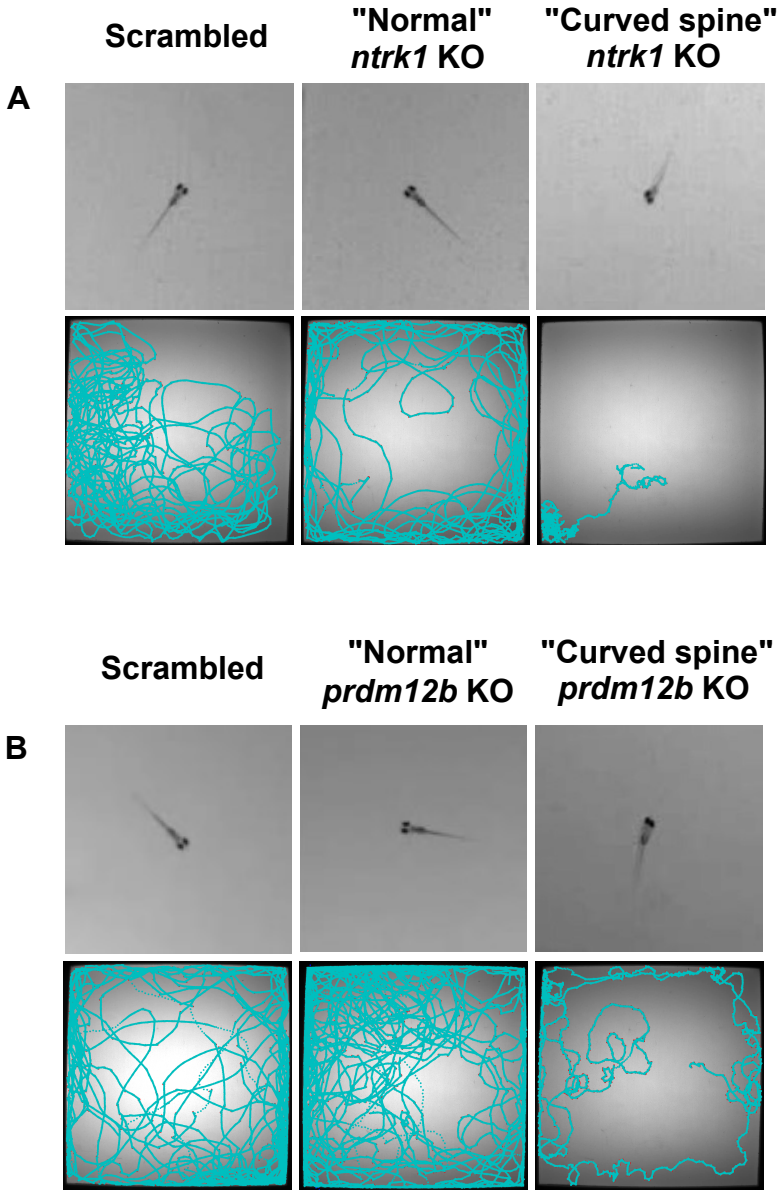

Figure 5.6: **F0 knockouts of *ntrk1* (A) and *prdm12b* (B) lead to swimming defects in a subset of larvae**. Two populations of mutants emerge. Mutants with no obvious anatomical deformities ("Normal" *ntrk1* KO and "Normal" *prdm12b* KO) resemble scrambled-injected fish in their swimming behaviour: they maintain their balance throughout the experiment (top panel of each figure) and explore the whole arena (bottom panel of each figure, which shows the tracked positions of a single fish over the course of the experiment). On the other hand, mutants with the anatomical defects ("Curved spine" *ntrk1* KO and "Curved spine" *prdm12b* KO) showed abnormal swimming behaviour: they could not maintain an upright position (top panel of each figure) which translated into decreased exploration of the arena (bottom panel of each figure).

Focusing on *prdm12b* F0 knockouts first, I then sought to quantify their locomotor activity in the free-swimming assay, to assess whether the apparently normal fish showed no defects in locomotion. This is because we rely on behavioural outputs (tail flick) as a readout for an animal's ability to sense noxious stimuli, and so using fish with locomotion defects would be a confounding factor. I observed their phenotypes were actually very heterogeneous: 7/15 fish showed different combinations of the "curved spine" phenotype (abnormal swimming, bent spines, and overinflated or deflated swim bladders); 5/15 fish appeared visually normal but performed erratic swims when touched with a pipette tip prior to the infrared stimulation assay; only 3/15 fish looked completely normal. Given there were only very few normal fish, and that the phenotypes of abnormal fish were so variable, I was unable to quantify their locomotor activity and compare it to scrambled controls, as my numbers within each group would be too low.

My ultimate goal was to determine whether mutations in *prdm12b* led to changes in sensitivity to noxious heat in our infrared laser assay. In mice, *Prdm12* conditional knockout from DRG neurons during embryogenesis causes defects in nociception, including to noxious heat, and defects in the proliferation of nociceptors (Landy et al., 2021). Unfortunately, as detailed above, the majority of *prdm12b* F0 knockouts (12/15 fish) did not appear normal and instead showed various anatomical defects. Since behavioural outputs are used as a readout for an animal's ability to sense noxious stimuli, I would be unable to properly quantify and characterise the response of these mutants to the laser, or to draw any conclusions from that data regarding their ability to sense noxious heat. However, I sought to understand whether some response to the laser was still observed. Strikingly, despite their anatomical defects, "curved spine" *prdm12b* mutants still consistently showed tail-flick behaviours when stimulated with the infrared laser (Figure 5.7.A). This was seen across different infrared laser intensities and the three rounds of stimulation. The latencies of these tail flicks were largely incompatible with a SL response (Figure 5.7.B) but this cannot be interpreted due to the developmental defects of these fish. Further, as mentioned, I did identify a small subset of *prdm12b* F0 knockouts (3/15 fish) that lacked overt anatomical or swimming abnormalities. These fish were also tested on the infrared laser setup and were found to reliably respond to the stimulus (Figure 5.8).

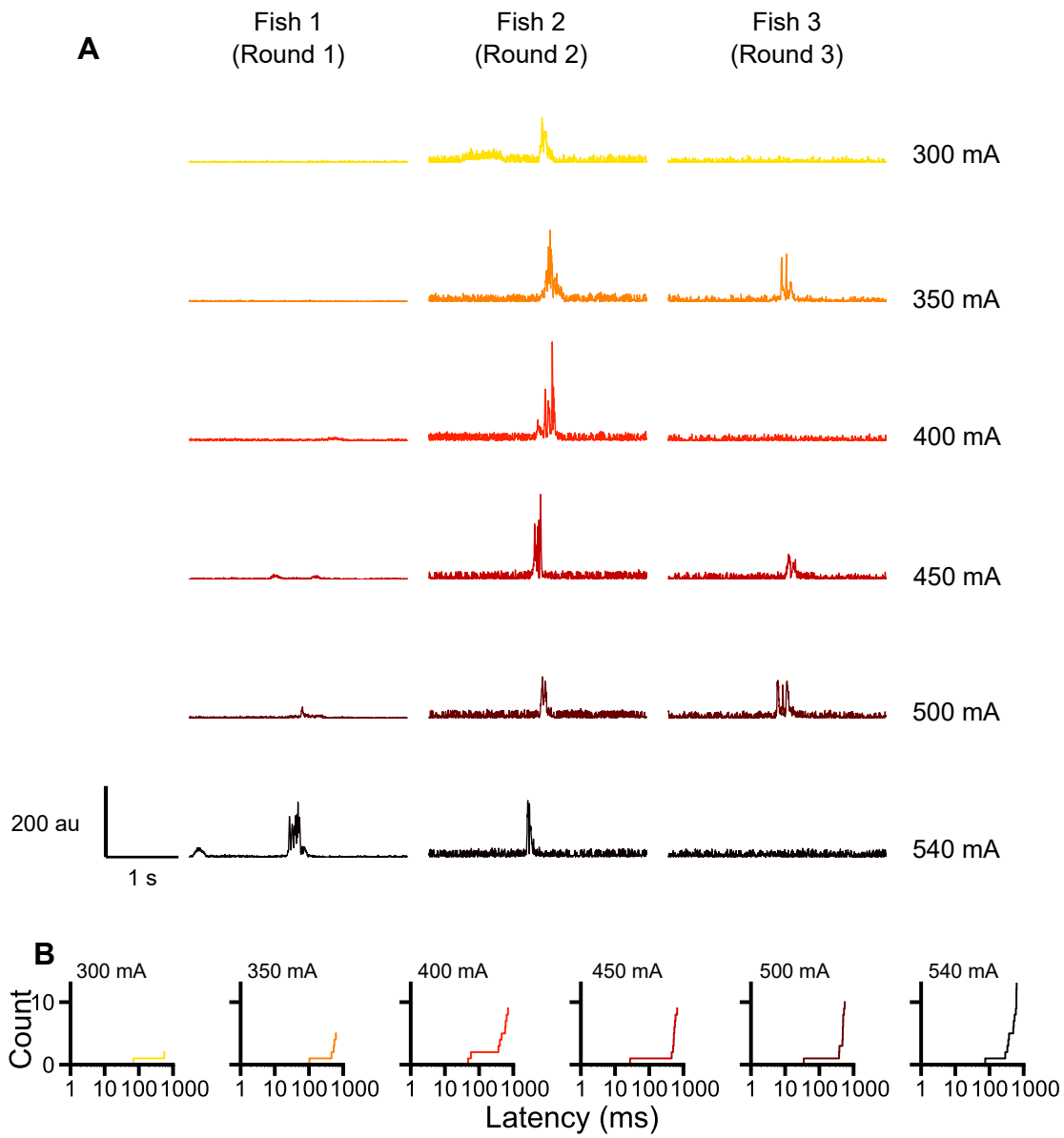

Figure 5.7: ***prdm12b* mutants with severe anatomical defects retain the ability to sense heat**. A: Representative motion traces of three different "curved spine" *prdm12b* mutant fish across different rounds of the infrared laser stimulation assay (round 1 is shown for fish 1; round 2 for fish 2; and round 3 for fish 3). X axis shows time in ms and ranges from -500 ms (before laser is switched on) to 2000 ms. B: Cumulative distribution of response latencies to the infrared laser (n=21 trials). The x axis is shown on a logarithmic scale.

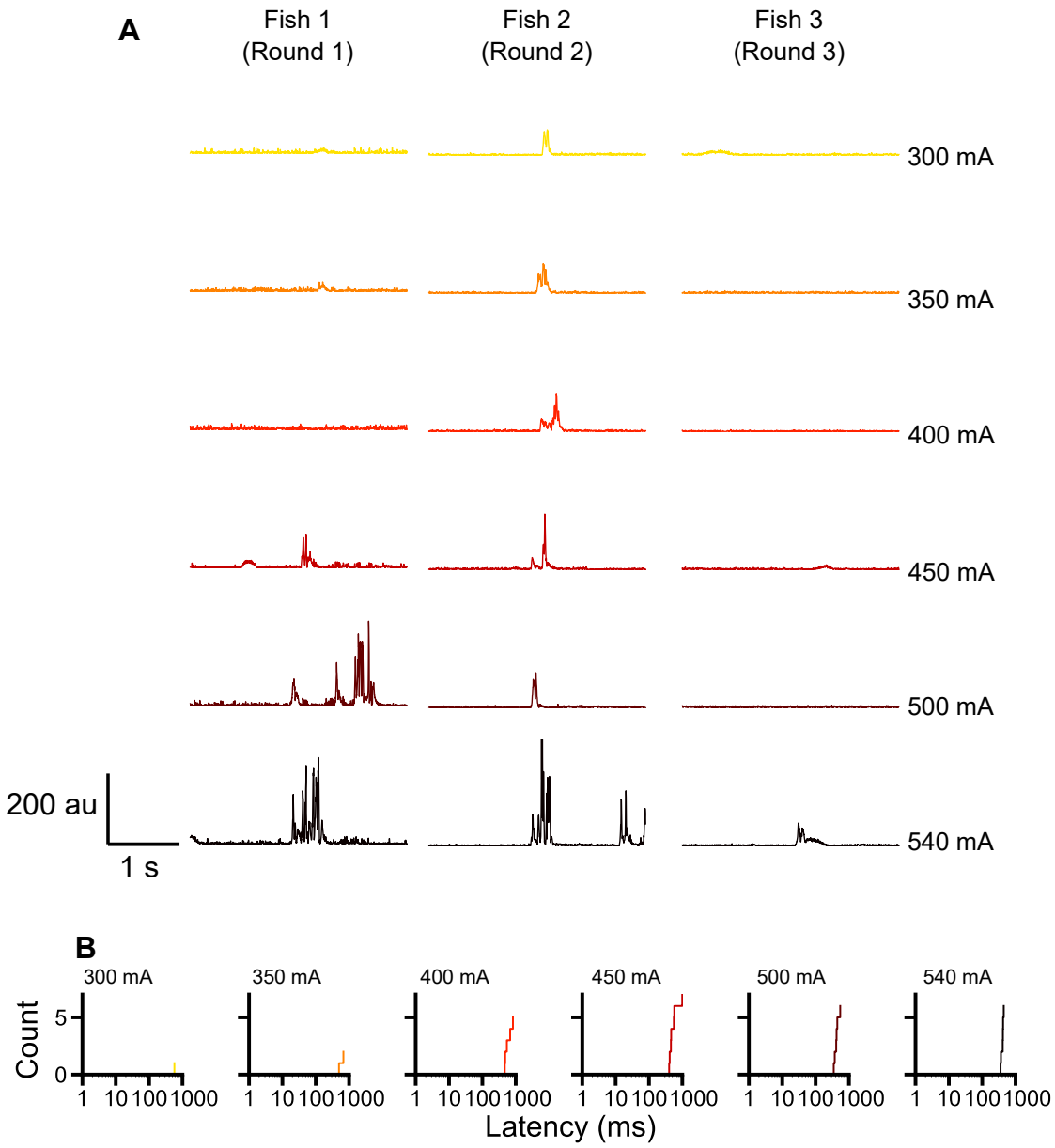

Figure 5.8: ***prdm12b*** **mutants lacking anatomical defects retain the ability to sense heat.** A: Representative motion traces of three different "normal" *prdm12b* mutant fish across different rounds of the infrared laser stimulation assay (round 1 is shown for fish 1; round 2 for fish 2; and round 3 for fish 3). X axis shows time in ms and ranges from -500 ms (before laser is switched on) to 2000 ms. B: Cumulative distribution of response latencies to the infrared laser (n=9 trials). The x axis is shown on a logarithmic scale.

Due to time constraints of the project and the small proportion of the mutant population they represented, I was unable to increase the sample size enough to be able to characterise their responses to the laser. Further studies on these *prdm12b* mutants are needed.

I then focused on *ntrk1* F0 knockouts. I sought to quantify the free-swimming behaviour of the population of “normal” *ntrk1* F0 knockouts, to confirm whether the apparently normal fish showed no defects in locomotion. I also examined the free-swimming behaviour of fish showing the “curved spine” phenotype as positive control, to determine whether differences in anatomy translated into quantifiable differences in locomotion. As predicted, I found that *ntrk1* F0 knockouts with a “curved spine” swam significantly less over the course of the experiment than scrambled controls (Figure 5.9.A), as shown by the lower value of total distance covered (Figure 5.9.B; p=0.003). Additionally, they performed smaller bouts (Figure 5.9.C), both in terms of peak bout velocity (Figure 5.9.D; p=0.004) and average bout velocity (Figure 5.9.E, right; p=0.003). On the other hand, and most importantly, *ntrk1* mutants without anatomical defects (“normal”, n=3) only showed a trend towards a decrease in total distance covered compared to scrambled controls (Figure 5.10.A), but this was not significant (Figure 5.10.B; p=0.210). Accordingly, no significant differences were detected with regards to bout size (Figure 5.10.C), both in terms of peak bout velocity (Figure 5.10.D; p=0.776) and average bout velocity (Figure 5.10.E; p=0.433). In short, there were two populations of *ntrk1* F0 knockout fish: one with anatomical and locomotion defects (“curved spine”), and another that seemed normal, showed no obvious anatomical defects and displayed locomotor activity that was indistinguishable from controls.

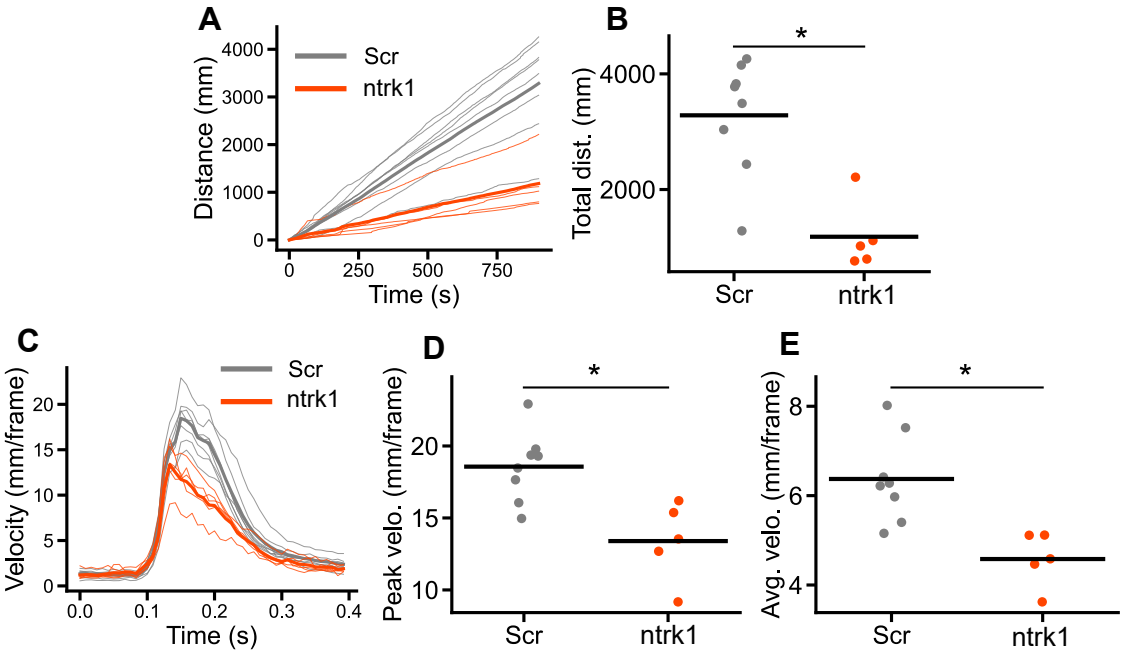

Figure 5.9: ***ntrk1* F0 knockouts with severe anatomical defects show swimming defects**. A: Cumulative distance covered by "curved spine" ntrk1 mutants ('ntrk1', n=5), compared to scrambled-injected controls ('Scr', n=8). B: The total distance covered over the course of the experiment is significantly lower in "curved spine" *ntrk1* mutants than scrambled-injected controls (F=39, p=0.003 with a Mann-Whitney U test). C: Bout velocity of "curved spine" *ntrk1* mutants compared to scrambled-injected controls. D-E: Peak bout velocity (D) and average bout velocity (E) of "curved spine" *ntrk1* mutants are significantly lower than scrambled-injected controls (peak bout velocity: F=3.55, p=0.005 with an Independent Samples t-Test; average bout velocity: F=3.65, p=0.004 with an Independent Samples t-Test)

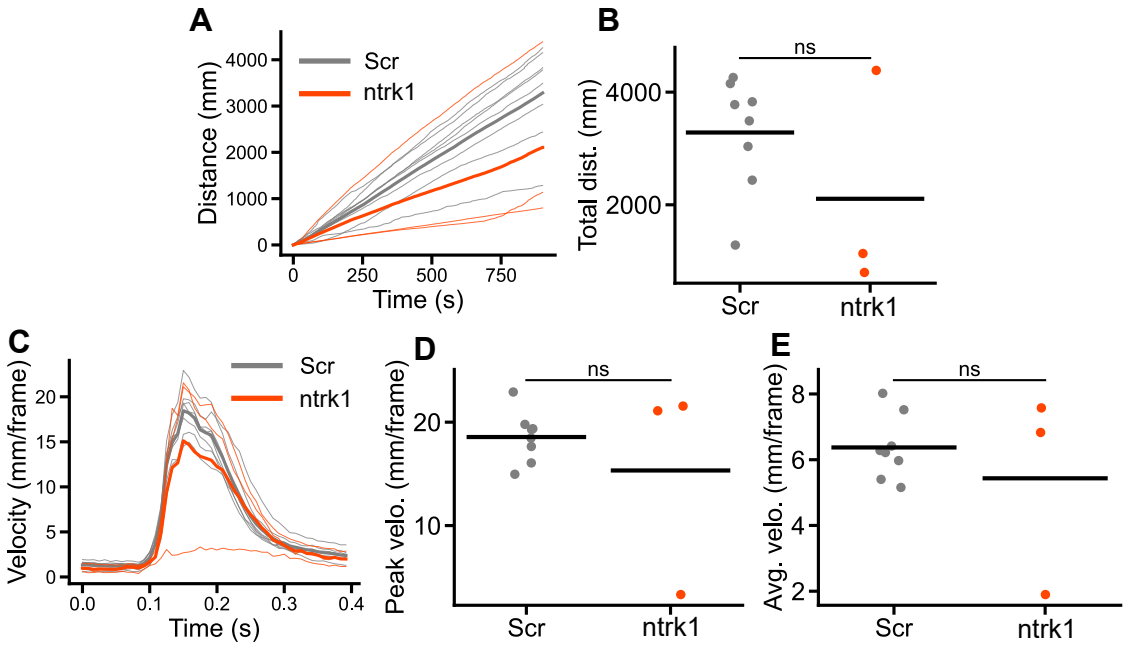

Figure 5.10: ***ntrk1* F0 knockouts without anatomical defects show locomotor activity indistinguishable from controls**. A: Cumulative distance covered by "normal" *ntrk1* mutants ('ntrk1', n=3), compared to scrambled-injected controls ('Scr', n=8). B: There is a trend towards a lower total distance covered by "normal" *ntrk1* mutants, compared to scrambled-injected controls, however this is not significant (F=1.35, p=0.210 with an Independent Samples t-Test). C: Bout velocity of "normal" *ntrk1* mutants compared to scrambled-injected controls. D-E: No significant differences could be detected on peak bout velocity (D) and average bout velocity (E) when comparing "normal" *ntrk1* mutants to scrambled-injected controls (peak bout velocity: F=10, p=0.776 with a Mann-Whitney U test; average bout velocity: F=0.82, p=0.433 with an Independent Samples t-Test).

The second population of *ntrk1* mutants was particularly promising, since the lack of obvious defects meant I could test those fish on the infrared laser setup to determine whether mutations in *ntrk1* led to changes in sensitivity to noxious heat. As shown in Figure 5.11.A, *ntrk1* mutants respond to a range of infrared laser intensities with both SL and LL responses. When compared to scrambled controls, no clear differences were observed in the LL response latency (Figure 5.11.B), LL response probability (Figure 5.11.C) or SL response probability (Figure 5.11.D). This was unexpected and contradicted what is seen in the mouse literature, where mice lacking *Ntrk1* show loss of responses to noxious stimuli (Smeyne et al., 1994). Therefore, I then looked more closely at the various response kinematics (peak cumulative angle, curvature, motion and vigour), for both the LL (Figure 5.12) and SL (Figure 5.13) responses, with the aim of detecting more subtle changes in the response to the laser. I focused on the five or two highest intensities, as they more reliably induced LL or SL responses, respectively. Using a Kolmogorov–Smirnov test, I was unable to detect any significant differences in the CDs of each of these kinematics when comparing scrambled controls to *ntrk1* F0 knockouts. In short, in *ntrk1* F0 knockout fish that were otherwise normal, I was unable to detect any differences in their behavioural responses to noxious heat in the form of an infrared laser, compared to controls.

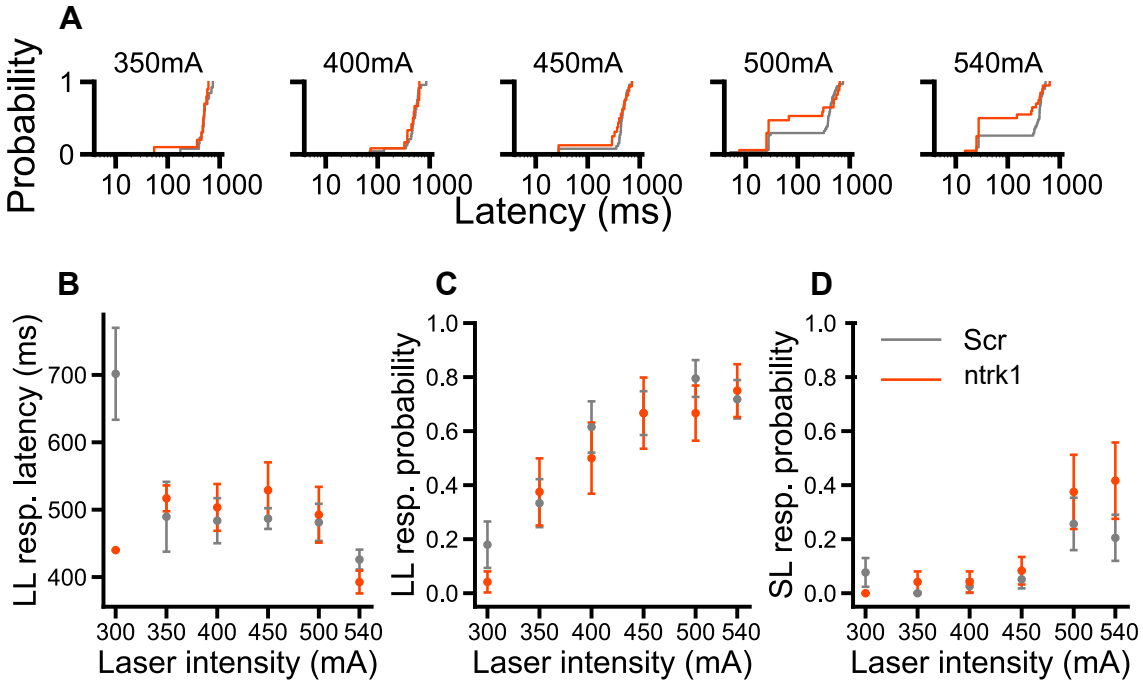

Figure 5.11: **"Normal" *ntrk1* F0 knockouts respond to a range of infrared laser intensities with both SL and LL responses**. A: Cumulative distribution of response latencies of scrambled-injected controls (grey, n=39 trials) and *ntrk1* (orange, n=24 trials) to the infrared laser. The x axis is shown on a logarithmic scale. B-D: "Normal" *ntrk1* F0 knockouts show LL response latencies (B), LL response probabilities (C) and SL response probabilities (D) that are indistinguishable from controls (scrambled: n=13 fish; ntrk1: n=8 fish). Error bars represent SEM.

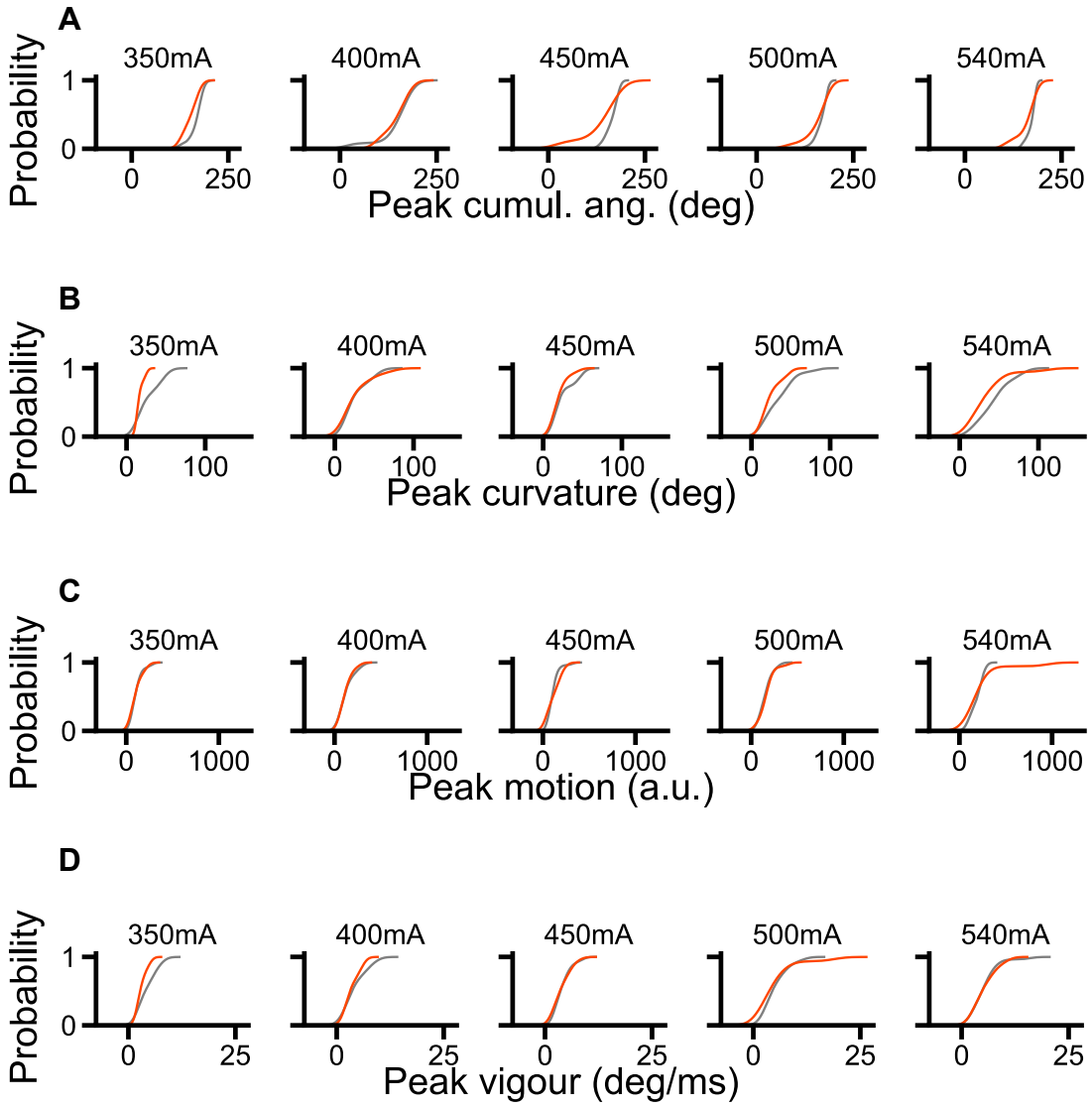

Figure 5.12: **"Normal" *ntrk1* F0 knockouts show LL responses which are kinematically indistinguishable from those of scrambled controls**. Kernel density estimate plots of LL peak cumulative angle (A), peak curvature (B), peak motion (C) and peak vigour (D) are shown for the five highest infrared laser intensities (350 mA – 540 mA), for both *ntrk1* mutants (orange, n=24 trials) and scrambled-injected controls (grey, n=39 trials). A Kolmogorov–Smirnov test was unable to detect significant differences in the distributions of controls and mutants. This was true for all kinematics and laser intensities (peak cumulative angle: F=0.470, p=0.139 (350 mA); F=0.208, p=0.867 (400 mA); F=0.346, p=0.144 (450 mA); F=0.216, p=0.602 (500 mA); F=0.349, p=0.105 (540 mA); peak curvature: F=0.479, p=0.115 (350 mA); F=0.25, p=0.684 (400 mA); F=0.337, p=0.166 (450 mA); F=0.296, p=0.259 (500 mA); F=0.345, p=0.112 (540 mA); peak motion: F=0.222, p=0.898 (350 mA), F=0.167, p=0.977 (400 mA); F= 0.346, p=0.144 (450 mA); F=0.232, p=0.542 (500 mA); F=0.365, p=0.081 (540 mA); peak vigour: F=0.385, p=0.325 (350 mA); F=0.25, p=0.684 (400 mA); F=0.197, p=0.757 (450 mA); F=0.280, p=0.288 (500 mA); F=0.198, p=0.690 (540 mA)).

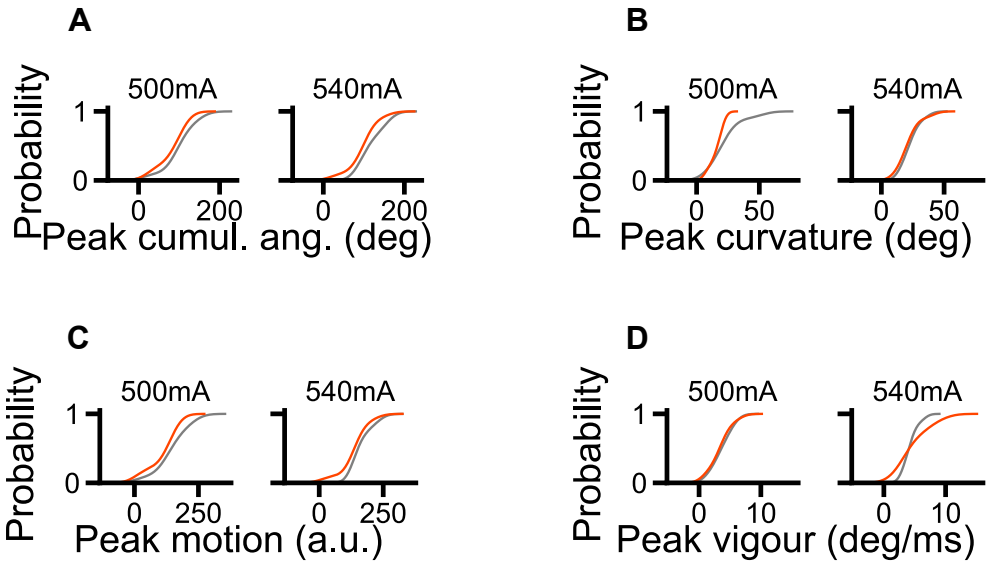

Figure 5.13: **"Normal" *ntrk1* F0 knockouts show SL responses which are kinematically indistinguishable from those of scrambled controls.** Kernel density estimate plots of SL peak cumulative angle (A), peak curvature (B), peak motion (C) and peak vigour (D) are shown for the two highest infrared laser intensities (500 mA and 540 mA), for both *ntrk1* mutants (orange, n=24 trials) and scrambled-injected controls (grey, n=39 trials). A Kolmogorov–Smirnov test was unable to detect significant differences in the distributions of controls and mutants. This was true for all kinematics and laser intensities (peak cumulative angle: F=0.278, p=0.740 (500 mA); F=0.275, p=0.823 (540 mA); peak curvature: F=0.389, p=0.343 (500 mA); F=0.25, p=0.898 (540 mA); peak motion: F=0.3, p=0.637 (500 mA); F=0.325, p=0.602 (540 mA); peak vigour: F=0.189, p=0.975 (500 mA); F=0.3, p=0.723 (540 mA)).

The F0 method for the generation of mutants can lead to mosaicism in the mutations generated, both across the population of mutants and within each animal (Kroll et al., 2021). Indeed, we could already see that, across our mutants, some looked anatomically normal while others didn't, potentially due to these differences. I hypothesised that mutants that appeared normal might have less severe mutations, which could perhaps explain why no changes in heat sensitivity were observed. Therefore, I then sought to test whether "curved spine" *ntrk1* mutants responded to noxious heat in the infrared laser setup. As explained previously, a detailed characterisation of any behaviours seen would not be possible due to the anatomical defects in these fish, but it might still be possible to understand whether noxious heat sensitivity is abolished in fish with potentially more disruptive mutations in the *ntrk1* gene. Strikingly, "curved spine" *ntrk1* F0 knockouts still consistently showed tail-flick behaviours when stimulated with the infrared laser (Figure 5.14.A). This was seen across different infrared laser intensities and throughout the three rounds of stimulation. These tail-flicks appear smaller than those performed by "normal" *ntrk1* mutants (Figure 5.14.B), and none of them occur in latencies compatible with a SL response (Figure 5.14.C) but, as mentioned, this cannot be interpreted due to their developmental defects. In short, *ntrk1* F0 knockout fish with clear anatomical effects, suggesting the occurrence of severe mutations, retained the ability to respond to noxious heat.

In conclusion, F0 knockout of *ntrk1* or *prdm12b* leads to severe anatomical and swimming defects in a subset of larvae, but sensitivity to noxious stimuli is not abolished. Additionally, *ntrk1* mutants without anatomical or swimming abnormalities show preserved responses to noxious heat, comparable to those of controls.

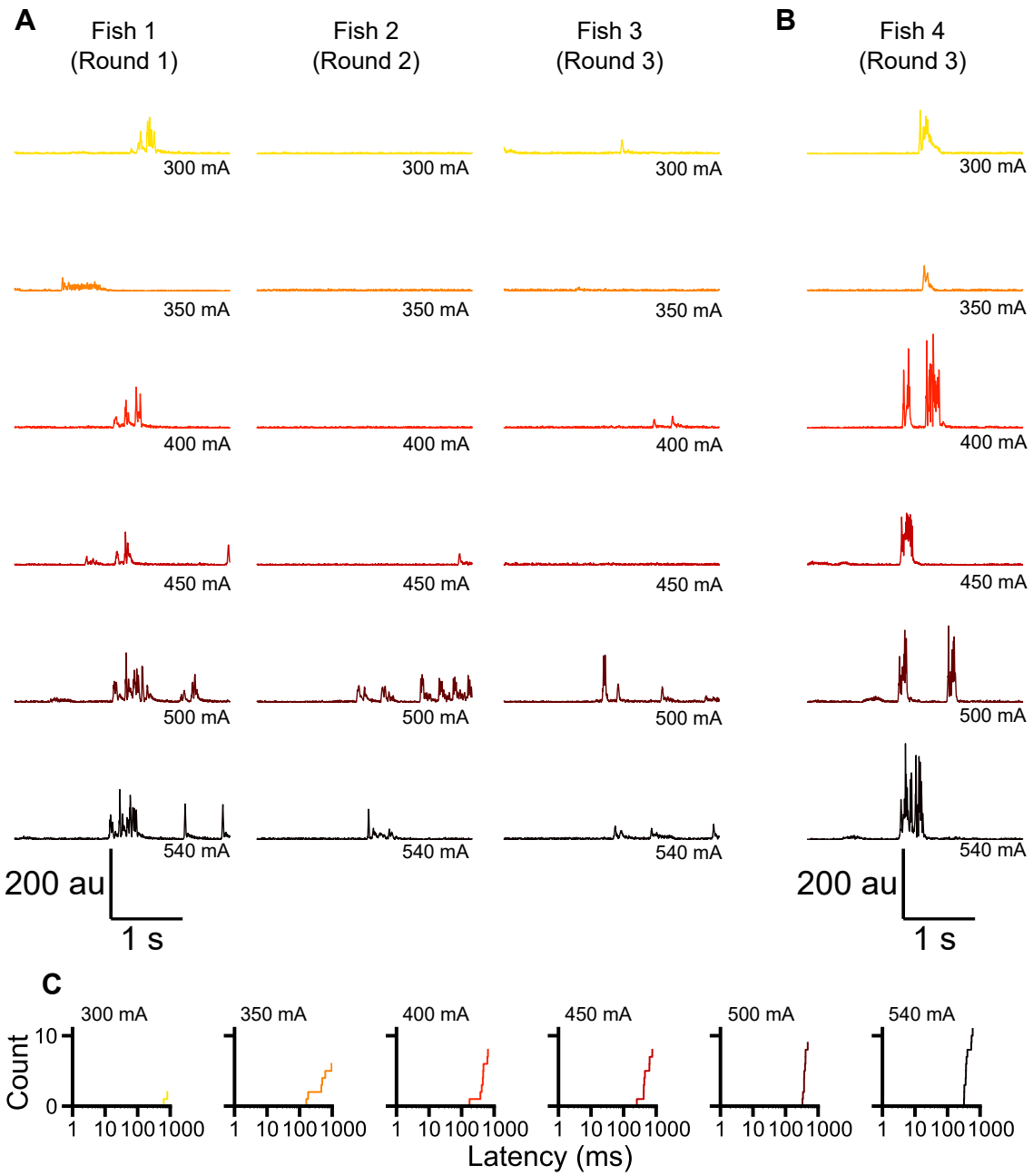

Figure 5.14: ***ntrk1* mutants with severe anatomical defects retain the ability to sense heat**. A and B: Representative motion traces of three "curved spine" *ntrk1* F0 knockout fish (fish 1, 2, and 3) across different rounds of stimulation (A), and one "normal" *ntrk1* F0 knockout fish (fish 4) across one round of stimulation (B) (round 1 is shown for fish 1; round 2 for fish 2; round 3 for fish 3; and round 3 for fish 4). X axis shows time in ms and ranges from -500 ms (before laser is switched on) to 2000 ms. R1, R2 and R3 represent rounds 1, 2 and 3, respectively. C: Cumulative distribution of response latencies of "curved spine" *ntrk1* F0 knockout fish to the infrared laser (n=12 trials). The x axis is shown on a logarithmic scale.

5.2.4 Single knockout of *ngfb* does not lead to reduced embryo viability or severe anatomical defects

In zebrafish, there are two orthologs of the human *NGF* gene, *ngfa* and *ngfb*. This is seen across many zebrafish genes as a result of a teleost-specific whole genome duplication event (Meyer and Schartl, 1999; Howe et al., 2013). In the early stages of development, *ngfb* is expressed in the TG and in the brain; it is also widely expressed across the brain and spinal cord of adult zebrafish (Nittoli et al., 2018; Cacialli et al., 2019; Hui et al., 2017; Sun et al., 2018). To the best of my knowledge, no studies have reported the expression pattern of *ngfa*. However, some studies have indirectly pointed towards a possible role of *ngfa* in sensory neuron development in zebrafish. For instance, Wu et al. (2019) showed that zebrafish embryos treated with Aflatoxin B1 display aberrant morphology of TG neurons and significantly down-regulated the expression of *ngfa*, amongst other genes. Therefore, I first targeted *ngfa* and *ngfb* simultaneously with the aim of generating double knockouts (where ngf function was completely abolished), and then targeted each ortholog separately to disentangle the role of each ortholog. Embryo viability was monitored from 1 to 4 dpf across the different groups: “uninjected” (WT embryos from the same batch that did not receive any injections), “scrambled” (embryos injected with ‘scrambled’ crRNA); and “*ngfa/b*-inj”, “*ngfa*-inj” and “*ngfb*-inj” (embryos injected with crRNA targeting both *ngfa* and *ngfb*, only *ngfa*, or only *ngfb*, respectively). In the “*ngfa/b*-inj” group, similar results were observed as to those seen after targeting *ntrk1* or *prdm12b*: the percentage of viable fish at 4 dpf was lower in “*ngfa/b*-inj” fish, compared to scrambled controls (Figure 5.15.A), and the “curved spine” phenotype, underlying the drop in viability from 3 to 4 dpf, was also present. On the other hand, viability in both the “*ngfa*-inj” group and the “*ngfb*-inj” group was slightly lower than in “scrambled” fish, but this difference was not as noticeable as when both orthologs were targeted simultaneously, and neither was the drop in viability between 3 and 4 dpf (Figures 5.15.C and E).

Brightfield images of a representative subset of larvae from each group (“scrambled”, “*ngfa/b*-inj”, “*ngfa*-inj” and “*ngfb*-inj”) were taken. Then, each larva was euthanised and its gDNA was extracted for genotyping. Since I was unable to use the HL-PCR method to test the efficiency of crRNA targeting *ngfa*, I could not genotype fish in the “*ngfa/b*-inj” and “*ngfa*-inj” groups. Consequently, we

cannot be sure about whether individual fish have been mutated. However, I successfully genotyped fish in the "*ngfb*-inj" group and found that most *ngfb* F0 knockout fish looked normal (Figure 5.15.F). Conversely, most fish in the "*ngfa/b*-inj" group showed anatomical defects at 7 dpf, particularly the "curved spine" phenotype and deflated swim bladders, and these defects often appeared more severe than in *ntrk1* or *prdm12b* mutants (Figure 5.15.B). This strongly suggests that, on a population level, at least one of the crRNA targeting *ngfa* was often successful at inducing mutations: in *ngfb* F0 knockout fish, the presence of a functional *ngfa* would compensate for the loss of *ngfb*, leading to fish with no defects (Figure 5.15.F)*;* in "*ngfa*-inj fish, the presence of a functional *ngfb* would compensate for the loss of *ngfa*, leading to fish with no defects (Figure 5.15.D); in "*ngfa/b*-inj" fish, the loss of both genes would lead to the observed anatomical defects (Figure 5.15.B). Indeed, Kroll et al. (2021) showed that using only two gRNA is sufficient to achieve a high rate of F0 biallelic knockouts (> 75% per gene).

However, since I was not able to genotype individual "*ngfa*-inj" or "*ngfa/b*-inj" fish, I was unable to analyse the behavioural experiments carried out on these fish. Instead, I focused on the *ngfb* F0 knockout fish. In the future, using alternative genotyping techniques, such as Sanger sequencing or MiSeq, would allow me to genotype "*ngfa*-inj" and "*ngfa/b*-inj" fish and pursue the behavioural experiments on confirmed mutants with those genotypes. Both Sanger sequencing and MiSeq have been successfully used by Kroll et al. (2021) to genotype F0 embryos following CRISPR-Cas9.

In short, F0 knockouts of *ngfb* do not show reduced embryo viability or severe anatomical defects, but embryos injected with gRNA targeting both *ngf* orthologs do.

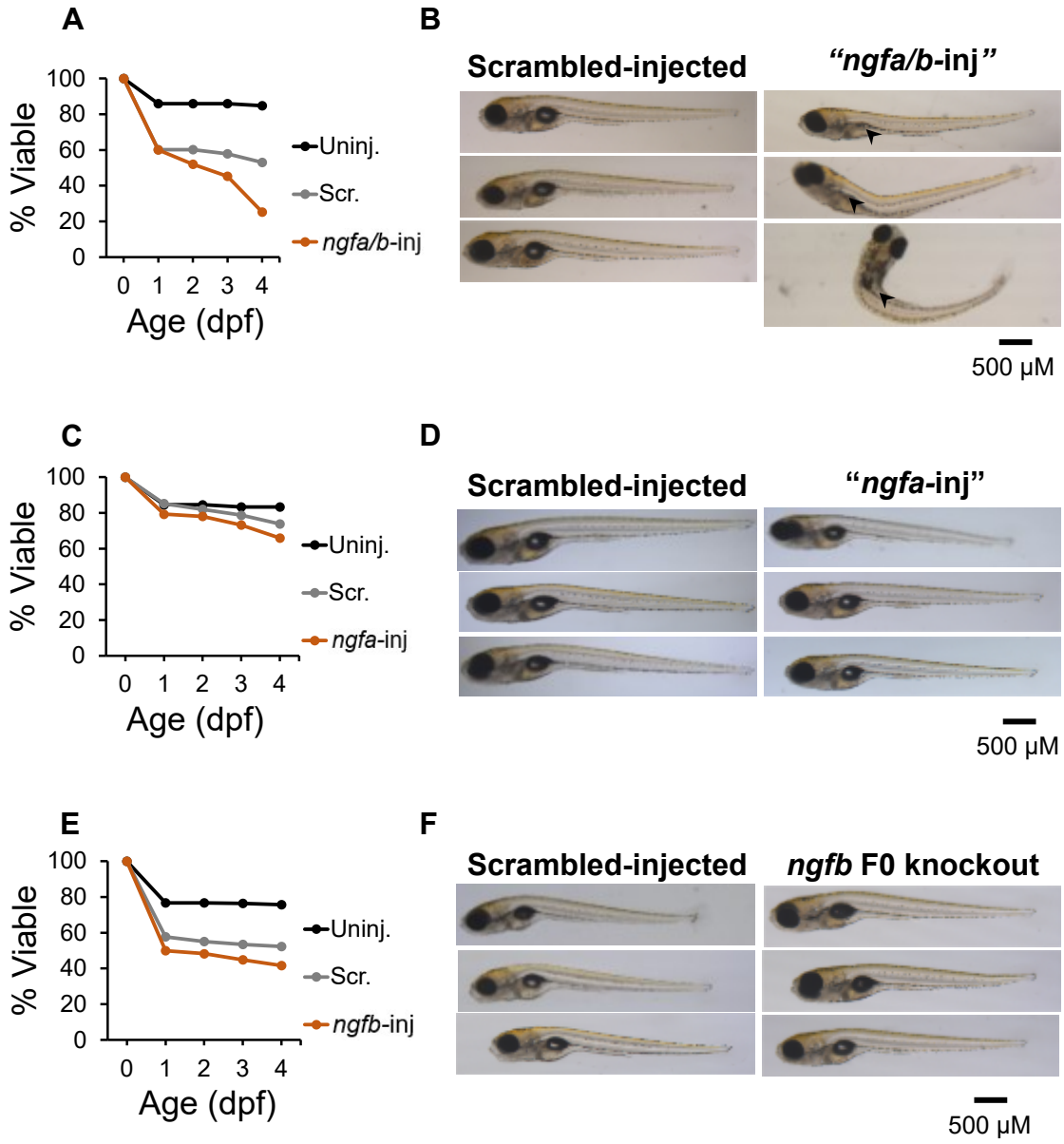

Figure 5.15: **Viability of embryos injected with crRNA targeting *ngfa*, *ngfb* or both *ngfa* and *ngfb***. A, C, and E show the percentage of injected embryos that were viable on each day (Day 0: injection day). Compared to scrambled-injected controls, the percentage of viable fish at 4 dpf was lower in the *ngfa/b*-inj group (A), but not in the *ngfa*-inj (C) or *ngfb*-inj groups (E). The striking drop in viability from 3 to 4 dpf in the *ngfa/b*-inj group was due to some developmental defects becoming apparent at that age. B, D, and F show representative brightfield images of scrambled controls (B, D, F), *ngfb* mutants (F), or fish injected with crRNA targeting *ngfa* (D), or both *ngfa* and ngfb (B). Several embryos injected with crRNA targeting both *ngfa* and *ngfb* showed a bent spine and swim bladder inflation defects (arrowhead). This was rarely seen in *ngfb* mutants or fish injected with crRNA targeting only *ngfa*. 'Uninj.': uninjected controls; 'Scr.' and 'Scrambled-injected': controls injected with scrambled crRNA; '*ngfa/b*-inj': embryos injected with crRNA targeting both *ngfa* and *ngfb*; '*ngfa*-inj': embryos injected with crRNA targeting *ngfa*; '*ngfb*-inj': embryos injected with crRNA targeting *ngfb*; '*ngfb* F0 knockout': confirmed *ngfb* F0 knockout.

5.2.5 *ngfb* F0 knockouts show normal swimming behaviours and normal LL responses to the laser but almost completely abolished SL responses

While *ngfb* F0 mutants showed no obvious anatomical defects, I first looked to confirm that their basal levels of locomotor activity were also unaffected before performing the infrared laser experiments. To do that, *ngfb* mutant fish (n=6 fish) and scrambled-injected controls (n=8 fish) were allowed to freely explore an open arena, as described previously. As predicted from their normal anatomy, *ngfb* F0 knockout fish resembled scrambled-injected fish in their swimming behaviour: they maintained their balance throughout the experiment (Figure 5.16.A, top panel) and explored the whole arena (Figure 5.16.A, bottom panel). Quantifying this behaviour across the whole population, I was unable to detect any significant differences between *ngfb* mutants and scrambled controls regarding total distance covered (Figures 5.16.B and C; p=0.711), or bout size (Figure 5.16.D), both in terms of peak bout velocity (Figure 5.16.E; p=0.460) and average bout velocity (Figure 5.16.F; p=0.833). This suggests that the locomotor activity of *ngfb* mutants is not deeply affected by the mutations.

Encouraged by these results, I proceeded to test these fish on the infrared laser setup to assess whether noxious heat sensitivity was altered in *ngfb* F0 knockouts. *ngfb* mutants (n=21 fish) show LL responses across all intensities tested (Figure 5.17.A), with response probabilities similar to those of scrambled controls (n=29 fish) (Figure 5.17.C). At the highest laser intensity there seemed to be a trend towards higher LL response probabilities in *ngfb* mutants, however this was not statistically significant (Figure 5.17.C; F=218.5; p=0.078 with a Mann–Whitney U test). This preserved response to the infrared laser in the *ngfb* mutants was not unexpected, since the presence of a functional *ngfa* in these fish could be compensating for the loss of *ngfb*. Moreover, these results would be in accordance with what I observed for the “normal” *ntrk1* F0 knockout fish, where no effect on LL response probability was seen (*ntrk1* encodes trka, the receptor that *ngfb* primarily binds to). Strikingly, however, the SL response was nearly completely abolished in *ngfb* mutants, with a Mann–Whitney U test revealing a statistically significant decrease in the SL response probability in *ngfb* mutants at the highest intensity, compared to controls (Figure 5.17.D; F= 394; p=0.016).

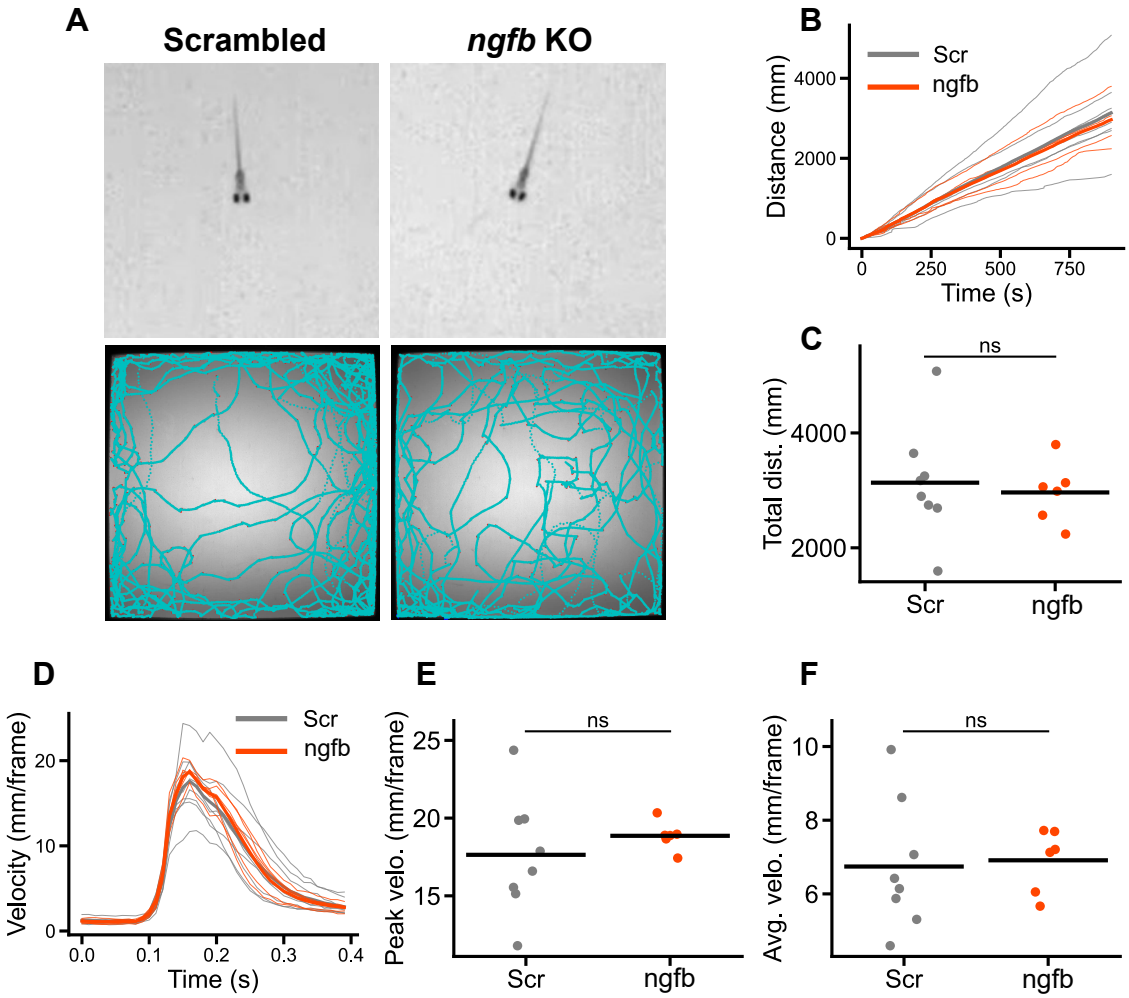

Figure 5.16: ***ngfb* F0 knockouts show locomotor activity indistinguishable form controls**. A: Mutants show no obvious anatomical deformities and resemble scrambled-injected fish in their swimming behaviour: they maintain their balance throughout the experiment (top panel) and explore the whole arena (bottom panel, which shows the tracked positions of the fish in the corresponding top panel over the course of the experiment). B: Cumulative distance covered by *ngfb* mutants ('ngfb', n=6), compared to scrambled-injected controls ('Scr', n=8). C: No significant differences could be detected between the total distance covered by *ngfb* mutants and controls (F=0.380, p=0.711 with an Independent Samples t-Test). D: Bout velocity of *ngfb* mutants compared to scrambled-injected controls. E-F: No significant differences were detected on peak bout velocity (E) and average bout velocity (F) when comparing *ngfb* mutants to scrambled-injected controls (peak bout velocity: F=-0.762, p=0.460; average bout velocity: F=-0.216, p=0.833, both with an Independent Samples t-Test).

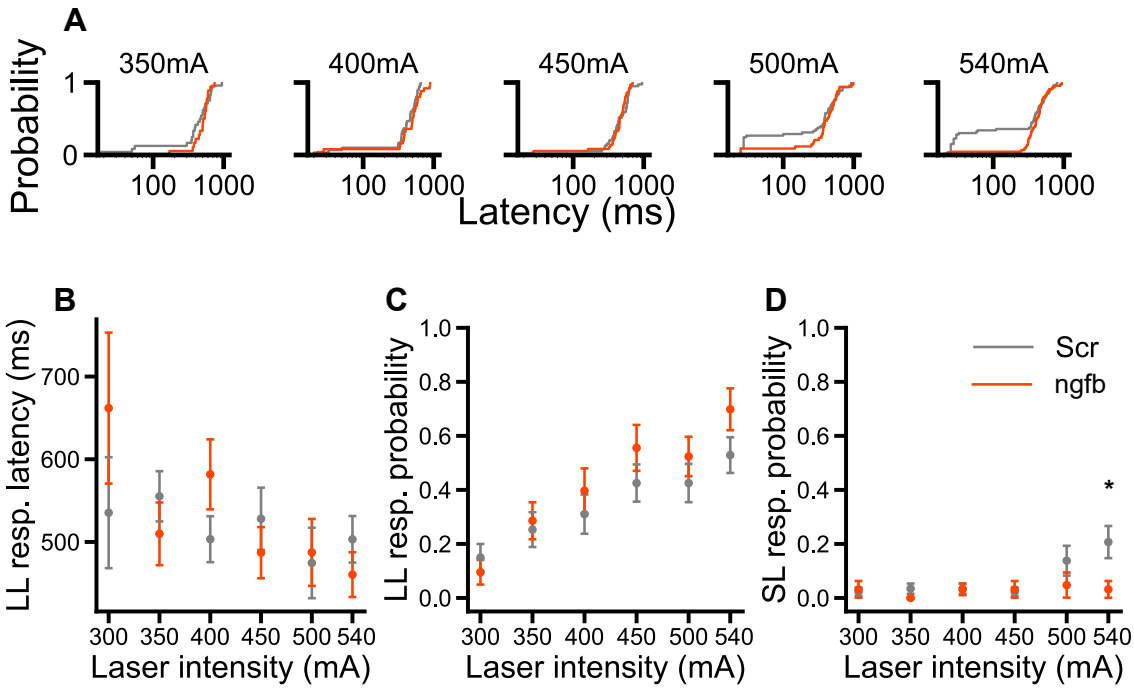

Figure 5.17: ***ngfb* F0 knockouts respond to a range of infrared laser intensities with LL responses but largely lack SL responses**. A: Cumulative distribution of response latencies of scrambled-injected controls (grey, n=87 trials) and *ngfb* (orange, n=63 trials) to the infrared laser. The x axis is shown on a logarithmic scale. B-D: *ngfb* mutants show LL response latencies (B) and LL response probabilities that are indistinguishable from controls but show significantly decreased SL response probabilities (e.g., at 540 mA: F=394, p=0.016 with a Mann-Whitney U test, as indicated by the asterisk) (scrambled: n=29 fish; ngfb: n=21 fish). Error bars represent SEM.

This nearly complete absence of a SL response suggested possible defects in heat sensation, which was unexpected given the normal LL response probability and latencies I observed in the mutants. As such, I first sought to determine whether there were more subtle defects in the LL response to heat. To do that, I compared the various LL response kinematics (peak cumulative angle, curvature, motion and vigour) in scrambled and *ngfb* mutants (Figure 5.18). Using a Kolmogorov–Smirnov test, I was unable to detect any significant differences in the CDs of each of these kinematics, suggesting the LL response is preserved in mutants. Looking more closely into the SL responses of individual fish, I found that while the population of scrambled fish showed a mix of SL response probabilities at 540 mA, with fish responding in 0/3, 1/3, 2/3 or 3/3 trials, the population of *ngfb* mutants actually contained a single responding fish at 540 mA, with all other 20 fish showing 0/3 SL responses (Figure 5.19.A). Interestingly, this fish actually drove the majority of the SL responses seen across all laser intensities: it responded reliably across multiple intensities and across all three rounds of stimulation (Figure 5.19.C), showing a SL response in a total of 8/18 trials (SL response probability = 0.44; Figure 5.19.B, right, Fish number 21). Apart from this fish, only two other *ngfb* mutants showed at least one SL response across the whole experiment (three rounds of six intensities), with one of them responding in 1/18 trials (SL response probability = 0.06) and the other in 2/18 trials (SL response probability = 0.11). The F0 method for the generation of mutants can lead to mosaicism in the mutations generated, both across the population of mutants and within each animal (Kroll et al., 2021). As such, it is possible that there was a mix between WT *ngfb* and mutated *ngfb* within the strongly responding fish shown in Figure 5.19.C: enough WT *ngfb* for the production of functional ngfb, but also enough mutated *ngfb* for the HL primers to fail to suppress DNA amplification (Figure 5.4.B), which would lead to a “mutant” outcome on the HL-PCR.

In short, *ngfb* F0 knockouts show LL responses to the laser that are indistinguishable from controls, but almost completely abolished SL responses. This was unexpected and suggested a specific impairment in the circuitry driving the SL response. Further experiments were carried out to address this, as detailed below.

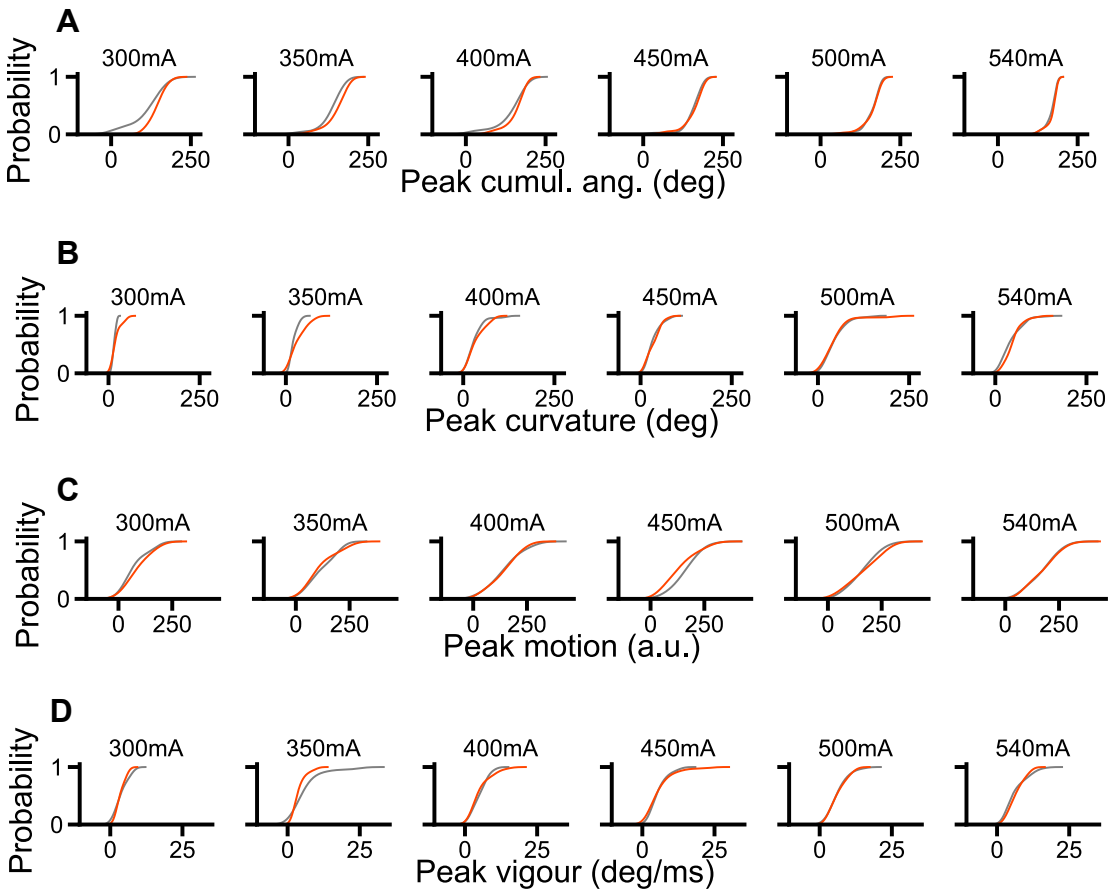

Figure 5.18: ***ngfb*** **F0 knockouts show LL responses which are kinematically indistinguishable from those of scrambled controls**. Kernel density estimate plots of LL peak cumulative angle (A), peak curvature (B), peak motion (C) and peak vigour (D) are shown for both *ngfb* mutants (orange, n=63 trials) and scrambled-injected controls (grey, n=87 trials). A Kolmogorov–Smirnov test was unable to detect significant differences in the distributions of controls and mutants. This was true for all kinematics and laser intensities (peak cumulative angle: F=0.436, p= 0.336 (300 mA); F=0.399, p=0.062 (350 mA); F=0.204, p=0.571 (400 mA); F=0.274, p=0.105 (450 mA); F=0.160, p=0.688 (500 mA); F=0.225, p=0.168 (540 mA); peak curvature: F=0.385, p=0.438 (300 mA); F=0.343, p=0.151 (350 mA); F=0.246, p=0.344 (400 mA); F=0.233, p=0.234 (450 mA); F=0.158, p=0.699 (500 mA); F=0.247, p=0.103 (540 mA); peak motion: F=0.295, p=0.765 (300 mA); F=0.222, p=0.624 (350 mA); F=0.111, p=0.985 (400 mA); F=0.277, p=0.099 (450 mA); F=0.168, p=0.627 (500 mA); F=0.103, p=0.941 (540 mA); peak vigour: F=0.231, p=0.931 (300 mA); F=0.298, p=0.279 (350 mA); F=0.236, p=0.393 (400 mA); F=0.179, p=0.536 (450 mA); F=0.090, p=0.995 (500 mA); F=0.208, p=0.245 (540 mA)).

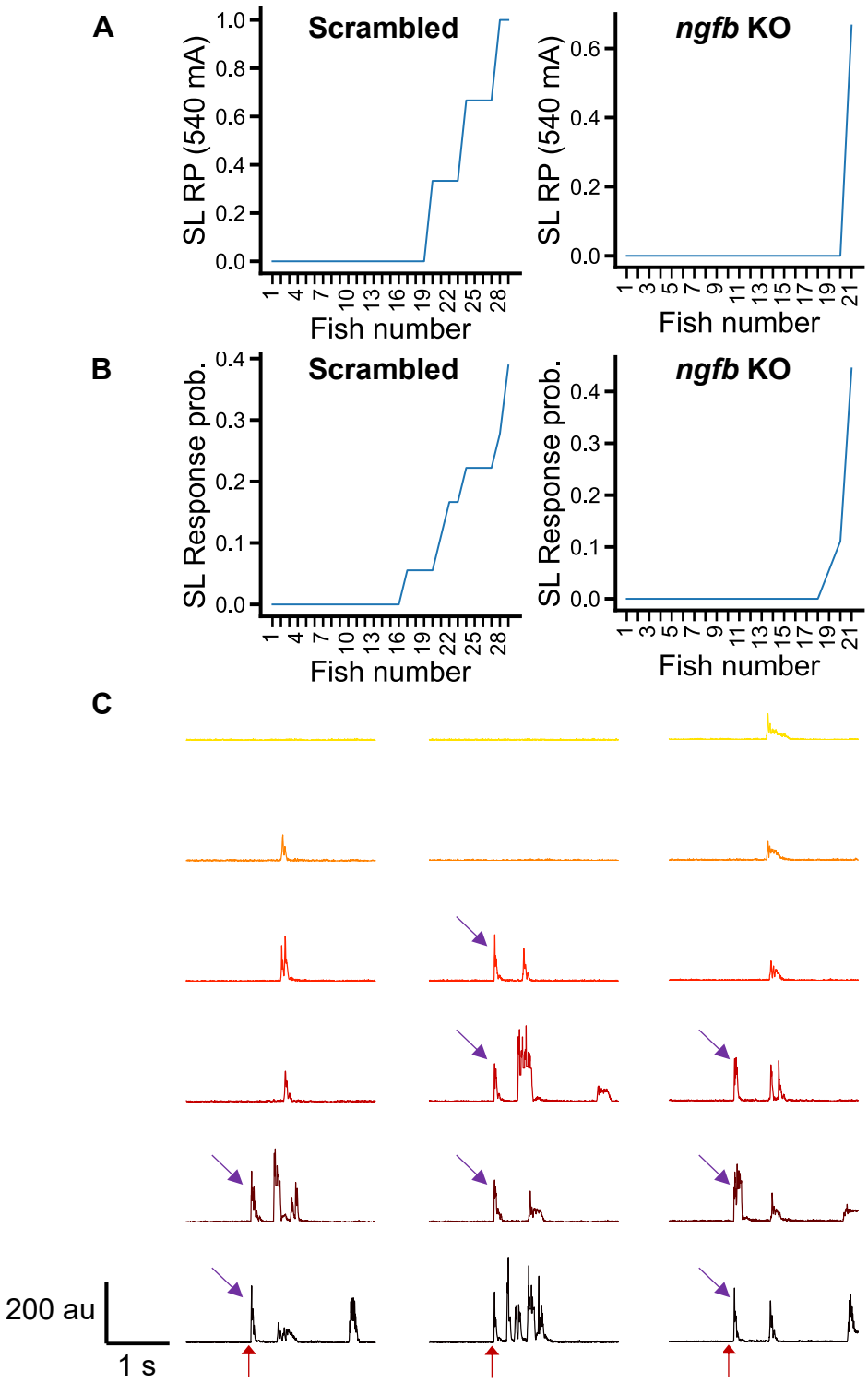

Figure 5.19: **The SL response is completely abolished in most *ngfb* F0 knockouts**. A: In scrambled-injected fish, at 540 mA, there was a mixed population within the responding fish, and 13/29 fish (SL response probability = 0.45) responded in at least one trial. Conversely, only 1/21 *ngfb* mutant fish (SL response probability = 0.05) showed at least one SL response. B: The only *ngfb* mutant that showed SL responses at 540 mA responded reliably across several laser intensities and all three rounds of stimulation, with an overall response rate of 0.44 (over three rounds of six intensities). C: Representative motion traces of the responsive *ngfb* mutant shown in A across rounds 1 (left), 2 (middle) and 3 (right). The red arrow indicates when the laser was switched on (t=0). A SL response is seen in all three rounds, across many intensities (purple arrows).

5.2.6 *ngfb* F0 knockouts can perform fast escape responses and visually-mediated escape responses

As detailed in Chapter 4, zebrafish larvae can perform very fast escape responses when exposed to acoustic/vibrational stimuli, with latencies of only a few tens of milliseconds. To understand if the absence of a SL response to the laser was due to an overall impairment in their ability to perform fast escapes, *ngfb* mutants were exposed to a 'tap' vibration assay. Here, a tap is delivered every 15 s to the bottom of the petri dish where larvae are freely swimming. Fish are tracked online (Figure 5.20.A) and the properties of their escape responses are measured. *ngfb* mutants were capable of executing fast escape responses with comparable probability to scrambled controls (Figure 5.20.B; p=0.277). Importantly, these responses were very fast, with latencies typically below 25 ms and comparable to those of controls (Figure 5.20.C; p=0.916), and angular velocities that were not significantly different to those displayed by scrambled-injected fish (Figure 5.20.D; p=0.279). This suggests *ngfb* mutants do not have an overall impairment in their ability to perform fast escapes.

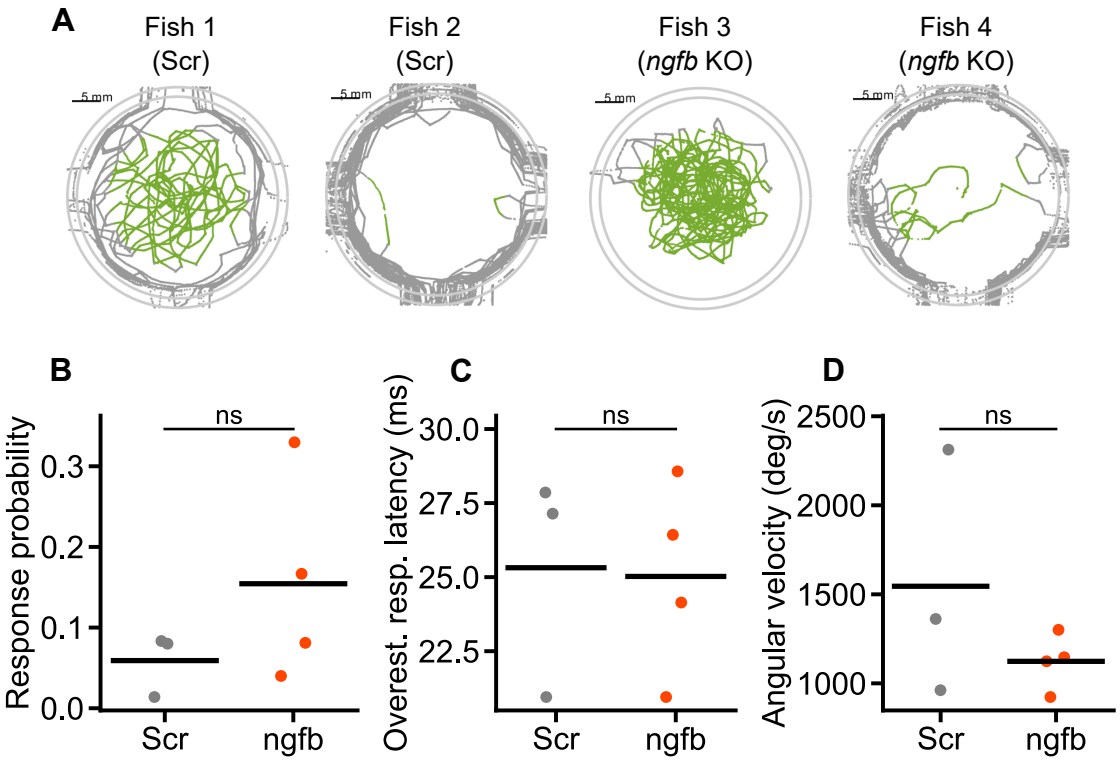

Figure 5.20: ***ngfb* F0 knockouts retain the ability to perform fast escape responses**. *ngfb* mutants (n=4 fish) and scrambled controls (n=3 fish) underwent a 'tap' vibration assay. Here, a tap is delivered every 15 s to the bottom of the petri dish where larvae are freely swimming. Fish are tracked online, and the properties of their escape responses are measured. A: Tracked positions of representative fish over the course of the experiment. Green traces indicate successful tracking. Grey traces indicate failures in tracking, which occur when fish approach the edge of the dish. During frames where tracking fails, no behavioural data is recorded. For a fish to be included in the analysis, escape data from at least ten 'taps' must have been successfully recorded (Fish 1, 3, and 4). Otherwise, fish are discarded (Fish 2). Scr: scrambled-injected; *ngfb* KO: *ngfb* F0 knockout. B: *ngfb* mutants executed fast escape responses with comparable probability to scrambled controls (F=-1.219, p=0.277 with an Independent Samples t-Test). C: The responses performed by *ngfb* mutants were fast, with latencies typically around 25 ms, which were also comparable to those of controls (F=0.110, p=0.916 with an Independent Samples t-Test). 'Overest. resp. latency': Overestimated response latency. In this setup, to calculate response latencies, an LED is placed adjacent to the petri dish (within the camera field of view) and is triggered at the same time as the solenoid tapper. The response latency is calculated in relation to the LED being switched on (t=0). Because the LED is switched on almost instantaneously but there is a slight delay between the tapper being triggered and the tap being delivered to the bottom of the petri dish, escape latencies calculated in relation to the LED being switched on are overestimated. D: Angular velocities of *ngfb* mutants were not significantly different to those displayed by scrambled-injected fish (F=1.213, p=0.279 with an Independent Samples t-Test).

Alternatively, there was a possibility that the SL response was absent in *ngfb* knockouts due to visual deficits present in these mutants. Indeed, *ngfb* is expressed early in development in visual areas such as the optic tectum (Nittoli et al., 2018) (although no expression could be found in the adult – Cacialli et al. (2019)), and, as detailed in Chapter 4, my control experiments using blind fish did not allow me to conclusively rule out a visual component partly or fully underlying the SL response to the laser. Therefore, my next aim was to assess whether *ngfb* mutants could execute escape responses to visual stimuli. To do that, freely swimming larvae were exposed to a series of looming stimuli and their escape response rate was measured. Firstly, it was important to distinguish fast escape responses from spontaneous bouts that simply happened to fall within 1 second of the presentation of a looming stimulus. This was necessary because larvae exhibited a high basal rate of swimming. Indeed, when looking at a 1 s window 30 seconds before stimulus presentation, both scrambled and *ngfb* mutants showed a high "response" rate (Figure 5.21.A, "unfilt."). Therefore, a filter was applied such that only responses with a high peak velocity were considered escape responses (see Chapter 2 – Methods). When this filter was applied to the 1 s window 30 seconds before stimulus presentation, virtually no "responses" were detected (Figure 5.21.A, "filt."), but responses were still recorded when looking at a 1 s window after stimulus presentation (Figure 5.21.A, "loom"). These were therefore considered visually-evoked escape responses. *ngfb* mutants were found to reliably perform escape responses to the looming stimuli, with response probabilities (Figure 5.21.B; $p=0.362$) and latencies (Figures 5.21.C and D; $p=0.263$) that were similar to those of scrambled-injected controls. This strongly suggests *ngfb* mutants can perform escape responses to visual stimuli. Nevertheless, it is worth mentioning that the latencies of these responses were greater than those of SL responses (> 200 ms vs ~ 25 ms), both in scrambled controls and *ngfb* mutants. As such, escape responses to these looming stimuli are not directly comparable to SL responses to the laser. It would be theoretically possible for different pathways to mediate each of them. This will be further discussed below. This data nevertheless indicates that *ngfb* mutants have preserved escape responses to visual stimuli.

Taken together, these results suggest that *ngfb* mutants can perform fast escape responses, with latencies compatible with those of SL responses, as well as visually-mediated escape responses.

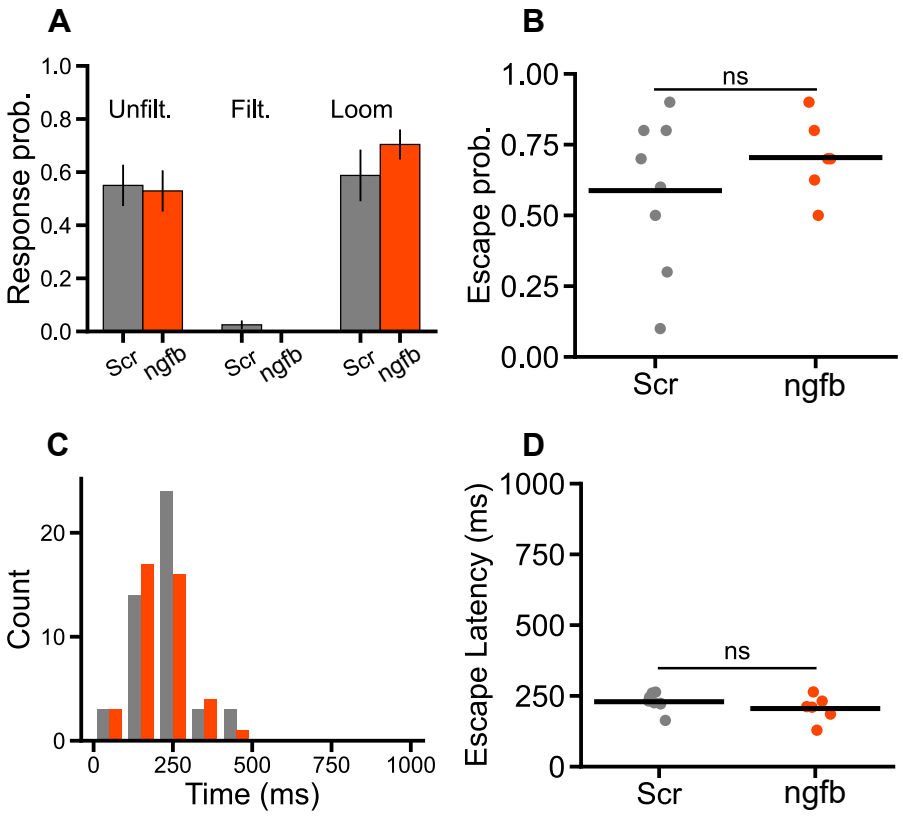

Figure 5.21: ***ngfb* F0 knockouts retain the ability to perform escape responses to visual stimuli.** Free-swimming larvae were exposed to a series of looming stimuli and their escape response rate and latency were measured. A: Looking at a 1 s window 30 seconds before stimulus presentation, both scrambled controls (n=8) and *ngfb* mutants (n=6) showed a high "response" rate ("Unfilt." – unfiltered, that is, before a filter was applied). Therefore, a filter was applied such that only responses with a high peak velocity were considered escape responses. When this filter was applied to the same 1 s window 30 seconds before stimulus presentation, virtually no "responses" were detected ("Filt." – filtered, that is, after a filter based on peak velocity was applied), but responses were recorded when looking at a 1 s window after stimulus presentation ("Loom"). These were therefore considered visually-evoked escape responses. B-D: *ngfb* mutants reliably performed escape responses to the looming stimuli, with response probabilities (B) and latencies (C and D) that were indistinguishable from those of scrambled-injected controls (escape probability: F=-0.947, p=0.362; escape latency: F=1.175, p=0.263 both with an Independent Samples t-Test). A histogram of the distribution of response latencies of scrambled controls (grey) and *ngfb* mutants (orange) is shown in C.

5.3 Discussion

In this chapter, I generated F0 knockouts of *ngfb*, *ntrk1* and *prdm12b*, the zebrafish orthologs of *NGF*, *NTRK1* and *PRDM12*. To the best of our knowledge, this is the first time *ntrk1* and *ngfb* have been mutated in zebrafish. F0 knockout of *ntrk1* or *prdm12b* leads to severe anatomical defects in a subset of larvae, particularly a curved spine and/or lack of inflation of the swim bladder at 6-7 dpf, which affect their swimming. Nevertheless, these fish retain the ability to respond to infrared laser stimulation with tail-flick behaviours. On the other hand, F0 knockouts of *ngfb* lead to mutants with no obvious anatomical or locomotor defects. These fish show normal LL responses to stimulation with the infrared laser but SL responses are almost completely abolished.

5.3.1 Generation of F0 knockouts

To generate F0 knockouts, I used a recently developed method in which the injection of three synthetic crRNAs per gene allows for the generation of biallelic knockouts with fully penetrant phenotypes in >90% of injected animals (Kroll et al., 2021). I then used HL-PCR to test their ability to induce mutations (Figure 5.4.B; Rand et al., 2005; Kroll et al., 2021). For *ngfb* and *prdm12b*, all three crRNA initially designed were successful at inducing mutations; for *ntrk1*, two of the three crRNA were successful at reliably inducing mutations, and a fourth crRNA was designed with the aim of identifying a third working crRNA.

Regarding *ngfa*, I found that one of the three crRNAs injected was not successful at generating mutations. This could potentially be due to undocumented single-nucleotide polymorphisms (SNPs) affecting the ability of the crRNA to recognise our DNA target sequence of interest. As for the other two crRNAs targeting *ngfa*, I was unable to use HL-PCR to determine their efficiency, since the headloop tag in my primers was not able to suppress DNA amplification in WT fish. *ngfa* is a short, single exon gene, meaning that all the crRNA target sequences within only a few dozen base pairs of each other. Therefore, one possible explanation for this could be that the mutations generated by the other gRNA disrupted the sequence that the headloop tag would normally be complementary to. Another possible explanation could be the presence of SNPs

in the sequence the headloop tag would normally be complementary to. HL-PCR has been shown to be highly sensitive, detecting even 1-bp deletions in stable mutant lines (Kroll et al., 2021). This means that SNPs in WT fish could affect the ability of the headloop tag to suppress DNA amplification, preventing its use as a genotyping method for those specific target sites. Indeed, for the third crRNA targeting *ngfa*, subsequent analysis did reveal a record on Ensembl of a synonymous mutation located within the sequence the tag should be complementary to (Figure 5.4.E). On the other hand, no SNPs were reported for the sequence relating to the second crRNA targeting *ngfa*, but as described previously, there could be undocumented SNPs in that area. Going forward, a possible solution would be to sequence the parents used to generate the embryos prior to designing the crRNA and HL-PCR primers. This is more time-consuming but would ensure there were no SNPs in my sequences of interest.

Nevertheless, the survival and anatomical results observed across *ngfa*-injected fish, *ngfa/b*-injected fish, and *ngfb* mutants suggest that at least one of the crRNA targeting *ngfa* was successful at inducing mutations. In fact, while most successful *ngfb* F0 knockouts looked normal (Figure 5.15.F), most fish injected with gRNA targeting simultaneously *ngfa* and *ngfb* showed severe anatomical defects at 7 dpf (Figure 5.15.B), alike those observed in *ntrk1* or *prdm12b* mutants. This strongly suggests that, on a population level, at least one of the crRNA targeting *ngfa* was successful at inducing mutations: in *ngfb* F0 knockout fish, the presence of a functional *ngfa* would compensate for the loss of *ngfb*, and vice-versa, resulting in largely normal fish; conversely, in fish where both isoforms are targeted, the loss of both genes leads to the observed anatomical defects. Indeed, the chances of designing three crRNA that are not effective are low, and injecting even just two functional crRNA already leads to a high mutation probability (Kroll et al., 2021). In the future, it would be interesting to explore the effect of a loss of *ngfa* on noxious heat sensation. Based on the HL-PCR technical difficulties described above, alternative genotyping techniques should be used for this gene, such as Sanger sequencing or MiSeq. Both have been successfully used by Kroll et al. (2021) to genotype F0 embryos following CRISPR-Cas9.

5.3.2 *prdm12b* F0 knockouts and *ntrk1* F0 knockouts display a similar phenotype

<u>*PRDM12* mutants</u>

PRDM12 mutations in mammals. In mammals, *PRDM12* encodes a transcription factor which regulates the expression of TRKA (encoded by *NTRK1*), the receptor that NGF preferentially binds to (Kaplan et al., 1991; Klein et al., 1991; Marmigère and Ernfors, 2007). In humans, *PRDM12* is expressed exclusively in the peripheral nervous system, and mutations in *PRDM12* have been shown to lead to HSAN8 (Chen et al., 2015). In rodents, *Prdm12* can also be found in some brain areas and is necessary for the development of nociceptive neurons by regulating the expression of TrkA, with loss of *Prdm12* during development causing defects in pain sensation (Kinameri et al., 2008; Desiderio et al., 2019; Landy et al., 2021; Imhof et al., 2020).

Effect of zebrafish prdm12b mutations on survival. In zebrafish, *prdm12b* expression is restricted to the hindbrain and spinal cord at 36 hpf (hours post-fertilisation) and 50 hpf. However, its expression in earlier stages is more widespread, including the forebrain (both telencephalon and diencephalon) at 24 hpf (Zannino et al., 2014). This could suggest a broader role of *prdm12b* in zebrafish. However, contrary to what is seen in mice, where animals in which *Prdm12* is constitutively knocked out die within a few hours from birth (Desiderio et al., 2019; Landy et al., 2021), I found *prdm12b* F0 knockouts to survive until at least 6-7 dpf, some of which without clear developmental abnormalities. This is consistent with what was previously reported in the zebrafish literature: studies using antisense morpholino oligonucleotides to knock down the expression of *prdm12b*, as well as those using CRISPR-Cas9 to generate germline mutants for *prdm12b*, found larvae to survive until at least 4 dpf (Zannino et al., 2014; Yildiz et al., 2019). Nevertheless, *prdm12b* homozygous mutants do not survive until adulthood and normally die by juvenile stages (~21 dpf) (Yildiz et al., 2019).

Effect of zebrafish prdm12b mutations on anatomy, neuroanatomy and behaviour. The majority of *prdm12b* F0 knockouts showed various anatomical defects, such as the “curved spine” phenotype (which includes defects in swim bladder inflation and/or a bent spine) and abnormal swimming. Surprisingly, neither Zannino et al. (2014) nor Yildiz et al. (2019) reported anatomical defects

resembling those. Indeed, Yildiz et al. (2019) were unable to detect any defects in the structure of tail/trunk musculature of *prdm12b* mutants, and Zannino et al. (2014) mainly reported mild differences in the number of abducens neurons, the migration of facial neurons and the number of oligodendrocyte precursor cells (the latter only in the very early stages of development) in *prdm12b* morphants. This could perhaps be explained by the fact that these defects become more apparent from 6-7 dpf, and these studies largely focused on younger larvae. Interestingly, however, both Zannino et al. (2014) and Yildiz et al. (2019) found mutations in *prdm12b* to lead to a loss of V1 interneurons in the hindbrain and spinal cord, and subsequent disruption of the stereotyped touch-evoked C-bend escape response, with M-cells remaining unaffected. This raises interesting questions about the circuitry underlying motor responses to somatosensory stimuli in zebrafish larvae. Importantly, the “curved spine” *prdm12b* mutants generated in the present study consistently showed tail-flick behaviours when stimulated with the infrared laser (Figure 5.7.A), which suggests that mutations in *prdm12b* do not lead to a complete loss of noxious heat sensing. Moreover, a small subset of *prdm12b* F0 knockouts (3/15) lacked overt anatomical or swimming abnormalities. As such, future studies on healthy *prdm12b* F0 knockouts could help elucidate the basis of these circuits underlying behavioural responses to noxious and (innocuous) sensory stimuli. For instance, it would be particularly interesting to assess whether healthy *prdm12b* F0 knockouts retain the ability to execute SL responses to noxious heat in the infrared laser assay.

***NTRK1* mutants**

NTRK1 mutations in mammals. In humans, various mutations in *NTRK1* have been shown to lead to congenital insensitivity to pain with anhidrosis (CIPA), also known as HSAN4 (Indo et al., 1996; Mardy et al., 1999; Indo 2001). This phenotype is mostly replicated in rodents: mice lacking *Ntrk1* show loss of responses to noxious stimuli and a complete loss of nociceptors in the DRG, as well as loss of sympathetic ganglia neurons and cholinergic neurons of the basal forebrain (Smeyne et al., 1994; Snider, 1994). *Ntrk1* homozygous mutants survive longer than *Prdm12* mutants, but also do not reach adulthood (Smeyne et al., 1994). In mice, *Ntrk1* is expressed in the DRG and some sensory cranial ganglia, including the TG (Martin-Zanca et al., 1990).

ntrk1 expression in zebrafish. There are some key differences between neurotrophin receptors in zebrafish, compared to rodents. Firstly, while *ntrk1* is expressed in RB neurons and TG in zebrafish larvae, expression in DRG neurons has not been detected (Gau et al., 2017; Pan et al., 2012; Hahn et al., 2020; Martin et al., 1995; Palanca et al., 2013). This provides further support to our targeting of the head (which is innervated by the TG) in our infrared laser experiments. Secondly, there are two zebrafish orthologs to each of the other two main TRK receptors found in mammals, TRKB and TRKC: *ntrk2a* and *ntrk2b* encode trkB1 and trkB2, and *ntrk3a* and *ntrk3b* encode trkC1 and trkC2, respectively (Martin et al., 1995). Of these, *ntrk2a* and *ntrk3a* seem to be the most relevant orthologs for our work, since they have been consistently found to be expressed in TG and RB neurons (Martin et al., 1995; Gau et al., 2017; Nittoli et al., 2018). *ntrk2b* has mainly been detected in the brain, with mutations in this gene affecting subsets of the dopaminergic and serotonergic neuronal populations that correlate with anxiety-like behaviours (Nittoli et al., 2018; Martin et al., 1995; Hahn et al., 2020; Sahu et al., 2019), and *ntrk3b* has been detected in the TG by some (Pan et al., 2012) but not others (Martin et al., 1995; Martin et al., 1998).

However, the expression of these genes in different TG subpopulations does not resemble that of mouse sensory neurons. Broadly speaking, during mouse development, expression of TrkA specifies nociceptors, expression of TrkC and Runx3 (without TrkB) specifies proprioceptors, and expression of TrkB (or a few other factors) specifies mechanoreceptors (Fitzgerald 2005; Marmigère and Ernfors, 2007; Lallemend and Ernfors, 2012; for more detail, see Chapter 1 – Introduction). In adult DRG, expression of Trpv1 and Trpa1 can only be found in nociceptors, which do not express TrkB or TrkC at any point in development (Usoskin et al., 2015). In zebrafish, on the other hand, trpa1b and trpv1 have both been found in a subset of trkC1+ TG neurons, and trpv1 has been found to co-localise with trkB1 (Pan et al., 2012; Gau et al., 2017). Importantly for us, however, a subset of trpv1+ neurons (and a small subset of trpa1b+ neurons) in the zebrafish larvae TG has been found to also express trkA, replicating what is seen in peptidergic and non-peptidergic unmyelinated DRG neurons in adult mice (Gau et al., 2017; Usoskin et al., 2015). This suggests that, despite the other differences reported, mutating *ntrk1* could potentially affect the development of trpv1+ neurons, which are known to play a role in heat sensation in zebrafish

(Gau et al., 2013), and therefore lead to changes in their response to the infrared laser. Indeed, the expression of *ntrk1* and *ntrk2a* has recently been found to precede that of other *ntrk* genes in the zebrafish embryo (Hahn et al., 2020), suggesting they might be key developmental players. Alternatively, it would be possible for no differences in heat sensitivity to be detected, even if zebrafish trkA is involved in the differentiation and maintenance of the neurons where it is expressed. This is because, contrary to what is seen in mice, trpv1 is expressed in other, trkA-, subpopulations of zebrafish TG neurons, which could in principle remain unaffected in *ntrk1* mutants (Gau et al., 2017). Indeed, the nociceptive system is particularly known for its redundancy, with mice retaining robust responses to somatosensory heat in the presence of only one of the three TRP channels involved in noxious heat sensation, Trpv1, Trpa1, and Trpm3 (Vandewauw et al., 2018). Additionally, the F0 method for the generation of mutants can lead to mosaicism in the mutations generated, both across the population of mutants and within each animal (Kroll et al., 2021).

Zebrafish ntrk1 F0 knockouts retain the ability to sense heat. In accordance with my second prediction, I was unable to detect any clear differences in the LL response latency (Figure 5.11.B), LL response probability (Figure 5.11.C) or SL response probability (Figure 5.11.D) of “normal” *ntrk1* F0 mutants, compared to scrambled controls, in the infrared laser assay. There were also no significant differences in the other response kinematics analysed (peak cumulative angle, curvature, motion and vigour – Figure 5.12 and 5.13). Moreover, “curved spine” mutants still retained the ability to respond to heat. In the future, it would be interesting to explore whether any of these mutants show changes in the number of trpv1+ neurons, which could be addressed by performing *in situ* hybridisation. This could help elucidate the developmental pathways underlying the differentiation and specification of both trpv1+ neurons and other TG neuron subtypes in zebrafish.

Developmental defects of *ntrk1* and *prdm12b* mutants

A subset of ntrk1 and prdm12b mutants show abnormal swimming. ntrk1 and *prdm12b* F0 knockouts, as well as the *ngfa/b*-injected fish, often displayed abnormal (spiral) swimming. This could potentially result from the swim bladder

inflation deficits, the curved spines, and/or other factors. Indeed, dozens of genes have been reported to lead to various abnormal swimming patterns, when mutated (Granato et al., 1996).

Mutations in different genes can lead to swim bladder inflation defects. Swim bladder inflation is a critical developmental stage for zebrafish, as it decreases body density, allowing fish to obtain neutral buoyancy. This relies on the "swim-up" behaviour, whereby fish swim towards the surface for initial inflation of the swim bladder (Lindsey et al., 2010). Defects in swim bladder inflation upon mutation of certain genes have been reported in the literature. For instance, homozygous mutants for *gbx1* and *gbx2* (genes important for cerebellum development) fail to form a swim bladder and die during early larval stages (Su et al., 2014). Moreover, *dolk* mutants, which have mutations in dolichol kinase (a broadly expressed regulator of the glycoprotein biosynthesis pathway), show no obvious morphological defects by 5 dpf except for failure to inflate their swim bladders, and die by 14 dpf, although the underlying mechanism was not investigated (Meserve et al., 2021). Finally, *gsx2* mutant zebrafish show swim bladder inflation failures and this also seems to prevent survival past larval stages, although again no causal relationships were established (Coltogirone et al., 2021). *Gsx2* and closely related *Gsx1* encode homeobox transcription factors expressed in the CNS, with roles in promoting regional neuronal identity in mice. *Gsx2* mutant mice show disrupted hindbrain and forebrain morphology and die shortly after birth (Szucsik et al., 1997). Interestingly, a recent study by Baba et al. (2022) has shown *Gsx2* expression to be decreased in *Prdm12*-knockout P19 cells (mouse embryonic tumour cells used as a model for neural differentiation). It would be interesting to study whether zebrafish *prdm12b* mutants also show decreased expression of *gsx2*, and whether that could partly explain the swim bladder inflation defects I report. However, other factors are likely to be involved, seeing as my *ntrk1* F0 knockouts, as well as fish injected with gRNA simultaneously targeting *ngfa* and *ngfb*, also showed those defects, which suggests this might be a consequence of disrupting the NGF/TRKA pathway in zebrafish.

The "curved spine" phenotype. It is unclear if the bent spines seen in a subset of *ntrk1* F0 knockouts, *prdm12b* F0 knockouts, and *ngfa/b*-injected fish are a consequence of the swim bladder inflation defects, or a direct consequence

of mutations in *ntrk1, prdm12b* or *ngfa/b*. For instance, Goolish and Okutake (1999) found that zebrafish larvae raised in the absence of an air–water interface fail to inflate their swim bladders and show increased spine curvature. On the other hand, Coltogirone et al. (2021) and Hageter et al. (2021) reported a lack of gross morphological abnormalities in *gsx2* mutants, despite the defects in swim bladder inflation. Interestingly, several toxins, such as TBBPA (tetrabromobisphenol A), TDCPP (tris(1,3-dichloro-2-propyl) phosphate) and chlorpyrifos, have also been found to lead to a “curved spine” (deflated swim bladder and/or bent tail) phenotype, with some suggesting thyroid disruption to be underlying the deflated swim bladder (Chen et al., 2016; Godfrey et al., 2017; Qiao et al., 2021; Richendrfer et al., 2012; Li et al., 2018; Noyes et al., 2015; Fu et al., 2013). Strikingly, exposure to TDCPP has been found to lead to decreased expression of *ntrk1* in Chinese rare minnow (*Gobiocypris rarus*) adults (Yuan et al., 2016), and rats treated with chlorpyrifos showed decreased levels of TrkA protein the prefrontal cortex (Terry et al., 2007), suggesting decreased *ntrk1* expression could be a possible link between toxin exposure and a “curved spine”. However, Chen et al. (2016) actually found increased *ntrk1* expression in zebrafish after exposure to TBBPA.

Additional effects of mutating *ntrk1* cannot be ruled out. For instance, *ntrk1* variants have been detected in patients with Hirschsprung's disease (which results from a failure of enteric nervous system progenitors to migrate, proliferate, differentiate, or survive), and zebrafish has been successfully used to model this disease by mutating other disease genes, suggesting similarities in the zebrafish ENS, compared to that of mammals (Yang et al., 2019; Jiang et al., 2015; Pu et al., 2017; Gui et al., 2017). In short, it is unclear what could be underlying the “curved spine” phenotype we observe in *prdm12b* and *ntrk1* mutants. However, as argued previously with regards to the swim bladder inflation defects, it seems likely that it results from a failure of the NGF/TRKA pathway, since a similar phenotype is found in *prdm12b* mutants, *ntrk1* mutants, and fish injected with gRNA targeting both *ngf* orthologs. This again suggests a key role of this pathway in zebrafish development.

Finally, it is worth noting that, as detailed, there were a range of phenotypes amongst *ntrk1* F0 knockouts and *prdm12b* F0 knockouts, with some mutants appearing normal and others showing a range of anatomical defects of various

degrees of severity. This may be explained by the fact that the F0 method can lead to mosaicism in the mutations generated (Kroll et al., 2021). It is possible that mutants with the most severe phenotypes had mutations in sequences of the gene that are more important for protein function, such as specific functional domains. In the future, it would be interesting to perform deep sequencing of *ntrk1* F0 knockouts and *prdm12b* F0 knockouts, for instance by Illumina MiSeq (Kroll et al., 2021), in order to establish these connections between each induced mutation and the resulting mutant phenotype. This may give us insight into which gene sequences are critical for protein function.

5.3.3 Understanding the phenotype of *ngfb* mutants

In humans, NGF is required for sensory neuron specification, and mutations in the *NGF* gene have been shown to lead to HSAN5, a developmental pain insensitivity disorder (Fitzgerald, 2005; Einarsdottir et al., 2004). Mice lacking Ngf fail to respond to noxious stimuli and show loss of sensory and sympathetic neurons (Crowley et al., 1994). Homozygous mutants for *Ngf* often survive for a few weeks, but show defects in food intake and are developmentally delayed. In zebrafish, there are two *ngf* orthologs, *ngfa* and *ngfb*, although previous studies in the zebrafish literature strikingly often fail to acknowledge this, and instead focus simply on *ngfb*, referring to it as "*ngf*". As detailed previously, I was unable to genotype fish where *ngfa* had been targeted and therefore focused on *ngfb* for subsequent experiments. In the early stages of development, *ngfb* can be found in the TG and in the brain, including in the optic tectum and otic vesicle; it is also widely expressed across the brain and spinal cord of adult zebrafish, and it is strongly expressed in rod photoreceptors of zebrafish larvae, juvenile and adult fish (Nittoli et al., 2018; Cacialli et al., 2019; Hui et al., 2017; Sun et al., 2018).

ngfb F0 mutant larvae appeared anatomically normal and did not have the "curved spine" phenotype seen in *ntrk1* and *prdm12b* mutants. This is likely due to the presence of a functional *ngfa* gene, since the "curved spine" was again found in fish injected with gRNA targeting both *ngf* orthologs simultaneously. I could not detect any differences in the LL response of these mutants to the infrared laser. This is not unexpected, since it is in accordance with what I observed for the "normal" *ntrk1* F0 knockout fish (*ntrk1* encodes trka, the receptor

that ngf primarily binds to), and the presence of a functional *ngfa* could be compensating for the loss of *ngfb*. Fast escape responses to vibrational stimuli and escape responses to looming stimuli were also unaffected, suggesting ngfb is not involved in these behaviours. However, the SL response was largely abolished.

It is unclear what might be underlying these results. The fact that these mutants can execute normal responses to vibrational stimuli (Figure 5.20), with latencies of less than 25 ms, suggests that there is not an overall impairment in the circuitry driving fast escape responses in these fish. Moreover, in Chapter 4 I showed the LL response to be driven by heat, rather visual or acoustic stimuli. A preserved, normal, LL response in the *ngfb* mutants therefore strongly suggests that there is not an overall impairment in the circuitry underlying escape-like responses to heat in these fish. Taken together, these results suggest there are two independent heat-sensing pathways, one driving the “LL heat response” and the other the “SL heat response”, with only the latter being affected in the mutants. One limitation to these conclusions is that I have not been able to conclusively rule out a visual contribution to the SL response in WT fish. It is true that *ngfb* F0 mutants showed normal responses to visual (looming) stimuli, which suggests their vision is not impaired, but these can be mediated by a variety of circuits, depending on the properties of the looming stimulus (Bhattacharyya et al., 2017). Indeed, the latencies observed were too long for these responses to be classed as a SL response, so it would be theoretically possible for an “ngfb-independent looming escape circuit” to be unaffected, and an “ngfb-dependent fast visual circuit” to be impaired. In the future, a detailed analysis of the TG subpopulations of *ngfb* F0 mutants should provide further insight on this matter (see below: Future work).

5.3.4 Future work

In the future, it would be especially interesting to explore the neuroanatomical basis of the loss of the SL response in *ngfb* mutants. A particularly promising avenue would be to assess whether there are changes in the overall population (or specific subpopulations) of TG sensory neurons. To that end, I have designed and tested (in WT fish) RNA probes for several genes which are known to play a role in nociception in mammals (and zebrafish). In WT larvae, I was able to use these probes to detect TG expression of several of these genes (*trpv1*, *cgrp*, *p2rx2*, and *trpa1b* but not *trpm3*) (Figure 5.22.A-E; also Gau et al., 2013; Pan et al., 2012; Appelbaum et al., 2007; Prober et al., 2008; Kastenhuber et al., 2013). Additionally, I optimised a protocol to combine fluorescent *in situ* hybridisation (FISH) with immunohistochemistry (Figure 5.22.F). Using these probes and protocols in the future will allow us to understand if the loss of the SL response is due to a loss of specific populations of TG neurons. Further, combining FISH with *c-fos* staining, a marker of neural activity (Herrera and Robertson, 1996), would give us an understanding of which cell populations are responding to the heat stimulus.

By advancing our knowledge of the mechanisms underlying noxious heat sensation in zebrafish larvae, and the role played by different genes in these processes, this will help further establish the zebrafish as a model to study the genetics of nociception.

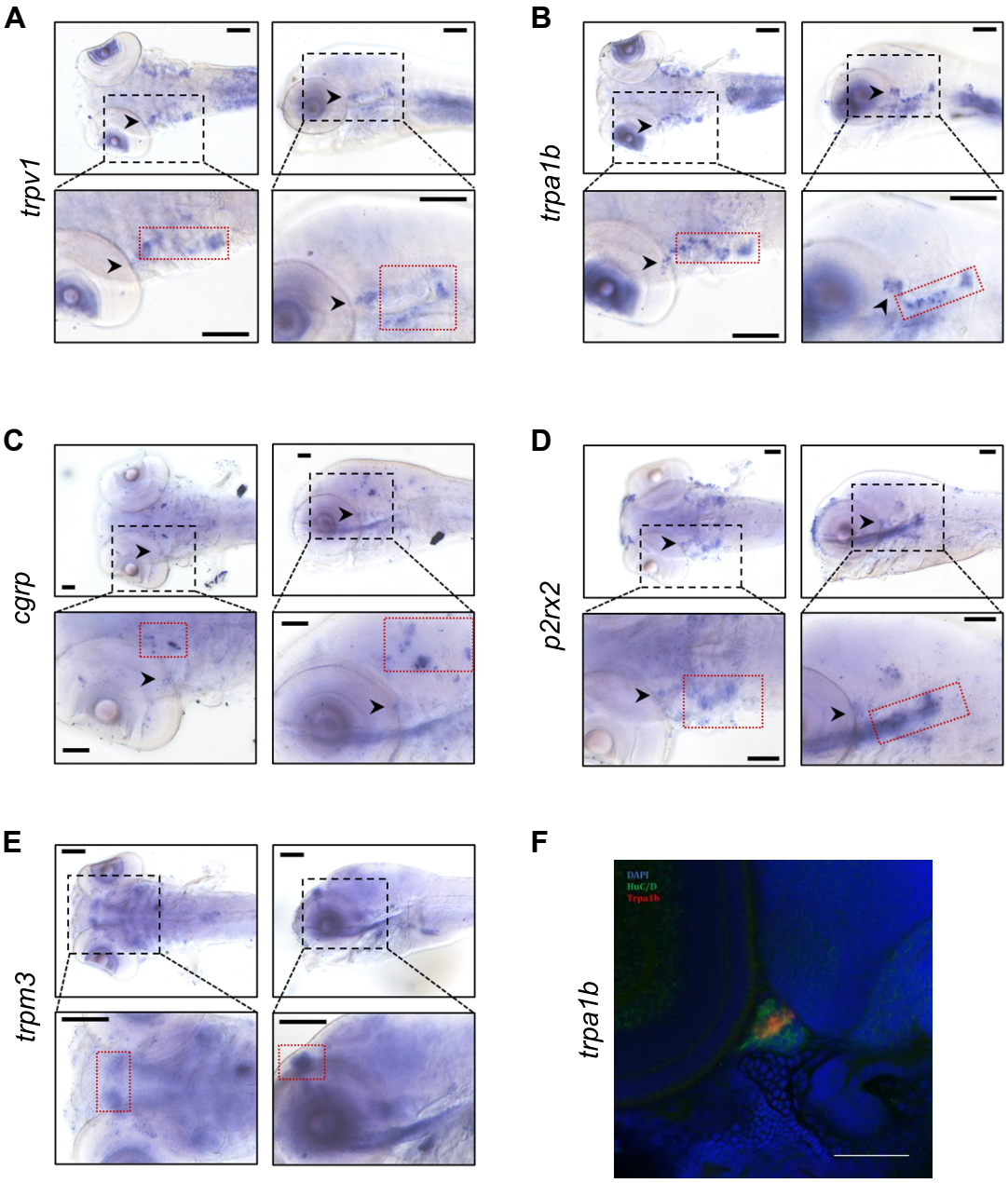

Figure 5.22: **Testing RNA probes for the detection of nociception-related genes in the TG of zebrafish larvae**. In situ hybridisation was performed on larval zebrafish for *trpv1* (A), *trpa1b* (B), *cgrp* (C), *p2rx2* (D) and *trpm3* (E), at 7 dpf. For each transcript, dorsal (left) and lateral (right) views are shown, at 10x (top) and 20x (bottom) magnifications. Black arrowheads indicate TG. The red dotted line indicates either other cranial nerve ganglia (for *trpv1*, *trpa1b* and *p2rx2*), the forebrain (for *trpm3*), and midbrain (for *cgrp*). Scale bar = 100 µm. F: A subpopulation of TG neurons (HuC/D-positive, in green) expresses *trpa1b* (red) at 4 dpf. DAPI staining shown in blue. Scale bar = 50 µm.

Chapter 6: General discussion

The role of the nervous system is ultimately to generate behaviour (Gomez-Marin and Ghazanfar, 2019; Datta et al., 2019). The ability to detect and escape from potentially harmful situations is crucial for survival, with injury causing a big selective pressure. These behavioural responses are advantageous from an evolutionary point of view and are shared across different species, from invertebrates, such as *Aplysia californica* (with its widely studied gill withdrawal reflex), *Caenorhabditis elegans* and *Drosophila melanogaster*, to rodents and primates (Castellucci et al., 1970; Wittenburg and Baumeister, 1999; Im and Galko, 2012; Caterina et al., 2000, Chudler et al., 1986; Walters and Moroz, 2009; Walters, 1994). As such, pain, “an unpleasant sensory and emotional experience associated with, or resembling that associated with, actual or potential tissue damage” (IASP, 2020), is critical for survival. It allows for the identification of the source of danger and shapes behaviour, by prompting immediate behavioural responses that minimise contact with potentially damaging situations, encouraging the adoption of behaviours that promote tissue repair after injury, such as resting a broken limb, and promoting the avoidance of potentially damaging situations or behaviours in the future through lasting associations made between those behaviours and pain, the unpleasant sensation (Barik et al., 2018; Khuong et al., 2019; Haggard et al., 2013; Honore et al., 2000; Huang et al., 2018; Seymour, 2019). Nevertheless, pain can also be undesirable and even become maladaptive, as is the case with chronic pain. Chronic pain can be extremely debilitating and negatively affect general and mental health, as well as social and economic wellbeing (Elliott et al., 1999; Elliott et al., 2002; Haack et al., 2019; Chopra and Arora, 2014; Serafini et al., 2020; Boersma et al., 2019; Van Damme et al., 2018). Therapeutic advances have been limited and the majority of analgesics used fall into the class of opioids. Despite their widespread use, they actually show limited efficacy in the treatment of chronic pain, while also presenting several side effects, such as physical dependence and addiction, and their misuse can lead to death by overdose (Serafini et al., 2020; Fields and Margolis, 2015; Elman and Borsook, 2016; White and Irvine, 1999). Indeed, opioid misuse, sometimes termed the “opioid epidemic”, is a long-standing issue in the United States, with over 33 thousand deaths per year, as of 2017 (Soelberg et al., 2017). Furthermore, acute pain, such as postoperative pain or pain

resulting from injury or tissue trauma, is also largely undermanaged and often reliant on opioids, in both adults and children (Apfelbaum et al., 2003; Breivik and Stubhaug, 2008; Joshi and Kehlet, 2019; Rosen et al., 2022; Ferland et al., 2019; Hsu et al., 2019). In short, pain represents a large unmet clinical need. Many promising drugs identified in pre-clinical studies in rodents fail to produce an analgesic effect in clinical trials. For instance, voltage-gated sodium channels are considered promising analgesic drug targets, due to their role in neuronal excitability and signalling, as well as having been implicated in human genetic pain disorders and chronic pain conditions. However, success in clinical trials has been limited so far, with antagonists targeting specific sodium channels, such as Nav1.7 and Nav1.8, often showing weak to no analgesic activity, despite showing anti-nociceptive properties in rodents (Momin and Wood, 2008; Emery et al., 2016; Jarvis et al., 2007; Yekkirala et al., 2017). The development of better drugs and treatments requires a better understanding of the mechanisms underlying pain and nociception.

The zebrafish has established itself as a model organism in a broad range of fields, including Neuroscience (Bianco et al., 2011; Spence et al., 2007; Tunbak et al., 2020; Oliveira, 2013; Stewart et al., 2014). Amongst other advantages, they have smaller, simpler brains than rodents, and are easily genetically manipulated, which allows for the identification of circuits underlying various behaviours and developmental processes through imaging and manipulation of neuronal activity (Antinucci and Hindges, 2016; Lau et al., 2019; Haesemeyer et al., 2018, Wee et al., 2019; Kalueff et al., 2014). Moreover, there are several similarities between primary afferent neurons in zebrafish and mammals, at a developmental, genetic, molecular and cellular level (Malafoglia et al., 2013a). In zebrafish, cutaneous afferents are also pseudounipolar neurons with cell bodies in either TG or DRG. TG neurons innervate and transmit sensory information from the head, with their peripheral axons arborising on the surface of the head and central axons projecting into the hindbrain (Kimmel et al., 1990; Metcalfe et al., 1990; Sagasti et al., 2005). DRG neurons innervate and transmit sensory information from the body, with their central axons projecting to the dorsal horn of the spinal cord (McGraw et al. 2008; Knafo et al., 2017; Figure 1.5). Zebrafish larvae have been found to express orthologs of several genes crucial for nociception in mammals, such as *TRPA1*, *TRPV1*, *TRPM3*, *P2RX2*, *P2RX3*, and *CGRP*, and there is some functional conservation across species,

with zebrafish trpv1 channels being critical for noxious heat-induced behaviours, and trpa1b channels underlying behavioural responses to chemical irritant AITC (Gau et al., 2013; Prober et al., 2008; Kastenhuber et al., 2013; Appelbaum et al., 2007; Pan et al., 2012; also Figure 5.22). Finally, zebrafish show a variety of behavioural responses to noxious stimuli, such as temperature and chemicals (Lima et al., 2012; Gau et al., 2013; Prober et al., 2008; Barrios et al., 2020). These behaviours are critical for survival. For instance, temperatures in the natural habitat of zebrafish can fluctuate widely, since they typically live in shallow pools, and zebrafish can be exposed to chemicals as well (for example, AITC is a biodegradation product used by plants from the Brassicaceae family as defence) (Engeszer et al., 2007; Haesemeyer 2020; Overby et al., 2015). Some of these behavioural responses include increased locomotor activity, avoidance of the hot side in a place preference assay, and large-angle tail bends upon optovin-based trpa1 stimulation (Gau et al., 2013; Prober et al., 2008; Esancy et al., 2018; Ko et al., 2019; Kroll et al., 2021; Wee et al., 2019). For all these reasons, the zebrafish has been increasingly seen as a potential model for nociception (Gonzalez-Nunez and Rodriguez, 2009; Malafoglia et al., 2013a; Taylor et al., 2017; Ohnesorge et al., 2021).

The overall goal of my project was to establish the zebrafish as a model to study the genetics of nociception. Specifically, I aimed to answer the following questions:

1. Do zebrafish show fast behavioural responses to noxious heat?
2. Can these responses be manipulated by mutating specific genes?

In **Chapter 3**, I set up an assay for the study of behavioural responses to noxious heat in zebrafish larvae. I used an infrared laser to deliver temporally-precise heat stimuli (based on a previously published assay, Haesemeyer et al., 2018), which were estimated to be in the noxious range and consistently elicited tail-flick behaviours over a range of intensities, which I was able to track for analysis.

These responses were characterised in **Chapter 4**. Tail-flick responses of tethered zebrafish larvae to noxious or innocuous stimuli have been reported in the literature (Wee et al., 2019; Haesemeyer et al., 2018). Here, I have shown for the first time that responses of head-fixed larvae to a thermal noxious stimulus in the form of an infrared laser have two components: a fast, short latency (SL) response, which happens less frequently, and a slower, long latency (LL) response, which happens more frequently. Both responses were likely driven by heat, rather than other sensory stimuli. An auditory contribution towards the SL or LL responses was ruled out, since moving the fish to a position immediately adjacent to that targeted by the laser completely abolished both components of the response. Further, retinally-blind fish showed LL response probabilities that were similar to those of sighted controls, which suggests this response was not visually driven. I was unable to completely rule out a potential visual contribution towards the SL response with certainty, due to the low SL response probabilities shown by both blind fish and sighted controls, likely as a result of their reduced pigmentation. Future experiments on pigmented blind fish are needed.

In **Chapter 5**, I generated and characterised F0 knockouts of the zebrafish orthologs of *NGF*, *NTRK1* and *PRDM12*. I selected these genes because their role in pain is unknown in zebrafish but well-established in mammals. Indeed, the NGF/TRKA pathway is known to be required for the development and specification of nociceptors in mammals, with mutations in all three of these genes leading to developmental pain insensitivity disorders in humans (Einarsdottir et al., 2004; Mardy et al., 1999; Chen et al., 2015; Cox et al., 2019), and decreased sensitivity to noxious stimuli and loss of sensory neurons in mice (Crowley et al.,1994; Smeyne et al., 1994; Desiderio et al., 2019; Landy et al., 2021). Moreover, I found the amino acid sequences of the proteins encoded by these genes to be highly conserved across zebrafish, mouse and human. To mutate these genes in zebrafish, I used a recently developed method for reliably generating biallelic knockouts directly in the injected embryos (the F0 generation) (Kroll et al., 2021). Targeting each gene at three different loci, this protocol allows for the generation of biallelic F0 knockouts with fully penetrant phenotypes in >90% of injected animals. I found that *ntrk1* F0 knockout fish and *prdm12b* F0 knockout fish showed a mixed phenotype: some fish appeared anatomically normal and showed no clear locomotion defects, while others had various anatomical defects, including a bent spine and deflated swim bladder, which

resulted in locomotor defects. The ability to respond to noxious heat was retained across these fish. On the other hand, *ngfb* F0 knockout fish showed no anatomical defects, normal swimming and a normal LL response, but almost completely absent SL responses.

In short, I have fulfilled my aims by showing that:

1. Tethered zebrafish larvae can show fast escape-like responses to noxious heat; and
2. Mutating the zebrafish ortholog of a gene with known roles in mammalian nociception nearly completely abolishes one of the components of these responses.

My results and promising future directions are discussed in more detail below.

6.1 How are noxious stimuli encoded by TG neurons?

In mammals, AITC, a chemical irritant, acts as a noxious stimulus through the activation of TRPA1 channels, which also play a role in sensing noxious heat, together with TRPV1 and TRPM3 (Bandell et al., 2004; Caterina et al., 2000; Vandewauw et al., 2018). In zebrafish, trpa1 channels have also been found to mediate behavioural responses to AITC, but are not thought to play a significant role in heat sensation, which is mediated by trpv1 channels (Prober et al., 2008; Gau et al., 2013). Interestingly, I found that the response to the infrared laser could be modulated with AITC, with incubation in subthreshold concentrations of AITC leading to significantly increased LL response probabilities. Therefore, my observed sensitisation of the response to the infrared laser by AITC raises interesting questions regarding how different noxious stimulus modalities are encoded by zebrafish PANs and second-order neurons. One possible explanation is that AITC is activating trpa1 channels in neurons that express both

trpa1 and trpv1 channels, thus decreasing their threshold of activation by heat. Indeed, characterisation of gene expression in TG neurons has found subpopulations of these neurons that express both trpa1 and trpv1 channels (Gau et al., 2013; Gau et al., 2017). Alternatively, this sensitisation could also be explained by an increased excitability of second-order neurons due to the summation of inputs (AITC and heat), which has been reported in rodents (Martin et al., 2004; Sawyer et al., 2009).

In rodents, several theories have been put forward to explain how different somatosensory stimuli are encoded by PANs and second- and third-order orders to ultimately result in pain (or pain-like) sensations. However, this remains a contentious topic, and rodent models have so far been unable to provide us with definite answers (Prescott et al., 2014). Taking advantage of the unique characteristics of the zebrafish as an animal model might allow us to answer some of these questions. For instance, Haesemeyer et al. (2018) previously generated a brain-wide circuit model of (innocuous) heat-evoked swimming behaviour in larval zebrafish, by simultaneously recording neuronal activity of sensory neurons and the behaviours elicited in response to an innocuous heat stimulus. Similarly, it would be possible to carry out our infrared laser experiments on zebrafish transgenic lines that expressed calcium reporters in subpopulations of TG neurons, simultaneously recording neuronal activity and the behaviours elicited, in the presence and absence of AITC. This could contribute towards a better understanding of how different noxious stimuli modalities are encoded by different populations of primary afferent neurons in zebrafish, and how that leads to the generation of escape behaviours.

6.2 What circuits underlie behavioural responses to noxious heat?

Both LL and SL responses could be elicited throughout the full duration of the experiment and neither habituation nor sensitisation to the stimulus was observed. Habituation or sensitisation to a stimulus depend on various factors, such as frequency and intensity of the stimulus, so it is possible that they could be elicited under different assay conditions (Thompson, 2009). Interestingly, the

LL response probability and latency reached a *plateau* at higher laser intensities, which further supports that the stimulus is noxious. The SL response could not be as reliably induced as the LL response, showing less than 30% response rates, even at the highest laser intensity. However, when it did occur, it appeared more stereotyped than the LL response, and its latency did not vary much. Indeed, increasing laser intensities led to LL responses which were faster, as shown by the rightward shift in the cumulative distribution (CD) curves of peak vigour and peak motion for higher laser intensities (Figure 4.3), and happened sooner, with LL response latencies decreasing with increasing laser intensities (until reaching a *plateau* from 450 mA; Figure 4.2.E). On the other hand, the CD curves of all SL response metrics analysed (peak cumulative angle, curvature, motion and vigour) did not appear to change across intensities, with the possible exception of peak motion and peak vigour at 450 mA (Figure 4.4), and the SL response latency was constantly around 25 ms (Figure 4.2.F). This suggests a generally stereotyped, possibly reflex-like, response. The clear temporal separation between the LL and SL responses (> 100 ms vs ~ 25 ms, respectively) suggests different circuits may be underlying each of them. This hypothesis is supported by the observation that there was a specific loss of the SL response in *ngfb* mutants that were otherwise normal, with the LL response remaining unaffected. Performing whole brain calcium imaging experiments during the infrared laser stimulation assay could help identify promising regions driving each response. Laser ablations and optogenetic stimulation and inhibition of identified neuronal populations could then help establish causal relationships between their activation and the execution of a SL and/or LL response to noxious heat.

Our experiments focused on stimulation of the head, which is sensed by primary sensory neurons with cell bodies in the TG. In the future, it would be interesting to explore if infrared laser stimulation of the tail can also elicit similar behaviours, particularly the temporally separated SL and LL responses, as well as studying the circuitry underlying these responses. This is likely to be more complex due to the presence of two populations of sensory neurons at larval stages, DRG neurons and RB neurons (Malafoglia et al., 2013a).

6.3 What is the role of the ngf/trkA pathway in zebrafish?

ntrk1 F0 knockout fish showed a mixed phenotype: some fish appeared anatomically normal and showed no clear behavioural defects when freely swimming in an open arena; others had various anatomical defects, including a bent spine and deflated swim bladder, which resulted in locomotor defects. The same was observed in *prdm12b* F0 knockout fish. *ntrk1* mutants lacking anatomical defects showed normal responses to the infrared laser, which were indistinguishable from those of controls. The F0 method for the generation of mutants can lead to mosaicism in the mutations generated, both across the population of mutants and within each animal (Kroll et al., 2021). As such, I first hypothesised that mutants that appeared normal might have less severe mutations, which could perhaps explain why no changes in heat sensitivity were observed. Strikingly, both *ntrk1* and *prdm12b* mutants with severe anatomical defects retained the ability to respond to the infrared laser. Due to their anatomical defects, it was not possible to assess whether there were more subtle changes in heat sensitivity. However, the observation that *ntrk1* and *prdm12b* F0 knockout fish maintained the ability to respond to heat (and that the responses of normal *ntrk1* mutants were indistinguishable from those of controls) raises questions regarding whether the ngf/trkA pathway plays a critical role in the development, maintenance, and specification of nociceptors in zebrafish, as it does in mammals (Fitzgerald, 2005; Lallemend and Ernfors, 2012; Koch et al., 2018). Further, contrary to what is seen in mammals (Usoskin et al., 2015), trpv1 channels are found in both trkA+ and trkA- populations of larval zebrafish TG neurons (Gau et al., 2017). These differences in the expression of mammalian nociceptive markers again raise questions on how zebrafish nociceptors develop. Future experiments could help address this. For instance, it would be interesting to carry out FISH in *ntrk1* and *prdm12b* mutants, looking at nociceptor markers, as well as combining calcium imaging with the infrared laser experiments in these mutants, both in the presence and absence of AITC. The behaviours and neuronal activity observed could provide us with insights into the role of these proteins in zebrafish.

Further studies are also needed to better understand what causes the anatomical defects seen in some *ntrk1* and *prdm12b* mutants. It is possible that they result from unspecific off-target effects of the gRNAs injected. However, these defects were seen in *ntrk1* mutants, *prdm12b* mutants, and fish injected with gRNA simultaneously targeting *ngfa* and *ngfb*, but rarely in fish that retained one functional *ngf* ortholog (*ngfb* mutants or fish injected with gRNA targeting *ngfa*). This suggests that they might result specifically from disrupting the ngf/trkA pathway in zebrafish. Indeed, the expression of *ntrk1* (and *ntrk2a*) has recently been found to precede that of other ntrk genes in the zebrafish embryo (Hahn et al., 2020), suggesting it might be a key developmental player. The expression of ngfb, ntrk1 and prdm12b is not restricted to sensory neurons. For instance, ngfb has been found to be expressed in the optic tectum, lateral line primordium, and posterior somites at 24 hpf, and across several brain areas (from diencephalon to mesencephalon and telencephalon) at adult stages (Cacialli et al., 2019; Nittoli et al., 2018); ntrk1 is expressed in the cerebellum and olfactory epithelium of adult zebrafish (Gatta et al., 2016; Catania et al., 2003); and prdm12b has been found in the hindbrain and diencephalon of larval fish, as well as many cranial nerve ganglia (Zannino et al., 2014). Given this broad expression, the phenotype of these mutants is not entirely unexpected. Indeed, Ngf, Ntrk1, or Prdm12 homozygous mutant mice do not survive until adulthood (Crowley et al.,1994; Smeyne et al., 1994; Landy et al., 2021), and neither do zebrafish *prdm12b* homozygous mutants, which normally die by juvenile stages (~21 dpf) (Yildiz et al., 2019). In the future, generating stable mutant lines for each of these genes, and studying heterozygous mutants, could provide further insight into this. It would also be particularly interesting to generate sensory neuron-specific conditional knockouts. This can be done in zebrafish using CRISPR-Cas9 (Ablain et al., 2015), and it is an approach that has been successfully used in mice to circumvent the early lethality issue of *Prdm12* knockouts, for instance (Landy et al., 2021). These mutant lines could then also be tested on the infrared laser setup. As such, these experiments would help elucidate the role of these three genes in both zebrafish development and zebrafish nociception.

Strikingly, *ngfb* F0 knockouts seemed anatomically normal, showed no obvious defects in locomotion and showed LL responses to the infrared laser that were indistinguishable from those of controls, but their SL responses were almost completely abolished. This further supports the hypothesis that different circuits

mediate the SL and LL responses and raises interesting questions that could be addressed in future work. Indeed, it would be interesting to explore the neuroanatomical basis of this phenomenon, for instance by assessing whether there were changes in the overall population of TG sensory neurons, or in specific subpopulations, in these mutants. This could be achieved by carrying out fluorescent in situ hybridisation targeting genes known to play a role in nociception in mammals and zebrafish. A more detailed characterisation of TG neurons, for instance using single-cell RNA sequencing, could provide further insight into genes that are down- (or up-) regulated in the mutants. This technique has been used extensively in both rodents and zebrafish (Raj et al., 2018; Farrell et al., 2018; Farnsworth et al., 2020; Schier, 2020; Usoskin et al., 2015; Tavares-Ferreira et al., 2022). It would also be interesting to assess the sensitivity of *ngfb* mutants to other noxious stimuli, such as AITC, as well as whether the AITC-induced sensitisation of the LL response to the laser is maintained in the mutants.

In zebrafish, there are two *ngf* orthologs, *ngfa* and *ngfb*, although previous studies often fail to acknowledge this, and instead focus simply on *ngfb*, referring to it as "*ngf*". Not much is known about the expression or function of ngfa. However, my data suggests that these two orthologs might share some functional roles. Indeed, *ngfb* F0 mutant larvae appeared anatomically normal and lacked the "curved spine" phenotype seen in *ntrk1* and *prdm12b* mutants, but this was again found in fish injected with gRNA targeting both *ngf* orthologs simultaneously. Nevertheless, the SL response was largely absent in *ngfb* mutants, which suggests a distinct, critical role of this ortholog in those behaviours. Interestingly, two recent studies have indirectly pointed towards a possible role of *ngfa* in sensory neuron development and nociception in zebrafish. Firstly, Wu et al. (2019) showed that zebrafish embryos treated with Aflatoxin B1 display aberrant morphology of TG and hindbrain neurons and significantly down-regulated the expression of *ngfa*, amongst other genes. Secondly, Jeong et al. (2021) showed that FAM19A5l, the zebrafish ortholog of FAM19A5 (Family with sequence similarity 19 (chemokine (C–C motif)-like) member A5), is expressed in TG and DRG neurons, with FAM19A5l+ neurons in the TG expressing *trpa1b* and *trpv1* and responding to AITC. Strikingly, FAM19A5l-knockout and FAM19A5l-overexpressing transgenic fish showed down- and up-regulated levels of *trpa1b* and *ngfa*, respectively, with FAM19A5l-knockouts showing decreased

responses to AITC. Therefore, pursuing the study of *ngfa* F0 knockouts may also help shed light on the role of the ngf/trkA pathway in zebrafish nociception.

6.4 Conclusion

In this work, I studied the responses of zebrafish larvae to a noxious heat stimulus in the form of an infrared laser. I found that there are often two components in these responses, which are temporally separated and have different properties, that they are largely driven by heat, and that they can be modulated using an irritant chemical. I also generated F0 knockouts of *ngfb*, *ntrk1* and *prdm12b*, the zebrafish orthologs of three genes known to play a critical role in human pain. My results suggest a role of the ngf/trkA pathway in zebrafish development, and a role of *ngfb* in underlying fast escape-like responses to noxious heat. This work helps establish the great potential of the zebrafish as a model to study the genetics of nociception and opens several promising avenues for future work. At the genetic level, other genes known to be critical for mammalian nociception could be studied, as well as promising candidate genes with unknown function, with the aim of gaining an in-depth mechanistic understanding of causal links between genes and behaviour. Furthermore, at the cellular and circuit level, brain-wide circuit models of protective behaviours in response to various noxious stimuli could be studied. Finally, the great potential of the zebrafish for high-throughput screening of drug compounds could be utilised for both targeted and unbiased analgesic discovery. Indeed, once a gene is found to play a role in nociception in zebrafish, drugs targeting that gene (e.g., receptor/channel antagonists), could be tested for analgesic function in high-throughput assays. For instance, systems such as a 96-well plate on a “hot plate” assay would allow for the testing of dozens of compounds simultaneously. At the same time, drug libraries of compounds of unknown function could be quickly screened for analgesics using the same high-throughput systems. Ultimately, a genetic approach to the study of zebrafish nociception can be used to gain a mechanistic understanding of the genes, cells and pathways involved in sensing noxious stimuli and generating protective behaviours, which may help the development of better drugs and treatments for pain.

References

Abbate, F., Madrigrano, M., Scopitteri, T., Levanti, M., Cobo, J. L., Germanà, A., Vega, J. A., & Laurà, R. (2016). Acid-sensing ion channel immunoreactivities in the cephalic neuromasts of adult zebrafish. Annals of Anatomy, 207, 27–31. https://doi.org/10.1016/j.aanat.2016.06.007

Ablain, J., Durand, E. M., Yang, S., Zhou, Y., & Zon, L. I. (2015). A CRISPR/Cas9 vector system for tissue-specific gene disruption in zebrafish. Developmental Cell, 32(6), 756–764. https://doi.org/10.1016/j.devcel.2015.01.032

Abraira, V. E., & Ginty, D. D. (2013). The sensory neurons of touch. Neuron, 79(4), 618–639. https://doi.org/10.1016/j.neuron.2013.07.051

Adedara, I. A., Costa, F. V., Biasuz, E., Canzian, J., Farombi, E. O., & Rosemberg, D. B. (2022). Influence of acid-sensing ion channel blocker on behavioral responses in a zebrafish model of acute visceral pain. Behavioural Brain Research, 416(August 2021), 113565. https://doi.org/10.1016/j.bbr.2021.113565

Al-Anzi, B., Tracey, W. D., & Benzer, S. (2006). Response of Drosophila to Wasabi Is Mediated by painless, the Fly Homolog of Mammalian TRPA1/ANKTM1. Current Biology, 16(10), 1034–1040. https://doi.org/10.1016/j.cub.2006.04.002

Albin, K. C., Carstens, M. I., & Carstens, E. (2008). Modulation of oral heat and cold pain by irritant chemicals. Chemical Senses, 33(1), 3–15. https://doi.org/10.1093/chemse/bjm056

Alday, A., Alonso, H., Gallego, M., Urrutia, J., Letamendia, A., Callol, C. and Casis, O., (2014). Ionic channels underlying the ventricular action potential in zebrafish embryo. Pharmacological research, 84, pp.26-31.

Altschul, S. F., Gish, W., Miller, W., Myers, E. W., & Lipman, D. J. (1990). Basic local alignment search tool. Journal of Molecular Biology, 215(3), 403–410. https://doi.org/10.1016/S0022-2836(05)80360-2

Andermann, P., Ungos, J. and Raible, D.W. (2002). Neurogenin1 defines zebrafish cranial sensory ganglia precursors. Developmental biology, 251(1), pp.45-58. https://doi.org/10.1006/dbio.2002.0820

Anderson, S. L., Coli, R., Daly, I. W., Kichula, E. A., Rork, M. J., Volpi, S. A., Ekstein, J., & Rubin, B. Y. (2001). Familial dysautonomia is caused by mutations of the IKAP gene. American Journal of Human Genetics, 68(3), 753–758. https://doi.org/10.1086/318808

Anderson, J.L., Mulligan, T.S., Shen, M.C., Wang, H., Scahill, C.M., Tan, F.J., Du, S.J., Busch-Nentwich, E.M. and Farber, S.A. (2017). mRNA processing in mutant zebrafish lines generated by chemical and CRISPR-mediated mutagenesis produces unexpected transcripts that escape nonsense-mediated decay. PLoS genetics, 13(11), p.e1007105.

Antinucci, P., Dumitrescu, A. S., Deleuze, C., Morley, H. J., Leung, K., Hagley, T., Kubo, F., Baier, H., Bianco, I. H., & Wyart, C. (2020). A calibrated optogenetic toolbox of stable zebrafish opsin lines. ELife, 9, 1–31. https://doi.org/10.7554/eLife.54937

Antinucci, Paride, & Hindges, R. (2016). A crystal-clear zebrafish for in vivo imaging. Scientific Reports, 6(June), 1–10. https://doi.org/10.1038/srep29490

Apfelbaum, J. L., Chen, C., Mehta, S. S., & Gan, T. J. (2003). Postoperative pain experience: Results from a national survey suggest postoperative pain continues to be undermanaged. Anesthesia and Analgesia, 97(2), 534–540. https://doi.org/10.1213/01.ANE.0000068822.10113.9E

Appelbaum, L., Skariah, G., Mourrain, P., & Mignot, E. (2007). Comparative expression of p2x receptors and ecto-nucleoside triphosphate diphosphohydrolase 3 in hypocretin and

sensory neurons in zebrafish. Brain Research, 1174(1), 66–75. https://doi.org/10.1016/j.brainres.2007.06.103

Aziz, Q., Barke, A., Bennett, M. I., Benoliel, R., Cohen, M., Evers, S., Finnerup, N. B., First, M. B., Giamberardino, M. A., Kaasa, S., Kosek, E., Lavand'homme, P., Nicholas, M., Perrot, S., Rief, W., Scholz, J., Schug, S., Smith, B. H., Svensson, P., … Wand, S.-J. (2015). A classification of chronic pain for ICD-11. Pain, 156(6), 1003–1007.

Baba, A., Suwada, T., Muta, S., Kuhara, S., & Tashiro, K. (2022). Prdm12 regulates inhibitory neuron differentiation in mouse embryonal carcinoma cells. Cytotechnology, 74(2), 329–339. https://doi.org/10.1007/s10616-022-00519-1

Ballantyne, J. C., & Sullivan, M. D. (2017). Discovery of endogenous opioid systems: What it has meant for the clinician's understanding of pain and its treatment. Pain, 158(12), 2290–2300. https://doi.org/10.1097/j.pain.0000000000001043

Ballini, E., Virginio, C., Medhurst, S. J., Summerfield, S. G., Aldegheri, L., Buson, A., Carignani, C., Chen, Y. H., Giacometti, A., Lago, I., Powell, A. J., & Jarolimek, W. (2011). Characterization of three diaminopyrimidines as potent and selective antagonists of P2X3 and P2X2/3 receptors with in vivo efficacy in a pain model. British Journal of Pharmacology, 163(6), 1315–1325. https://doi.org/10.1111/j.1476-5381.2011.01322.x

Bandell, M., Story, G.M., Hwang, S.W., Viswanath, V., Eid, S.R., Petrus, M.J., Earley, T.J. and Patapoutian, A. (2004). Noxious cold ion channel TRPA1 is activated by pungent compounds and bradykinin. Neuron, 41(6), pp.849-857. https://doi.org/10.1016/S0896-6273(04)00150-3

Barik, A., & Chesler, A. T. (2020). Parallel Parabrachial Pathways Provide Pieces of the Pain Puzzle. Neuron, 106(6), 873–875. https://doi.org/10.1016/j.neuron.2020.05.034

Barik, A., Thompson, J. H., Seltzer, M., Ghitani, N., & Chesler, A. T. (2018). A Brainstem-Spinal Circuit Controlling Nocifensive Behavior. Neuron, 100(6), 1491-1503.e3. https://doi.org/10.1016/j.neuron.2018.10.037

Barrios, J. P., Wang, W. C., England, R., Reifenberg, E., & Douglass, A. D. (2020). Hypothalamic Dopamine Neurons Control Sensorimotor Behavior by Modulating Brainstem Premotor Nuclei in Zebrafish. Current Biology, 30(23), 4606-4618.e4. https://doi.org/10.1016/j.cub.2020.09.002

Bartesaghi, L., Wang, Y., Fontanet, P., Wanderoy, S., Berger, F., Wu, H., Akkuratova, N., Bouçanova, F., Médard, J. J., Petitpré, C., Landy, M. A., Zhang, M. D., Harrer, P., Stendel, C., Stucka, R., Dusl, M., Kastriti, M. E., Croci, L., Lai, H. C., … Chrast, R. (2019). PRDM12 Is Required for Initiation of the Nociceptive Neuron Lineage during Neurogenesis. Cell Reports, 26(13), 3484-3492.e4. https://doi.org/10.1016/j.celrep.2019.02.098

Barth, K. A., Miklosi, A., Watkins, J., Bianco, I. H., Wilson, S. W., & Andrew, R. J. (2005). Fsi Zebrafish Show Concordant Reversal of Laterality of Viscera, Neuroanatomy, and a Subset of Behavioral Responses. Current Biology, 15(9), 844–850. https://doi.org/10.1016/j.cub.2005.03.047

Basbaum, A. I., Bautista, D. M., Scherrer, G., & Julius, D. (2009). Cellular and Molecular Mechanisms of Pain. Cell, 139(2), 267–284. https://doi.org/10.1016/j.cell.2009.09.028

Bateman, A., Martin, M. J., Orchard, S., Magrane, M., Agivetova, R., Ahmad, S., Alpi, E., Bowler-Barnett, E. H., Britto, R., Bursteinas, B., Bye-A-Jee, H., Coetzee, R., Cukura, A., Silva, A. D., Denny, P., Dogan, T., Ebenezer, T. G., Fan, J., Castro, L. G., … Zhang, J. (2021). UniProt: The universal protein knowledgebase in 2021. Nucleic Acids Research, 49(D1), D480–D489. https://doi.org/10.1093/nar/gkaa1100

Bautista, D. M., Jordt, S. E., Nikai, T., Tsuruda, P. R., Read, A. J., Poblete, J., Yamoah, E. N., Basbaum, A. I., & Julius, D. (2006). TRPA1 Mediates the Inflammatory Actions of Environmental Irritants and Proalgesic Agents. Cell, 124(6), 1269–1282. https://doi.org/10.1016/j.cell.2006.02.023

Bejaoui, K., Wu, C., Scheffler, M. D., Haan, G., Ashby, P., Wu, L., De Jong, P., & Brown, R. H. (2001). SPTLC1 is mutated in hereditary sensory neuropathy, type 1. Nature Genetics, 27(3), 261–262. https://doi.org/10.1038/85817

Bennett, D. L. H., & Woods, C. G. (2014). Painful and painless channelopathies. The Lancet Neurology, 13(6), 587–599. https://doi.org/10.1016/S1474-4422(14)70024-9

Berson, D. M., Dunn, F. A., & Takao, M. (2002). Phototransduction by retinal ganglion cells that set the circadian clock. Science, 295(5557), 1070–1073. https://doi.org/10.1126/science.1067262

Bhatt, D. H., McLean, D. L., Hale, M. E., & Fetcho, J. R. (2007). Grading Movement Strength by Changes in Firing Intensity versus Recruitment of Spinal Interneurons. Neuron, 53(1), 91–102. https://doi.org/10.1016/j.neuron.2006.11.011

Bhattacharyya, K., McLean, D. L., & MacIver, M. A. (2017). Visual Threat Assessment and Reticulospinal Encoding of Calibrated Responses in Larval Zebrafish. Current Biology, 27(18), 2751-2762.e6. https://doi.org/10.1016/j.cub.2017.08.012

Bianco, I. H., Kampff, A. R., & Engert, F. (2011). Prey capture behavior evoked by simple visual stimuli in larval zebrafish. Frontiers in Systems Neuroscience, 5(DECEMBER 2011), 1–13. https://doi.org/10.3389/fnsys.2011.00101

Binshtok, A. M., Gerner, P., Oh, S. B., Puopolo, M., Suzuki, S., Roberson, D. P., Herbert, T., Wang, C. F., Kim, D., Chung, G., Mitani, A. A., Wang, G. K., Bean, B. P., & Woolf, C. J. (2009). Coapplication of lidocaine and the permanently charged sodium channel blocker QX-314 produces a long-lasting nociceptive blockade in rodents. Anesthesiology, 111(1), 127–137. https://doi.org/10.1097/ALN.0b013e3181a915e7

Blanco-Sánchez, B., Clément, A., Phillips, J. B., & Westerfield, M. (2017). Zebrafish models of human eye and inner ear diseases. Methods in Cell Biology, 138(1), 415–467. https://doi.org/10.1016/bs.mcb.2016.10.006

Boersma, K., Sö Dermark, M., Hesser, H., Flinka, I. K., Gerdle, B. O., & Lintona, S. J. (2019). Efficacy of a transdiagnostic emotion focused exposure treatment for chronic pain patients with comorbid anxiety and depression: A randomized controlled trial. Pain, 160(8), 1708–1718. https://doi.org/10.1097/j.pain.0000000000001575

Bossé, G. D., & Peterson, R. T. (2017). Development of an opioid self-administration assay to study drug seeking in zebrafish. Behavioural Brain Research, 335(August), 158–166. https://doi.org/10.1016/j.bbr.2017.08.001

Breivik, H., Collett, B., Ventafridda, V., Cohen, R., & Gallacher, D. (2006). Survey of chronic pain in Europe: Prevalence, impact on daily life, and treatment. European Journal of Pain, 10(4), 287. https://doi.org/10.1016/j.ejpain.2005.06.009

Breivik, H., & Stubhaug, A. (2008). Management of acute postoperative pain: Still a long way to go! Pain, 137(2), 233–234. https://doi.org/10.1016/j.pain.2008.04.014

Browne, L. E., Latremoliere, A., Lehnert, B. P., Grantham, A., Ward, C., Alexandre, C., Costigan, M., Michoud, F., Roberson, D. P., Ginty, D. D., & Woolf, C. J. (2017). Time-Resolved Fast Mammalian Behavior Reveals the Complexity of Protective Pain Responses. Cell Reports, 20(1), 89–98. https://doi.org/10.1016/j.celrep.2017.06.024

Brunet, S., Sardon, T., Zimmerman, T., Wittmann, T., Pepperkok, R., Karsenti, E., & Vernos, I. (2004). Characterization of the TPX2 Domains Involved in Microtubule Nucleation and Spindle Assembly in Xenopus nucleation around chromatin and functions in a network of other molecules , some of which also are regulated by. Mol Biol Cell, 15(December), 5318–5328. https://doi.org/10.1091/mbc.E04

Budick, S. A., & O'Malley, D. M. (2000). Locomotor repertoire of the larval zebrafish: Swimming, turning and prey capture. Journal of Experimental Biology, 203(17), 2565–2579. https://doi.org/10.1242/jeb.203.17.2565

Burgess, H. A., & Granato, M. (2007a). Modulation of locomotor activity in larval zebrafish during light adaptation. Journal of Experimental Biology, 210(14), 2526–2539. https://doi.org/10.1242/jeb.003939

Burgess, H. A., & Granato, M. (2007b). Sensorimotor gating in larval zebrafish. Journal of Neuroscience, 27(18), 4984–4994. https://doi.org/10.1523/JNEUROSCI.0615-07.2007

Burton, C. E., Zhou, Y., Bai, Q., & Burton, E. A. (2017). Spectral properties of the zebrafish visual motor response. Neuroscience Letters, 646, 62–67. https://doi.org/10.1016/j.neulet.2017.03.002

Bushnell, M. C., Čeko, M., & Low, L. A. (2013). Cognitive and emotional control of pain and its disruption in chronic pain. Nature Reviews Neuroscience, 14(7), 502–511. https://doi.org/10.1038/nrn3516

Cacialli, P., Gatta, C., D'Angelo, L., Leggieri, A., Palladino, A., de Girolamo, P., Pellegrini, E., & Lucini, C. (2019). Nerve growth factor is expressed and stored in central neurons of adult zebrafish. Journal of Anatomy, 235(1), 167–179. https://doi.org/10.1111/joa.12986

Canfield, J. G. (2003). Temporal constraints on visually directed C-start responses: Behavioral and physiological correlates. Brain, Behavior and Evolution, 61(3), 148–158. https://doi.org/10.1159/000069751

Caron, S.J., Prober, D., Choy, M. and Schier, A.F. (2008). In vivo birthdating by BAPTISM reveals that trigeminal sensory neuron diversity depends on early neurogenesis. https://doi.org/10.1242/dev.023200

Catania, S., Germanà, A., Laurà, R., Gonzalez-Martinez, T., Ciriaco, E., & Vega, J. A. (2003). The crypt neurons in the olfactory epithelium of the adult zebrafish express TrkA-like immunoreactivity. Neuroscience Letters, 350(1), 5–8. https://doi.org/10.1016/S0304-3940(03)00751-1

Caterina, M. J., Leffler, A., Malmberg, A. B., Martin, W. J., Trafton, J., Petersen-Zeitz, K. R., Koltzenburg, M., Basbaum, A. I., & Julius, D. (2000). Impaired nociception and pain sensation in mice lacking the capsaicin receptor. Science, 288(5464), 306–313. https://doi.org/10.1126/science.288.5464.306

Caterina, Michael J., Schumacher, M. A., Tominaga, M., Rosen, T. A., Levine, J. D., & Julius, D. (1997). The capsaicin receptor: A heat-activated ion channel in the pain pathway. Nature, 389(6653), 816–824. https://doi.org/10.1038/39807

Chang, Y. T., Lin, J. W., & Faber, D. S. (1987). Spinal inputs to the ventral dendrite of the teleost Mauthner cell. Brain Research, 417(2), 205–213. https://doi.org/10.1016/0006-8993(87)90444-6

Chapman, H., Waclaw, R. R., Pei, Z., Nakafuku, M., & Campbell, K. (2012). The homeobox gene Gsx2 controls the timing of oligodendroglial fate specification in mouse lateral ganglionic eminence progenitors. Development (Cambridge), 140(11), 2289–2298. https://doi.org/10.1242/dev.091090

Castellucci V, Pinsker H, Kupfermann I, Kandel ER. Neuronal mechanisms of habituation and dishabituation of the gill-withdrawal reflex in Aplysia. Science. 1970 Mar 27;167(3926):1745-8.

Chen, Y. C., Auer-Grumbach, M., Matsukawa, S., Zitzelsberger, M., Themistocleous, A. C., Strom, T. M., Samara, C., Moore, A. W., Cho, L. T. Y., Young, G. T., Weiss, C., Schabhüttl, M., Stucka, R., Schmid, A. B., Parman, Y., Graul-Neumann, L., Heinritz, W., Passarge, E., Watson, R. M., … Senderek, J. (2015). Transcriptional regulator PRDM12 is essential for human pain perception. Nature Genetics, 47(7), 803–808. https://doi.org/10.1038/ng.3308

Chen, J., Tanguay, R. L., Xiao, Y., Haggard, D. E., Ge, X., Jia, Y., Zheng, Y., Dong, Q., Huang, C., & Lin, K. (2016). TBBPA exposure during a sensitive developmental window produces neurobehavioral changes in larval zebrafish. Environmental Pollution, 216, 53–63. https://doi.org/10.1016/j.envpol.2016.05.059

Chen, Z., Donnelly, C.R., Dominguez, B., Harada, Y., Lin, W., Halim, A.S., Bengoechea, T.G., Pierchala, B.A. and Lee, K.F. (2017). p75 is required for the establishment of postnatal sensory neuron diversity by potentiating Ret signaling. Cell reports, 21(3), pp.707-720.

Cheng, W. W. C., Tang, C. S. M., Gui, H. S., So, M. T., Lui, V. C. H., Tam, P. K. H., & Garcia-Barcelo, M. M. (2015). Depletion of the IKBKAP ortholog in zebrafish leads to hirschsprung disease-like phenotype. World Journal of Gastroenterology, 21(7), 2040–2046. https://doi.org/10.3748/wjg.v21.i7.2040

Chiabrando, D., Castori, M., di Rocco, M., Ungelenk, M., Gießelmann, S., Di Capua, M., Madeo, A., Grammatico, P., Bartsch, S., Hübner, C. A., Altruda, F., Silengo, L., Tolosano, E., & Kurth, I. (2016). Mutations in the Heme Exporter FLVCR1 Cause Sensory Neurodegeneration with Loss of Pain Perception. PLoS Genetics, 12(12), 1–18. https://doi.org/10.1371/journal.pgen.1006461

Chiabrando, D., Fiorito, V., Petrillo, S., Bertino, F., & Tolosano, E. (2021). HEME: a neglected player in nociception? Neuroscience and Biobehavioral Reviews, 124(March 2020), 124–136. https://doi.org/10.1016/j.neubiorev.2021.01.011

Chiang, M. C., Nguyen, E. K., Canto-Bustos, M., Papale, A. E., Oswald, A. M. M., & Ross, S. E. (2020). Divergent Neural Pathways Emanating from the Lateral Parabrachial Nucleus Mediate Distinct Components of the Pain Response. Neuron, 106(6), 927-939.e5. https://doi.org/10.1016/j.neuron.2020.03.014

Chinen, A., Hamaoka, T., Yamada, Y., & Kawamura, S. (2003). Gene duplication and spectral diversification of cone visual pigments of zebrafish. Genetics, 163(2), 663–675. https://doi.org/10.1093/genetics/163.2.663

Chopra, K., & Arora, V. (2014). An intricate relationship between pain and depression: Clinical correlates, coactivation factors and therapeutic targets. Expert Opinion on Therapeutic Targets, 18(2), 159–176. https://doi.org/10.1517/14728222.2014.855720

Chudler, E. H., Dong, W. K., & Kawakami, Y. (1986). Cortical nociceptive responses and behavioral correlates in the monkey. Brain Research, 397(1), 47–60. https://doi.org/10.1016/0006-8993(86)91368-5

Citterio, A., Arnoldi, A., Panzeri, E., Merlini, L., D'Angelo, M. G., Musumeci, O., Toscano, A., Bondi, A., Martinuzzi, A., Bresolin, N., & Bassi, M. T. (2015). Variants in KIF1A gene in dominant and sporadic forms of hereditary spastic paraparesis. Journal of Neurology, 262(12), 2684–2690. https://doi.org/10.1007/s00415-015-7899-9

Collymore, C., Tolwani, A., Lieggi, C. and Rasmussen, S. (2014). Efficacy and safety of 5 anesthetics in adult zebrafish (Danio rerio). Journal of the American Association for Laboratory Animal Science, 53(2), pp.198-203.

Collymore, C., Banks, E.K. and Turner, P.V. (2016). Lidocaine hydrochloride compared with MS222 for the euthanasia of zebrafish (Danio rerio). Journal of the American Association for Laboratory Animal Science, 55(6), pp.816-820.

Coltogirone RA, Sherfinski EI, Dobler ZA, Peterson SN, Andlinger AR, Fadel LC, Patrick RL, Bergeron SA. Gsx2 but not Gsx1 is necessary for early forebrain patterning and long-term survival in zebrafish. Biorxiv. 2021 Jan 1. https://doi.org/10.1101/2021.09.13.460150

Cornell, R. A., & Eisen, J. S. (2000). Delta signaling mediates segregation of neural crest and spinal sensory neurons from zebrafish lateral neural plate. Development, 127(13), 2873–2882. https://doi.org/10.1242/dev.127.13.2873

Correia, A. D., Cunha, S. R., Scholze, M., & Stevens, E. D. (2011). A novel behavioral fish model of nociception for Testing Analgesics. Pharmaceuticals, 4(4), 665–680. https://doi.org/10.3390/ph4040665

Costa, F. V., Rosa, L. V., Quadros, V. A., Santos, A. R. S., Kalueff, A. V., & Rosemberg, D. B. (2019). Understanding nociception-related phenotypes in adult zebrafish: Behavioral and

pharmacological characterization using a new acetic acid model. Behavioural Brain Research, 359(September 2018), 570–578. https://doi.org/10.1016/j.bbr.2018.10.009

Cox, J. J., Kurth, I., & Geoffrey Woods, C. (2018). Human genetics of pain. In The Oxford Handbook of the Neurobiology of Pain (pp. 101–127). https://doi.org/10.1093/oxfordhb/9780190860509.013.1

Cox, J. J., Reimann, F., Nicholas, A. K., Thornton, G., Roberts, E., Springell, K., Karbani, G., Jafri, H., Mannan, J., Raashid, Y., Al-Gazali, L., Hamamy, H., Valente, E. M., Gorman, S., Williams, R., McHale, D. P., Wood, J. N., Gribble, F. M., & Woods, C. G. (2006). An SCN9A channelopathy causes congenital inability to experience pain. Nature, 444(7121), 894–898. https://doi.org/10.1038/nature05413

Cregg, R., Momin, A., Rugiero, F., Wood, J. N., & Zhao, J. (2010). Pain channelopathies. Journal of Physiology, 588(11), 1897–1904. https://doi.org/10.1113/jphysiol.2010.187807

Crowley, C., Spencer, S. D., Nishimura, M. C., Chen, K. S., Pitts-Meek, S., Armaninl, M. P., Ling, L. H., McMahon, S. B., Shelton, D. L., Levinson, A. D., & Phillips, H. S. (1994). Mice lacking nerve growth factor display perinatal loss of sensory and sympathetic neurons yet develop basal forebrain cholinergic neurons. Cell, 76(6), 1001–1011. https://doi.org/10.1016/0092-8674(94)90378-6

Cunningham, F., Achuthan, P., Akanni, W., Allen, J., Amode, M. R., Armean, I. M., Bennett, R., Bhai, J., Billis, K., Boddu, S., Cummins, C., Davidson, C., Dodiya, K. J., Gall, A., Girón, C. G., Gil, L., Grego, T., Haggerty, L., Haskell, E., … Flicek, P. (2019). Ensembl 2019. Nucleic Acids Research, 47(D1), D745–D751. https://doi.org/10.1093/nar/gky1113

Curtright, A., Rosser, M., Goh, S., Keown, B., Wagner, E., Sharifi, J., Raible, D. W., & Dhaka, A. (2015). Modeling nociception in zebrafish: A way forward for unbiased analgesic discovery. PLoS ONE, 10(1), 1–18. https://doi.org/10.1371/journal.pone.0116766

Dakin, P., DiMartino, S. J., Gao, H., Maloney, J., Kivitz, A. J., Schnitzer, T. J., Stahl, N., Yancopoulos, G. D., & Geba, G. P. (2019). The Efficacy, Tolerability, and Joint Safety of Fasinumab in Osteoarthritis Pain: A Phase IIb/III Double-Blind, Placebo-Controlled, Randomized Clinical Trial. Arthritis and Rheumatology, 71(11), 1824–1834. https://doi.org/10.1002/art.41012

Dalla Rosa, I., Cámara, Y., Durigon, R., Moss, C. F., Vidoni, S., Akman, G., Hunt, L., Johnson, M. A., Grocott, S., Wang, L., Thorburn, D. R., Hirano, M., Poulton, J., Taylor, R. W., Elgar, G., Martí, R., Voshol, P., Holt, I. J., & Spinazzola, A. (2016). MPV17 Loss Causes Deoxynucleotide Insufficiency and Slow DNA Replication in Mitochondria. PLoS Genetics, 12(1). https://doi.org/10.1371/journal.pgen.1005779

D'Amora, M., & Giordani, S. (2018). The utility of zebrafish as a model for screening developmental neurotoxicity. Frontiers in Neuroscience, 12(December), 1–6. https://doi.org/10.3389/fnins.2018.00976

Daneshjou, K., Jafarieh, H., & Raaeskarami, S. R. (2012). Congenital insensitivity to pain and anhydrosis (CIPA) syndrome; A report of 4 cases. Iranian Journal of Pediatrics, 22(3), 412–416.

Datta, S. R., Anderson, D. J., Branson, K., Perona, P., & Leifer, A. (2019). Computational Neuroethology: A Call to Action. Neuron, 104(1), 11–24. https://doi.org/10.1016/j.neuron.2019.09.038

Davies, W. I. L., Zheng, L., Hughes, S., Katherine Tamai, T., Turton, M., Halford, S., Foster, R. G., Whitmore, D., & Hankins, M. W. (2011). Functional diversity of melanopsins and their global expression in the teleost retina. Cellular and Molecular Life Sciences, 68(24), 4115–4132. https://doi.org/10.1007/s00018-011-0785-4

Dawkins, J. L., Hulme, D. J., Brahmbhatt, S. B., Auer-Grumbach, M., & Nicholson, G. A. (2001). Mutations in SPTLC1, encoding serine palmitoyltransferase, long chain base subunit-1, cause hereditary sensory neuropathy type I. Nature Genetics, 27(3), 309–312. https://doi.org/10.1038/85879

De Fusco, M., Marconi, R., Silvestri, L., Atorino, L., Rampoldi, L., Morgante, L., Ballabio, A., Aridon, P., & Casari, G. (2003). Haploinsufficiency of ATP1A2 encoding the Na+/K+ pump α2 subunit associated with familial hemiplegic migraine type 2. Nature Genetics, 33(2), 192–196. https://doi.org/10.1038/ng1081

Deakin, A. G., Buckley, J., AlZu'bi, H. S., Cossins, A. R., Spencer, J. W., Al'Nuaimy, W., Young, I. S., Thomson, J. S., & Sneddon, L. U. (2019). Automated monitoring of behaviour in zebrafish after invasive procedures. Scientific Reports, 9(1), 1–13. https://doi.org/10.1038/s41598-019-45464-w

Demin, K. A., Meshalkina, D. A., Kysil, E. V., Antonova, K. A., Volgin, A. D., Yakovlev, O. A., Alekseeva, P. A., Firuleva, M. M., Lakstygal, A. M., de Abreu, M. S., Barcellos, L. J. G., Bao, W., Friend, A. J., Amstislavskaya, T. G., Rosemberg, D. B., Musienko, P. E., Song, C., & Kalueff, A. V. (2018). Zebrafish models relevant to studying central opioid and endocannabinoid systems. Progress in Neuro-Psychopharmacology and Biological Psychiatry, 86(March), 301–312. https://doi.org/10.1016/j.pnpbp.2018.03.024

Denk, F., Bennett, D. L., & McMahon, S. B. (2017). Nerve Growth Factor and Pain Mechanisms. Annual Review of Neuroscience, 40, 307–325. https://doi.org/10.1146/annurev-neuro-072116-031121

Desiderio, S., Vermeiren, S., Van Campenhout, C., Kricha, S., Malki, E., Richts, S., Fletcher, E. V., Vanwelden, T., Schmidt, B. Z., Henningfeld, K. A., Pieler, T., Woods, C. G., Nagy, V., Verfaillie, C., & Bellefroid, E. J. (2019). Prdm12 Directs Nociceptive Sensory Neuron Development by Regulating the Expression of the NGF Receptor TrkA. Cell Reports, 26(13), 3522-3536.e5. https://doi.org/10.1016/j.celrep.2019.02.097

Dhaka, A., Murray, A. N., Mathur, J., Earley, T. J., Petrus, M. J., & Patapoutian, A. (2007). TRPM8 Is Required for Cold Sensation in Mice. Neuron, 54(3), 371–378. https://doi.org/10.1016/j.neuron.2007.02.024

Dib-Hajj, S. D., Rush, A. M., Cummins, T. R., Hisama, F. M., Novella, S., Tyrrell, L., Marshall, L., & Waxman, S. G. (2005). Gain-of-function mutation in Nav1.7 in familial erythromelalgia induces bursting of sensory neurons. Brain, 128(8), 1847–1854. https://doi.org/10.1093/brain/awh514

Dichgans, M., Freilinger, T., Eckstein, G., Babini, E., Lorenz-Depiereux, B., Biskup, S., Ferrari, M. D., Herzog, J., Van Den Maagdenberg, A. M. J. M., Pusch, M., & Strom, T. M. (2005). Mutation in the neuronal voltage-gated sodium channel SCN1A in familial hemiplegic migraine. Lancet, 366(9483), 371–377. https://doi.org/10.1016/S0140-6736(05)66786-4

Dinakar, P., & Stillman, A. M. (2016). Pathogenesis of Pain. Seminars in Pediatric Neurology, 23(3), 201–208. https://doi.org/10.1016/j.spen.2016.10.003

Dolensek, N., Gehrlach, D. A., Klein, A. S., & Gogolla, N. (2020). Facial expressions of emotion states and their neuronal correlates in mice. Science, 368(6486), 89–94. https://doi.org/10.1126/science.aaz9468

Dooley, K., & Zon, L. I. (2000). Zebrafish: A model system for the study of human disease. Current Opinion in Genetics and Development, 10(3), 252–256. https://doi.org/10.1016/S0959-437X(00)00074-5

Douglass, A. D., Kraves, S., Deisseroth, K., Schier, A. F., & Engert, F. (2008). Escape Behavior Elicited by Single, Channelrhodopsin-2-Evoked Spikes in Zebrafish Somatosensory Neurons. Current Biology, 18(15), 1133–1137. https://doi.org/10.1016/j.cub.2008.06.077

Driever, W., Schier, A. F., Neuhauss, S. C. F., Malicki, J., Stemple, D. L., & Stainier, D. Y. R. (1996). A genetic screen for mutations affecting embryogenesis in zebrafish. Development, 123, 37–46.

Drissi, I., Woods, W. A., & Woods, C. G. (2020). Understanding the genetic basis of congenital insensitivity to pain. British Medical Bulletin, 133(1), 65–78. https://doi.org/10.1093/bmb/ldaa003

Dunn, T. W., Gebhardt, C., Naumann, E. A., Riegler, C., Ahrens, M. B., Engert, F., & Del Bene, F. (2016). Neural Circuits Underlying Visually Evoked Escapes in Larval Zebrafish. Neuron, 89(3), 613–628. https://doi.org/10.1016/j.neuron.2015.12.021

Dux, M., Rosta, J., & Messlinger, K. (2020). TRP channels in the focus of trigeminal nociceptor sensitization contributing to primary headaches. International Journal of Molecular Sciences, 21(1). https://doi.org/10.3390/ijms21010342

Dykes, I. M., Lanier, J., Raisa Eng, S., & Turner, E. E. (2010). Brn3a regulates neuronal subtype specification in the trigeminal ganglion by promoting Runx expression during sensory differentiation. Neural Development, 5(1), 1–18. https://doi.org/10.1186/1749-8104-5-3

Easter Jr, S. S., & Nicola, G. N. (1996). The Development of Vision in the Zebrafish. Developmental Biology, 180(2), 646–663. https://ac.els-cdn.com/S0012160696903358/1-s2.0-S0012160696903358-main.pdf?_tid=5127746c-bbc2-4d6b-99ba-76814082f1d5&acdnat=1549017063_e3b9adb656fb244c4fe9fc5d7a0f7c72%0Ahttp://www.sciencedirect.com/science/article/pii/S0012160696903358

Edvardson, S., Cinnamon, Y., Jalas, C., Shaag, A., Maayan, C., Axelrod, F. B., & Elpeleg, O. (2012). Hereditary sensory autonomic neuropathy caused by a mutation in dystonin. Annals of Neurology, 71(4), 569–572. https://doi.org/10.1002/ana.23524

Efremova, M., & Teichmann, S. A. (2020). FOCUS | comment |. 17(January), 17–20.

Einarsdottir, E., Carlsson, A., Minde, J., Toolanen, G., Svensson, O., Solders, G., Holmgren, G., Holmberg, D., & Holmberg, M. (2004). A mutation in the nerve growth factor beta gene (NGFB) causes loss of pain perception. Human Molecular Genetics, 13(8), 799–805. https://doi.org/10.1093/hmg/ddh096

Elliott, A. M., Smith, B. H., Hannaford, P. C., Smith, W. C., & Chambers, W. A. (2002). The course of chronic pain in the community: Results of a 4-year follow-up study. Pain, 99(1–2), 299–307. https://doi.org/10.1016/S0304-3959(02)00138-0

Elliott, A.M., Smith, B.H., Penny, K.I., Smith, W.C. and Chambers, W.A., 1999. The epidemiology of chronic pain in the community. The lancet, 354(9186), pp.1248-1252.

Elman, I., & Borsook, D. (2016). Common Brain Mechanisms of Chronic Pain and Addiction. Neuron, 89(1), 11–36. https://doi.org/10.1016/j.neuron.2015.11.027

Emery, E. C., Luiz, A. P., & Wood, J. N. (2016). Nav1.7 and other voltage-gated sodium channels as drug targets for pain relief. Expert Opinion on Therapeutic Targets, 20(8), 975–983. https://doi.org/10.1517/14728222.2016.1162295

Emran, F., Rihel, J., & Dowling, J. E. (2008). A behavioral assay to measure responsiveness of Zebrafish to changes in light intensities. Journal of Visualized Experiments, 20. https://doi.org/10.3791/923

Engeszer, R. E., Patterson, L. B., Rao, A. A., & Parichy, D. M. (2007). Zebrafish in the wild: A review of natural history and new notes from the field. Zebrafish, 4(1), 21–40. https://doi.org/10.1089/zeb.2006.9997

Esancy, K., Condon, L., Feng, J., Kimball, C., Curtright, A., & Dhaka, A. (2018). A zebrafish and mouse model for selective pruritus via direct activation of TRPA1. ELife, 7, 1–24. https://doi.org/10.7554/eLife.32036

Faber, C. G., Hoeijmakers, J. G. J., Ahn, H. S., Cheng, X., Han, C., Choi, J. S., Estacion, M., Lauria, G., Vanhoutte, E. K., Gerrits, M. M., Dib-Hajj, S., Drenth, J. P. H., Waxman, S. G., & Merkies, I. S. J. (2012). Gain of function Na V1.7 mutations in idiopathic small fiber neuropathy. Annals of Neurology, 71(1), 26–39. https://doi.org/10.1002/ana.22485

Faber, C. G., Lauria, G., Merkies, I. S. J., Cheng, X., Han, C., Ahn, H. S., Persson, A. K., Hoeijmakers, J. G. J., Gerrits, M. M., Pierro, T., Lombardi, R., Kapetis, D., Dib-Hajj, S. D., & Waxman, S. G. (2012). Gain-of-function Nav1.8 mutations in painful neuropathy. Proceedings of the National Academy of Sciences of the United States of America, 109(47), 19444–19449. https://doi.org/10.1073/pnas.1216080109

Fajardo, O., Zhu, P., & Friedrich, R. W. (2013). Control of a specific motor program by a small brain area in zebrafish. Frontiers in Neural Circuits, 7(MAR), 1–19. https://doi.org/10.3389/fncir.2013.00067

Farnsworth, D. R., Saunders, L. M., & Miller, A. C. (2020). A single-cell transcriptome atlas for zebrafish development. Developmental Biology, 459(2), 100–108. https://doi.org/10.1016/j.ydbio.2019.11.008

Farrell, J. A., Wang, Y., Riesenfeld, S. J., Shekhar, K., Regev, A., & Schier, A. F. (2018). Single-cell reconstruction of developmental trajectories during zebrafish embryogenesis. Science, 360(6392). https://doi.org/10.1126/science.aar3131

Fassier, C., Hutt, J. A., Scholpp, S., Lumsden, A., Giros, B., Nothias, F., Schneider-Maunoury, S., Houart, C., & Hazan, J. (2010). Zebrafish atlastin controls motility and spinal motor axon architecture via inhibition of the BMP pathway. Nature Neuroscience, 13(11), 1380–1387. https://doi.org/10.1038/nn.2662

Fazio, M., Ablain, J., Chuan, Y., Langenau, D. M., & Zon, L. I. (2020). Zebrafish patient avatars in cancer biology and precision cancer therapy. Nature Reviews Cancer, 20(5), 263–273. https://doi.org/10.1038/s41568-020-0252-3

Feitsma, H., & Cuppen, E. (2008). Zebrafish as a cancer model. Molecular Cancer Research, 6(5), 685–694. https://doi.org/10.1158/1541-7786.MCR-07-2167

Ferland, C. E., Vega, E., & Ingelmo, P. M. (2018). Acute pain management in children: Challenges and recent improvements. Current Opinion in Anaesthesiology, 31(3), 327–332. https://doi.org/10.1097/ACO.0000000000000579

Fernandes, A. M., Fero, K., Arrenberg, A. B., Bergeron, S. A., Driever, W., & Burgess, H. A. (2012). Deep brain photoreceptors control light-seeking behavior in zebrafish larvae. Current Biology, 22(21), 2042–2047. https://doi.org/10.1016/j.cub.2012.08.016

Ferrier, A., De Repentigny, Y., Lynch-Godrei, A., Gibeault, S., Eid, W., Kuo, D., Zha, X., & Kothary, R. (2015). Disruption in the autophagic process underlies the sensory neuropathy in dystonia musculorum mice. Autophagy, 11(7), 1025–1036. https://doi.org/10.1080/15548627.2015.1052207

Fertleman, C. R., Baker, M. D., Parker, K. A., Moffatt, S., Elmslie, F. V., Abrahamsen, B., Ostman, J., Klugbauer, N., Wood, J. N., Gardiner, R. M., & Rees, M. (2006). SCN9A Mutations in Paroxysmal Extreme Pain Disorder: Allelic Variants Underlie Distinct Channel Defects and Phenotypes. Neuron, 52(5), 767–774. https://doi.org/10.1016/j.neuron.2006.10.006

Fields, H. L., & Margolis, E. B. (2015). Understanding opioid reward. Trends in Neurosciences, 38(4), 217–225. https://doi.org/10.1016/j.tins.2015.01.002

Fischer, D., Schabhüttl, M., Wieland, T., Windhager, R., Strom, T. M., & Auer-Grumbach, M. (2014). A novel missense mutation confirms ATL3 as a gene for hereditary sensory neuropathy type 1. Brain, 137(7), 91–92. https://doi.org/10.1093/brain/awu091

Fitzgerald, M. (2005). The development of nociceptive circuits. Nature Reviews Neuroscience, 6(7), 507–520. https://doi.org/10.1038/nrn1701

Fontana, B. D., Mezzomo, N. J., Kalueff, A. V., & Rosemberg, D. B. (2018). The developing utility of zebrafish models of neurological and neuropsychiatric disorders: A critical review. Experimental Neurology, 299(May 2017), 157–171. https://doi.org/10.1016/j.expneurol.2017.10.004

Fu, J., Han, J., Zhou, B., Gong, Z., Santos, E. M., Huo, X., Zheng, W., Liu, H., Yu, H., & Liu, C. (2013). Toxicogenomic responses of zebrafish embryos/larvae to tris(1,3-dichloro-2-propyl) phosphate (TDCPP) reveal possible molecular mechanisms of developmental toxicity. Environmental Science and Technology, 47(18), 10574–10582. https://doi.org/10.1021/es401265q

Gahtan, E., Sankrithi, N., Campos, J. B., & O'Malley, D. M. (2002). Evidence for a widespread brain stem escape network in larval zebrafish. Journal of Neurophysiology, 87(1), 608–614. https://doi.org/10.1152/jn.00596.2001

Ganz, J. (2018). Gut feelings: Studying enteric nervous system development, function, and disease in the zebrafish model system. Developmental Dynamics, 247(2), 268–278. https://doi.org/10.1002/dvdy.24597

Gatta, C., Altamura, G., Avallone, L., Castaldo, L., Corteggio, A., D'Angelo, L., de Girolamo, P., & Lucini, C. (2016). Neurotrophins and their Trk-receptors in the cerebellum of zebrafish. Journal of Morphology, 277(6), 725–736. https://doi.org/10.1002/jmor.20530

Gau, P., Curtright, A., Condon, L., Raible, D. W., & Dhaka, A. (2017). An ancient neurotrophin receptor code; a single Runx/Cbfβ complex determines somatosensory neuron fate specification in zebrafish. PLoS Genetics, 13(7), 1–30. https://doi.org/10.1371/journal.pgen.1006884

Gau, P., Poon, J., Ufret-Vincenty, C., Snelson, C. D., Gordon, S. E., Raible, D. W., & Dhaka, A. (2013). The zebrafish ortholog of TRPV1 is required for heat-induced locomotion. Annals of Internal Medicine, 158(6), 5249–5260. https://doi.org/10.1523/JNEUROSCI.5403-12.2013

Gavva, N. R., Klionsky, L., Qu, Y., Shi, L., Tamir, R., Edenson, S., Zhang, T. J., Viswanadhan, V. N., Toth, A., Pearce, L. V., Vanderah, T. W., Porreca, F., Blumberg, P. M., Lile, J., Sun, Y., Wild, K., Louis, J. C., & Treanor, J. J. S. (2004). Molecular Determinants of Vanilloid Sensitivity in TRPV1. Journal of Biological Chemistry, 279(19), 20283–20295. https://doi.org/10.1074/jbc.M312577200

Gemberling, M., Bailey, T. J., Hyde, D. R., & Poss, K. D. (2013). The zebrafish as a model for complex tissue regeneration. Trends in Genetics, 29(11), 611–620. https://doi.org/10.1016/j.tig.2013.07.003

Ghisleni, G., Capiotti, K. M., Da Silva, R. S., Oses, J. P., Piato, Â. L., Soares, V., Bogo, M. R., & Bonan, C. D. (2012). The role of CRH in behavioral responses to acute restraint stress in zebrafish. Progress in Neuro-Psychopharmacology and Biological Psychiatry, 36(1), 176–182. https://doi.org/10.1016/j.pnpbp.2011.08.016

Ghosh, M., & Rihel, J. (2019). Hierarchical Compression Reveals Sub-Second to Day-Long Structure in Larval Zebrafish Behaviour. BioRxiv, 7(August), 1–21. https://doi.org/10.1101/694471

Ghosh, S., Li, L., & Tourtellotte, W. G. (2021). Retrograde nerve growth factor signaling abnormalities and the pathogenesis of familial dysautonomia. Neural Regeneration Research, 16(9), 1795–1796. https://doi.org/10.4103/1673-5374.306081

Ghysen, A., & Dambly-Chaudière, C. (2007). The lateral line microcosmos. Genes and Development, 21(17), 2118–2130. https://doi.org/10.1101/gad.1568407

Gilron, I., Jensen, T. S., & Dickenson, A. H. (2013). Combination pharmacotherapy for management of chronic pain: From bench to bedside. The Lancet Neurology, 12(11), 1084–1095. https://doi.org/10.1016/S1474-4422(13)70193-5

Gilron, I., Jensen, T. S., & Dickenson, A. H. (2022). Combined pharmacotherapy for chronic pain management. Clinical Pain Management, 218–228. https://doi.org/10.1002/9781119701170.ch21

Glass, A. S., & Dahm, R. (2004). The zebrafish as a model organism for eye development. Ophthalmic Research, 36(1), 4–24. https://doi.org/10.1159/000076105

Godfrey, A., Hooser, B., Abdelmoneim, A., Horzmann, K. A., Freemanc, J. L., & Sepúlveda, M. S. (2017). Thyroid disrupting effects of halogenated and next generation chemicals on the swim bladder development of zebrafish. Aquatic Toxicology, 193(October), 228–235. https://doi.org/10.1016/j.aquatox.2017.10.024

Gokin, A. P., Philip, B., & Strichartz, G. R. (2001). Preferential block of small myelinated sensory and motor fibers by lidocaine: In vivo electrophysiology in the rat sciatic nerve. Anesthesiology, 95(6), 1441–1454. https://doi.org/10.1097/00000542-200112000-00025

Gomez-Marin, A., & Ghazanfar, A. A. (2019). The Life of Behavior. Neuron, 104(1), 25–36. https://doi.org/10.1016/j.neuron.2019.09.017

Gonzalez-Nunez, V., & Rodríguez, R. E. (2009). The zebrafish: A model to study the endogenous mechanisms of pain. ILAR Journal, 50(4), 373–386. https://doi.org/10.1093/ilar.50.4.373

Goolish, E. M., & Okutake, K. (1999). Lack of gas bladder inflation by the larvae of zebrafish in the absence of an air-water interface. Journal of Fish Biology, 55(5), 1054–1063. https://doi.org/10.1006/jfbi.1999.1110

Granato M., Van Eeden F. J. M., Schach U., Trowe T., Brand M., Furutani-Seiki M., Haffter P., Hammerschimdt M., Heisenberg C., Jiang Y., Kane D. A., Kelsh R., Mullins M. C., Odenthal J., & Nusslein-Volhard C. (1996). Genes controlling and mediating locomotion behavior of the zebrafish embryo and larva. Development, 123, 399–413.

Guelly, C., Zhu, P. P., Leonardis, L., Papić, L., Zidar, J., Schabhüttl, M., Strohmaier, H., Weis, J., Strom, T. M., Baets, J., Willems, J., De Jonghe, P., Reilly, M. M., Fröhlich, E., Hatz, M., Trajanoski, S., Pieber, T. R., Janecke, A. R., Blackstone, C., & Auer-Grumbach, M. (2011). Targeted high-throughput sequencing identifies mutations in atlastin-1 as a cause of hereditary sensory neuropathy type i. American Journal of Human Genetics, 88(1), 99–105. https://doi.org/10.1016/j.ajhg.2010.12.003

Gui, H., Schriemer, D., Cheng, W. W., Chauhan, R. K., Antiňolo, G., Berrios, C., Bleda, M., Brooks, A. S., Brouwer, R. W. W., Burns, A. J., Cherny, S. S., Dopazo, J., Eggen, B. J. L., Griseri, P., Jalloh, B., Le, T. L., Lui, V. C. H., Luzón-Toro, B., Matera, I., … Hofstra, R. M. W. (2017). Whole exome sequencing coupled with unbiased functional analysis reveals new Hirschsprung disease genes. Genome Biology, 18(1), 1–13. https://doi.org/10.1186/s13059-017-1174-6

Guo, Y., Chen, Y., Yang, M., Xu, X., Lin, Z., Ma, J., Chen, H., Hu, Y., Ma, Y., Wang, X., & Tian, X. (2020). A Rare KIF1A Missense Mutation Enhances Synaptic Function and Increases Seizure Activity. Frontiers in Genetics, 11(February), 1–11. https://doi.org/10.3389/fgene.2020.00061

Haack, M., Simpson, N., Sethna, N., Kaur, S., & Mullington, J. (2020). Sleep deficiency and chronic pain: potential underlying mechanisms and clinical implications. Neuropsychopharmacology, 45(1), 205–216. https://doi.org/10.1038/s41386-019-0439-z

Habib, A. M., Matsuyama, A., Okorokov, A. L., Santana-Varela, S., Bras, J. T., Aloisi, A. M., Emery, E. C., Bogdanov, Y. D., Follenfant, M., Gossage, S. J., Gras, M., Humphrey, J., Kolesnikov, A., Le Cann, K., Li, S., Minett, M. S., Pereira, V., Ponsolles, C., Sikandar, S., … Cox, J. J. (2018). A novel human pain insensitivity disorder caused by a point mutation in ZFHX2. Brain, 141(2), 365–376. https://doi.org/10.1093/brain/awx326

Haehnel-Taguchi, M., Fernandes, A. M., Böhler, M., Schmitt, I., Tittel, L., & Driever, W. (2018). Projections of the diencephalospinal dopaminergic system to peripheral sense organs in larval zebrafish (Danio rerio). Frontiers in Neuroanatomy, 12(March), 1–21. https://doi.org/10.3389/fnana.2018.00020

Haesemeyer, M. (2020). Thermoregulation in fish. Molecular and Cellular Endocrinology, 518(December 2019), 110986. https://doi.org/10.1016/j.mce.2020.110986

Haesemeyer, M., Robson, D. N., Li, J. M., Schier, A. F., & Engert, F. (2015). The Structure and Timescales of Heat Perception in Larval Zebrafish. Cell Systems, 1(5), 338–348. https://doi.org/10.1016/j.cels.2015.10.010

Haesemeyer, M., Robson, D. N., Li, J. M., Schier, A. F., & Engert, F. (2018). A Brain-wide Circuit Model of Heat-Evoked Swimming Behavior in Larval Zebrafish. Neuron, 98(4), 817-831.e6. https://doi.org/10.1016/j.neuron.2018.04.013

Haffter, P., Granato, M., Brand, M., Mullins, M. C., Hammerschmidt, M., Kane, D. A., Odenthal, J., Van Eeden, F. J. M., Jiang, Y. J., Heisenberg, C. P., Kelsh, R. N., Furutani-Seiki, M., Vogelsang, E., Beuchle, D., Schach, U., Fabian, C., & Nüsslein-Volhard, C. (1996). The identification of genes with unique and essential functions in the development of the zebrafish, Danio rerio. Development, 123, 1–36. https://doi.org/10.1242/dev.123.1.1

Hageter, J., Waalkes, M., Starkey, J., Copeland, H., Price, H., Bays, L., Showman, C., Laverty, S., Bergeron, S. A., & Horstick, E. J. (2021). Environmental and Molecular Modulation of Motor Individuality in Larval Zebrafish. Frontiers in Behavioral Neuroscience, 15(December), 1–19. https://doi.org/10.3389/fnbeh.2021.777778

Haggard, P., Iannetti, G. D., & Longo, M. R. (2013). Spatial sensory organization and body representation in pain perception. Current Biology, 23(4), R164–R176. https://doi.org/10.1016/j.cub.2013.01.047

Hahn, K., Manuel, P., & Bouldin, C. (2020). Expression of the neurotrophic tyrosine kinase receptors, ntrk1 and ntrk2a, precedes expression of other ntrk genes in embryonic zebrafish. PeerJ, 8, 1–15. https://doi.org/10.7717/peerj.10479

Hartmann, S., Vogt, R., Kunze, J., Rauschert, A., Kuhnert, K. D., Wanzenböck, J., Lamatsch, D. K., & Witte, K. (2018). Zebrafish larvae show negative phototaxis to near-infrared light. PLoS ONE, 13(11), 1–16. https://doi.org/10.1371/journal.pone.0207264

Hauptmann, G., Söll, I., Krautz, R., & Theopold, U. (2016). Multi-target chromogenic whole-mount In Situ hybridization for comparing gene expression domains in Drosophila embryos. Journal of Visualized Experiments, 2016(107), 1–9. https://doi.org/10.3791/53830

Hempstead, B.L., Martin-Zanca, D., Kaplan, D.R., Parada, L.F. and Chao, M.V. (1991). High-affinity NGF binding requires coexpression of the trk proto-oncogene and the low-affinity NGF receptor. Nature, 350(6320), pp.678-683.

Henriques, P. M., Rahman, N., Jackson, S. E., & Bianco, I. H. (2019). Nucleus Isthmi Is Required to Sustain Target Pursuit during Visually Guided Prey-Catching. Current Biology, 29(11), 1771-1786.e5. https://doi.org/10.1016/j.cub.2019.04.064

Hermanns, H., Hollmann, M. W., Stevens, M. F., Lirk, P., Brandenburger, T., Piegeler, T., & Werdehausen, R. (2019). Molecular mechanisms of action of systemic lidocaine in acute and chronic pain: a narrative review. British Journal of Anaesthesia, 123(3), 335–349. https://doi.org/10.1016/j.bja.2019.06.014

Herrera, D. G., & Robertson, H. A. (1996). Activation of c-fos in the brain. Progress in Neurobiology, 50(2–3), 83–107. https://doi.org/10.1016/S0301-0082(96)00021-4

Higashijima, S. I., Hotta, Y., & Okamoto, H. (2000). Visualization of cranial motor neurons in live transgenic zebrafish expressing green fluorescent protein under the control of the Islet-1 promoter/enhancer. Journal of Neuroscience, 20(1), 206–218. https://doi.org/10.1523/jneurosci.20-01-00206.2000

Hohenauer, T., & Moore, A. W. (2012). The Prdm family: Expanding roles in stem cells and development. Development (Cambridge), 139(13), 2267–2282. https://doi.org/10.1242/dev.070110

Honore, P., Luger, N. M., Sabino, M. A. C., Schwei, M. J., Rogers, S. D., Mach, D. B., O'Keefe, P. F., Ramnaraine, M. L., Clohisy, D. R., & Mantyh, P. W. (2000). Osteoprotegerin blocks bone cancer-induced skeletal destruction, skeletal pain and pain-related neurochemical reorganization of the spinal cord. Nature Medicine, 6(5), 521–528. https://doi.org/10.1038/74999

Horstick, E. J., Bayleyen, Y., & Burgess, H. A. (2020). Molecular and cellular determinants of motor asymmetry in zebrafish. Nature Communications, 11(1), 1–15. https://doi.org/10.1038/s41467-020-14965-y

Howe, K., Clark, M. D., Torroja, C. F., Torrance, J., Berthelot, C., Muffato, M., Collins, J. E., Humphray, S., McLaren, K., Matthews, L., McLaren, S., Sealy, I., Caccamo, M., Churcher, C., Scott, C., Barrett, J. C., Koch, R., Rauch, G. J., White, S., … Stemple, D. L. (2013). The zebrafish reference genome sequence and its relationship to the human genome. Nature, 496(7446), 498–503. https://doi.org/10.1038/nature12111

Hsu, J. R., Mir, H., Wally, M. K., Seymour, R. B., Archer, K. R., Attum, B., Chad Coles, K. Y., Dumpe, J., Harvey, E., Higgins, T., Hoegler, J., Liu, J. Z., Lowe, J., Mamczak, C., Lawrence Marsh, J., Miller, A. N., Obremskey, W., Ransone, M., Ricci, W., … Shafiq, B. (2019). Clinical Practice Guidelines for Pain Management in Acute Musculoskeletal Injury. Journal of Orthopaedic Trauma, 33(5), E158–E182. https://doi.org/10.1097/BOT.0000000000001430

Hu, B., Chiang, C. Y., Hu, J. W., Dostrovsky, J. O., & Sessle, B. J. (2002). P2X receptors in trigeminal subnucleus caudalis modulate central sensitization in trigeminal subnucleus oralis. Journal of Neurophysiology, 88(4), 1614–1624. https://doi.org/10.1152/jn.2002.88.4.1614

Huang, J., Han, C., Estacion, M., Vasylyev, D., Hoeijmakers, J. G. J., Gerrits, M. M., Tyrrell, L., Lauria, G., Faber, C. G., Dib-Hajj, S. D., Merkies, I. S. J., & Waxman, S. G. (2014). Gain-of-function mutations in sodium channel NaV1.9 in painful neuropathy. Brain, 137(6), 1627–1642. https://doi.org/10.1093/brain/awu079

Huang, T., Lin, S. H., Malewicz, N. M., Zhang, Y., Zhang, Y., Goulding, M., LaMotte, R. H., & Ma, Q. (2019). Identifying the pathways required for coping behaviours associated with sustained pain. Nature, 565(7737), 86–90. https://doi.org/10.1038/s41586-018-0793-8

Hui, S. P., Sheng, D. Z., Sugimoto, K., Gonzalez-Rajal, A., Nakagawa, S., Hesselson, D., & Kikuchi, K. (2017). Zebrafish Regulatory T Cells Mediate Organ-Specific Regenerative Programs. Developmental Cell, 43(6), 659-672.e5. https://doi.org/10.1016/j.devcel.2017.11.010

Hwang, W. Y., Fu, Y., Reyon, D., Maeder, M. L., Tsai, S. Q., Sander, J. D., Peterson, R. T., Yeh, J. R. J., & Joung, J. K. (2013). Efficient genome editing in zebrafish using a CRISPR-Cas system. Nature Biotechnology, 31(3), 227–229. https://doi.org/10.1038/nbt.2501

International Association for the Study of Pain (IASP). https://www.iasp-pain.org/resources/terminology/ (accessed April 2022).

Im, S. H., & Galko, M. J. (2012). Pokes, sunburn, and hot sauce: Drosophila as an emerging model for the biology of nociception. Developmental Dynamics, 241(1), 16–26. https://doi.org/10.1002/dvdy.22737

Imhof, S., Kokotović, T., & Nagy, V. (2020). PRDM12: New Opportunity in Pain Research. Trends in Molecular Medicine, 26(10), 895–897. https://doi.org/10.1016/j.molmed.2020.07.007

Indo, Y., Tsuruta, M., Hayashida, Y., Karim, M. A., Ohta, K., Kawano, T., Mitsubuchi, H., & Tonoki, H. (1966). • © 199 6. 485–488.

Jarvis, M. F., Burgard, E. C., McGaraughty, S., Honore, P., Lynch, K., Brennan, T. J., Subieta, A., Van Biesen, T., Cartmell, J., Bianchi, B., Niforatos, W., Kage, K., Yu, H., Mikusa, J., Wismer, C. T., Zhu, C. Z., Chu, K., Lee, C. H., Stewart, A. O., … Faltynek, C. (2002). A-317491, a novel potent and selective non-nucleotide antagonist of P2X3 and P2X2/3 receptors, reduces chronic inflammatory and neuropathic pain in the rat. Proceedings of the National Academy of Sciences of the United States of America, 99(26), 17179–17184. https://doi.org/10.1073/pnas.252537299

Jarvis, M. F., Honore, P., Shieh, C. C., Chapman, M., Joshi, S., Zhang, X. F., Kort, M., Carroll, W., Marron, B., Atkinson, R., Thomas, J., Liu, D., Krambis, M., Liu, Y.,

McGaraughty, S., Chu, K., Roeloffs, R., Zhong, C., Mikusa, J. P., … Krafte, D. S. (2007). A-803467, a potent and selective Nav1.8 sodium channel blocker, attenuates neuropathic and inflammatory pain in the rat. Proceedings of the National Academy of Sciences of the United States of America, 104(20), 8520–8525. https://doi.org/10.1073/pnas.0611364104

Jeong, I., Yun, S., Shahapal, A., Cho, E. B., Hwang, S. W., Seong, J. Y., & Park, H. C. (2021). FAM19A5l Affects Mustard Oil-Induced Peripheral Nociception in Zebrafish. Molecular Neurobiology, 58(9), 4770–4785. https://doi.org/10.1007/s12035-021-02449-z

Jepma, M., Jones, M., & Wager, T. D. (2014). The dynamics of pain: Evidence for simultaneous site-specific habituation and site-nonspecific sensitization in thermal pain. Journal of Pain, 15(7), 734–746. https://doi.org/10.1016/j.jpain.2014.02.010

Jiang, Q., Arnold, S., Heanue, T., Kilambi, K. P., Doan, B., Kapoor, A., Ling, A. Y., Sosa, M. X., Guy, M., Jiang, Q., Burzynski, G., West, K., Bessling, S., Griseri, P., Amiel, J., Fernandez, R. M., Verheij, J. B. G. M., Hofstra, R. M. W., Borrego, S., … Chakravarti, A. (2015). Functional loss of semaphorin 3C and/or semaphorin 3D and their epistatic interaction with ret are critical to hirschsprung disease liability. American Journal of Human Genetics, 96(4), 581–596. https://doi.org/10.1016/j.ajhg.2015.02.014

Johnson, R. E., Linderman, S., Panier, T., Wee, C. L., Song, E., Herrera, K. J., Miller, A., & Engert, F. (2020). Probabilistic Models of Larval Zebrafish Behavior Reveal Structure on Many Scales. Current Biology, 30(1), 70-82.e4. https://doi.org/10.1016/j.cub.2019.11.026

Jordt, S. E., Bautista, D. M., Chuang, H. H., McKemy, D. D., Zygmunt, P. M., Högestätt, E. D., Meng, I. D., & Julius, D. (2004). Mustard oils and cannabinoids excite sensory nerve fibres through the TRP channel ANKTM1. Nature, 427(6971), 260–265. https://doi.org/10.1038/nature02282

Jordt, S. E., & Julius, D. (2002). Molecular basis for species-specific sensitivity to “hot” chili peppers. Cell, 108(3), 421–430. https://doi.org/10.1016/S0092-8674(02)00637-2

Joshi, G. P., & Kehlet, H. (2019). Postoperative pain management in the era of ERAS: An overview. Best Practice and Research: Clinical Anaesthesiology, 33(3), 259–267. https://doi.org/10.1016/j.bpa.2019.07.016

Kalueff, A. V., Echevarria, D. J., Homechaudhuri, S., Stewart, A. M., Collier, A. D., Kaluyeva, A. A., Li, S., Liu, Y., Chen, P., Wang, J. J., Yang, L., Mitra, A., Pal, S., Chaudhuri, A., Roy, A., Biswas, M., Roy, D., Podder, A., Poudel, M. K., … Song, C. (2016). Zebrafish neurobehavioral phenomics for aquatic neuropharmacology and toxicology research. Aquatic Toxicology, 170, 297–309. https://doi.org/10.1016/j.aquatox.2015.08.007

Kalueff, A. V., Echevarria, D. J., & Stewart, A. M. (2014). Gaining translational momentum: More zebrafish models for neuroscience research. Progress in Neuro-Psychopharmacology and Biological Psychiatry, 55, 1–6. https://doi.org/10.1016/j.pnpbp.2014.01.022

Kalueff, A. V., Gebhardt, M., Stewart, A. M., Cachat, J. M., Brimmer, M., Chawla, J. S., Craddock, C., Kyzar, E. J., Roth, A., Landsman, S., Gaikwad, S., Robinson, K., Baatrup, E., Tierney, K., Shamchuk, A., Norton, W., Miller, N., Nicolson, T., Braubach, O., … Schneider, H. (2013). Towards a comprehensive catalog of zebrafish behavior 1.0 and beyond. Zebrafish, 10(1), 70–86. https://doi.org/10.1089/zeb.2012.0861

Kalueff, A. V., Stewart, A. M., & Gerlai, R. (2014). Zebrafish as an emerging model for studying complex brain disorders. Trends in Pharmacological Sciences, 35(2), 63–75. https://doi.org/10.1016/j.tips.2013.12.002

Kang, K., Pulver, S. R., Panzano, V. C., Chang, E. C., Griffith, L. C., Theobald, D. L., & Garrity, P. A. (2010). Analysis of Drosophila TRPA1 reveals an ancient origin for human chemical nociception. Nature, 464(7288), 597–600. https://doi.org/10.1038/nature08848

Kaplan, D. R., Hempstead, B. L., Martin-Zanca, D., Chao, M. V., & Parada, L. F. (1991). The trk proto-oncogene product: A signal transducing receptor for nerve growth factor. Science, 252(5005), 554–558. https://doi.org/10.1126/science.1850549

Karadimas, C. L., Vu, T. H., Holve, S. A., Chronopoulou, P., Quinzii, C., Johnsen, S. D., Kurth, J., Eggers, E., Palenzuela, L., Tanji, K., Bonilla, E., De Vivo, D. C., DiMauro, S., & Hirano, M. (2006). Navajo neurohepatopathy is caused by a mutation in the MPV17 gene. American Journal of Human Genetics, 79(3), 544–548. https://doi.org/10.1086/506913

Kastenhuber, E., Gesemann, M., Mickoleit, M., & Neuhauss, S. C. F. (2013). Phylogenetic analysis and expression of zebrafish transient receptor potential melastatin family genes. Developmental Dynamics, 242(11), 1236–1249. https://doi.org/10.1002/dvdy.24020

Kay, J. N., Finger-Baier, K. C., Roeser, T., Staub, W., & Baier, H. (2001). Retinal ganglion cell genesis requires lakritz, a zebrafish atonal homolog. Neuron, 30(3), 725–736. https://doi.org/10.1016/S0896-6273(01)00312-9

Khaminets, A., Heinrich, T., Mari, M., Grumati, P., Huebner, A. K., Akutsu, M., Liebmann, L., Stolz, A., Nietzsche, S., Koch, N., Mauthe, M., Katona, I., Qualmann, B., Weis, J., Reggiori, F., Kurth, I., Hübner, C. A., & Dikic, I. (2015). Regulation of endoplasmic reticulum turnover by selective autophagy. Nature, 522(7556), 354–358. https://doi.org/10.1038/nature14498

Khuong, T. M., Wang, Q. P., Manion, J., Oyston, L. J., Lau, M. T., Towler, H., Lin, Y. Q., & Neely, G. G. (2019). Nerve injury drives a heightened state of vigilance and neuropathic sensitization in Drosophila. Science Advances, 5(7), 1–13. https://doi.org/10.1126/sciadv.aaw4099

Kim, C. H., Ueshima, E., Muraoka, O., Tanaka, H., Yeo, S. Y., Huh, T. L., & Miki, N. (1996). Zebrafish elav/HuC homologue as a very early neuronal marker. Neuroscience Letters, 216(2), 109–112. https://doi.org/10.1016/0304-3940(96)13021-4

Kimmel, C. B., Hatta, K., & Metcalfe, W. K. (1990). Early axonal contacts during development of an identified dendrite in the brain of the zebrafish. Neuron, 4(4), 535–545. https://doi.org/10.1016/0896-6273(90)90111-R

Kimmel, C. B., Patterson, J., & Kimmel, R. O. (1974). The development and behavioral characteristics of the startle response in the zebra fish. Developmental Psychobiology, 7(1), 47–60. https://doi.org/10.1002/dev.420070109

Kinameri, E., Inoue, T., Aruga, J., Imayoshi, I., Kageyama, R., Shimogori, T., & Moore, A. W. (2008). Prdm proto-oncogene transcription factor family expression and interaction with the Notch-Hes pathway in mouse neurogenesis. PLoS ONE, 3(12), 1–10. https://doi.org/10.1371/journal.pone.0003859

Klein, C. J., Botuyan, M. V., Wu, Y., Ward, C. J., Nicholson, G. A., Hammans, S., Hojo, K., Yamanishi, H., Karpf, A. R., Wallace, D. C., Simon, M., Lander, C., Boardman, L. A., Cunningham, J. M., Smith, G. E., Litchy, W. J., Boes, B., Atkinson, E. J., Middha, S., … Dyck, P. J. (2011). Mutations in DNMT1 cause hereditary sensory neuropathy with dementia and hearing loss. Nature Genetics, 43(6), 595–600. https://doi.org/10.1038/ng.830

Klein, R., Lamballe, F., Bryant, S. and Barbacid, M., 1992. The trkB tyrosine protein kinase is a receptor for neurotrophin-4. Neuron, 8(5), pp.947-956. https://doi.org/10.1016/0896-6273(92)90209-V

Klein, Rüdiger, Nanduri, V., Jing, S., Lamballe, F., Tapley, P., Bryant, S., Cordon-Cardo, C., Jones, K. R., Reichardt, L. F., & Barbacid, M. (1991). The trkB tyrosine protein kinase is a receptor for brain-derived neurotrophic factor and neurotrophin-3. Cell, 66(2), 395–403. https://doi.org/10.1016/0092-8674(91)90628-C

Knafo, S., Fidelin, K., Prendergast, A., Tseng, P. E. B., Parrin, A., Dickey, C., Böhm, U. L., Figueiredo, S. N., Thouvenin, O., Pascal-Moussellard, H., & Wyart, C. (2017). Mechanosensory neurons control the timing of spinal microcircuit selection during locomotion. ELife, 6, 1–21. https://doi.org/10.7554/eLife.25260

Ko, M. J., Ganzen, L. C., Coskun, E., Mukadam, A. A., Leung, Y. F., & van Rijn, R. M. (2019). A critical evaluation of TRPA1-mediated locomotor behavior in zebrafish as a

screening tool for novel anti-nociceptive drug discovery. Scientific Reports, 9(1), 1–11. https://doi.org/10.1038/s41598-019-38852-9

Koch, S. C., Acton, D., & Goulding, M. (2018). Spinal Circuits for Touch, Pain, and Itch. Annual Review of Physiology, 80, 189–217. https://doi.org/10.1146/annurev-physiol-022516-034303

Kogelman, L. J. A., Christensen, R. E., Pedersen, S. H., Bertalan, M., Hansen, T. F., Jansen-Olesen, I., & Olesen, J. (2017). Whole transcriptome expression of trigeminal ganglia compared to dorsal root ganglia in Rattus Norvegicus. Neuroscience, 350, 169–179. https://doi.org/10.1016/j.neuroscience.2017.03.027

Koltzenburg, M., Lundberg, L. E. R., & Torebjörk, H. E. (1992). Dynamic and static components of mechanical hyperalgesia in human hairy skin. Pain, 51(2), 207–219. https://doi.org/10.1016/0304-3959(92)90262-A

Korn, H., & Faber, D. S. (2005). The Mauthner cell half a century later: A neurobiological model for decision-making? Neuron, 47(1), 13–28. https://doi.org/10.1016/j.neuron.2005.05.019

Kornak, U., Mademan, I., Schinke, M., Voigt, M., Krawitz, P., Hecht, J., Barvencik, F., Schinke, T., Gießelmann, S., Beil, F. T., Pou-Serradell, A., Vílchez, J. J., Beetz, C., Deconinck, T., Timmerman, V., Kaether, C., De Jonghe, P., Hübner, C. A., Gal, A., … Kurth, I. (2014). Sensory neuropathy with bone destruction due to a mutation in the membrane-shaping atlastin GTPase 3. Brain, 137(3), 683–692. https://doi.org/10.1093/brain/awt357

Krauss, J., Astrinides, P., Frohnhöfer, H. G., Walderich, B., & Nüsslein-Volhard, C. (2013). Transparent, a gene affecting stripe formation in Zebrafish, encodes the mitochondrial protein Mpv17 that is required for iridophore survival. Biology Open, 2(7), 703–710. https://doi.org/10.1242/bio.20135132

Kremeyer, B., Lopera, F., Cox, J. J., Momin, A., Rugiero, F., Marsh, S., Woods, C. G., Jones, N. G., Paterson, K. J., Fricker, F. R., Villegas, A., Acosta, N., Pineda-Trujillo, N. G., Ramírez, J. D., Zea, J., Burley, M. W., Bedoya, G., Bennett, D. L. H., Wood, J. N., & Ruiz-Linares, A. (2010). A Gain-of-Function Mutation in TRPA1 Causes Familial Episodic Pain Syndrome. Neuron, 66(5), 671–680. https://doi.org/10.1016/j.neuron.2010.04.030

Kroll, F., Powell, G. T., Ghosh, M., Gestri, G., Antinucci, P., Hearn, T. J., Tunbak, H., Lim, S., Dennis, H. W., Fernandez, J. M., Whitmore, D., Dreosti, E., Wilson, S. W., Hoffman, E. J., & Rihel, J. (2021). A simple and effective f0 knockout method for rapid screening of behaviour and other complex phenotypes. In eLife (Vol. 10, pp. 1–34). https://doi.org/10.7554/eLife.59683

Kucenas, S., Soto, F., Cox, J. A., & Voigt, M. M. (2006). Selective labeling of central and peripheral sensory neurons in the developing zebrafish using P2X3 receptor subunit transgenes. Neuroscience, 138(2), 641–652. https://doi.org/10.1016/j.neuroscience.2005.11.058

Kupari, J., Usoskin, D., Parisien, M., Lou, D., Hu, Y., Fatt, M., Lönnerberg, P., Sp\aangberg, M., Eriksson, B., Barkas, N., Kharchenko, P. V., Loré, K., Khoury, S., Diatchenko, L., & Ernfors, P. (2021). Single cell transcriptomics of primate sensory neurons identifies cell types associated with chronic pain. Nature Communications, 12(1). https://doi.org/10.1038/s41467-021-21725-z

Kurth, I., Pamminger, T., Hennings, J. C., Soehendra, D., Huebner, A. K., Rotthier, A., Baets, J., Senderek, J., Topaloglu, H., Farrell, S. A., Nürnberg, G., Nürnberg, P., De Jonghe, P., Gal, A., Kaether, C., Timmerman, V., & Hübner, C. A. (2009). Mutations in FAM134B, encoding a newly identified Golgi protein, cause severe sensory and autonomic neuropathy. Nature Genetics, 41(11), 1179–1181. https://doi.org/10.1038/ng.464

Labun, K., Montague, T. G., Gagnon, J. A., Thyme, S. B., & Valen, E. (2016). CHOPCHOP v2: a web tool for the next generation of CRISPR genome engineering. Nucleic Acids Research, 44(W1), W272–W276. https://doi.org/10.1093/nar/gkw398

Labun, K., Montague, T. G., Krause, M., Torres Cleuren, Y. N., Tjeldnes, H., & Valen, E. (2019). CHOPCHOP v3: Expanding the CRISPR web toolbox beyond genome editing. Nucleic Acids Research, 47(W1), W171–W174. https://doi.org/10.1093/nar/gkz365

Lacoste, A. M. B., Schoppik, D., Robson, D. N., Haesemeyer, M., Portugues, R., Li, J. M., Randlett, O., Wee, C. L., Engert, F., & Schier, A. F. (2015). A Convergent and essential interneuron pathway for mauthner-cell-mediated escapes. Current Biology, 25(11), 1526–1534. https://doi.org/10.1016/j.cub.2015.04.025

Lai, J. G., Tsai, S. M., Tu, H. C., Chen, W. C., Kou, F. J., Lu, J. W., Wang, H. D., Huang, C. L., & Yuh, C. H. (2014). Zebrafish WNK lysine deficient protein kinase 1 (wnk1) affects angiogenesis associated with VEGF signaling. PLoS ONE, 9(8). https://doi.org/10.1371/journal.pone.0106129

Lallemend, F., & Ernfors, P. (2012). Molecular interactions underlying the specification of sensory neurons. Trends in Neurosciences, 35(6), 373–381. https://doi.org/10.1016/j.tins.2012.03.006

Lalonde, S., Stone, O.A., Lessard, S., Lavertu, A., Desjardins, J., Beaudoin, M., Rivas, M., Stainier, D.Y. and Lettre, G. (2017). Frameshift indels introduced by genome editing can lead to in-frame exon skipping. PloS one, 12(6), p.e0178700.

Lam, C. S., Korzh, V., & Strahle, U. (2005). Zebrafish embryos are susceptible to the dopaminergic neurotoxin MPTP. European Journal of Neuroscience, 21(6), 1758–1762. https://doi.org/10.1111/j.1460-9568.2005.03988.x

Lamballe, F., Klein, R., & Barbacid, M. (1991). trkC, a new member of the trk family of tyrosine protein kinases, is a receptor for neurotrophin-3. Cell, 66(5), 967–979. https://doi.org/10.1016/0092-8674(91)90442-2

Lanave, C., Colangelo, A. M., Saccone, C., & Alberghina, L. (2007). Molecular evolution of the neurotrophin family members and their Trk receptors. Gene, 394(1–2), 1–12. https://doi.org/10.1016/j.gene.2007.01.021

Landy, M. A., Goyal, M., Casey, K. M., Liu, C., & Lai, H. C. (2021). Loss of Prdm12 during development, but not in mature nociceptors, causes defects in pain sensation. Cell Reports, 34(13), 108913. https://doi.org/10.1016/j.celrep.2021.108913

Larsson, E., Kuma, R., Norberg, A., Minde, J., & Holmberg, M. (2009). Nerve growth factor R221W responsible for insensitivity to pain is defectively processed and accumulates as proNGF. Neurobiology of Disease, 33(2), 221–228. https://doi.org/10.1016/j.nbd.2008.10.012

Lau, J. Y., Bianco, I. H., & Severi, K. E. (2019). Cellular-level understanding of supraspinal control: what can be learned from zebrafish? Current Opinion in Physiology, 8, 141–145. https://doi.org/10.1016/j.cophys.2019.01.013

Lee, D. A., Andreev, A., Truong, T. V., Chen, A., Hill, A. J., Oikonomou, G., Pham, U., Hong, Y. K., Tran, S., Glass, L., Sapin, V., Engle, J., Fraser, S. E., & Prober, D. A. (2017). Genetic and neuronal regulation of sleep by neuropeptide VF. ELife, 6, 1–35. https://doi.org/10.7554/eLife.25727

Lee, J. R., Srour, M., Kim, D., Hamdan, F. F., Lim, S. H., Brunel-Guitton, C., Décarie, J. C., Rossignol, E., Mitchell, G. A., Schreiber, A., Moran, R., Van Haren, K., Richardson, R., Nicolai, J., Oberndorff, K. M. E. J., Wagner, J. D., Boycott, K. M., Rahikkala, E., Junna, N., … Michaud, J. L. (2015). De novo mutations in the motor domain of KIF1A cause cognitive impairment, spastic paraparesis, axonal neuropathy, and cerebellar atrophy. Human Mutation, 36(1), 69–78. https://doi.org/10.1002/humu.22709

Leipold, E., Hanson-Kahn, A., Frick, M., Gong, P., Bernstein, J. A., Voigt, M., Katona, I., Goral, R. O., Altmüller, J., Nürnberg, P., Weis, J., Hübner, C. A., Heinemann, S. H., & Kurth, I. (2015). Cold-aggravated pain in humans caused by a hyperactive NaV1.9 channel mutant. Nature Communications, 6(Cmmc), 1–11. https://doi.org/10.1038/ncomms10049

Leipold, E., Liebmann, L., Korenke, G. C., Heinrich, T., Gießelmann, S., Baets, J., Ebbinghaus, M., Goral, R. O., Stödberg, T., Hennings, J. C., Bergmann, M., Altmüller, J., Thiele, H., Wetzel, A., Nürnberg, P., Timmerman, V., De Jonghe, P., Blum, R., Schaible, H. G., … Kurth, I. (2013). A de novo gain-of-function mutation in SCN11A causes loss of pain perception. Nature Genetics, 45(11), 1399–1407. https://doi.org/10.1038/ng.2767

Li, J. M. (2012). Identification of an Operant Learning Circuit by Whole Brain Functional Imaging in Larval Zebrafish. Doctoral dissertation, Harvard University. Available online at: http://nrs.harvard.edu/urn-3:HUL.InstRepos:10974703.

Li, C. L., Li, K. C., Wu, D., Chen, Y., Luo, H., Zhao, J. R., Wang, S. S., Sun, M. M., Lu, Y. J., Zhong, Y. Q., Hu, X. Y., Hou, R., Zhou, B. B., Bao, L., Xiao, H. S., & Zhang, X. (2016). Somatosensory neuron types identified by high-coverage single-cell RNA-sequencing and functional heterogeneity. Cell Research, 26(1), 83–102. https://doi.org/10.1038/cr.2015.149

Li, R., Zhang, L., Shi, Q., Guo, Y., Zhang, W., & Zhou, B. (2018). A protective role of autophagy in TDCIPP-induced developmental neurotoxicity in zebrafish larvae. Aquatic Toxicology, 199(March), 46–54. https://doi.org/10.1016/j.aquatox.2018.03.016

Lima M.G., Maximino C., de Jesus Oliveira Batista E., Oliveira K.R.M., Herculano A.M. (2012) Nocifensive Behavior in Adult and Larval Zebrafish. In: Kalueff A., Stewart A. (eds) Zebrafish Protocols for Neurobehavioral Research. Neuromethods, vol 66. Humana Press, Totowa, NJ. https://doi.org/10.1007/978-1-61779-597-8_11

Lindsey, B. W., Smith, F. M., & Croll, R. P. (2010). From inflation to flotation: Contribution of the swimbladder to whole-body density and swimming depth during development of the zebrafish (Danio rerio). Zebrafish, 7(1), 85–96. https://doi.org/10.1089/zeb.2009.0616

Link, B. A., & Collery, R. F. (2015). Zebrafish Models of Retinal Disease. Annual Review of Vision Science, 1(1), 125–153. https://doi.org/10.1146/annurev-vision-082114-035717

Lister, J. A., Robertson, C. P., Lepage, T., Johnson, S. L., & Raible, D. W. (1999). Nacre Encodes a Zebrafish Microphthalmia-Related Protein That Regulates Neural-Crest-Derived Pigment Cell Fate. Development, 126(17), 3757–3767. https://doi.org/10.1242/dev.126.17.3757

Liu, K. S., & Fetcho, J. R. (1999). Laser ablations reveal functional relationships of segmental hindbrain neurons in zebrafish. Neuron, 23(2), 325–335. https://doi.org/10.1016/S0896-6273(00)80783-7

Lopes, D. M., Denk, F., & McMahon, S. B. (2017). The molecular fingerprint of dorsal root and trigeminal ganglion neurons. Frontiers in Molecular Neuroscience, 10(September), 1–11. https://doi.org/10.3389/fnmol.2017.00304

Lopes, G., Bonacchi, N., Frazão, J., Neto, J. P., Atallah, B. V., Soares, S., Moreira, L., Matias, S., Itskov, P. M., Correia, P. A., Medina, R. E., Calcaterra, L., Dreosti, E., Paton, J. J., & Kampff, A. R. (2015). Bonsai: An event-based framework for processing and controlling data streams. Frontiers in Neuroinformatics, 9(APR), 1–14. https://doi.org/10.3389/fninf.2015.00007

Lopez-Luna, J., Al-Jubouri, Q., Al-Nuaimy, W., & Sneddon, L. U. (2017). Reduction in activity by noxious chemical stimulation is ameliorated by immersion in analgesic drugs in zebrafish. Journal of Experimental Biology, 220(8), 1451–1458. https://doi.org/10.1242/jeb.146969

López-Schier, H. (2019). Neuroplasticity in the acoustic startle reflex in larval zebrafish. Current Opinion in Neurobiology, 54, 134–139. https://doi.org/10.1016/j.conb.2018.10.004

Ma, Q., Chen, Z., Barrantes, I. D. B., De La Pompa, J. L., & Anderson, D. J. (1998). Neurogenin1 Is Essential for the Determination of Neuronal Precursors for Proximal Cranial Sensory Ganglia. Neuron, 20(3), 469–482. https://doi.org/10.1016/S0896-6273(00)80988-5

Madeira, F., Park, Y. M., Lee, J., Buso, N., Gur, T., Madhusoodanan, N., Basutkar, P., Tivey, A. R. N., Potter, S. C., Finn, R. D., & Lopez, R. (2019). The EMBL-EBI search and

sequence analysis tools APIs in 2019. Nucleic Acids Research, 47(W1), W636–W641. https://doi.org/10.1093/nar/gkz268

Malafoglia, V., Bryant, B., Raffaeli, W., Giordano, A., & Bellipanni, G. (2013a). The zebrafish as a model for nociception studies. Journal of Cellular Physiology, 228(10), 1956–1966. https://doi.org/10.1002/jcp.24379

Malafoglia, V., Colasanti, M., Raffaeli, W., Balciunas, D., Giordano, A., & Bellipanni, G. (2013b). Extreme thermal noxious stimuli induce pain responses in zebrafish larvae. Journal of Cellular Physiology, 229(3), 300–308. https://doi.org/10.1002/jcp.24447

Manganelli, F., Parisi, S., Nolano, M., Tao, F., Paladino, S., Pisciotta, C., Tozza, S., Nesti, C., Rebelo, A. P., Provitera, V., Santorelli, F. M., Shy, M. E., Russo, T., Zuchner, S., & Santoro, L. (2017). Novel mutations in dystonin provide clues to the pathomechanisms of HSAN-VI. Neurology, 88(22), 2132–2140. https://doi.org/10.1212/WNL.0000000000003992

Manteniotis, S., Lehmann, R., Flegel, C., Vogel, F., Hofreuter, A., Schreiner, B. S. P., Altmüller, J., Becker, C., Schöbel, N., Hatt, H., & Gisselmann, G. (2013). Comprehensive RNA-Seq expression analysis of sensory ganglia with a focus on ion channels and GPCRs in trigeminal ganglia. PLoS ONE, 8(11), 1–30. https://doi.org/10.1371/journal.pone.0079523

Mardy, S., Miura, Y., Endo, F., Matsuda, I., & Indo, Y. (2001). Congenital insensitivity to pain with anhidrosis (CIPA): Effect of TRKA (NTRK1) missense mutations on autophosphorylation of the receptor tyrosine kinase for nerve growth factor. Human Molecular Genetics, 10(3), 179–188. https://doi.org/10.1093/hmg/10.3.179

Mardy, S., Miura, Y., Endo, F., Matsuda, I., Sztriha, L., Frossard, P., Moosa, A., Ismail, E. A. R., Macaya, A., Andria, G., Toscano, E., Gibson, W., Graham, G. E., & Indo, Y. (1999). Congenital insensitivity to pain with anhidrosis: Novel mutations in the TRKA (NTRK1)gene encoding a high-affinity receptor for nerve growth factor. American Journal of Human Genetics, 64(6), 1570–1579. https://doi.org/10.1086/302422

Marmigère, F., & Ernfors, P. (2007). Specification and connectivity of neuronal subtypes in the sensory lineage. Nature Reviews Neuroscience, 8(2), 114–127. https://doi.org/10.1038/nrn2057

Marmigère, F., Montelius, A., Wegner, M., Groner, Y., Reichardt, L. F., & Ernfors, P. (2006). The Runx1/AML1 transcription factor selectively regulates development and survival of TrkA nociceptive sensory neurons. Nature Neuroscience, 9(2), 180–187. https://doi.org/10.1038/nn1631

Marquart, G. D., Tabor, K. M., Bergeron, S. A., Briggman, K. L., & Burgess, H. A. (2019). Prepontine non-giant neurons drive flexible escape behavior in zebrafish. PLoS Biology, 17(10), 1–19. https://doi.org/10.1371/journal.pbio.3000480

Marques, I. J., Lupi, E., & Mercader, N. (2019). Model systems for regeneration: Zebrafish. Development (Cambridge), 146(18). https://doi.org/10.1242/dev.167692

Marques, J.C., Lackner, S., Félix, R. and Orger, M.B. (2018). Structure of the zebrafish locomotor repertoire revealed with unsupervised behavioral clustering. Current Biology, 28(2), pp.181-195. https://doi.org/10.1016/j.cub.2017.12.002

Marquez-Legorreta, E., Piber, M., & Scott, E. K. (2020). Visual escape in larval zebrafish: stimuli, circuits, and behavior. In Behavioral and Neural Genetics of Zebrafish (pp. 49–71). Elsevier Inc. https://doi.org/10.1016/b978-0-12-817528-6.00004-8

Marsden, K. C., & Granato, M. (2015). In Vivo Ca2+ Imaging Reveals that Decreased Dendritic Excitability Drives Startle Habituation. Cell Reports, 13(9), 1733–1740. https://doi.org/10.1016/j.celrep.2015.10.060

Martin, S. C., Sandell, J. H., & Heinrich, G. (1998). Zebrafish TrkC1 and TrkC2 receptors define two different cell populations in the nervous system during the period of axonogenesis. Developmental Biology, 195(2), 114–130. https://doi.org/10.1006/dbio.1997.8839

Martin, W. J., Cao, Y. Q., & Basbaum, A. I. (2004). Characterization of Wide Dynamic Range Neurons in the Deep Dorsal Horn of the Spinal Cord in Preprotachykinin-A Null Mice in Vivo. Journal of Neurophysiology, 91(5), 1945–1954. https://doi.org/10.1152/jn.00945.2003

Martin SC, Marazzi G, Sandell JH, Heinrich G. Five Trk receptors in the zebrafish. Developmental biology. 1995 Jun 1;169(2):745-58.

Martin-Zanca, D., Barbacid, M., & Parada, L. F. (1990). Expression of the trk proto-oncogene is restricted to the sensory cranial and spinal ganglia of neural crest origin in mouse development. Genes and Development, 4(5), 683–694. https://doi.org/10.1101/gad.4.5.683

Martorano, L., Peron, M., Laquatra, C., Lidron, E., Facchinello, N., Meneghetti, G., Tiso, N., Rasola, A., Ghezzi, D., & Argenton, F. (2019). The zebrafish orthologue of the human hepatocerebral disease gene MPV17 plays pleiotropic roles in mitochondria. DMM Disease Models and Mechanisms, 12(3). https://doi.org/10.1242/dmm.037226

Matos-Cruz, V., Blasic, J., Nickle, B., Robinson, P. R., Hattar, S., & Halpern, M. E. (2011). Unexpected diversity and photoperiod dependence of the zebrafish melanopsin system. PLoS ONE, 6(9). https://doi.org/10.1371/journal.pone.0025111

McElligott, M. B., & O'Malley, D. M. (2005). Prey tracking by larval zebrafish: Axial kinematics and visual control. Brain, Behavior and Evolution, 66(3), 177–196. https://doi.org/10.1159/000087158

McGraw, H. F., Nechiporuk, A., & Raible, D. W. (2008). Zebrafish dorsal root ganglia neural precursor cells adopt a glial fate in the absence of neurogenin1. Journal of Neuroscience, 28(47), 12558–12569. https://doi.org/10.1523/JNEUROSCI.2079-08.2008

McMahon, S & Koltzenburg, M (eds) 2005, Wall and Melzack's Textbook of Pain E-dition. 5 Rev ed edn, Churchill Livingstone (Elsevier Health Sciences)

Mearns, D. S., Donovan, J. C., Fernandes, A. M., Semmelhack, J. L., & Baier, H. (2020). Deconstructing Hunting Behavior Reveals a Tightly Coupled Stimulus-Response Loop. Current Biology, 30(1), 54-69.e9. https://doi.org/10.1016/j.cub.2019.11.022

Medan, V., & Preuss, T. (2014). The Mauthner-cell circuit of fish as a model system for startle plasticity. Journal of Physiology Paris, 108(2–3), 129–140. https://doi.org/10.1016/j.jphysparis.2014.07.006

Meeker, N. D., Hutchinson, S. A., Ho, L., & Trede, N. S. (2007). Method for isolation of PCR-ready genomic DNA from zebrafish tissues. BioTechniques, 43(5), 610–614. https://doi.org/10.2144/000112619

Meeker, R.B. and Williams, K.S. (2015). The p75 neurotrophin receptor: at the crossroad of neural repair and death. Neural regeneration research, 10(5), pp.721-725.

Megat, S., Ray, P. R., Tavares-Ferreira, D., Moy, J. K., Sankaranarayanan, I., Wanghzou, A., Lou, T. F., Barragan-Iglesias, P., Campbell, Z. T., Dussor, G., & Price, T. J. (2019). Differences between dorsal root and trigeminal ganglion nociceptors in mice revealed by translational profiling. Journal of Neuroscience, 39(35), 6829–6847. https://doi.org/10.1523/JNEUROSCI.2663-18.2019

Mendelson, B. (1986). Development of reticulospinal neurons of the zebrafish. II. Early axonal outgrowth and cell body position. Journal of Comparative Neurology, 251(2), 172–184. https://doi.org/10.1002/cne.902510204

Mercurio, S., Petrillo, S., Chiabrando, D., Bassi, Z. I., Gays, D., Camporeale, A., Vacaru, A., Miniscalco, B., Valperga, G., Silengo, L., Altruda, F., Baron, M. H., Santoro, M. M., & Tolosano, E. (2015). The heme exporter Flvcr1 regulates expansion and differentiation of committed erythroid progenitors by controlling intracellular heme accumulation. Haematologica, 100(6), 720–729. https://doi.org/10.3324/haematol.2014.114488

Merrill, A.W., Cuellar, J.M., Judd, J.H., Carstens, M.I. and Carstens, E. (2008). Effects of TRPA1 agonists mustard oil and cinnamaldehyde on lumbar spinal wide-dynamic range neuronal responses to innocuous and noxious cutaneous stimuli in rats. Journal of neurophysiology, 99(2), pp.415-425. https://doi.org/10.1152/jn.00883.2007

Meserve, J. H., Nelson, J. C., Marsden, K. C., Hsu, J., Echeverry, F. A., Jain, R. A., Wolman, M. A., Pereda, A. E., & Granato, M. (2021). A forward genetic screen identifies Dolk as a regulator of startle magnitude through the potassium channel subunit Kv1.1. PLoS Genetics, 17(6), 1–28. https://doi.org/10.1371/journal.pgen.1008943

Messlinger, K., Balcziak, L. K., & Russo, A. F. (2020). Cross-talk signaling in the trigeminal ganglion: role of neuropeptides and other mediators. Journal of Neural Transmission, 127(4), 431–444. https://doi.org/10.1007/s00702-020-02161-7

Metcalfe, W. K., Myers, P. Z., Trevarrow, B., Bass, M. B., & Kimmel, C. B. (1990). Primary neurons that express the L2/HNK-1 carbohydrate during early development in the zebrafish. Development, 110(2), 491–504. https://doi.org/10.1242/dev.110.2.491

Meyer, A., & Schartl, M. (1999). Gene and genome duplications in vertebrates: The one-to-four (-to-eight in fish) rule and the evolution of novel gene functions. Current Opinion in Cell Biology, 11(6), 699–704. https://doi.org/10.1016/S0955-0674(99)00039-3

Miklósi, A., Andrew, R. J., & Savage, H. (1997). Behavioural lateralisation of the tetrapod type in the zebrafish (Brachydanio rerio). Physiology and Behavior, 63(1), 127–135. https://doi.org/10.1016/S0031-9384(97)00418-6

Minett, M. S., Pereira, V., Sikandar, S., Matsuyama, A., Lolignier, S., Kanellopoulos, A. H., Mancini, F., Iannetti, G. D., Bogdanov, Y. D., Santana-Varela, S., Millet, Q., Baskozos, G., MacAllister, R., Cox, J. J., Zhao, J., & Wood, J. N. (2015). Endogenous opioids contribute to insensitivity to pain in humans and mice lacking sodium channel Nav1.7. Nature Communications, 6(May). https://doi.org/10.1038/ncomms9967

Mocho, J.P., Lang, F., Valentin, G., Bedu, S., McKimm, R., Ramos, J., Saavedra Torres, Y., Wheatley, S.E., Higgins, J., Millington, M.E. and Lundegaard, P.R. (2022). A Multi-Site Assessment of Anesthetic Overdose, Hypothermic Shock, and Electrical Stunning as Methods of Euthanasia for Zebrafish (Danio rerio) Embryos and Larvae. Biology, 11(4), p.546.

Moens, C. B., & Prince, V. E. (2002). Constructing the hindbrain: Insights from the zebrafish. Developmental Dynamics, 224(1), 1–17. https://doi.org/10.1002/dvdy.10086

Mogil, J. S. (2009). Animal models of pain: Progress and challenges. Nature Reviews Neuroscience, 10(4), 283–294. https://doi.org/10.1038/nrn2606

Montague, T. G., Cruz, J. M., Gagnon, J. A., Church, G. M., & Valen, E. (2014). CHOPCHOP: A CRISPR/Cas9 and TALEN web tool for genome editing. Nucleic Acids Research, 42(W1), 401–407. https://doi.org/10.1093/nar/gku410

Montalbano, G., Levanti, M., Mhalhel, K., Abbate, F., Laurà, R., Guerrera, M. C., Aragona, M., & Germanà, A. (2021). Acid-sensing ion channels in zebrafish. Animals, 11(8). https://doi.org/10.3390/ani11082471

Mu, Y., quan Li, X., Zhang, B., & lin Du, J. (2012). Visual Input Modulates Audiomotor Function via Hypothalamic Dopaminergic Neurons through a Cooperative Mechanism. Neuron, 75(4), 688–699. https://doi.org/10.1016/j.neuron.2012.05.035

Murphy, S. M., Ernst, D., Wei, Y., Laurà, M., Liu, Y. T., Polke, J., Blake, J., Winer, J., Houlden, H., Hornemann, T., & Reilly, M. M. (2013). Hereditary sensory and autonomic neuropathy type 1 (HSANI) caused by a novel mutation in SPTLC2. Neurology, 80(23), 2106–2111. https://doi.org/10.1212/WNL.0b013e318295d789

Naarendorp, F., Esdaille, T. M., Banden, S. M., Andrews-Labenski, J., Gross, O. P., & Pugh, E. N. (2010). Dark light, rod saturation, and the absolute and incremental sensitivity of mouse cone vision. Journal of Neuroscience, 30(37), 12495–12507. https://doi.org/10.1523/JNEUROSCI.2186-10.2010

Nahorski, M. S., Al-Gazali, L., Hertecant, J., Owen, D. J., Borner, G. H. H., Chen, Y. C., Benn, C. L., Carvalho, O. P., Shaikh, S. S., Phelan, A., Robinson, M. S., Royle, S. J., & Woods, C. G. (2015). A novel disorder reveals clathrin heavy chain-22 is essential for human pain and touch development. Brain, 138(8), 2147–2160. https://doi.org/10.1093/brain/awv149

Nahorski, M. S., Chen, Y. C., & Woods, C. G. (2015). New Mendelian Disorders of Painlessness. Trends in Neurosciences, 38(11), 712–724. https://doi.org/10.1016/j.tins.2015.08.010

Nassar, M. A., Stirling, L. C., Forlani, G., Baker, M. D., Matthewst, E. A., Dickenson, A. H., & Wood, J. N. (2004). Nociceptor-specific gene deletion reveals a major role for Nav 1.7 (PN1) in acute and inflammatory pain. Proceedings of the National Academy of Sciences of the United States of America, 101(34), 12706–12711. https://doi.org/10.1073/pnas.0404915101

Nelson, R. F., Balraj, A., Suresh, T., Torvund, M., & Patterson, S. S. (2019). Strain variations in cone wavelength peaks in situ during zebrafish development. Visual Neuroscience, 36, E010. https://doi.org/10.1017/S0952523819000075

Nemani, T., Steel, D., Kaliakatsos, M., DeVile, C., Ververi, A., Scott, R., Getov, S., Sudhakar, S., Male, A., Mankad, K., Muntoni, F., Reilly, M. M., Kurian, M. A., Carr, L., & Munot, P. (2020). KIF1A-related disorders in children: A wide spectrum of central and peripheral nervous system involvement. Journal of the Peripheral Nervous System, 25(2), 117–124. https://doi.org/10.1111/jns.12368

Nguyen, M. Q., Wu, Y., Bonilla, L. S., von Buchholtz, L. J., & Ryba, N. J. P. (2017). Diversity amongst trigeminal neurons revealed by high throughput single cell sequencing. PLoS ONE, 12(9), 1–22. https://doi.org/10.1371/JOURNAL.PONE.0185543

Nikbakht, N., & Diamond, M. E. (2021). Conserved visual capacity of rats under red light. ELife, 10, 1–12. https://doi.org/10.7554/eLife.66429

Nittoli, V., Sepe, R. M., Coppola, U., D'Agostino, Y., De Felice, E., Palladino, A., Vassalli, Q. A., Locascio, A., Ristoratore, F., Spagnuolo, A., D'Aniello, S., & Sordino, P. (2018). A comprehensive analysis of neurotrophins and neurotrophin tyrosine kinase receptors expression during development of zebrafish. Journal of Comparative Neurology, 526(6), 1057–1072. https://doi.org/10.1002/cne.24391

Noyes, P. D., Haggard, D. E., Gonnerman, G. D., & Tanguay, R. L. (2015). Advanced morphological - behavioral test platform reveals neurodevelopmental defects in embryonic zebrafish exposed to comprehensive suite of halogenated and organophosphate flame retardants. Toxicological Sciences, 145(1), 177–195. https://doi.org/10.1093/toxsci/kfv044

Nugraha, B., Gutenbrunner, C., Barke, A., Karst, M., Schiller, J., Schäfer, P., Falter, S., Korwisi, B., Rief, W., & Treede, R. D. (2019). The IASP classification of chronic pain for ICD-11: Functioning properties of chronic pain. Pain, 160(1), 88–94. https://doi.org/10.1097/j.pain.0000000000001433

Odstrcil, I., Petkova, M. D., Haesemeyer, M., Boulanger-Weill, J., Nikitchenko, M., Gagnon, J. A., Oteiza, P., Schalek, R., Peleg, A., Portugues, R., Lichtman, J. W., & Engert, F. (2022). Functional and ultrastructural analysis of reafferent mechanosensation in larval zebrafish. Current Biology, 32(1), 176-189.e5. https://doi.org/10.1016/j.cub.2021.11.007

Ohnesorge, N., Heinl, C., & Lewejohann, L. (2021). Current Methods to Investigate Nociception and Pain in Zebrafish. Frontiers in Neuroscience, 15(April), 1–13. https://doi.org/10.3389/fnins.2021.632634

Oliveira, M. C. G., Pelegrini-da Silva, A., Tambeli, C. H., & Parada, C. A. (2009). Peripheral mechanisms underlying the essential role of P2X3,2/3 receptors in the development of inflammatory hyperalgesia. Pain, 141(1–2), 127–134. https://doi.org/10.1016/j.pain.2008.10.024

Oliveira, R. F. (2013). Mind the fish: Zebrafish as a model in cognitive social neuroscience. Frontiers in Neural Circuits, 7(JUL), 1–15. https://doi.org/10.3389/fncir.2013.00131

O'Malley, D. M., Kao, Y. H., & Fetcho, J. R. (1996). Imaging the functional organization of zebrafish hindbrain segments during escape behaviors. Neuron, 17(6), 1145–1155. https://doi.org/10.1016/S0896-6273(00)80246-9

Ophoff, R. A., Terwindt, G. M., Vergouwe, M. N., Van Eijk, R., Oefner, P. J., Hoffman, S. M. G., Lamerdin, J. E., Mohrenweiser, H. W., Bulman, D. E., Ferrari, M., Haan, J., Lindhout, D., Van Ommen, G. J. B., Hofker, M. H., Ferrari, M. D., & Frants, R. R. (1996). Familial hemiplegic migraine and episodic ataxia type-2 are caused by mutations in the Ca2+ channel gene CACNL1A4. Cell, 87(3), 543–552. https://doi.org/10.1016/S0092-8674(00)81373-2

Orger, M. B., Kampff, A. R., Severi, K. E., Bollmann, J. H., & Engert, F. (2008). Control of visually guided behavior by distinct populations of spinal projection neurons. Nature Neuroscience, 11(3), 327–333. https://doi.org/10.1038/nn2048

Øverby, A., Stokland, R. A., \AAsberg, S. E., Sporsheim, B., & Bones, A. M. (2015). Allyl isothiocyanate depletes glutathione and upregulates expression of glutathione S-transferases in Arabidopsis thaliana. Frontiers in Plant Science, 6(APR), 1–9. https://doi.org/10.3389/fpls.2015.00277

Palanca, A. M. S., Lee, S. L., Yee, L. E., Joe-Wong, C., Trinh, L. A., Hiroyasu, E., Husain, M., Fraser, S. E., Pellegrini, M., & Sagasti, A. (2013). New transgenic reporters identify somatosensory neuron subtypes in larval zebrafish. Developmental Neurobiology, 73(2), 152–167. https://doi.org/10.1002/dneu.22049

Pan, Y. A., Choy, M., Prober, D. A., & Schier, A. F. (2012). Robo2 determines subtype-specific axonal projections of trigeminal sensory neurons. Development, 139(3), 591–600. https://doi.org/10.1242/dev.076588

Pantoja, C., Hoagland, A., Carroll, E. C., Karalis, V., Conner, A., & Isacoff, E. Y. (2016). Neuromodulatory Regulation of Behavioral Individuality in Zebrafish. Neuron, 91(3), 587–601. https://doi.org/10.1016/j.neuron.2016.06.016

Patton, E. E., Zon, L. I., & Langenau, D. M. (2021). Zebrafish disease models in drug discovery: from preclinical modelling to clinical trials. Nature Reviews Drug Discovery, 20(8), 611–628. https://doi.org/10.1038/s41573-021-00210-8

Paukert, M., Sidi, S., Russell, C., Siba, M., Wilson, S. W., Nicolson, T., & Gründer, S. (2004). A family of acid-sensing ion channels from the zebrafish: Widespread expression in the central nervous system suggests a conserved role in neuronal communication. Journal of Biological Chemistry, 279(18), 18783–18791. https://doi.org/10.1074/jbc.M401477200

Peirs, C., & Seal, R. P. (2016). Recent advances and current views. Science, 354(6312), 578–584.

Pereira, T. D., Shaevitz, J. W., & Murthy, M. (2020). Quantifying behavior to understand the brain. Nature Neuroscience, 23(12), 1537–1549. https://doi.org/10.1038/s41593-020-00734-z

Pietrobon, D., & Brennan, K. C. (2019). Genetic mouse models of migraine. Journal of Headache and Pain, 20(1). https://doi.org/10.1186/s10194-019-1029-5

Pogorzala, L. A., Mishra, S. K., & Hoon, M. A. (2013). The cellular code for mammalian thermosensation. Journal of Neuroscience, 33(13), 5533–5541. https://doi.org/10.1523/JNEUROSCI.5788-12.2013

Portugues, R., & Engert, F. (2009). The neural basis of visual behaviors in the larval zebrafish. Current Opinion in Neurobiology, 19(6), 644–647. https://doi.org/10.1016/j.conb.2009.10.007

Powell GT (2020) Headloop, version 39ef51c GitHub. https://github.com/GTPowell21/Headloop

Power, I. (2005). Recent advances in postoperative pain therapy. British Journal of Anaesthesia, 95(1), 43–51. https://doi.org/10.1093/bja/aei037

Prescott, S. A., Ma, Q., & De Koninck, Y. (2014). Normal and abnormal coding of somatosensory stimuli causing pain. Nature Neuroscience, 17(2), 183–191. https://doi.org/10.1038/nn.3629

Preuss, T., Osei-Bonsu, P. E., Weiss, S. A., Wang, C., & Faber, D. S. (2006). Neural representation of object approach in a decision-making motor circuit. Journal of Neuroscience, 26(13), 3454–3464. https://doi.org/10.1523/JNEUROSCI.5259-05.2006

Price, M.P., Lewin, G.R., McIlwrath, S.L., Cheng, C., Xie, J., Heppenstall, P.A., Stucky, C.L., Mannsfeldt, A.G., Brennan, T.J., Drummond, H.A. and Qiao, J., 2000. The mammalian sodium channel BNC1 is required for normal touch sensation. Nature, 407(6807), pp.1007-1011. https://doi.org/10.1038/35039512

Price, M. P., McIlwrath, S. L., Xie, J., Cheng, C., Qiao, J., Tarr, D. E., Sluka, K. A., Brennan, T. J., Lewin, G. R., & Welsh, M. J. (2002). Erratum: The DRASIC cation channel contributes to the detection of cutaneous touch and acid stimuli in mice (Neuron (December 20, 2001) 32 (1071-1083)). Neuron, 35(2), 407. https://doi.org/10.1016/S0896-6273(02)00772-9

Price, T. J., & Flores, C. M. (2007). Critical Evaluation of the Colocalization Between Calcitonin Gene-Related Peptide, Substance P, Transient Receptor Potential Vanilloid Subfamily Type 1 Immunoreactivities, and Isolectin B4 Binding in Primary Afferent Neurons of the Rat and Mouse. Journal of Pain, 8(3), 263–272. https://doi.org/10.1016/j.jpain.2006.09.005

Prober, D. A., Zimmerman, S., Myers, B. R., McDermott, B. M., Kim, S. H., Caron, S., Rihel, J., Solnica-Krezel, L., Julius, D., Hudspeth, A. J., & Schier, A. F. (2008). Zebrafish TRPA1 channels are required for chemosensation but not for thermosensation or mechanosensory hair cell function. Journal of Neuroscience, 28(40), 10102–10110. https://doi.org/10.1523/JNEUROSCI.2740-08.2008

Pu, J., Tang, S., Tong, Q., Wang, G., Jia, H., Jia, Q., Li, K., Li, D., Yang, D., Yang, J., Li, H., Li, S., & Mei, H. (2017). Neuregulin 1 is involved in enteric nervous system development in zebrafish. Journal of Pediatric Surgery, 52(7), 1182–1187. https://doi.org/10.1016/j.jpedsurg.2017.01.005

Purves, D., Augustine, G.J., Fitzpatrick, D., Hall, W.C., LaMantia, A.S., McNamara, J.O. and White, L.E. (2004). *Neuroscience*. 3rd edn. Sinauer Associates. Inc., USA.

Qiao, K., Hu, T., Jiang, Y., Huang, J., Hu, J., Gui, W., Ye, Q., Li, S., & Zhu, G. (2021). Crosstalk of cholinergic pathway on thyroid disrupting effects of the insecticide chlorpyrifos in zebrafish (Danio rerio). Science of the Total Environment, 757, 143769. https://doi.org/10.1016/j.scitotenv.2020.143769

Raj, B., Wagner, D. E., McKenna, A., Pandey, S., Klein, A. M., Shendure, J., Gagnon, J. A., & Schier, A. F. (2018). Simultaneous single-cell profiling of lineages and cell types in the vertebrate brain. Nature Biotechnology, 36(5), 442–450. https://doi.org/10.1038/nbt.4103

Rajadhyaksha, A. M., Elemento, O., Puffenberger, E. G., Schierberl, K. C., Xiang, J. Z., Putorti, M. L., Berciano, J., Poulin, C., Brais, B., Michaelides, M., Weleber, R. G., & Higgins, J. J. (2010). Mutations in FLVCR1 cause posterior column ataxia and retinitis pigmentosa. American Journal of Human Genetics, 87(5), 643–654. https://doi.org/10.1016/j.ajhg.2010.10.013

Rand, K. N., Ho, T., Qu, W., Mitchell, S. M., White, R., Clark, S. J., & Molloy, P. L. (2005). Headloop suppression PCR and its application to selective amplification of methylated DNA sequences. Nucleic Acids Research, 33(14), 1–11. https://doi.org/10.1093/nar/gni120

Raouf, R., Quick, K., & Wood, J. N. (2010). Pain as a channelopathy. Journal of Clinical Investigation, 120(11), 3745–3752. https://doi.org/10.1172/JCI43158

Reilly, S. C., Quinn, J. P., Cossins, A. R., & Sneddon, L. U. (2008). Behavioural analysis of a nociceptive event in fish: Comparisons between three species demonstrate specific responses. Applied Animal Behaviour Science, 114(1–2), 248–259. https://doi.org/10.1016/j.applanim.2008.01.016

Reinig, S., Driever, W., & Arrenberg, A. B. (2017). The Descending Diencephalic Dopamine System Is Tuned to Sensory Stimuli. Current Biology, 27(3), 318–333. https://doi.org/10.1016/j.cub.2016.11.059

Rennefeld, C., Wiech, K., Schoell, E. D., Lorenz, J., & Bingel, U. (2010). Habituation to pain: Further support for a central component. Pain, 148(3), 503–508. https://doi.org/10.1016/j.pain.2009.12.014

Richendrfer, H., Pelkowski, S. D., Colwill, R. M., & Créton, R. (2012). Developmental sub-chronic exposure to chlorpyrifos reduces anxiety-related behavior in zebrafish larvae. Neurotoxicology and Teratology, 34(4), 458–465. https://doi.org/10.1016/j.ntt.2012.04.010

Rihel, J., Prober, D.A., Arvanites, A., Lam, K., Zimmerman, S., Jang, S., Haggarty, S.J., Kokel, D., Rubin, L.L., Peterson, R.T. and Schier, A.F. (2010). Zebrafish behavioral profiling links drugs to biological targets and rest/wake regulation. Science, 327(5963), pp.348-351. DOI: 10.1126/science.1183090

Rihel, J., & Schier, A. F. (2012). Behavioral screening for neuroactive drugs in zebrafish. Developmental Neurobiology, 72(3), 373–385. https://doi.org/10.1002/dneu.20910

Robertson, G.N., McGee, C.A.S., Dumbarton, T.C., Croll, R.P. and Smith, F.M. (2007). Development of the swimbladder and its innervation in the zebrafish, Danio rerio. Journal of Morphology, 268(11), pp.967-985. https://doi.org/10.1002/jmor.10558

Rodriguez, E., Sakurai, K., Xu, J., Chen, Y., Toda, K., Zhao, S., Han, B. X., Ryu, D., Yin, H., Liedtke, W., & Wang, F. (2018). Publisher Correction: A craniofacial?specific monosynaptic circuit enables heightened affective pain (Nature Neuroscience DOI: 10.1038/s41593-017-0012-1). Nature Neuroscience, 21(6), 896. https://doi.org/10.1038/s41593-018-0103-7

Rosen, D. M., Alcock, M. M., & Palmer, G. M. (2022). Opioids for acute pain management in children. Anaesthesia and Intensive Care, 50(1–2), 81–94. https://doi.org/10.1177/0310057X211065769

Rostock, C., Schrenk-Siemens, K., Pohle, J., & Siemens, J. (2018). Human vs. Mouse Nociceptors – Similarities and Differences. Neuroscience, 387, 13–27. https://doi.org/10.1016/j.neuroscience.2017.11.047

Rotthier, A., Auer-Grumbach, M., Janssens, K., Baets, J., Penno, A., Almeida-Souza, L., Van Hoof, K., Jacobs, A., De Vriendt, E., Schlotter-Weigel, B., Löscher, W., Vondráček, P., Seeman, P., De Jonghe, P., Van Dijck, P., Jordanova, A., Hornemann, T., & Timmerman, V. (2010). Mutations in the SPTLC2 subunit of serine palmitoyltransferase cause hereditary sensory and autonomic neuropathy type i. American Journal of Human Genetics, 87(4), 513–522. https://doi.org/10.1016/j.ajhg.2010.09.010

Rotthier, A., Baets, J., Timmerman, V., & Janssens, K. (2012). Mechanisms of disease in hereditary sensory and autonomic neuropathies. Nature Reviews Neurology, 8(2), 73–85. https://doi.org/10.1038/nrneurol.2011.227

Sagasti, A., Guido, M. R., Raible, D. W., & Schier, A. F. (2005). Repulsive interactions shape the morphologies and functional arrangement of zebrafish peripheral sensory arbors. Current Biology, 15(9), 804–814. https://doi.org/10.1016/j.cub.2005.03.048

Sahu, M. P., Pazos-Boubeta, Y., Pajanoja, C., Rozov, S., Panula, P., & Castrén, E. (2019). Neurotrophin receptor Ntrk2b function in the maintenance of dopamine and serotonin neurons in zebrafish. Scientific Reports, 9(1), 1–13. https://doi.org/10.1038/s41598-019-39347-3

Sankrithi, N. S., & O'Malley, D. M. (2010). Activation of a multisensory, multifunctional nucleus in the zebrafish midbrain during diverse locomotor behaviors. Neuroscience, 166(3), 970–993. https://doi.org/10.1016/j.neuroscience.2010.01.003

Sapède, D., Chaigne, C., Blader, P., & Cau, E. (2020). Functional heterogeneity in the pineal projection neurons of zebrafish. Molecular and Cellular Neuroscience, 103(February), 103468. https://doi.org/10.1016/j.mcn.2020.103468

Sawyer, C. M., Carstens, M. I., & Carstens, E. (2009). Mustard oil enhances spinal neuronal responses to noxious heat but not cooling. Neuroscience Letters, 461(3), 271–274. https://doi.org/10.1016/j.neulet.2009.06.036

Schnider TW, Gaeta R, Brose W, Minto CF, Gregg KM, Shafer SL. Derivation and cross-validation of pharmacokinetic parameters for computer-controlled infusion of lidocaine in pain therapy. The Journal of the American Society of Anesthesiologists. 1996 May 1;84(5):1043-50.

Schorscher-Petcu, A., Takács, F., & Browne, L. E. (2021). Scanned optogenetic control of mammalian somatosensory input to map input-specific behavioral outputs. ELife, 10, 1–19. https://doi.org/10.7554/eLife.62026

Schroeder, P. G., & Sneddon, L. U. (2017). Exploring the efficacy of immersion analgesics in zebrafish using an integrative approach. Applied Animal Behaviour Science, 187, 93–102. https://doi.org/10.1016/j.applanim.2016.12.003

Senzaki, K., Ozaki, S., Yoshikawa, M., Ito, Y., & Shiga, T. (2010). Runx3 is required for the specification of TrkC-expressing mechanoreceptive trigeminal ganglion neurons. Molecular and Cellular Neuroscience, 43(3), 296–307. https://doi.org/10.1016/j.mcn.2009.12.003

Serafini, R. A., Pryce, K. D., & Zachariou, V. (2020). The Mesolimbic Dopamine System in Chronic Pain and Associated Affective Comorbidities. Biological Psychiatry, 87(1), 64–73. https://doi.org/10.1016/j.biopsych.2019.10.018

Severi, K. E., Portugues, R., Marques, J. C., O'Malley, D. M., Orger, M. B., & Engert, F. (2014). Neural Control and Modulation of Swimming Speed in the Larval Zebrafish. Neuron, 83(3), 692–707. https://doi.org/10.1016/j.neuron.2014.06.032

Seymour, B. (2019). Pain: A Precision Signal for Reinforcement Learning and Control. Neuron, 101(6), 1029–1041. https://doi.org/10.1016/j.neuron.2019.01.055

Sharma, N., Flaherty, K., Lezgiyeva, K., Wagner, D. E., Klein, A. M., & Ginty, D. D. (2020). The emergence of transcriptional identity in somatosensory neurons. Nature, 577(7790), 392–398. https://doi.org/10.1038/s41586-019-1900-1

Shekarabi, M., Girard, N., Rivière, J. B., Dion, P., Houle, M., Toulouse, A., Lafrenière, R. G., Vercauteren, F., Hince, P., Laganiere, J., Rochefort, D., Faivre, L., Samuels, M., & Rouleau, G. A. (2008). Mutations in the nervous system-specific HSN2 exon of WNK1 cause hereditary sensory neuropathy type II. Journal of Clinical Investigation, 118(7), 2496–2505. https://doi.org/10.1172/JC134088

Shimazaki, T., Tanimoto, M., Oda, Y., & Higashijima, S. I. (2019). Behavioral role of the reciprocal inhibition between a pair of mauthner cells during fast escapes in Zebrafish. Journal of Neuroscience, 39(7), 1182–1194. https://doi.org/10.1523/JNEUROSCI.1964-18.2018

Shore, S.E., Vass, Z., Wys, N.L. and Altschuler, R.A., 2000. Trigeminal ganglion innervates the auditory brainstem. Journal of Comparative Neurology, 419(3), pp.271-285. https://doi.org/10.1002/(SICI)1096-9861(20000410)419:3<271::AID-CNE1>3.0.CO;2-M

Sievers, F., Wilm, A., Dineen, D., Gibson, T. J., Karplus, K., Li, W., Lopez, R., McWilliam, H., Remmert, M., Söding, J., Thompson, J. D., & Higgins, D. G. (2011a). Fast, scalable generation of high-quality protein multiple sequence alignments using Clustal Omega. Molecular Systems Biology, 7(539). https://doi.org/10.1038/msb.2011.75

Sievers, F., Wilm, A., Dineen, D., Gibson, T. J., Karplus, K., Li, W., Lopez, R., McWilliam, H., Remmert, M., Söding, J., Thompson, J. D., & Higgins, D. G. (2011b). Fast, scalable generation of high-quality protein multiple sequence alignments using Clustal Omega. Molecular Systems Biology, 7(539). https://doi.org/10.1038/msb.2011.75

Slatter, C. A. B., Kanji, H., Coutts, C. A., & Ali, D. W. (2005). Expression of PKC in the developing zebrafish, Danio rerio. Journal of Neurobiology, 62(4), 425–438. https://doi.org/10.1002/neu.20110

Smeyne, R. J., Klein, R., Schnapp, A., Long, L. K., Bryant, S., Lewin, A., Lira, S. A., & Barbacid, M. (1994). Severe sensory and sympathetic neuropathies in mice carrying a disrupted Trk/NGF receptor gene. Nature, 368(6468), 246–249. https://doi.org/10.1038/368246a0

Sneddon, L. U. (2002). Anatomical and electrophysiological analysis of the trigeminal nerve in a teleost fish, Oncorhynchus mykiss. Neuroscience Letters, 319(3), 167–171. https://doi.org/10.1016/S0304-3940(01)02584-8

Sneddon, L. U. (2003). Trigeminal somatosensory innervation of the head of a teleost fish with particular reference to nociception. Brain Research, 972(1–2), 44–52. https://doi.org/10.1016/S0006-8993(03)02483-1

Sneddon, L. U. (2018). Comparative physiology of nociception and pain. Physiology, 33(1), 63–73. https://doi.org/10.1152/physiol.00022.2017

Sneddon, L. U. (2019). Evolution of nociception and pain: Evidence from fish models. Philosophical Transactions of the Royal Society B: Biological Sciences, 374(1785). https://doi.org/10.1098/rstb.2019.0290

Snider, W. D. (1994). Functions of the neurotrophins during nervous system development: What the knockouts are teaching us. Cell, 77(5), 627–638. https://doi.org/10.1016/0092-8674(94)90048-5

Soelberg, C. D., Brown, R. E., Du Vivier, D., Meyer, J. E., & Ramachandran, B. K. (2017). The US Opioid Crisis: Current Federal and State Legal Issues. Anesthesia and Analgesia, 125(5), 1675–1681. https://doi.org/10.1213/ANE.0000000000002403

Sorlien, E. L., Witucki, M. A., & Ogas, J. (2018). Efficient production and identification of CRISPR/Cas9-generated gene knockouts in the model system Danio rerio. Journal of Visualized Experiments, 2018(138), 1–10. https://doi.org/10.3791/56969

Sovrano, V. A., & Andrew, R. J. (2006). Eye use during viewing a reflection: Behavioural lateralisation in zebrafish larvae. Behavioural Brain Research, 167(2), 226–231. https://doi.org/10.1016/j.bbr.2005.09.021

Spence, R., Gerlach, G., Lawrence, C., & Smith, C. (2008). The behaviour and ecology of the zebrafish, Danio rerio. Biological Reviews, 83(1), 13–34. https://doi.org/10.1111/j.1469-185X.2007.00030.x

Steinhart, J. S., & Hart, S. R. (1968). Calibration curves for thermistors. Deep-Sea Research and Oceanographic Abstracts, 15(4), 497–503. https://doi.org/10.1016/0011-7471(68)90057-0

Stewart, A. M., Braubach, O., Spitsbergen, J., Gerlai, R., & Kalueff, A. V. (2014). Zebrafish models for translational neuroscience research: From tank to bedside. Trends in Neurosciences, 37(5), 264–278. https://doi.org/10.1016/j.tins.2014.02.011

Stewart, W. J., & McHenry, M. J. (2010). Sensing the strike of a predator fish depends on the specific gravity of a prey fish. Journal of Experimental Biology, 213(22), 3769–3777. https://doi.org/10.1242/jeb.046946

Streisinger, G., Walker, C., Dower, N., Knauber, D. and Singer, F. (1981). Production of clones of homozygous diploid zebra fish (Brachydanio rerio). Nature, 291(5813), pp.293-296. https://doi.org/10.1038/291293a0

Su, C. Y., Kemp, H. A., & Moens, C. B. (2014). Cerebellar development in the absence of Gbx function in zebrafish. Developmental Biology, 386(1), 181–190. https://doi.org/10.1016/j.ydbio.2013.10.026

Subedi, B., Anderson, S., Croft, T. L., Rouchka, E. C., Zhang, M., & Hammond-Weinberger, D. R. (2021). Gene alteration in zebrafish exposed to a mixture of substances of abuse. Environmental Pollution, 278. https://doi.org/10.1016/j.envpol.2021.116777

Sun, C., Galicia, C., & Stenkamp, D. L. (2018). Transcripts within rod photoreceptors of the Zebrafish retina. BMC Genomics, 19(1), 1–18. https://doi.org/10.1186/s12864-018-4499-y

Suriyanarayanan, S., Othman, A., Dräger, B., Schirmacher, A., Young, P., Mulahasanovic, L., Hörtnagel, K., Biskup, S., von Eckardstein, A., Hornemann, T., & Lone, M. A. (2019). A Novel Variant (Asn177Asp) in SPTLC2 Causing Hereditary Sensory Autonomic Neuropathy Type 1C. NeuroMolecular Medicine, 21(2), 182–191. https://doi.org/10.1007/s12017-019-08534-w

Svedružić, Ž. M. (2011). Dnmt1: Structure and function. In Progress in Molecular Biology and Translational Science (Vol. 101, pp. 221–254). https://doi.org/10.1016/B978-0-12-387685-0.00006-8

Szucsik, J. C., Witte, D. P., Li, H., Pixley, S. K., Small, K. M., & Potter, S. S. (1997). Altered forebrain and hindbrain development in mice mutant for the Gsh- 2 homeobox gene. Developmental Biology, 191(2), 230–242. https://doi.org/10.1006/dbio.1997.8733

Takahashi, M., Narushima, M., & Oda, Y. (2002). In Vivo Imaging of Functional Inhibitory Networks on the Mauthner Cell of Larval Zebrafish. Journal of Neuroscience, 22(10), 3929–3938. https://doi.org/10.1523/jneurosci.22-10-03929.2002

Tan, L. L., & Kuner, R. (2021). Neocortical circuits in pain and pain relief. Nature Reviews Neuroscience, 22(8), 458–471. https://doi.org/10.1038/s41583-021-00468-2

Tanaka, H., Maeda, R., Shoji, W., Wada, H., Masai, I., Shiraki, T., Kobayashi, M., Nakayama, R., & Okamoto, H. (2007). Novel mutations affecting axon guidance in zebrafish and a role for plexin signalling in the guidance of trigeminal and facial nerve axons. Development, 134(18), 3259–3269. https://doi.org/10.1242/dev.004267

Tang, W., Davidson, J. D., Zhang, G., Conen, K. E., Fang, J., Serluca, F., Li, J., Xiong, X., Coble, M., Tsai, T., Molind, G., Fawcett, C. H., Sanchez, E., Zhu, P., Couzin, I. D., & Fishman, M. C. (2020). Genetic Control of Collective Behavior in Zebrafish. IScience, 23(3), 100942. https://doi.org/10.1016/j.isci.2020.100942

Tang, Z., Chen, Z., Tang, B., & Jiang, H. (2015). Primary erythromelalgia: A review. Orphanet Journal of Rare Diseases, 10(1), 1–11. https://doi.org/10.1186/s13023-015-0347-1

Tavares-Ferreira, D., Shiers, S., Ray, P. R., Wangzhou, A., Jeevakumar, V., Sankaranarayanan, I., Cervantes, A. M., Reese, J. C., Chamessian, A., Copits, B. A., Dougherty, P. M., Gereau IV, R. W., Burton, M. D., Dussor, G., & Price, T. J. (2022). Spatial transcriptomics of dorsal root ganglia identifies molecular signatures of human nociceptors. Science Translational Medicine, 14(632), 1–18. https://doi.org/10.1126/scitranslmed.abj8186

Taylor, J. C., Dewberry, L. S., Totsch, S. K., Yessick, L. R., DeBerry, J. J., Watts, S. A., & Sorge, R. E. (2017). A novel zebrafish-based model of nociception. Physiology and Behavior, 174, 83–88. https://doi.org/10.1016/j.physbeh.2017.03.009

Temizer, I., Donovan, J. C., Baier, H., & Semmelhack, J. L. (2015). A Visual Pathway for Looming-Evoked Escape in Larval Zebrafish. Current Biology, 25(14), 1823–1834. https://doi.org/10.1016/j.cub.2015.06.002

Terry, A. V., Gearhart, D. A., Beck, W. D., Truan, J. N., Middlemore, M. L., Williamson, L. N., Bartlett, M. G., Prendergast, M. A., Sickles, D. W., & Buccafusco, J. J. (2007). Chronic, intermittent exposure to chlorpyrifos in rats: Protracted effects on axonal transport, neurotrophin receptors, cholinergic markers, and information processing. Journal of

Pharmacology and Experimental Therapeutics, 322(3), 1117–1128. https://doi.org/10.1124/jpet.107.125625

Testa, G., Mainardi, M., Morelli, C., Olimpico, F., Pancrazi, L., Petrella, C., Severini, C., Florio, R., Malerba, F., Stefanov, A., Strettoi, E., Brandi, R., Arisi, I., Heppenstall, P., Costa, M., Capsoni, S., & Cattaneo, A. (2019). The NGFR100W mutation specifically impairs nociception without affecting cognitive performance in a mouse model of hereditary sensory and autonomic neuropathy type V. Journal of Neuroscience, 39(49), 9702–9715. https://doi.org/10.1523/JNEUROSCI.0688-19.2019

Theriault, F. M., Roy, P., & Stifani, S. (2004). AML1/Runx1 is important for the development of hindbrain cholinergic branchiovisceral motor neurons and selected cranial sensory neurons. Proceedings of the National Academy of Sciences of the United States of America, 101(28), 10343–10348. https://doi.org/10.1073/pnas.0400768101

Thompson, R.F., 2009. Habituation: a history. Neurobiology of learning and memory, 92(2), p.127. doi: 10.1016/j.nlm.2008.07.011

Thyme, S. B., Pieper, L. M., Li, E. H., Pandey, S., Wang, Y., Morris, N. S., Sha, C., Choi, J. W., Herrera, K. J., Soucy, E. R., Zimmerman, S., Randlett, O., Greenwood, J., McCarroll, S. A., & Schier, A. F. (2019). Phenotypic Landscape of Schizophrenia-Associated Genes Defines Candidates and Their Shared Functions. Cell, 177(2), 478-491.e20. https://doi.org/10.1016/j.cell.2019.01.048

Tian, L., Andrew Hires, S., & Looger, L. L. (2012). Imaging neuronal activity with genetically encoded calcium indicators. Cold Spring Harbor Protocols, 7(6), 647–656. https://doi.org/10.1101/pdb.top069609

Tittle, R. K., Sze, R., Ng, A., Nuckels, R. J., Swartz, M. E., Anderson, R. M., Bosch, J., Stainier, D. Y. R., Eberhart, J. K., & Gross, J. M. (2011). Uhrf1 and Dnmt1 are required for development and maintenance of the zebrafish lens. Developmental Biology, 350(1), 50–63. https://doi.org/10.1016/j.ydbio.2010.11.009

Todd, A. J. (2010). Neuronal circuitry for pain processing in the dorsal horn. Nature Reviews Neuroscience, 11(12), 823–836. https://doi.org/10.1038/nrn2947

Trang, T., Quirion, R., & Jhamandas, K. (2005). The spinal basis of opioid tolerance and physical dependence: Involvement of calcitonin gene-related peptide, substance P, and arachidonic acid-derived metabolites. Peptides, 26(8), 1346–1355. https://doi.org/10.1016/j.peptides.2005.03.031

Tsang, A., Von Korff, M., Lee, S., Alonso, J., Karam, E., Angermeyer, M. C., Borges, G. L. G., Bromet, E. J., de Girolamo, G., de Graaf, R., Gureje, O., Lepine, J. P., Haro, J. M., Levinson, D., Oakley Browne, M. A., Posada-Villa, J., Seedat, S., & Watanabe, M. (2008). Common Chronic Pain Conditions in Developed and Developing Countries: Gender and Age Differences and Comorbidity With Depression-Anxiety Disorders. Journal of Pain, 9(10), 883–891. https://doi.org/10.1016/j.jpain.2008.05.005

Tunbak, H., Vazquez-Prada, M., Ryan, T., Kampff, A. R., & Dreosti, E. (2020). Whole-brain mapping of socially isolated zebrafish reveals that lonely fish are not loners. ELife, 9, 1–14. https://doi.org/10.7554/eLife.55863

Usoskin, D., Furlan, A., Islam, S., Abdo, H., Lönnerberg, P., Lou, D., Hjerling-Leffler, J., Haeggström, J., Kharchenko, O., Kharchenko, P. V., Linnarsson, S., & Ernfors, P. (2015). Unbiased classification of sensory neuron types by large-scale single-cell RNA sequencing. Nature Neuroscience. https://doi.org/10.1038/nn.3881

Van Damme, S., Becker, S., & Van Der Linden, D. (2018). Tired of pain? Toward a better understanding of fatigue in chronic pain. Pain, 159(1), 7–10. https://doi.org/10.1097/j.pain.0000000000001054

Van Den Maagdenberg, A. M. J. M., Pietrobon, D., Pizzorusso, T., Kaja, S., Broos, L. A. M., Cesetti, T., Van De Ven, R. C. G., Tottene, A., Van Der Kaa, J., Plomp, J. J., Frants, R. R., & Ferrari, M. D. (2004). A Cacna1a knockin migraine mouse model with increased

susceptibility to cortical spreading depression. Neuron, 41(5), 701–710. https://doi.org/10.1016/S0896-6273(04)00085-6

von Krogh, K., Higgins, J., Saavedra Torres, Y. and Mocho, J.P. (2021). Screening of anaesthetics in adult zebrafish (Danio rerio) for the induction of euthanasia by overdose. Biology, 10(11), p.1133.

Vandewauw, I., De Clercq, K., Mulier, M., Held, K., Pinto, S., Van Ranst, N., Segal, A., Voet, T., Vennekens, R., Zimmermann, K., Vriens, J., & Voets, T. (2018). A TRP channel trio mediates acute noxious heat sensing. Nature, 555(7698), 662–666. https://doi.org/10.1038/nature26137

Vassilopoulos, S., Esk, C., Hoshino, S., Funke, B. H., Chen, C. Y., Plocik, A. M., Wright, W. E., Kucherlapati, R., & Brodsky, F. M. (2009). A Role for the CHC22 clathrin heavy-chain isoform in human glucose metabolism. Science, 324(5931), 1192–1196. https://doi.org/10.1126/science.1171529

Waldmann, R., Champigny, G., Bassilana, F., Heurteaux, C., & Lazdunski, M. (1997). A proton-gated cation channel involved in acid-sensing. Nature, 386(6621), 173–177. https://doi.org/10.1038/386173a0

Walters, E.T., 1994. Injury-related behavior and neuronal plasticity: an evolutionary perspective on sensitization, hyperalgesia, and analgesia. International review of neurobiology, 36, pp.325-427.

Walters, E. T., & Moroz, L. L. (2009). Molluscan memory of injury: Evolutionary insights into Chronic pain and neurological disorders. Brain, Behavior and Evolution, 74(3), 206–218. https://doi.org/10.1159/000258667

Watkins, J., Miklósi, A., & Andrew, R. J. (2004). Early asymmetries in the behaviour of zebrafish larvae. Behavioural Brain Research, 151(1–2), 177–183. https://doi.org/10.1016/j.bbr.2003.08.012

Watson, J. J., Allen, S. J., & Dawbarn, D. (2008). Targeting nerve growth factor in pain: What is the therapeutic potential? BioDrugs, 22(6), 349–359. https://doi.org/10.2165/0063030-200822060-00002

Wee, C. L., Nikitchenko, M., Wang, W.-C., Luks-Morgan, S. J., Song, E., Gagnon, J. A., Randlett, O., Bianco, I. H., Lacoste, A. M. B., Glushenkova, E., Barrios, J. P., Schier, A. F., Kunes, S., Engert, F., & Douglass, A. D. (2019). Zebrafish oxytocin neurons drive nocifensive behavior via brainstem premotor targets. Nature Neuroscience, 22(9), 1477–1492. https://doi.org/10.1038/s41593-019-0452-x

Wemmie, J. A., Taugher, R. J., & Kreple, C. J. (2013). Acid-sensing ion channels in pain and disease. Nature Reviews Neuroscience, 14(7), 461–471. https://doi.org/10.1038/nrn3529

White, J. M., & Irvine, R. J. (1999). Mechanisms of fatal opioid overdose. Addiction, 94(7), 961–972. https://doi.org/10.1046/j.1360-0443.1999.9479612.x

Williams, J. A., Barrios, A., Gatchalian, C., Rubin, L., Wilson, S. W., & Holder, N. (2000). Programmed cell death in zebrafish Rohon Beard neurons is influenced by TrkC1/NT-3 signaling. Developmental Biology, 226(2), 220–230. https://doi.org/10.1006/dbio.2000.9860

Winata, C. L., Korzh, S., Kondrychyn, I., Zheng, W., Korzh, V., & Gong, Z. (2009). Development of zebrafish swimbladder: The requirement of Hedgehog signaling in specification and organization of the three tissue layers. Developmental Biology, 331(2), 222–236. https://doi.org/10.1016/j.ydbio.2009.04.035

Winkelmann, J., Lin, L., Schormair, B., Kornum, B. R., Faraco, J., Plazzi, G., Melberg, A., Cornelio, F., Urban, A. E., Pizza, F., Poli, F., Grubert, F., Wieland, T., Graf, E., Hallmayer, J., Strom, T. M., & Mignot, E. (2012). Mutations in DNMT1 cause autosomal dominant cerebellar ataxia, deafness and narcolepsy. Human Molecular Genetics, 21(10), 2205–2210. https://doi.org/10.1093/hmg/dds035

Wittenburg, N., & Baumeister, R. (1999). Thermal avoidance in Caenorhabditis elegans: An approach to the study of nociception. Proceedings of the National Academy of Sciences of the United States of America, 96(18), 10477–10482. https://doi.org/10.1073/pnas.96.18.10477

Wolman, M., & Granato, M. (2012). Behavioral genetics in larval zebrafish: Learning from the young. Developmental Neurobiology, 72(3), 366–372. https://doi.org/10.1002/dneu.20872

Wu, R.S., Lam, I.I., Clay, H., Duong, D.N., Deo, R.C. and Coughlin, S.R. (2018). A rapid method for directed gene knockout for screening in G0 zebrafish. Developmental cell, 46(1), pp.112-125.

Wu, T. S., Cheng, Y. C., Chen, P. J., Huang, Y. T., Yu, F. Y., & Liu, B. H. (2019). Exposure to aflatoxin B1 interferes with locomotion and neural development in zebrafish embryos and larvae. Chemosphere, 217(110), 905–913. https://doi.org/10.1016/j.chemosphere.2018.11.058

Xie, J., Wu, T., Xu, K., Huang, I. K., Cleaver, O., & Huang, C. L. (2009). Endothelial-specific expression of WNK1 kinase is essential for angiogenesis and heart development in mice. American Journal of Pathology, 175(3), 1315–1327. https://doi.org/10.2353/ajpath.2009.090094

Yang, W., Chen, S. C., Lai, J. Y., Ming, Y. C., Chen, J. C., & Chen, P. L. (2019). Distinctive genetic variation of long-segment Hirschsprung's disease in Taiwan. Neurogastroenterology and Motility, 31(11), 1–10. https://doi.org/10.1111/nmo.13665

Yang, Y., Wang, Y., Li, S., Xu, Z., Li, H., Ma, L., Fan, J., Bu, D., Liu, B., Fan, Z., Wu, G., Jin, J., Ding, B., Zhu, X., & Shen, Y. (2004). Mutations in SCN9A, encoding a sodium channel alpha subunit, in patients with primary erythermalgia. Journal of Medical Genetics, 41(3), 171–174. https://doi.org/10.1136/jmg.2003.012153

Yao, C., Vanderpool, K. G., Delfiner, M., Eddy, V., Lucaci, L. G., Soto-Riveros, C., Yasumura, T., Rash, J. E., & Pereda, A. E. (2014). Electrical synaptic transmission in developing zebrafish: Properties and molecular composition of gap junctions at a central auditory synapse. Journal of Neurophysiology, 112(9), 2102–2113. https://doi.org/10.1152/jn.00397.2014

Yao, Y., Li, X., Zhang, B., Yin, C., Liu, Y., Chen, W., Zeng, S., & Du, J. (2016). Visual Cue-Discriminative Dopaminergic Control of Visuomotor Transformation and Behavior Selection. Neuron, 89(3), 598–612. https://doi.org/10.1016/j.neuron.2015.12.036

Ye, J., Coulouris, G., Zaretskaya, I., Cutcutache, I., Rozen, S., & Madden, T. L. (2012). Primer-BLAST: a tool to design target-specific primers for polymerase chain reaction. BMC Bioinformatics, 13, 134. https://doi.org/10.1186/1471-2105-13-134

Yekkirala, A. S., Roberson, D. P., Bean, B. P., & Woolf, C. J. (2017). Breaking barriers to novel analgesic drug development. Nature Reviews Drug Discovery, 16(8), 545–564. https://doi.org/10.1038/nrd.2017.87

Yeo, S. Y., Miyashita, T., Fricke, C., Little, M. H., Yamada, T., Kuwada, J. Y., Huh, T. L., Chien, C. B., & Okamoto, H. (2004). Involvement of Islet-2 in the Slit signaling for axonal branching and defasciculation of the sensory neurons in embryonic zebrafish. Mechanisms of Development, 121(4), 315–324. https://doi.org/10.1016/j.mod.2004.03.006

Yildiz, O., Downes, G. B., & Sagerström, C. G. (2019). Zebrafish prdm12b acts independently of nkx6.1 repression to promote eng1b expression in the neural tube p1 domain. Neural Development, 14(1), 1–19. https://doi.org/10.1186/s13064-019-0129-x

Yu, L. C., Hanson, P., & Lundeberg, T. (1994). The calcitonin gene-related peptide antagonist CGRP8-37 increases the latency to withdrawal responses in rats. Brain Research, 666(2), 295. https://doi.org/10.1016/0006-8993(94)90787-0

Yu, Y., Chen, Z., Li, W. G., Cao, H., Feng, E. G., Yu, F., Liu, H., Jiang, H., & Xu, T. L. (2010). A nonproton ligand sensor in the acid-sensing ion channel. Neuron, 68(1), 61–72. https://doi.org/10.1016/j.neuron.2010.09.001

Yuan, J., Matsuura, E., Higuchi, Y., Hashiguchi, A., Nakamura, T., Nozuma, S., Sakiyama, Y., Yoshimura, A., Izumo, S., & Takashima, H. (2013). Hereditary sensory and autonomic neuropathy type IID caused by an SCN9A mutation. Neurology, 80(18), 1641–1649. https://doi.org/10.1212/WNL.0b013e3182904fdd

Yuan, L., Li, J., Zha, J., & Wang, Z. (2016). Targeting neurotrophic factors and their receptors, but not cholinesterase or neurotransmitter, in the neurotoxicity of TDCPP in Chinese rare minnow adults (Gobiocypris rarus). Environmental Pollution, 208, 670–677. https://doi.org/10.1016/j.envpol.2015.10.045

Zaig, S., Scarpellini, C., & Montandon, G. (2021). Respiratory depression and analgesia by opioid drugs in freely-behaving larval zebrafish. ELife, 10, 1–20. https://doi.org/10.7554/eLife.63407

Zannino, D. A., Downes, G. B., & Sagerström, C. G. (2014). Prdm12b specifies the p1 progenitor domain and reveals a role for V1 interneurons in swim movements. Developmental Biology, 390(2), 247–260. https://doi.org/10.1016/j.ydbio.2014.02.025

Zeisel, A., Hochgerner, H., Lönnerberg, P., Johnsson, A., Memic, F., van der Zwan, J., Häring, M., Braun, E., Borm, L. E., La Manno, G., Codeluppi, S., Furlan, A., Lee, K., Skene, N., Harris, K. D., Hjerling-Leffler, J., Arenas, E., Ernfors, P., Marklund, U., & Linnarsson, S. (2018). Molecular Architecture of the Mouse Nervous System. Cell, 174(4), 999-1014.e22. https://doi.org/10.1016/j.cell.2018.06.021

Zhang, X. Y., Wen, J., Yang, W., Wang, C., Gao, L., Zheng, L. H., Wang, T., Ran, K., Li, Y., Li, X., Xu, M., Luo, J., Feng, S., Ma, X., Ma, H., Chai, Z., Zhou, Z., Yao, J., Zhang, X., & Liu, J. Y. (2013). Gain-of-Function mutations in SCN11A cause familial episodic pain. American Journal of Human Genetics, 93(5), 957–966. https://doi.org/10.1016/j.ajhg.2013.09.016

Zhao, X., Alvarado, D., Rainier, S., Lemons, R., Hedera, P., Weber, C. H., Tukel, T., Apak, M., Heiman-Patterson, T., Ming, L., Bui, M., & Fink, J. K. (2001). Mutations in a newly identified GTPase gene cause autosomal dominant hereditary spastic paraplegia. Nature Genetics, 29(3), 326–331. https://doi.org/10.1038/ng758

Zheng, Y., Liu, P., Bai, L., Trimmer, J. S., Bean, B. P., & Ginty, D. D. (2019). Deep Sequencing of Somatosensory Neurons Reveals Molecular Determinants of Intrinsic Physiological Properties. Neuron, 103(4), 598-616.e7. https://doi.org/10.1016/j.neuron.2019.05.039

Zhu, P. P., Patterson, A., Lavoie, B., Stadler, J., Shoeb, M., Patel, R., & Blackstone, C. (2003). Cellular localization, oligomerization, and membrane association of the hereditary spastic paraplegia 3A (SPG3A) protein atlastin. The Journal of Biological Chemistry, 278(49), 49063–49071. https://doi.org/10.1074/jbc.M306702200

Ziemann, A. E., Allen, J. E., Dahdaleh, N. S., Drebot, I. I., Coryell, M. W., Wunsch, A. M., Lynch, C. M., Faraci, F. M., Howard, M. A., Welsh, M. J., & Wemmie, J. A. (2009). The Amygdala Is a Chemosensor that Detects Carbon Dioxide and Acidosis to Elicit Fear Behavior. Cell, 139(5), 1012–1021. https://doi.org/10.1016/j.cell.2009.10.029